Identification and Validation of an Aircraft Performance Model for the Study of Flight Trajectories of the Cessna Citation X

by

Georges GHAZI

MANUSCRIPT-BASED THESIS PRESENTED TO ÉCOLE DE TECHNOLOGIE SUPÉRIEURE
IN PARTIAL FULFILLMENT FOR THE DEGREE OF
DOCTOR OF PHILOSOPHY
Ph.D.

MONTREAL, NOVEMBER 11TH, 2020

ÉCOLE DE TECHNOLOGIE SUPÉRIEURE
UNIVERSITÉ DU QUÉBEC

BOARD OF EXAMINERS

THIS THESIS HAS BEEN EVALUATED

BY THE FOLLOWING BOARD OF EXAMINERS

Mrs. Ruxandra Mihæla Botez, Thesis Supervisor
Department of Systems Engineering, École de technologie supérieure

Mr. Kamal Al-Haddad, Chair, Board of Examiners
Department of Electrical Engineering, École de technologie supérieure

Mr. Rachid Aissaoui, Member of the Jury
Department of Systems Engineering, École de technologie supérieure

Mr. Adrian Hiliuta, External Examiner
CMC Electronics

THIS THESIS WAS PRESENTED AND DEFENDED

IN THE PRESENCE OF A BOARD OF EXAMINERS AND THE PUBLIC

ON OCTOBER 29TH, 2020

AT ÉCOLE DE TECHNOLOGIE SUPÉRIEURE

ACKNOWLEDGEMENTS

First of all, I would like to express my sincere gratitude to my thesis supervisor, Dr. Ruxandra Mihaela Botez, for giving me this wonderful opportunity to conduct my PhD thesis at the Laboratory of Applied Research in Active Control, Avionics, and AeroServoElasticity (LARCASE). Without her support, guidance and constant feedback, this PhD would not have been achieved. I would also thank her for giving me the great opportunity to share my knowledge to students as a Lecturer for the courses "Introduction à l'avionique" (GPA745) and "Systèmes de commande des avions" (GPA741).

Many thanks are also dues to Mr. Oscar Carranza for his very good humor and all the long discussions we had, but above all for sharing with me all his knowledge. I also thank him for his help and support on the two research aircraft flight simulators available at the LARCASE.

I would also like to thank to CMC Electronics team for its support and collaboration in this research. In particular, I would like to thank Mr. Reza Neshat and Mr. Oussama Abdul-Baki for their invaluable advices and feedback on my research.

I am also very thankful to all the members and researchers of LARCASE, and more specifically to all students I had the pleasure to work with and share ideas. I especially thank Andréa Mennequin, Aurélie George, Charles Bourrely, Alina Turculet, Mathias Barret, Maxime Lussier, Marc Henri Devillers, Magali Gelhaye and Benoit Gerardin. I would not have been able to accomplish as much as I did without their research efforts and implication in my research.

A very special "thank you" to Margaux, Marine and Polo for all the very good times we had at LARCASE, and for all the great conversations we had during lunch hours. I also would like to thank Alejandro Murrieta-Mendoza AKA "El Sabroson" for his friendship, and for all the fun moments we had at the LARCASE and during our travels around the world. His advice and comments were of great help in writing my papers.

I am also indebted to all my friends, far too numerous to be listed here, but my thoughts are particularly with Kevin Rezk AKA "Boy Pou", Ahmed Khalil AKA "Boy Zin", Jonathan

Brulatout, Mariana Castaneda-Gonzalez, and Sitraka Razanamparany, who have been a major source of support. Thanks guys for your sincere friendships, for all the moments we spent together, for our crazy laughs and especially for your good humor.

I owe thanks to a very special person, the woman with whom I have shared my life for the past four years. Throughout my PhD studies, you never stopped supporting and encouraging me. I spent unforgettable moments with you and I hope that the years to come will only be better. Today, I consider myself the luckiest in the world to have you by my side. For all that you have done and your unconditional love: Thank You.

Finally, I would like to say a heartfelt thank you to my family for always believing in me and encouraging me to follow my dreams. Thank you for all the support you give me at every moment of my life, and for all the sacrifice you did to shape my life. I hope you will see in this thesis the accomplishment of all that you have done for me; I dedicate this PhD thesis to you.

Identification et validation d'un modèle de performance pour l'étude des trajectoires de vol de l'avion Cessna Citation X

Georges GHAZI

RÉSUMÉ

L'optimisation des trajectoires de vol a été identifiée comme l'une des solutions permettant de réduire la consommation de carburant et l'empreinte carbone des avions à court terme. Pour pouvoir analyser et optimiser les trajectoires de vol d'un avion, il nécessaire de développer des modèles mathématiques capables de prédire avec une grande précision les performances de ce dernier. Dans ce contexte, l'enjeu de cette thèse a été de proposer différentes techniques permettant d'une part d'identifier un modèle mathématique d'un avion, et d'autre part, de pouvoir prédire les trajectoires et les performances de vol d'un avion.

Les études présentées dans cette thèse ont été réalisées en collaboration avec les partenaires industriels du LARCASE, et ont été expérimentalement validées sur l'avion d'affaire Cessna Citation X pour lequel un simulateur de vol hautement qualifié était disponible.

La première partie de cette thèse portait sur l'identification et la création d'un modèle performance de l'avion Cessna Citation X à partir de données publiées dans les manuels de vol de l'avion (ou d'une source équivalente). Ce modèle avait pour objectif de représenter les performances aérodynamiques et propulsives de l'avion. Deux approches ont été alors envisagées. La première approche consistait à identifier un modèle de propulsion de l'avion en supposant que les données publiées dans les manuels de vol incluaient des informations suffisamment pertinentes sur les performances de moteurs de l'avion. La deuxième approche, quant à elle, faisait l'hypothèse qu'aucune information sur les moteurs n'était disponible, et que seules les données de trajectoire de vol étaient accessible à l'utilisateur. Dans les deux approches, il a été possible d'obtenir un modèle mathématique de l'avion à la fois fiable et précis.

La deuxième partie de cette thèse était axée sur l'étude et la prédiction des trajectoires de vol. En partant d'un modèle mathématique de l'avion, différents algorithmes ont été développés pour prédire les performances et les trajectoires de vol du Cessna Citation X. Encore une fois, cette étude a été divisée en deux sous-parties : une première sous-partie portait sur l'étude de la phase de décollage, tandis que la deuxième sous-partie était consacrée à la portion du vol au-dessus de 1500 pieds (i.e., excluant les phases de décollage et d'atterrissage). Les algorithmes et les techniques proposées dans cette thèse ont permis de prendre en compte les effets du vent, mais également de modéliser les techniques de pilotage.

Finalement, la dernière partie de cette thèse s'intéressait à la surveillance des performances d'un avion, et à la mise à jour automatique du modèle mathématique de ce dernier. Pour ce faire, un algorithme permettant d'analyser les performances de l'avion en croisière a été développé. Cet algorithme permettait dans un premier temps, de collecter des paramètres de vol de l'avion et de réaliser des analyses pour identifier les segments de vol dans lesquels l'avion se trouvait en conditions d'équilibre. Une fois ces segments de vol identifiés, l'algorithme effectuait des

corrélations entre les paramètres de vol mesurés, et ceux prédits par le modèle mathématique de l'avion. Cette analyse était ensuite utilisée pour évaluer le degré de précision du modèle mathématique de l'avion. Dans le cas où le modèle n'était plus suffisamment précis, alors une mise à jour automatique de ce dernier était réalisée.

La combinaison de toutes les études présentées dans cette thèse a permis de créer des outils mathématiques pour l'étude, l'analyse et la prédiction des trajectoires de vol de l'avion Cessna Citation X. Ces outils ont été développés pour répondre à des besoins spécifiques de l'industrie aéronautique, mais également pour aider les chercheurs du LARCASE dans leurs recherches.

Mots-clés: modélisation, identification, aérodynamique, propulsions, performances avion, trajectoire de vol

Identification and Validation of an Aircraft Performance Model for the Study of Flight Trajectories of the Cessna Citation X

Georges GHAZI

ABSTRACT

Flight trajectories optimization has been identified as one of the solutions to reduce fuel consumption, and carbon footprint of aircraft in the short term. To be able to analyze and optimize aircraft flight trajectories, it is necessary to develop mathematical models capable of predicting aircraft performance with great accuracy. Within this context, the main goal of this thesis was to propose different techniques to identify a mathematical model of an aircraft, and to predict the trajectories and flight performance of an aircraft.

The studies presented in this thesis were carried out in collaboration with the LARCASE industrial partners, and were applied on the well-known Cessna Citation X business jet for which a highly qualified research aircraft flight simulator was available.

The first part of this thesis focused on the identification and creation of a mathematical model of the Cessna Citation X based on data published in the aircraft flight manuals (or equivalent source). The objective of this mathematical model was to represent the aerodynamic and propulsive performance of the aircraft. Two approaches were then considered. The first approach consisted of identifying a propulsion model of the aircraft assuming that the data published in the flight manuals included sufficiently relevant information regarding the engine performance. The second approach assumed that no engine information was available, and that only flight trajectories data was accessible to the user. In both approaches, it was possible to obtain a mathematical model of the aircraft that was both reliable and accurate.

The second part of this thesis focused on the study and prediction of aircraft flight trajectories. A mathematical model of the aircraft, different algorithms have been developed to predict the performance, and flight trajectories of the Cessna Citation X. Once again, this study was divided into two subparts; the first subpart was devoted to the takeoff phase study, while the second subpart was devoted to the portion of the flight above 1500 feet (i.e., excluding the takeoff and landing phases). The algorithms and techniques proposed in this thesis made it possible to account for the effects of the wind, but also to take into account the piloting techniques.

Finally, the last part of this thesis focused on the monitoring of the aircraft performance, and on the automatic update of the mathematical model of the aircraft. For this purpose, an algorithm to analyze the aircraft performance in cruise was developed. This algorithm allowed, in a first step, to collect various aircraft flight parameters and to perform different analyses to identify the flight segments in which the aircraft was in trim conditions. Once these flight segments were identified, the algorithm correlated the measured flight parameters with those predicted by the aircraft mathematical model. This analysis was then used to assess the accuracy of the aircraft mathematical model. If the model was no longer accurate, then its automatic update was performed.

The combination of all the studies presented in this thesis has allowed the design of mathematical tools for the study, analysis and prediction of the flight trajectories of the Cessna Citation X aircraft. These tools were developed to meet specific needs of the aeronautical industry, but also to help LARCASE researchers in their research.

Keywords: modeling, identification, aerodynamics, propulsion, aircraft performance, flight trajectories

TABLE OF CONTENTS

Page

LIST OF TABLES

LIST OF FIGURES

LIST OF ALGORITHMS

LIST OF ABBREVIATIONS

ADS-B	Automatic Dependent Surveillance Broadcast
AF	Acceleration Factor
AFM	Aircraft Flight Manual
AGL	Above Ground Level
AH	Acceleration Height
ATC	Air Traffic Control
ATM	Air Traffic Management
BADA	Base of Aircraft Data
CAS	Calibrated Airspeed
CFD	Computational Fluid Dynamics
CLM	Component Level Model
CDO	Continuous Descent Operations
CO_2	Carbon Dioxyde
CVG	Compressor Variable Geometry
FAA	Federal Aviation Administration
FADEC	Full Authority Digital Electronics Control
FCOM	Flight Crew Operating Manual
F/B, F/O	Fly-By, or Fly-Over
FMS	Flight Management System

FPG	Flight Planning Guide
GARDN	Green Aviation Research & Developement Network
IATA	International Air Transport Association
IFP	In-Flight Performance
ISA	International Standard Atmosphere
LARCASE	Laboratory of Applied Research in Active Control, Avionics, and AeroServoElasticity
NADP	Noise Abatement Departure Procedure
NextGen	Next Generation of Air Transport
NO_x	Nitrogen Oxides
OAT	Outside Air Temperature
RAFS	Research Aircraft Flight Simulator
SESAR	Single European Sky ATM Research
SID	Standard Instrument Departure
SO_x	Sulfure Oxydes
STAR	Standard Terminal Arrival Route
T/C, T/D	Top-of-Climb, and Top-of-Descent
TBO	Trajectory Based Operation
TO/GA	Take-Off/Go-Around
TRH	Thrust Reduction Height
TSFC	Thust Specific Fuel Consumption

LIST OF VARIABLES AND SYMBOLS

List of Variables

CD_0	Zero-lift drag coefficient
CD_s	Drag aerodynamic coefficient
Cm_s	Pitching moment coefficient
CL_s	Lift aerodynamic coefficient
D	Drag force
F_B	Fuel burned
F_N	Engine net thrust
FD	Excess-thrust
g_0	Acceleration due to gravity
h	Pressure altitude
$\bar{h}$	Altitude above ground level
K	Lift-dependent drag coefficient
k_a, k_c	Adaptive, and conservative gains
L	Lift force
m	Aircraft mass
M	Mach number
M_y	Pitching moment
N_1	Engine fan speed

N_2	Engine core speed
n_z	Load factor
P	Ambient/Static air pressure
R_{air}	Specific air constant
R_M, R_N	Main, and nose gear reaction force (in Chapter 4)
R_N	Nominal turn radius (in Chapter 5)
S	Aircraft wing reference area
S_{ref}	Engine inlet section
t	time, or simulation time
T	Ambient/Static air temperature
V/S	Vertical speed
V_2	Takeoff safety speed
V_C	Calibrated airspeed
V_{GS}	Ground speed
V_{LOF}	Lift-off speed
V_T	True airspeed
V_R	Rotation speed
V_W, V'_W	Wind speed magnitude, and wind gradient
$V_{W,x}, V_{W,y}$	Horizontal wind components
V_{ZF}	Flaps up speed

W	Aircraft weight
W_{TO}	Aircraft Takeoff Weight
x	Ground/horizontal distance

Greek Symbols

α	Angle of attack
β	Interception angle
γ	Air-relative flight path angle
γ_R	Runway slope angle
δ	Static air pressure ratio / Normalized distance (in Chapter 6)
δ_e	Elevators deflection
δ_f	Flaps position
δ_g	Gears position
δ_s	Horizontal stabilizer position
θ	Static air temperature ratio
λ	Smoothing parameter (in Chapter 2) / Aircraft longitude (in Chapter 5) / Confidence coefficient (in Chapter 6)
μ	Friction coefficient runway (in Chapter 4) / Aircraft latitude (in Chapter 5)
ρ	Static air density
ϕ, ϕ_N	Aircraft bank angle, and nominal bank angle
ϕ_T	Engine thrust inclination

ψ	Aircraft heading
ψ_c	Aircraft course
ψ_w	Horizontal wind direction

INTRODUCTION

Today, aviation has become one of the most convenient mode of transportation. With a rapid worldwide transportation network, airlines are connecting more people and countries than ever before. According to the International Air Transport Association (IATA), about 4.4 billion people traveled around the world on an aircraft in 2018, which represented an increase of 6.9% compared to the number of people statistics established in 2017 (IATA, 2019).

The aviation industry is growing rapidly and will continue to grow as the demand for air transportation is expected to increase by an average of 4.3% per year over the next years (IATA, 2020). Such an expansion has both social and economic benefits; "social" because it allows people to travel for leisure, to explore new regions of the world or to reunite with family during the holidays; and "economic" because by facilitating trade between continents, it contributes to global economic growth and the development of countries.

Despite these many benefits, there are concerns about the growth of the aviation industry. More and more experts are questioning regarding the impact that such growth could have on the environment and the capacity of current systems to handle such a large aircraft flow.

0.1 Problem Statement

One of the main problems of aviation is that it is an energy-intensive transport sector that relies heavily on fossil fuels. By burning fuel, aircraft engines produce and emit staggering amounts of Carbon Dioxide (CO_2) which is known for its contribution to global warming, but also various other substances such as Nitrogen Oxides (NO_x) and Sulfur Oxides (SO_x) whose effects on the environment and human health are less well known. In 2017, the aviation industry produced around 859 million tonnes of CO_2, which accounted for 2 to 3% of global emissions (IATA, 2018). Although this share may seem relatively small, it does not really reflect the impact of aviation on the environment. Indeed, according to studies (Lee, Fahey, Forster, Newton, Wit, Lim, Owen & Sausen, 2009), emissions at high altitudes have a greater impact on global warming than if they were released at low altitudes (or at ground level).

In addition to emissions, the noise produced by aircraft during near-ground operations (i.e., takeoff, departures, approach and landing) has also been identified as a significant problem for people living near airports. The noise of an aircraft engine during a conventional takeoff, for example, can vary between 130 and 160 dB (Antuñano & Spanyers, 1998). This noise is often

defined as “unwanted sound” which, in the long term, can become a source of discomfort or annoyance. However, recent studies have shown that the effects of aircraft noise are not limited to only these two aspects, but could also cause adverse health effects, including: stress, anxiety, sleep disturbance and cardiovascular diseases (Correia, Peters, Levy, Melly & Dominici, 2013; Basner, Clark, Hansell, Hileman, Janssen, Shepherd & Sparrow, 2017).

Another problem related to the continuous growth of air transport concerns the capacity of current systems to handle the flow of aircraft. Indeed, in order to meet the high demand for air transport, airlines must enlarge their fleets, which results in an overload of airspace. Today, airports in major cities are reaching their capacity limits for arriving and departing flights (Silk, 2017). This saturation leads to flight delays, ineffective routes and complex air traffic control procedures. Studies have estimated that airlines waste an average of 740 million gallons of fuel per year due to domestic flight delays in the United States, which represents a loss of revenue of USD 19 billion (Balakrishnan, 2016). In terms of emissions, this loss corresponds to an additional 7.1 billion kilograms of CO_2 released into the atmosphere.

Finally, from an airline perspective, fuel consumption is not only an environmental issue, but is also an economic one. The two main expenses that affect the economy of airlines are labor and fuel costs. Labor costs are based on the time the aircraft spends in flight, and are usually quasi constant in the short term. Fuel costs, on the other hand, are more difficult to predict since they vary considerably depending on the price of oil. In 2018, IATA (2018) estimated that airlines spent an average of 23.5% of their operating fuel expenses. Given the highly competitive nature of the industry, airlines are paying more attention to fuel costs and are researching for strategies that could reduce their fuel consumption.

Faced with all these concerns, aviation stakeholders are asking themselves many questions, including the following question: “how to ensure responsible and sustainable growth in air transport, while remaining competitive?”.

0.2 Solutions and Research Motivations

To ensure sustainable growth in the aviation industry, three major challenges must be addressed: 1) reducing aircraft emissions (or fuel consumption), 2) reducing aircraft noise, and 3) improving air traffic management. In recent decades, different solutions have been proposed by researchers and engineers to address one or more of these challenges.

One of the most effective solutions, but also probably the most expensive one, to address the first two challenges is undoubtedly the use of new technologies in the design of next-generation engines (Marsh, 2012; Haselbach, Newby & Parker, 2015; Celis, Sethi, Singh & Pilidis, 2015). Indeed, since engines are largely responsible for the production of greenhouse gases and noise, improving their design would be a radical solution. Such an idea prompted engine manufacturers to improve current concepts, and to develop a new generation of more fuel-efficient and quieter engines.

According to Pratt & Whitney (2018), the inclusion of various technological improvements in their new Geared Turbofan (GTF) has led to the design of a next-generation engine with revolutionary economical and environmental performance. Similarly, the new Leap engine designed by CFM International is more efficient in comparison to today's best CMF56 engine due to the integration of lightweight materials, such as carbon fiber (Safran Aircraft Engines, 2017). The two engines have been deployed on different versions of the Airbus A320-NEO family, and have allowed a reduction in fuel consumption of 15 to 16%. In terms of noise reduction, the two engines are 15 to 20 dB quieter than the older generations of engines.

Although this solution is very effective, it is unfortunately not applicable to aircraft that are already in service. Indeed, to be able to benefit from such an improvement, all aircraft should replace their current engines with new generation engines, which would be very expensive.

Another equally effective solution for reducing fuel consumption, and therefore emissions, is to improve the overall aerodynamic characteristics of an aircraft. Studies have shown that a 20% reduction in aircraft drag could lead to an 18% fuel reduction (Okamoto, Rhee & Mourtos, 2005). In this research direction, the concept of morphing is attracting increasing interest from industry and academia (Apuleo, 2018; Michaud, Dalir & Joncas, 2018).

Taking inspiration from birds, the concept of morphing was introduced to aircraft during the 90s with the aim of adapting the shape of a wing in order to improve its aerodynamic characteristics, mostly by reducing the wing-friction (Apuleo, 2018). The ideal scenario would be that the wing of an aircraft could be morphed, and thus adapted during the flight in order to be able to operate optimally under all operating flight conditions. Since commercial aircraft generally operate in a wide range of flight conditions (altitude, speed, weight, etc.), adapting the shape of the wing to obtain the best possible performance for each flight condition could be an important asset in the goal of reducing fuel consumption (Segui & Botez, 2018; Segui, Mantilla, Ghazi & Botez, 2018; Segui, Rogoli & Botez, 2019).

Morphing wing concept is a promising solution for the development of the next generation of green aircraft. However, although several studies have shown promising results (Koreanschi, Gabor, Acotto, Brianchon, Portier, Botez, Mamou & Mebarki, 2017a,b), research is still needed in this field to convince the aviation industry of its potential benefits in terms of fuel consumption reduction while ensuring flight safety (Apuleo, 2018). In addition, as with engines improvement, the concept of morphing wings is more suited to next-generation aircraft, which means that current aircraft will not be able to benefit from this technology.

A third alternative, which is probably the easiest one to deploy in the short term and to all aircraft that are already in service, relies on the optimization of flight trajectories and flight procedures (Altus, 2009). Today, every commercial airline must define a flight plan prior to each flight in order to help the crew members to fly the aircraft safely, but also to coordinate their flights according to Air Traffic Control (ATC) requirements. A flight plan defines the route, expressed in terms of altitudes, speeds, and waypoints, that the aircraft is to fly from a departure airport to a destination airport (Altus, 2009; Dancila & Botez, 2018).

While flight plan is necessary to ensure that an aircraft meets the airlines criteria, it also provides an important opportunity to reduce the operating costs and fuel consumption (Roberson & Johns, 2007; Dancila & Botez, 2016, 2018). Various studies have shown that operational, economical and environmental benefits could be achieved by optimizing the horizontal route (Patrón, Kessaci & Botez, 2014; Murrieta-Mendoza, Beuze, Ternisien & Botez, 2017a), cruise speeds (Jensen, Hansman, Venuti & Reynolds, 2013), cruise altitudes (Jensen, Hansman, Venuti & Reynolds, 2014), or a combination of these parameters (Patrón, Berrou & Botez, 2015; Murrieta-Mendoza, Hamy & Botez, 2017b). A study by Boeing performance engineers found that the potential annual savings that a typical airline could expect by optimizing its aircraft cruising speed is between 4 and USD 5 millions (Roberson & Johns, 2007).

Optimizing flight trajectories and flight procedures can also be a solution to mitigate aircraft noise. Today, many cities have adopted Noise Abatement Procedures (NAP) to reduce the noise exposure of residents leaving in the vicinity of airports (Hebly & Visser, 2008; Khardi, 2009; Prats, Puig & Quevedo, 2011). These procedures are designed in order to prevent aircraft for flying over residential areas during its departure and arrival. In addition, aircraft must also comply with several restrictions, such as maintaining takeoff thrust and flaps settings for as long as possible. These restrictions are intended to force aircraft to climb faster and move it away from residential areas as quickly as possible.

Another notable example of improvement achieved through optimization of flight procedures, is the implementation of Continuous Descent Operations (CDOs) (Robinson & Kamgarpour, 2010). Unlike conventional operations where aircraft descend stepwise, CDOs were designed to allow arriving aircraft to descent from cruise altitude to the airport in a continuous way and with lower engine thrust. Reduction of the number of level flight segments allows reducing the need for aircraft engine thrust, and thereby decreasing fuel consumption as well as engine emissions and noise. However, it should be noted that the use of CDO requires a very good coordination with the ATC in order to allow crew members to optimize their descent rate. It is also necessary to estimate with high accuracy the moment when to start the aircraft descent, otherwise level flight segments will be necessary to adjust the trajectory of the aircraft.

Faced with the potential and multiple benefits of flight trajectories optimization, countries are redefining their national airspace in order to improve current flight procedures. To encourage them in this initiative, worldwide programs, such as the Next Generation Air Transport System (NextGen) in North America, and the Single European Sky ATM Research (SESAR) in Europe have been initiated (Brooker, 2008). The aim of these programs is to propose different solutions to modernize airspace by giving to the aircraft the flexibility to move more efficiently from departure to arrival, while at the same time, would ensure a degree of harmonization within air traffic. To achieve this ultimate objective, it is necessary to develop various decision support tools with the aim to enable airlines and air traffic controllers to improve the management of aircraft flight trajectories.

0.3 Research Areas and Research Projects

In 2010, the Laboratory of Applied Research in Active Control, Avionics and AeroServoElasticity (LARCASE) team started the investigation of new algorithms for optimizing aircraft flight trajectories, in partnership with CMC Electronics, and as part of a research program launched by the Green Aviation Research & Development Network (GARDN) which encourages the development of environmentally friendly aircraft technology in Canada. Within this context, the main objective of this research was to develop new methods and algorithms to calculate the performance, and flight trajectories of an aircraft.

Following the needs and requirements from CMC Electronics, and under the supervision of Dr. Ruxandra Mihaela Botez, the research presented in this thesis revolved around three main projects.

The first project focused on the development of new methods for identifying a mathematical model to predict the performance of an aircraft from accessible data. For this purpose, an initial study was conducted to determine the type and the minimum number of data necessary to identify an aircraft performance model. A second study was then conducted to propose practical methods and algorithms for the identification of a performance model, which should be both easy to handle and accurate to predict the aero-propulsive characteristics of the aircraft.

The second project focused on the development of new methods and algorithms for predicting aircraft flight trajectories. Two studies were considered for this second project. The first study consisted in developing algorithms for calculating aircraft takeoff and initial-climb trajectories. These algorithms were next adapted for the other flight phases (except for the landing phase). It should be noted that the flight phases were studied separately due to the structure of the aircraft mathematical model, which is generally more complex for the takeoff phase than for the other flight phases.

The third project focused on the investigation of new methods to account for airframe/engine degradation due to aircraft aging. Current mathematical models encoded on most on-board avionics systems, such as the Flight Management System (FMS), do not take this aspect into account, and consequently become less reliable over time. The objective of this project was therefore to propose a solution to overcome this problem by continuously monitoring the performance of the aircraft, and by automatically correcting (or updating) the models when necessary.

All the methods and algorithms presented in this thesis were applied to well-known Cessna Citation X business jet aircraft. This aircraft was chosen because of the availability of a qualified Research Aircraft Flight Simulator (RAFS) at the LARCASE. This simulator was designed and built by CAE Inc. based on flight tests data provided by the Cessna Textron aircraft manufacturer. The flight dynamics and engine models encoded in the RAFS have been validated with real flight tests data, and satisfy all criteria imposed in the Airplane Simulator Qualification (FAA, AC 120-40B) corresponding to highest level of certification (i.e., level-D). The RAFS was therefore considered as a reliable and adequate source of data for the verification and validation of the proposed methods and algorithms presented in this thesis could be easily adapted to other types of aircraft.

0.4 Thesis Organization

The **Chapter 1** of the thesis is devoted to the state of the art on the various themes addressed in this research. These themes include the modeling of the aero-propulsive characteristics of an aircraft, the calculation of aircraft flight trajectories, and finally the monitoring of aircraft performance. The chapter ends with the different specific objectives of the thesis, as well as with the contributions of each article which were published during this research.

The rest of the thesis is divided into three main parts, each subdivided into chapters. The first part aims to present the methods and algorithms developed with the aim to identify an aero-propulsive model of the Cessna Citation X. This part is divided into two chapters. The first chapter (**Chapter 2**) focused on modeling the engine performance of the Cessna Citation X. The second chapter (**Chapter 3**) deals with techniques for identifying an aero-propulsive model of the aircraft which includes both the aerodynamic model, and the propulsion model.

The second part of the thesis is dedicated to the prediction of aircraft flight trajectories. Once again, this part is divided into two chapters. The first chapter (**Chapter 4**) presents several techniques and algorithms for calculating aircraft flight trajectories during takeoff and departure procedures. The second chapter (**Chapter 5**) completes **Chapter 4** by presenting additional methods and algorithms for the calculation of aircraft flight trajectories for all the other flight phases (except for the landing phase).

The third part of this thesis is presented in **Chapter 5**. This chapter deals with a new innovative methodology developed at LARCASE to monitor aircraft performance, and to automatically correct the mathematical model of the aircraft based on flight parameters collected during the cruise phase.

Finally, the thesis ends with a general discussion of the results obtained from the different approaches proposed. This discussion is followed by a summary of the contributions, as well as by a list of recommendations for future work.

CHAPTER 1

LITERATURE REVIEW, OBJECTIVES & CONTRIBUTIONS

The first chapter of this thesis begins with a review of the literature on the various themes mentioned in the introduction. For reasons of consistency and for the convenience of the reader, the literature review presented in this chapter is intended to provide a general view of existing methods to address aircraft performance modeling and flight trajectories prediction problems. Nevertheless, a more detailed literature review will be presented in the following chapters, as each one of them contains a specialized literature review for its corresponding article.

Based on the literature review, the specific objectives of this thesis, as well as the main research contributions will be presented.

1.1 Literature Review

The research presented in this thesis involves different aspects which can be studied separately. First of all, it is question of proposing techniques for designing a mathematical model to predict the performance of an aircraft. This aspect is followed by the development of methods and algorithms for calculating the aircraft performance and flight trajectories for different flight regimes (i.e., takeoff, climb, cruise and descent). Finally, the last aspect of interest concerns the monitoring of aircraft performance and the automatic correction of mathematical models to account for modeling uncertainties as well as degradations dues to aircraft aging. Each of these three aspects will be therefore analyzed in the following sections.

1.1.1 Aircraft Performance modeling

The main goal of an aircraft performance model is to predict with a certain level of accuracy the actual aircraft and engine performance. The word “performance” in this context refers mainly to flight parameters describing the aircraft motion in the vertical plan (i.e. rate of climb/descent, acceleration, etc.), and also to the quantity of fuel required to perform a specific maneuver.

The typical structure of most aircraft performance models generally consists of a set of ordinary differential equations (used to describe the aircraft behavior) and two sub-models: a propulsion model and an aerodynamic model. The propulsion model allows, as its name suggests, to estimate the characteristics of the engines of the aircraft (i.e., thrust and fuel flow). The aerodynamic model, on the other hand, is used to estimate the aerodynamic characteristics of the aircraft, often expressed as its aerodynamic coefficients.

Nowadays, there are two main alternatives for researchers to obtain and/or design performance models. These alternatives are either to use "ready-to-use" performance models provided by specialized organizations, or to develop their own models based on available data. However, in some cases, accessing these data might be very difficult due to confidentiality issues.

1.1.1.1 BADA Aircraft Performance Models

Currently, one of best solution for researchers to access aircraft performance models is to use the well-known Base of Aircraft DAta (BADA, family 3). BADA is a collection of more than 300 aircraft performance models developed and maintained by Eurocontrol Experimental Center (ECC) (Nuic, Poles & Mouillet, 2010). The popularity of BADA models can be explained in part by two reasons. Firstly, the models are developed with the active cooperation of aircraft manufacturers and airlines, and secondly, they are available free of charge under certain conditions.

BADA models are provided to users as ASCII files containing a set of aircraft-specific coefficients. These coefficients must be used with a set of equations established by Eurocontrol in order to calculate the engine performance and the aircraft drag. According to the "BADA Performance Modeling Report" (Poles, 2009), theses coefficients are determined from trajectories data published in aircraft flight manuals. These manuals typically include the Aircraft Flight Manual (AFM), the Flight Crew Operating Manual (FCOM), the Flight Planning Guide (FPG), or any equivalent numerical documents/software capable of generating trajectories data (Nuic, 2010).

The procedure used by Eurocontrol to derive their models is based on the Least Squares (LS) technique. More specifically, this technique is applied to identify the coefficients for drag, thrust, and fuel flow equations that satisfy the rate of climb/descent and fuel consumption data published in the aircraft flight manuals for different flight profiles (i.e., climb, cruise and descent). Such a technique has the advantage of being straightforward and relatively simple. However, it also has several drawbacks because the equations used to model thrust, drag and fuel flow would need to be simplified in order to facilitate the identification process.

The approach used in BADA to model the engine thrust in descent, for instance, is to assume that the idle thrust (i.e., thrust setting during the descent) is proportional to the maximum climb thrust (Poles, 2009, p. 21). Such an assumption is not justified in practice because of the fact that the engine behavior in descent is often more complex than in climb. In addition, the net engine thrust may be negative during the descent phase due to the ram drag, which may be greater than the gross thrust at high speed and high altitude, while it is always positive during the climb phase. Another simplification which can lead to modeling uncertainties concerns the influence of the Mach number on the drag coefficient. This aspect is neglected, which means that the compressibility effects above Mach 0.6 are not considered in the drag model equations (Poles, 2009, p. 24).

Thus, although widely accepted as a reference for trajectory prediction and simulation applications, studies have shown that the models of BADA family 3 do not robustly represent the actual aircraft performance over their entire flight envelope (Nuic, Poinsot, Iagaru, Gallo, Navarro & Querejeta, 2005; Nuic *et al.*, 2010).

In 2005, a new family of BADA (family 4) was introduced with the objective of improving the accuracy of its BADA previous models (Nuic *et al.*, 2005, 2010). This action was accomplished by modifying the model equations, and by using more detailed reference data from manufacturers. However, this version is available under strict license restrictions, which considerably limits its use. In addition, there are no technical publications allowing to evaluate the quality of the BADA family 4 models since Eurocontrol does not allow the publication of this kind of studies.

It should be noted that there are also commercial software that provide access to performance data or performance models. A notable example is Piano-X developed by Lyssis and which includes a large database of performance models for more than 500 commercial aircraft (Simos, 2006). A detailed list of this software can be found in (Filippone, 2008). Unfortunately, these software are expensive, and come with strict license agreements which prevents their use for commercial purposes. In addition, the aircraft models encompassed in this software are not necessarily developed in cooperation with aircraft manufacturers or airlines operators. Consequently, their reliability is not always guaranteed (Filippone, 2008).

1.1.1.2 Engine Performance Modeling

A direct approach for predicting engine performance would involve the use of Computational Fluid Dynamics (CFD) methods (Chen, Langella & Swaminathan, 2019). These methods aim to analyze the properties of the air flow from the inlet to the outlet of the engine by solving the Reynolds-Averaged Navier-Stokes (RANS) equations using highly sophisticated software. They are commonly used by manufacturers to improve the design of their engines. Blackburn, Frendt, Gagné, Genest, Kohler & Nolan (2007), for instance, showed how CFD methods have been used to increase the efficiency of the Rolls-Royce Avon engine by 0.4%. However, these methods are generally computationally time expensive and require a very good knowledge of the structure of the engine. As a result, this type of methods is more suitable for design studies than for engine performance studies.

Another way to model engine performance is based on the Component Level Model (CLM) approach. As the name suggests it, the CLM approach consists in decomposing the engine into several components (i.e., fan, compressor, combustor, turbine, etc.), and in modeling the behavior of each component using appropriate equations. This approach has been widely used by researchers over the past two decades to model engine behavior (Bazazzade, Shahriari & Badihi, 2009; Roberts & Eastbourn, 2014; Botez, Bardela & Bournisien, 2019), to assess engine performance deterioration (Ogaji, Sampath, Singh & Probert, 2002), or for engine fault diagnosis (Junjie Lu, Feng Lu & Jinquan Huang, 2018).

Although the CLM approach has led to very good results in all of these studies, it is unfortunately not suitable for the research presented in this thesis. Indeed, the equations used to model the different engine components are usually unknown functions of detailed geometrical characteristics of the engine, and this information is not available in the public domain. In addition, the CLM approach requires to model various internal parameters of the engines which are not necessary for the studies of aircraft performance.

A very simple way to model engine performance is to use empirical or semi-empirical models. These models are expressed using polynomials or power law equations, that describe the variations in engine thrust and fuel flow as functions of aircraft operating conditions (i.e., altitude, airspeed and flight phase). Most of these models can be found in various manuals dealing with engine/aircraft performance, such as those written by Ojha (1995), Raymer (2012), Torenbeek (2013), Young (2017), and Mattingly, Heiser, Pratt, Boyer & Haven (2018).

A comparison of several empirical equations was conducted by Ghazi, Botez & Messi Achigui (2015c) in order to model the engine thrust of the Cessna Citation X. The results obtained in this study demonstrated that the accuracy of the models varied depending on the operating conditions. In another study, Bartel & Young (2008) improved the model proposed by Torenbeek (2013) for the estimation of the thrust of a turbofan engine during takeoff and climb phases. The author also provided additional equations to model the engine fuel consumption in cruise. Rodriguez & Botez (2013), have used a similar technique to propose a generic model for the prediction of the maximum thrust of turbofan based on previous studies conducted by Howe (2000). Senzig, Fleming & Iovinelli (2009) investigated a new empirical model to estimate aircraft fuel consumption during terminal procedures.

One of the main advantages of empirical models is that they provide implicit functional relationships between the desired engine performance and aircraft flight conditions. However, although practical and useful, empirical models are usually too much simplified, and do not accurately represent the engine characteristics over the entire aircraft flight envelope. Moreover,

they are not universally valid for all types of aircraft/engines, especially for modern turbofan engines exhibiting non-linear characteristics (Young, 2017).

Another method for obtaining an engine performance model consists in scaling an already existing engine model. This technique was for instance used by Gong & Chan (2002) to model the maximum climb thrust of a CFM65-3B1 based on an existing model of a Pratt & Whittney PW4056. A similar approach was also employed by Cavcar & Cavcar (2004) and by Baklacioglu & Cavcar (2014). In these two studies, the authors used cruise performance data of a Pratt & Whittney JT9D-7A provided by McCormick (1995) to approximate the thrust of a CFM65-3B1. Such technique has clearly the advantage of being relatively simple. However, no comparison has been made by the authors between their models versus experimental data to demonstrate the effectiveness of this technique. In addition, as shown later in the thesis, the performance of modern engines highly depends on thrust-ratings established by the manufacturers. These thrust-ratings are specific to an aircraft/engine configuration, and do not vary proportionally from one configuration to another. Also, Gong & Chan (2002) suggested that improvement should be done as attempts to apply their technique to the descent phase did not yield satisfactory results.

Finally, with the emergence of artificial intelligence, several researchers have proposed to model engine performance with Artificial Neural Networks (ANN) techniques. Trani, Wing-Ho, Schilling, Baik & Seshadri (2004) developed a neural network based model to predict the fuel consumption of a Fokker F-100. Turgut & Rosen (2012) combined a neural network with a genetic algorithm to model the fuel flow of a commercial aircraft during the descent phase as function of the altitude. A similar approach was used by Baklacioglu (2016) to model the fuel flow of transport aircraft. Zaag, Botez & Wong (2019) developed a neural network to model the engine fan speed, thrust and fuel flow of a Cessna Citation X based on flight data collected from a research aircraft flight simulator.

Neural networks and fuzzy logic are very powerful tools capable of learning and modeling non-linear and complex relationships (Hiliuta, Botez & Brenner, 2005; Hiliuta & Botez,

2007; Kouba, Botez & Boely, 2010; Boely & Botez, 2010; Boely, Botez & Kouba, 2011; De Jesus Mota & Botez, 2011). However, these tools are database-based methods, which means that they work well as long as all possible scenarios have been covered in the learning process. Consequently, it is often necessary to have a very large database for the creation of the network, which goes against the objectives set in this thesis (one of the objectives being to be able to identify models with the least data possible). Another drawback is that these are black boxes, which means that the elements of the network structure have no physical meaning for engineers.

1.1.1.3 Aerodynamic Performance Modeling

To complete the aircraft performance model, it is also necessary to represent the aerodynamic characteristics of the aircraft. In general, for the studies of aircraft performance and flight trajectories, the aerodynamic characteristics are mainly represented through the aircraft drag polar. This drag polar, also known as the lift-to-drag equation, describes the dependence of the drag coefficient on the lift coefficient.

Fundamentally, most of the techniques presented in the previous section for modeling engine performance can also be used to approximate the drag polar of an aircraft. However, for the sake of simplicity, empirical methods are generally preferred despite their imprecision. Once again, different drag polar models can be found in aircraft design textbooks, such as those cited in the previous section. Van Es (2002) proposed an empirical model for estimating the zero-lift drag coefficient based on data available in the literature. Filippone (2008) provided a comprehensive study on the prediction of drag coefficient for different transport aircraft using semi-empirical models. Camilleri, Chircop, Zammit-Mangion, Sabatini & Sethi (2012) used empirical equations provided by Ojha (1995) and Asselin (1997) to design a lift-to-drag model for an Airbus A320. Metz, Hoekstra, Ellerbroek & Kügler (2016) combined equations published in Raymer's textbook (Raymer, 2012) with flight tests data provided by Obert, Slingerland, Leusink, Berg, Koning & Tooren (2009) to develop a drag polar model for various commercial aircraft.

One problem that can arise when engine and drag models are both obtained empirically is that there is no guarantee that the resulting model reflects the actual aircraft performance. To overcome this problem, it is then necessary to either optimize the two models, or to consider one as a reference and to adjust the other accordingly. Given the complexity of engines, it is often simpler to adjust the drag model, assuming that the engine model is reliable. This approach was considered by Gong & Chan (2002), Cavcar & Cavcar (2004), and by Baklacioglu & Cavcar (2014). In all these studies, the authors presupposed an engine model and derived/optimized the drag polar model accordingly for a Boeing 737 based on trajectory data available in the aircraft flight manuals. Cavcar & Cavcar (2004) concluded that any combination of thrust/drag models that accurately reflects the rate of climb can be used to develop aircraft performance to calculate climb trajectories. However, Gong & Chan (2002) suggested that additional research should be conducted as attempts to apply their technique to the descent phase did not yield satisfactory results. Another problem relates to the quantity of trajectory data which is necessary to obtain a performance model which robustly reflects the performance of the aircraft over its entire flight envelope.

To solve the data accessibility problem, few researchers have recently proposed techniques to identify aircraft performance models based on ADS-B (Automatic Dependent Surveillance Broadcast) data. This technology allows aircraft to periodically share their information, such as identification, position, altitude, heading, ground speed, and vertical speed. This information could therefore be combined with a posteriori engine model to derive a drag coefficient model. Sun, Hoekstra & Ellerbroek (2018b; 2020) combined, for instance, the engine thrust model developed by Bartel & Young (2008) with ADS-B data with the aim to develop a drag polar model for various aircraft types. The authors demonstrated that it was possible to obtain drag models as precise as those available in the BADA family 3.

The main drawback of ADS-B data is the lack of information regarding the aircraft weight and fuel consumption. Indeed, airlines consider the mass of their aircraft as a very sensitive parameter and are therefore reluctant to share this information. Although several researchers have elaborated techniques to predict the aircraft weight at takeoff (Sun *et al.*, 2018b), these

methods do not yet allow to accurately estimate the weight of the aircraft for other phases of flight.

1.1.2 Flight Trajectories Prediction

After the modeling of aircraft performance, the second theme addressed in this thesis concerns the calculation and prediction of aircraft flight trajectories.

One of the most direct approach to calculate aircraft trajectories consists in solving and integrating a set of ordinary differential equations by assuming certain initial conditions and constraints (Quanbeck, 1982). These equations, also called equations of motion, are obtained from the Newton's second law, and describe the influences of the forces/moments applied to the aircraft center of gravity on its accelerations. Depending on the level of accuracy required, the equations of motion can vary in number and complexity, ranging from full six degrees-of-freedom kinetic models to simplified lookup table models.

1.1.2.1 Kinetic Models

Kinetic models are the most complex and detailed models that describe the behavior of an aircraft. These models allow to determine all the forces and moments applied to the aircraft, and therefore to describe the aircraft translational and rotational motion. This category of models is suited to the development of very accurate flight simulators such as the one presented in (Ghazi & Botez, 2015).

Although they provide a very good representation of the behavior of an aircraft, kinetic models require too much computational effort, and, for this reason, they are not suitable for studies of aircraft flight trajectories.

1.1.2.2 Point-Mass Models

Point-mass models are simplified kinetic models for which only the translational motion of the aircraft in a vertical plane is considered. This category of models, although less precise than kinetic models, is adequate for modeling aircraft motion in a fast-time simulation environment (Slattery & Zhao, 1997). Over the past few decades, point-mass models have been widely used by researchers for studying and optimizing aircraft flight trajectories.

Slattery & Zhao (1997), for instance, presented a technique that was implemented in the Center-TRACON Automation System (CTAS) tool developed at NASA Ames Research Center to generate aircraft vertical trajectories for air traffic automation. A similar approach was also used by Filippone (2008) and by Zhu, Wang, Chen & Wu (2016) to predict the trajectory of a commercial aircraft during the takeoff phase. Other researchers have used a point-mass model combined with the optimal control theory to optimize aircraft departure trajectories for minimum noise (Visser & Wijnen, 2001; Prats *et al.*, 2011; McEnteggart & Whidborne, 2018).

In most of the studies found in the literature, the authors always assumed that the aircraft flight path angle was sufficiently small to be neglected in certain equations of the point-mass model. While it is true that assuming small flight path angle reduces the complexity of the equations of motion, and thus its facilitates the integration process, this assumption can lead to modeling uncertainties. For example, neglecting the flight path angle implies that for a given aircraft weight, the lift coefficient remains constant regardless of the flight phase (i.e., climb, cruise and descent). Another simplification commonly used in most of the studies concerns the wind influence. In general, the inclusion of wind acceleration due to a non-zero wind gradient is not considered in the model. This aspect is important because it affects the aircraft vertical speed during a climb or a descent.

In fact, the inclusion of wind acceleration and flight path angle conducts to non-linear equations, thus making them more complex to solve. In this case, an optimization algorithm is required to solve the equations of motion, and to find the flight path angle required to perform a specific maneuver (Quanbeck, 1982).

Another drawback of point-mass models relies on the fact that the rotational motion about the pitching axis is ignored. As a result, these models do not allow to accurately represent the aircraft behavior during the takeoff phase, and more specifically during the rotation and transitions phases. A solution to overcome this aspect, is to use empirical models (Angeiras, 2015) or flight test data (Zammit-Mangion & Eshelby, 2008) to approximate the aircraft behavior during these flight phases. However, these techniques aim to model the average aircraft performance, and are therefore not always precise. For example, all empirical methods assume that the time to rotate the aircraft during the takeoff is always between 2 and 3 seconds, while in practice this parameter varies considerably depending on the aircraft configuration (i.e., weight and center of gravity location), the thrust and flaps settings, environment and runway conditions.

1.1.2.3 Kinematics Models

Another category of models that can be used to study aircraft flight trajectories are kinematic models. Unlike the two previous categories (i.e., kinetics and point-mass), kinematic models do not require mathematical representations of forces/moments applied to the aircraft. Instead, they intent to directly model several flight parameters, such as the aircraft acceleration or the rate of climb/descent. In most of cases, these parameters are obtained based on statistical analysis, as shown in (Sun, Ellerbroek & Hoekstra, 2019).

Although practical, kinematic models are unfortunately too much simplified, and because of their stochastic natures, they have a limited range of validity. These models are therefore useful for performing statistical analyses of flight trajectories, but they are not precise enough to predict and optimize aircraft flight trajectories.

1.1.2.4 Lookup Tables based Models

Finally, aircraft flight trajectories can be also calculated using lookup tables or performance databases. Such an approach was considered by researchers at LARCASE to optimize flight trajectories (Patrón *et al.*, 2015; Murrieta-Mendoza *et al.*, 2017b). Murrieta-Mendoza & Botez

(2015) described a complete method for calculating the vertical trajectory of a commercial aircraft using a set of performance databases. A similar approach was also considered by Ghazi, Botez & Tudor (2015b; 2015a) for predicting the climb and cruise trajectories of a Cessna Citation X using a lookup table-based aero-propulsive model. Tudor in (2017) also used a lookup table approach to model the flight trajectories of two commercial aircraft for the climb and descent phases.

One of the main advantages of using lookup table-based models is the simplicity of their structure. Indeed, because of their simplicity, these models are very easy to implement and above all computationally inexpensive. They can be used to generate flight trajectories over a few-seconds time span. However, their structure has also a major disadvantage as they cannot be adapted to consider certain aspects such as the influence of the wind or turns.

1.1.3 Aircraft Performance Monitoring

Finally, the last theme discussed in this thesis concerns the evaluation of the reliability of the aircraft performance model over time. Indeed, in addition to the modeling of uncertainties that may be introduced due to the quality of the data used in the identification process, there are other factors that may affect the reliability of the aircraft performance model.

Throughout its life cycle, an aircraft is constantly exposed to dynamic loads that degrade its flight characteristics. These degradations can have two main origins: airframe deterioration (control surfaces rigging, seals missing or damaged, etc.) and engine performance degradation (fuel consumption increase for a given thrust).

Airbus (2002a) conducted a study to evaluate the impact of engine/aircraft degradation on aircraft efficiency. The results of this study have shown that the “specific range” (i.e., distance covered per unit quantity of fuel consumed) of a typical commercial aircraft could be reduced by around 1.3% per year without engine replacement, and by around 0.3% per year with engine replacement. In the same study, they also concluded that the accumulation of imperfections on

the surface of the wings or the fuselage can cause the drag of an aircraft to increase by up to 2% every five years.

Longmuir & Ahmed (2009) also evaluated the correlation between fuel consumption and surface roughness variations caused by the accumulation of impurities. Based on wind-tunnel tests, the authors showed that for an increase in surface roughness, there was a corresponding increase in skin friction drag. For an aircraft, this increase in drag significantly reduces the aerodynamic efficiency of the wing, thus resulting in increased fuel consumption in cruise.

Therefore, by ignoring these factors, it is evident that, after several years of service, the actual performance of the aircraft will be different from that which it had when it entered in service. It is, therefore, more than important to monitor the aircraft performance and to apply appropriate corrective measures to maintain the level of reliability of the performance model.

Although this problem is of great interest in the aviation industry, there is unfortunately (to the knowledge of the author of this thesis) no study in the literature that deals with it. As it will be shown in **Chapter 6**, the majority of studies found in the literature related to this topic were more oriented towards engine fault diagnosis and condition monitoring. These methods are therefore more suitable for aircraft/engine maintenance, but none of these studies presented a method for correcting aircraft performance models. The study presented in **Chapter 6** is therefore the first study to address this topic.

1.2 Research Objectives, Approach and Contributions

The main objective of this research was to explore new methods and algorithms for developing mathematical tools for the study of aircraft performance and flight trajectories. The research was conducted in partnership with CMC Electronics, and as part of a research program launched by the Green Aviation Research & Development Network (GARDN) which encourages the development of environment friendly aircraft technology in Canada.

Considering the different axes discussed in the literature review, the main research objective of this thesis was divided into the three following objectives:

1. Develop a method and algorithms to identify a mathematical model to predict the performance an aircraft;
2. Develop prediction algorithms to calculate aircraft performance and flight trajectories for different flight phases;
3. Explore a new technique for monitoring aircraft performance in order to account for airframe/engine degradations and automatically correct aircraft mathematical models.

In the following sub-sections, a discussion relative to each objective is given, as well as the approach used to achieve these objectives and the contributions made.

1.2.1 Objective 1: Aircraft Performance Model Identification

The first objective was to develop new methods for the identification of an aircraft performance model. As explained in the review of the literature, a performance model is usually composed of two sub-models; a propulsion model and an aerodynamic model. In addition, it was also explained that for the sake of simplicity and in order to obtain good results, the aerodynamic model should be derived from an existing engine model. Based on these two aspects, two directions were proposed to achieve objective 1.

First Study: Engine Performance Modeling

In a first study, it was decided to focus the research on modeling engine performance using data available in the flight manuals of an aircraft, or in equivalent documents. The purpose of this study was twofold. The first purpose consisted in verifying if the data published in the flight manuals was sufficiently detailed to obtain an accurate engine model. The second purpose consisted in proposing a step-by-step method to identify the various elements defining the engine model.

The structure of the model was developed by combining a CLM approach with lookup tables. The advantage of this combination is that it allows to benefit from the simplicity of lookup tables while keeping a structure that reflects the physical architecture of the engine. A detailed analysis of the data published in the aircraft flight manuals was performed to determine the most relevant data allowing to identify an engine performance model. Functional relationships were then developed using dimensional analyzes in order to quantify the dependencies between the engine parameters and operating conditions. Each functional relationship was approximated using spline curves or surfaces. Validation of the methodology was accomplished by comparing the predictions obtained from the model with a series of engine data collected with the RAFS for different operating conditions.

The originality of this research is based on the use of data published in flight manuals, as well as on the flexibility of the structure of the engine performance model. Unlike most of studies in the literature, the model developed in this research was not limited to engine performance, but also enabled to take into account the thrust settings for all flight regimes (i.e., takeoff, climb, cruise and descent). Finally, the use of splines to approximate the different functional relationships defining the models makes it possible to easily adapt the methodology to any type of engine and aircraft.

The contribution of this first study was therefore essentially methodological and applicative. In addition, the engine performance model was developed for the needs of the LARCASE to allow researchers to perform performance analyzes and predict the flight trajectories of the Cessna Citation X. The results obtained in this study led to the publication of a first article:

Article 1: **Ghazi G.**, and Botez, R. M. (2019). Identification and Validation of an Engine Performance Database Model for the Flight Management System. *AIAA Journal of Aerospace Information Systems*, 16(8), 307-326.
DOI: https://doi.org/10.2514/1.I010663.

This article was co-authored with Dr. Ruxandra Mihaela Botez, who also supervised the progress of this research through regular meetings in collaboration with CMC Electronics team.

Second Study: Aero-Engine Performance Modeling

In the previous study, it was assumed that the data available in the aircraft flight manuals were sufficiently detailed to allow the identification of an engine performance model. However, this assumption is not always guaranteed, and the data published in the flight manuals can be limited to trajectories data only. In this case, it is necessary to identify the engine and aerodynamic model through an iterative process.

This second study therefore complements the research presented in the first article by proposing another method for identifying an aero-propulsive model of an aircraft using only trajectory data. The proposed technique consisted of starting from a set of trajectory data and then using an iterative process to obtain a combination of thrust and drag models to predict the performance of the aircraft in climb, cruise and descent. Techniques for modeling engine fuel flow and predicting aircraft fuel consumption were also presented. The method was successfully applied to the Cessna Citation X. Validation of the method was accomplished by comparing trajectory data predicted by the model with trajectory data measured with the RAFS.

The originality of this research lies in the fact that, unlike studies in the literature such as those carried out by (Gong & Chan, 2002) and (Cavcar & Cavcar, 2004), no engine data or a priori model was necessary to identify the performance model. In addition, the proposed methodology was not limited to the climb phase, but also included the cruise and descent phases. Finally, the method also enabled to model the engine fuel flow, whereas most of the studies in the literature have not taken this parameter into account.

The contribution of this second study is essentially methodological and applicative. The results obtained in this study led to the publication of a second article:

Article 2: **Ghazi G.**, Botez, R. M., and Domanti, S. (2020). New Methodology for Aircraft Performance Model Identification for Flight Management System Applications. *AIAA Journal of Aerospace Information Systems*, 17(6), 294-310. DOI: https://doi.org/10.2514/1.I010791.

This article was co-authored with Dr. Ruxandra Mihaela Botez, who also supervised the progress of this research through regular meetings in collaboration with CMC Electronics team. Mr. Simon Domanti, bachelor student, was also included as co-author as he contributed in the development and testing of the proposed methodology during his internships.

1.2.2 Objective 2: Aircraft Flight Trajectories Prediction

The second objective of this thesis was to propose new methods and algorithms for predicting aircraft flight trajectories. Once again, this objective was achieved through two studies.

First Study: Aircraft Takeoff and Departure Trajectories Prediction

The first study mainly focused on the analysis of aircraft departure trajectories. The main objective of this first study was to develop new methods and algorithms for calculating the aircraft performance and predicting its trajectory during the takeoff phase and the initial-climb phase to 3000 ft. It should be noted that the aerodynamic model structure used in this study was imposed by CMC Electronics. The engine performance, on the other hand, was based on the model identified in the first article.

The approach considered in this study consisted in numerically integrating the aircraft equations of motion for each segment that composed a typical takeoff and departure profile. For this purpose, the aircraft trajectory was divided into five segments, including ground acceleration, rotation, transition, climb at constant speed, and climb acceleration. For each segment, detailed and flexible algorithms were developed in order to solve the equations of motion, and to trim the aircraft under different environmental and operating conditions. The complete aircraft trajectory was obtained by combining these segments in a specified order depending on the departure procedure profile. The validation of the methodology was accomplished by comparing trajectory data predicted by the algorithms with those measured with the RAFS of the Cessna Citation X.

The originality of this research consists in the proposal of new methods and algorithms for solving and integrating the equations of motion of an aircraft during takeoff and initial-climb

phases. Unlike the methods available in the literature, the algorithms proposed have enabled to model the influence of a non-zero wind gradient or of the runway slope on the aircraft takeoff performance. In addition, techniques for modeling piloting procedures such as thrust management at the beginning of the ground acceleration phase, or the use of reduced thrust were presented. Finally, another originality of this research consisted in including the moment equation to predict the position of the control surfaces and to model the influence of the center of gravity location on the aircraft takeoff performance.

The contribution of this study is theoretical and methodological. In addition, the proposed algorithms were used to develop tools for the needs of CMC Electronics and for the needs of the LARCASE team. These tools can be used to calculate the performance of an aircraft, trim an aircraft under wide range of operating conditions, and predict the departure trajectories of an aircraft. The results obtained in this study have also led to the submission of a third article in the AIAA Journal of Aerospace Information Systems:

Article 3: **Ghazi G.**, Botez, R. M., and Maniette, N. (2020). Cessna Citation X Takeoff and Departure Trajectories Prediction in Presence of Winds. This article was published in the *AIAA Journal of Aerospace Information Systems* (Article in advance).
DOI: https://doi.org/10.2514/1.I010854

This article was co-authored with Dr. Ruxandra Mihaela Botez, who also supervised the progress of this research through regular meetings in collaboration with CMC Electronics team. Mr. Nicolas Maniette, bachelor student, was also included as co-author as he contributed in the development and testing of the proposed methodology.

Second Study: Aircraft Flight Trajectories Prediction above 1500 ft

The second study completes the first one by providing new methods and algorithms to predict the aircraft flight trajectories for the other flight phases (except for the landing phase). The approach, originality, and contributions of this study are globally the same as those mentioned

for the takeoff and departure procedures study. In addition, a fourth article was written based on the results obtained in this study:

Article 3: **Ghazi G.**, Botez, R. M., Bourrely, C., and Turculet, A. Method for Calculating Cessna Citation X 4D Flight Trajectories in Presence of Winds. This article was submitted for review and publication in the *AIAA Journal of Aerospace Information Systems* in July 2020.

This article was co-authored with Dr. Ruxandra Mihaela Botez, who also supervised the progress of this research through regular meetings in collaboration with CMC Electronics team. Mr. Charles Bourrely, bachelor student, and Miss. Alina-Andreea Turculet, master student, were also included as co-authors as they contributed in the development and testing of the proposed methodology.

1.2.3 Objective 3: Aircraft Performance Monitoring

Finally, the last objective of this thesis was to propose a new method for monitoring aircraft performance, and to auto correct the aircraft performance model to take into account the airframe/engine degradation.

The approach consisted in firstly developing a simplified aircraft performance model of the Citation Citation X for the cruise phase. The engine model was developed based on an empirical model found in the literature, while the aircraft drag polar model was established based on fuel consumption data available in the Flight Planning Guide (FPG). An algorithm capable of analyzing the aircraft flight parameters in cruise, and correcting the performance model was next developed. The first part of the algorithm consisted in collecting the information recorded during the cruise for the estimation of several additional flight parameters, such as the aircraft weight and acceleration. The second part of the algorithm consisted in evaluating the equilibrium of the aircraft by identifying all the stabilized flight segments during the cruise. The last part of the algorithm consisted in verifying the accuracy of the current drag coefficient model, and in the application of a correction when necessary. Various simulations were finally conducted with the

RAFS available at LARCASE to verify if the algorithm was able to correct the uncertainties of the initial model, and therefore to improve the prediction of the aircraft fuel consumption.

The originality and main contribution of this study lies in the development of a new method for monitoring aircraft performance, and in the automatic correction of a performance model based on flight data collected during the cruise phase. The results obtained in this study have led to the publication of a fifth article:

Article 5: **Ghazi G.**, Gerardin, B., Gelhaye, M., and Botez, R. M. (2019). New Adaptive Algorithm Development for Monitoring Aircraft Performance and Improving Flight Management System Predictions. *AIAA Journal of Aerospace Information Systems*, 17(2), 97-112.
DOI:https://doi.org/10.2514/1.I010748.

This article was co-authored with Dr. Ruxandra Mihaela Botez, who also supervised the progress of this research through regular meetings in collaboration with CMC Electronics team. Mr. Benoit Gerardin and Miss. Magali Gelhaye, bachelor students, were also included as co-authors as both of them contributed in the development and testing of the proposed methodology.

CHAPTER 2

IDENTIFICATION AND VALIDATION OF AN ENGINE PERFORMANCE DATABASE MODEL FOR THE FLIGHT MANAGEMENT SYSTEM

Georges Ghazi [a] and Ruxandra Mihaela Botez [b]

[a, b] Department of Automated Production Engineering, École de Technologie Supérieure, 1100 Notre-Dame West, Montréal, Québec, Canada H3C 1K3

Paper published in the *AIAA Journal of Aerospace Information Systems*, Vol. 16, No. 8, August 2019, pp. 307-326.
DOI: https://doi.org/10.2514/1.I010663

Résumé

Cet article présente les résultats d'une étude menée au Laboratoire de Recherche en Commande Active en Contrôle, Avionique et AéroSevoÉlasticité (LARCASE) pour identifier un modèle mathématique de moteur pour le système de gestion de vol, et pour la prédiction et l'optimisation des trajectoires de vol. La méthodologie a été appliquée à l'avion d'affaires Cessna Citation X, pour lequel le manuel de vol de l'avion et le manuel d'opération de l'équipage étaient disponibles. En plus de ces deux documents, une troisième source de données basée sur des trajectoires simulées a également été utilisée afin de générer plusieurs profils de vol en montée et end descente nécessaires au processus d'identification du modèle de moteur. Pour démontrer et valider la précision du modèle de performance du moteur proposé, un simulateur de vol pour la recherche de niveau D du Cessna Citation X a été utilisé comme référence. Selon l'Administration Fédérale de l'Aviation (FAA, AC 120-40B), le niveau D correspond au plus haut niveau de qualification pour la dynamique de vol et la modélisation du moteur. La validation de la méthodologie a été réalisée en comparant les prédictions du modèle avec une série de données de vol obtenues avec le simulateur de vol pour différentes conditions de vol et différentes phases de vol, incluant le décollage, la montée, la croisière et la descente. Les résultats issus de la comparaison ont été validés avec une tolérance de ±5% pour chaque performance du moteur calculée par le modèle en termes de vitesse de la soufflante, de vitesse de l'arbre haute pression, de poussée et de débit de carburant.

Abstract

This paper presents the results of a validation study conducted at the Laboratory of Applied Research in Active Controls, Avionics, and AeroServoElasticity (LARCASE) to identify an engine mathematical model for Flight Management System (FMS), trajectory prediction and optimization applications. The methodology was applied to the well-known Cessna Citation X business aircraft, for which the Aircraft Flight Manual (AFM) and the Flight Crew Operating Manual (FCOM) were available. In addition to these two documents, a third data source based on computerized trajectory was also used in order to generate several climb and descent flight profiles required in the identification process of the engine model. In order to demonstrate and further validate the accuracy of the proposed engine performance model, a level-D Research Aircraft Flight Simulator (RAFS) of the Cessna Citation X was used as a reference. According to the Federal Aviation Administration (FAA, AC 120-40B), the level-D corresponds to the highest qualification level for the flight dynamics and engine modeling. Validation of the methodology was accomplished by comparing the prediction model with a series of flight data collected with the flight simulator for different flight conditions and different flight phases including takeoff, climb, cruise and idle descent. Comparison results were validated with a tolerance of ±5% for each engine performance predicted by the model in terms of fan speed, core speed, thrust and fuel flow.

2.1 Introduction

Nowadays, the growing public awareness of the impact of aviation engine emissions on the environment forces the aviation stakeholders to search for environmentally friendly solutions. Compared to other modes of transport, the aviation industry (commercial and private) is responsible for approximately 1.5 to 2% of global carbon dioxide (CO_2) emissions (IATA, 2018). Although this percentage may seem relatively small, it has in reality a disproportionate large impact on the environment. Indeed, the impact per kilogram of CO_2 emissions at high-altitudes on climate change is about twice than that of emissions at ground-level Lee *et al.* (2009). Faced with this awareness, the International Air Transportation Association (IATA) has recognized

the need to address the global challenge of climate change and has set the ambitious goal of improving aviation fuel efficiency by 1.5% per year from 2009 to 2020 (ICAO, 2016 ; IATA, 2018).

To reach this ambitious goal, extensive research is being conducted by academia and industry in order to bring solutions that could minimize aircraft fuel consumption. Among the many solutions that have been elaborated to date – the use of biofuels to reduce engine environmental impact (Hendricks, Bushnell & Shouse, 2011; Sandquist & Guell, 2012), the use of new composite materials to reduce aircraft weight (Calado, Leite & Silva, 2018), the development of new generation of jet engines (Haselbach *et al.*, 2015), the improvement of wing aerodynamic performance using morphing technology (Koreanschi *et al.*, 2017a,b), etc. – one of solutions that seems to offer very good results in the short term relies on improving the efficiency of the aircraft flight trajectories (Jensen *et al.*, 2013, 2014; Murrieta-Mendoza *et al.*, 2017b).

Presently, improving the efficiency of the aircraft trajectory from takeoff to landing is one of the fundamental functions of the Flight Management System (FMS) (Liden, 1994). The FMS is an onboard computer located in the cockpit that assists the pilot in a multitude of in-flight operations including flight planning, trajectory prediction, aircraft/engine performance estimation, and navigation (Zhao & Vaddi, 2013). In addition to reducing the pilot's workload by programming the optimal route from one destination to the next, the FMS can also provide the pilots with several profile optimization advisories in order to minimize costs associated to fuel consumption and flight time. These advisories include for example the determination of the optimal cruise altitude, the computation of the economic speed for each flight regime and thrust limit data to prevent engine failure (Liden, 1994; Walter, 2001). Since its first implementation on the Boeing-767 in 1982, the Flight Management System continues to evolve to include a variety of functionalities that contributes to improve flight safety and efficiency (Miller, 2009; Walter, 2001; Avery, 2011).

2.1.1 Research Problem and Motivations

To compute the most efficient flight plan that the aircraft has to fly from one destination to the next, the different algorithms encoded within the FMS memory require an explicit mathematical model of the aircraft (Walter, 2001). Such a model, also called aircraft performance model, is supposed to represent with a certain level of accuracy the actual aircraft and engine performance. In most modern flight management systems, the aircraft performance model is established by the FMS manufacturer prior to the entry into service of the aircraft; this model results from the combination of a set of ordinary differential equations (used to characterize the aircraft motion) and a set of performance databases (used to quantify the aircraft performance) (Liden, 1994; Walter, 2001). These databases form the core element of the performance model and contain the engine and aerodynamic model data. The data includes the lift and drag aerodynamic coefficients, engine performance such as thrust force, thrust limits, and fuel flow, and other optimized performance that are specific to the aircraft/engine (Sibin, Guixian & Junwei, 2010).

FMS performance databases are usually obtained from manufacturer performance reports, flight simulators, and/or recorded flight data. The determination of the engine databases is a complex process that requires much more data than the aerodynamic database. This fact is due to the reason that modern aircraft have large flight envelopes and complex propulsion systems, which create a matrix of flight conditions that is nearly impossible to encompass without a very large dataset (Marshall & Schweikhard, 1973). Unfortunately, as manufacturers consider individual engine characteristics to be strictly confidential, all these data are increasingly difficult to obtain, as they are limited or available only under strict license agreements. Since the quality of the engine performance databases directly depends on the quality of the reference data, such a difficulty in obtaining information obliges FMS designers to develop aircraft performance models that are very costly.

To overcome problems related to intellectual property rights and reduce the associated costs, the avionics industry is seeking for alternative methods and reference sources that could be used to identify a model of aircraft/engine performance without the need of excessive data from

the production companies. Such a challenge has motivated several industrial and academic researchers to propose new solutions addressing this problem. However, although different approaches and methods exist to derive aerodynamic performance databases from available flight-test and flight data (Gong & Chan, 2002; Cavcar & Cavcar, 2004; Baklacioglu & Cavcar, 2014), there are unfortunately few studies related to engine performance database modeling in the literature.

2.1.2 Engine Performance Modeling Techniques

For trajectory optimization and flight management system applications, the desired engine performance data usually refers to the maximum available thrust and the fuel burn rate. The former is used to estimate the aircraft flight trajectory; the latter is used to estimate the amount of fuel needed to perform the flight.

A traditional way to determine these two performances is based on the Component-Level Modeling (CLM) technique (Kobayashi & Simon, 2005). As the name suggests it, this technique aims to decompose the engine into an assembly of components or sub-systems (for example, fan, compressor, turbine, etc.). Each sub-system is then modeled independently from the others using appropriate conservation physical laws that determine the change in state properties (e.g. pressure, temperature, etc.) at the entrances and exits of each component. The complete model results therefore in a set of differential equations which can be further used to simulate the entire engine behavior for any operating conditions. Although this approach has proved its efficacy in several studies (Martin, Wallace & Bates, 2008; Roberts & Eastbourn, 2014; Bardela & Botez, 2017), the inclusion of such detailed model would not be appropriate for the purposes of this study. Indeed, the equations used to model the different engine components are usually unknown functions of detailed geometrical characteristics of the engine, and are not available in the public domain. Moreover, since the FMS processing unit has a limited capacity, it is preferable to have the simplest model possible to allow fast trajectory computations during flight.

To reduce the complexity of the equations and the number of unknown parameters, several authors in the literature have elaborated empirical and semi-empirical models that describe the variation of the thrust and fuel flow as functions of environmental parameters, pressure altitude, and flight speed (Torenbeek, 2013; Mattingly *et al.*, 2018; Young, 2017). These equations are usually expressed as a polynomial and include a set of unknown parameters that must be identified from flight test data or engine manufacturer data (Bartel & Young, 2008; Ghazi *et al.*, 2015c). An important advantage of empirical models is that the equations result in an implicit functional relationship between the performance of the engine and operating conditions. However, because of their simplifications, these relationships are not universally valid throughout the entire flight envelope. It is therefore necessary to have different models to correctly represent the engine thrust and fuel flow for each flight regime (for example, takeoff) and operating conditions (Bartel & Young, 2008).

Based on this analysis, it can be concluded that the two techniques presented above (CLM and empirical equations) have some aspects that would be interesting to use for the purposes of this paper. Indeed, on one hand, the CLM approach has the advantage of describing the engine parameters using a unique model, while on the other hand, empirical equations have the advantages of describing the engine performance using simple relationships. Thus in this paper, by combining these two assets, it is possible to deduct an intermediate model that, is sufficiently complex to represent the performance of an engine over the entire flight range of the aircraft, while being simple enough to be implemented in a FMS.

The second problem raised in this paper concerns the availability of data to identify the mathematical model. To solve this problem, several researchers have proposed to use information published in the aircraft manuals (Gong & Chan, 2002; Cavcar & Cavcar, 2004; Roberts & Eastbourn, 2014). Indeed, every aircraft produced by a manufacturer must be provided with different documentations that are more or less relevant to the aircraft performance. These documentations include for instance the Airplane Flight Manual (AFM) and the Flight Crew Operations Manual (FCOM). Typically, the AFM is a complete document that contains flight procedures and performance data needed to operate the aircraft at a level of safety imposed by the airplane's

certification rules. The FCOM, for its part, describes in details the characteristics and operation of the airplane and its systems, including the propulsion system. Based on these two documents, it is then possible to determine the fuel flow for different flight phases including for example takeoff, climb, cruise and descent (Roberts & Eastbourn, 2014). However, a considerable drawback of aircraft flight manuals is that they do not provide valuable information regarding the thrust value of the engine. Thus, using only the AFM and FCOM to derive an engine performance model is not enough, and a complementary source needs to be found.

Nowadays, aircraft production companies develop performance algorithms and programs that can be used to generate a high quality of aircraft/engine performance data. Notable examples of such programs are the INFLT/REPORT Boeing Performance Software (developed by Boeing) and the PEP Airbus Performance Engineering Program (developed by Airbus) (Gong & Chan, 2002; Suchkov, Swierstra & Nuic, 2003). Both programs allow users to generate climb, cruise, descent, and other simple flight planning data for a complete range of operating conditions in terms of weight, speeds, and temperature with a high level of precision. The direct advantage of these programs is that the parameters of the engine can be collected during the simulation, giving the user the possibility to quantify the thrust variation as a function of pressure altitude, flight speed and environmental conditions. This kind of data could be therefore coupled with information available in the AFM and the FCOM for the development of better quality of engine performance models capable of meeting requirements for flight management systems.

2.1.3 Research Objectives and Paper Organization

Based on the review of the literature, the main objective of this paper can be the following: proposition of a methodology to identify an engine performance mathematical model of the Cessna Citation X using the minimum amount of data. Once the model created, it could be next used to derive a set of engine performance databases required to operate the flight management system algorithms. To reach this objective and develop such a methodology, the Aircraft Flight Manual (AFM), the Flight Crew Operating Manual (FCOM) and a set of computerized flight trajectories were used to gather a maximum information regarding the

Citation X propulsion system. A mathematical model was next proposed by combining a set of mathematical relationships with a component-level structure of the engine. In order to validate the proposed model, comparisons of its data with the level D Research Aircraft Flight Simulator (RAFS) of the Cessna Citation X data used as a reference were done (see Figure 2.1). According to the Federal Aviation Administration (FAA, AC 120-40B), the level-D corresponds to the highest qualification level for the flight dynamics and engine modeling. Each flight test performed with the RAFS aimed to represent a portion of a typical flight including takeoff, climb, cruise and idle descent.

Figure 2.1 Cessna Citation X Level-D Flight Simulator

The structure of this paper is the following: **Section 2.2** describes the Cessna Citation X propulsion system. **Section 2.3** deals with the complete methodology to identify the engine performance. This section includes the data collection, the mathematical equations describing the engine performance, and the identification process used to create the engine performance database that defines the model. In **Section 2.4** comparisons between the identified model and the level-D RAFS data are presented and discussed. Finally, the paper ends with some conclusion and remarks concerning further possible research and developments.

2.2 Cessna Citation X Propulsion System

The modeling of any physical system begins with an in-depth analysis of its characteristics. The purpose of this section is double. The first objective is to establish a complete and detailed description of the propulsion system that equips the Cessna Citation X. However, it is important to mention that, since the study presented in this paper focuses primarily on the development of an engine performance model for flight management system and trajectory optimization applications, only the properties of the propulsion system that directly affect the flight performance of the aircraft are discussed. The second objective is to demonstrate that the FCOM is a reliable data source that can be used to develop a performance model. At the end of this section, all the information collected will be used to provide a block diagram that represents the Cessna Citation X propulsion system model.

2.2.1 Cessna Citation X Engine Description

The Cessna Citation X is a medium-sized business jet designed to fly at a ceiling altitude of 51,000 ft and a maximum operating limit speed of 350 KCAS (Mach number of 0.92). To reach these high-performances, the aircraft has been equipped with two powerful Roll-Royce/Allison AE3007C1 engines, both installed on each side of the rear fuselage. The AE3007C1 is a high-bypass, dual-spool, axial flow turbofan. The engine is rated at 6,764 pound-force static thrust at sea level and up to 30°C ambient temperature (ISA+15°C). A schematic illustration of the principal elements that compose the core of the engine is given in Figure 2.2. The engine consists of a 24-blade single stage fan, a fourteen-stage axial flow compressor, a combustion chamber, two mechanical turbines, and an exhaust nozzle. The low-pressure shaft (represented by the block in black) connects the fan at the front of the engine to the three-stage low-pressure turbine assembly at the rear of the engine. The high-pressure shaft (represented by the block in grey) connects the high-pressure compressor to the two-stage high-pressure turbine.

Unlike several other turbofan technologies, the high-pressure and low-pressure shafts of the AE3007C1 are mounted concentrically but are not mechanically connected through a gearbox.

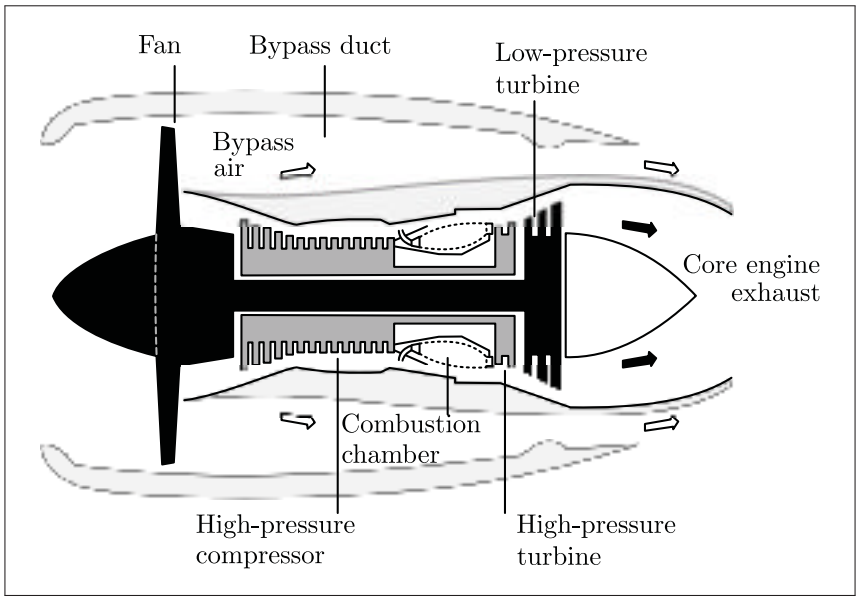

Figure 2.2 Diagram of the AE3007C1 Turbofan Engine

Instead, the engine is equipped with a set of Compressor Variable Geometry (CVG) vanes. These vanes are used to decouple the low-pressure shaft from the high-pressure shaft. In this way, the engine control system can optimize the compressor stages to different operating conditions while maintaining the rotational speed of the turbines at the most efficient value. Advantages include for examples optimal engine efficiency during idle descent, higher engine RPM during approach and optimal power for go-around procedure (aborted landing on final approach).

2.2.2 Engine Thrust Generation

To generate a propulsive force (i.e., thrust) that propels the Cessna Citation X forward, the AE3007C1 needs to accelerate the air between the front and the back of its structure. This principle is directly deriving from Newton's third law of motion, which states that "*for every action, there is an equal and opposite reaction*" (Torenbeek, 2013; Mattingly *et al.*, 2018; Young, 2017). Typically, as the aircraft flies, the air captured in the inlet-fan case is sucked and then compressed by the fan. Immediately after the fan, the incoming air is divided by a concentric duct into two parts. A major portion of the air is directed to the bypass duct, referred to as bypass air, whereas the rest of the air is routed directly to the engine core, referred to as core air. The

ratio of the airflow through the bypass duct to the airflow through the engine core is defined as the bypass ratio. For the Cessna Citation X engine, the bypass ratio is approximately 5.0 to 1.0.

As the core air continues to flow inside the engine structure, it is further compressed by the multi-stage high-pressure compressor to gradually increase its temperature. The hot core air at high pressure then passes through the combustion chamber where it is mixed and burned with fuel. The resulting energy converted during the combustion is extracted in both turbines in order to be converted into mechanical (rotational) energy. Part of the energy is first absorbed by the high-pressure turbine and transmitted forward by the high-pressure shaft to the compressor. The remaining energy is recovered by the low-pressure turbine to drive the fan through the low-pressure shaft. Finally, the hot air leaving the turbines is expanded through the nozzle at the rear of the engine and at a speed greater than the flight speed, producing a small thrust for propulsion. In parallel, the bypass air continues outside the engine core through the bypass duct where it is aerodynamically accelerated before being expanded with the core engine exhaust at a speed greater than the flight speed, thus producing a large proportion of thrust for propulsion.

The AE3007C1 is therefore a power plant that combines two interdependent propulsion mechanisms. One mechanism of this engine is designed to produce energy in the form of hot air at high speed, while the second mechanism uses a portion of that hot air to provide the required power to rotate the fan.

2.2.3 Engine Limitations, Thrust Ratings and Thrust Control

The amount of thrust that the AE3007C1 turbofan engine can produce in flight is controllable by the pilot using the throttle levers (or the thrust levers) located in the flight deck. When the pilot advances the thrust levers from one position to another, a signal is sent to the engine fuel control system to supply more fuel to the combustion chamber. This increase in fuel causes the low-pressure and high-pressure turbines to rotate faster, which in turn drive the fan at a higher speed. As the fan speed increases, more incoming air is compressed at high temperature and high speed, which produces more thrust for propulsion. Clearly, exceeding a certain thrust level

could cause the critical components of the engine to operate under conditions that exceed their design limitations. If such case occurs, the structural integrity of the engine, as well as the safety of the flight, could be compromised (Blake, 2009; Young, 2017).

2.2.3.1 Engine Limitations and Thrust Ratings

To protect the engine from failure and deterioration, manufacturers specify flight phase-dependent thrust limitations (Walter, 2001). These limitations, also known as thrust ratings, represent in certain way the maximum recommended thrust that the engine can produce under certain flight conditions. To better illustrate this concept, an example of thrust ratings for different flight phases is given in Figure 2.3 (Airbus, 2002b; Blake, 2009).

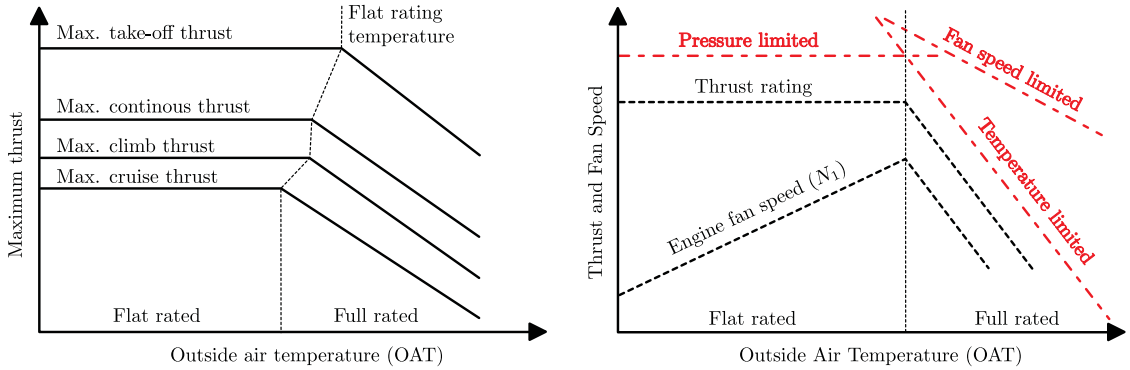

a) Flight-Phase Thrust Limitations due Outside Air Temperature

b) Thrust Limitations due to Temperature, Pressure and Fan Speed

Figure 2.3 Thrust Limitations and Thrust Ratings

As shown in Figure 2.3a, the maximum thrust that the pilot can use to perform a maneuver (takeoff, climb, cruise, etc.) remains constant until a critical outside air temperature. This critical temperature is usually referred as the flat rating temperature or kink temperature (Airbus, 2002b; Blake, 2009). For most engines, this temperature varies between ISA+0°C and ISA+15°C, where ISA is the value of the outside air temperature according to the International Standard Atmosphere model. Above this "breaking temperature", the maximum allowable thrust is

reduced as the outside air temperature increases. This limitation is generally determined by the engine manufacturer in order to protect the turbines from exceeding their design limit temperature.

It is important to mention that engine thrust ratings are not only functions of the outside air temperature, but also take into account other limitations due to high pressure differential across the engine case (pressure limited), and high centrifugal forces at the tips of the fan blades (fan speed limit). These limitations are illustrated in Figure 2.3b. The algorithms used to determine the thrust ratings of an engine vary among manufacturers and are specific to the engine. This is the reason why it is necessary to have access to reliable information when developing an engine performance model. For the Cessna Citation X case study, there are a number of five thrust ratings that the pilot can select in flight to safely carry out a maneuver. These ratings are listed below, together with relevant comments as to their purpose.

- **Maximum Take-Off/Go-Around Thrust** – This rating defines the maximum thrust that the engine can produce for a takeoff or a go-around procedure. For most engines, including the AE3007C1, this rating is certified to be maintained for a maximum of five minutes with all engines operative, and for a maximum of ten minutes in case of one engine failure;
- **Maximum Continuous Thrust** – This rating corresponds to the maximum thrust that one single engine can maintain during a flight when the remaining engine is inoperative. For instance, if one engine fails immediately after takeoff or during climb/cruise, the pilot has to continue the flight at maximum continuous thrust. This thrust rating may not be therefore used in normal operation;
- **Maximum Climb Thrust** – This rating determines the thrust level recommended by the engine manufacturer during a normal climb operation after takeoff or when performing a step-climb from one cruise altitude to the next. This rating does not represent a real limitation of engine performance, but rather a compromise between the engine maintenance objectives and the aircraft operational performance. For this reason, normal climb to altitude are conducted using this recommended thrust level;

- **Maximum Cruise Thrust** – This rating defines the maximum recommended thrust during normal cruise operation. In general, it is not a particularly useful rating since in cruise the pilot (or the autopilot) needs to adjust the thrust in order to maintain a constant altitude and flight speed to meet air traffic control requirements. Within this context, the maximum cruise thrust rating is more a reference level that the pilot should not exceed during a normal cruise;
- **Flight Idle Thrust** – This rating determines the minimum thrust that the pilot (or autopilot) can use during the descent phase. It is established by the engine manufacturer in order to keep the engine running, and to provide other services to the aircraft such as power, hydraulic supply pressure, and cabin pressurization.

Each of the five above ratings is computed automatically by the Full Authority Digital Electronic Control (FADEC) depending on flight conditions (pressure altitude, air temperature and flight speed) and thrust lever positions using predefined lookup tables. The FADEC is a modern system that controls the engine fuel supply in order to provide the pilot with the maximum thrust required to perform a specific maneuver. However, it is worth noting that since the thrust of an engine cannot be measured in flight, the FADEC does not control directly the thrust, but rather a parameter which can be measured in flight, and has a close relationship to the engine thrust (Airbus, 2002b; Blake, 2009; Young, 2017). The two most common parameters used by engine manufacturers to indirectly control the engine thrust are the engine fan speed (N_1) and the engine pressure ratio (EPR). This is the reason why thrust ratings are usually expressed in terms of N_1 or EPR, instead of maximum thrust values.

2.2.3.2 Impact of Bleed Air on Engine Performance

In addition to design limitations, engine performance may be also affected by the use of bleed air (Young, 2017). Indeed, according to the aircraft flight manuals, each engine of the Citation X has low-pressure and high-pressure ports from which compressor discharge air is bled off. These ports are respectively located on the eighth and fourteenth stages of the engine compressor (see high-pressure compressor in Figure 2.2). This hot and high-pressure air is required by the

aircraft's system for fuel tank pressurization, environmental control systems, air conditioning systems and anti-ice systems. From an aircraft performance perspective, bleed air can be seen as a performance penalty on the engine since it causes thrust to decrease and specific fuel consumption (ratio between the fuel flow and the thrust) to increase (Young, 2017). However, because of the complexity of the pressurization and environmental control system, only two bleed configurations are considered in this study. In the first configuration, only bleed air from the low-pressure system is considered, and the anti-ice systems are switched to "off". In the second configuration, the bleed air is extracted from the high-pressure system and the anti-ice systems (including wing, stabilizer and engine anti-ice) are switched "on".

2.2.3.3 In-Flight Thrust Logic Control

Finally, the last part of this section concerns the engine thrust control logic. As mentioned previously, the maximum amount of thrust that the pilot can select to perform a maneuver can be controlled by use of the throttle levers. To help the pilot in selecting the most appropriate thrust, the throttle levers of the Cessna Citation X are designed to rotate through a segment of an arc composed of five specific positions, also called "detents". Each of these five positions represents a specific thrust rating as shown in Figure 2.4.

When the pilot places the thrust levers in the IDLE position, a signal is sent to the FADEC to control the flight idle thrust. As the pilot advances the throttle levers beyond IDLE, a signal is sent to the FADEC to vary the thrust linearly until reaching a series of three consecutive detents. The first of the three detents is labeled CRU and commands the maximum cruise thrust. The second detent is labeled CLB and commands the maximum climb thrust. The third detent, labeled TO/MC, commands the maximum takeoff thrust. In case of one engine inoperative, this position will command the maximum continuous thrust. Finally, when pushing the throttle levers beyond the TO/MC position, the FADEC will still command the maximum take-off/go-around thrust.

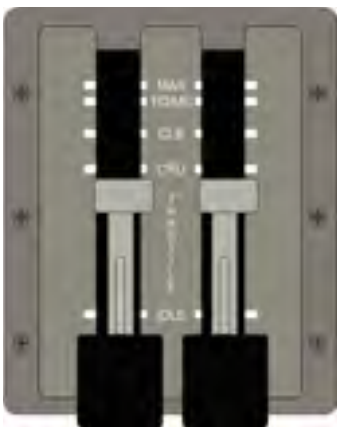

a) Cessna Citation X Throttle Levers

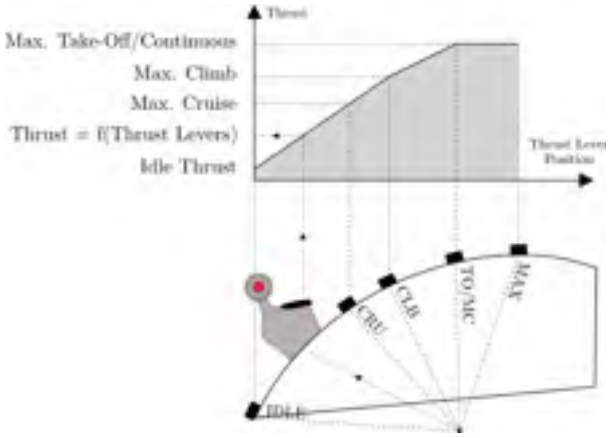

b) Throttle Lever Angle (TLA) and Thrust Value

Figure 2.4 Cessna Citation X Thrust Control

2.2.4 Summary and Conclusion

In this section, a complete and detailed description of the Cessna Citation X propulsion system was given. Based on the information gathered in this section, it can be now concluded that the development of a performance model for the AE3007C1 turbofan is a very complex procedure that includes the development of two sub-models. A first sub-model, called "FADEC/Thrust Ratings", is used to determine the thrust rating parameter (N_1 for the Cessna Citation X) depending on the flight condition (i.e., altitude, temperature and flight speed), throttle lever positions and bleed configuration. The second sub-model, called "Engine Performance", for its part, is used to determine the main engine performance based on the N_1 input. In this study, the three parameters that were considered to represent well the engine performance are the engine core speed, thrust and fuel flow. A block diagram which summarizes this concept is presented in Figure 2.5.

Finally, the main objective of this research paper can be reformulated as follows: propose a complete methodology to identify the different lookup tables of the proposed model in Figure 2.5. Such a methodology is presented and discussed in detail in the following section.

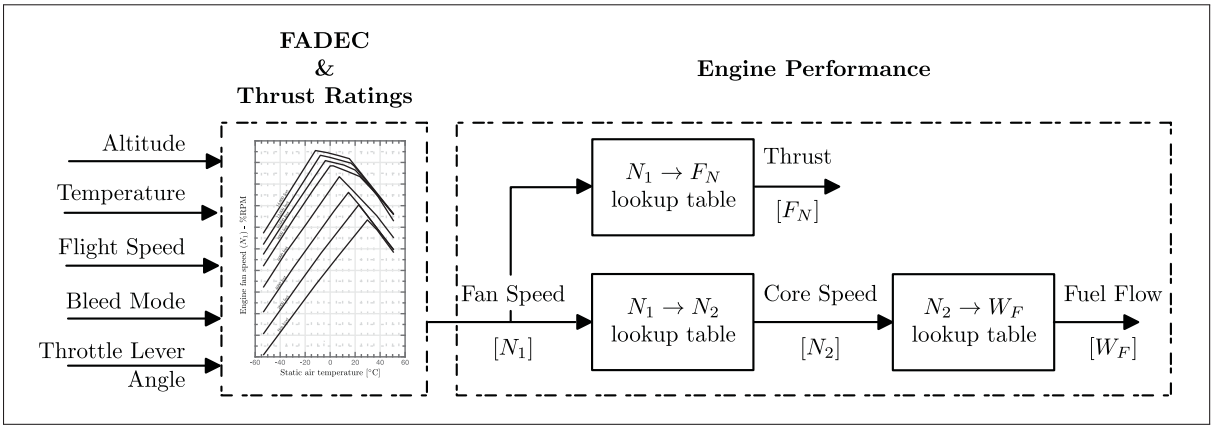

Figure 2.5 Proposed Engine Performance Model Block Diagram

2.3 Engine Performance Model Identification

The identification of a mathematical model is a complex procedure which consists in conducting an experiment with a system, measuring the system response, and finally using the collected data to propose a set of fundamental relationships that is supposed to represents the system behavior. The main objective of this section is to examine the reference data and theoretical equations required to identify an accurate performance model of the Cessna Citation X propulsion system. To this end, the section begins with the data collection process that has been used to gather information from a variety of sources. Afterward, the section presents the mathematical development of several fundamental relationships of the engine. These relationships aim to express the main engine performance (i.e., thrust, rotational speeds and fuel flow) as functions of measured flight parameters. Finally, the gathered data and engine fundamental relationships are then combined with an identification process to complete the methodology.

2.3.1 Data Collection and Database Generation

Gathering information from experimental observations is a key aspect for any scientific work. The objective of the data collection is to allow the modeler to collect enough information from a variety of sources in order to obtain a complete and accurate representation of the system of

interest. For the purposes of this study, three types of documents were used to gather a maximum amount of information regarding the Cessna Citation X propulsion system performance.

2.3.1.1 Aircraft Flight Manual and Certified Thrust Ratings

The first document used in this study to determine the engine characteristics is the Aircraft Flight Manual (AFM). This manual is a comprehensive document produced by the aircraft manufacturer, and it contains detailed information necessary to operate the aircraft at the level of safety established by the airplane certification basis. This information includes for instance aircraft operating techniques recommended for normal, abnormal and emergency procedures and the aircraft performance that should be achieved when the aircraft is operated in accordance with these procedures. Regarding the engine performance, the most relevant information published in the AFM concerns the three certified thrust ratings that are: the maximum takeoff thrust, maximum go-around thrust, and maximum continuous thrust. The publication of these three thrust limitations is mandatory by world-wide certification authorities such as the United States Federal Aviation Administration (FAA) and the European Aviation and Space Agency (EASA) (Blake, 2009; Young, 2017).

For the Cessna Citation X, these data are published in the AFM in graphical form as shown in Figure 2.6a. As illustrated here, each chart provided in the AFM aims to represent the maximum fan speed (in percentage of rotational speed, %RPM) as a function of pressure altitude, static/ram air temperature, and for a given anti-ice system configuration (“on” and “off”). To better explain how this type of data was extracted from the AFM and then converted into a numerical form, Figure 2.6 shows a case example corresponding to the maximum takeoff thrust rating.

As depicted in Figure 2.6, the original chart image was first scanned from the flight manual and then digitized using the Engauge Digitizer tool[1]. This tool is a free open-source software for extracting data point from a graphic image. This process is divided in four main steps. Firstly, the original image must be scanned and imported in the Engauge Digitizer environment. Then,

[1] Software available at: http://markummitchell.github.io/engauge-digitizer.

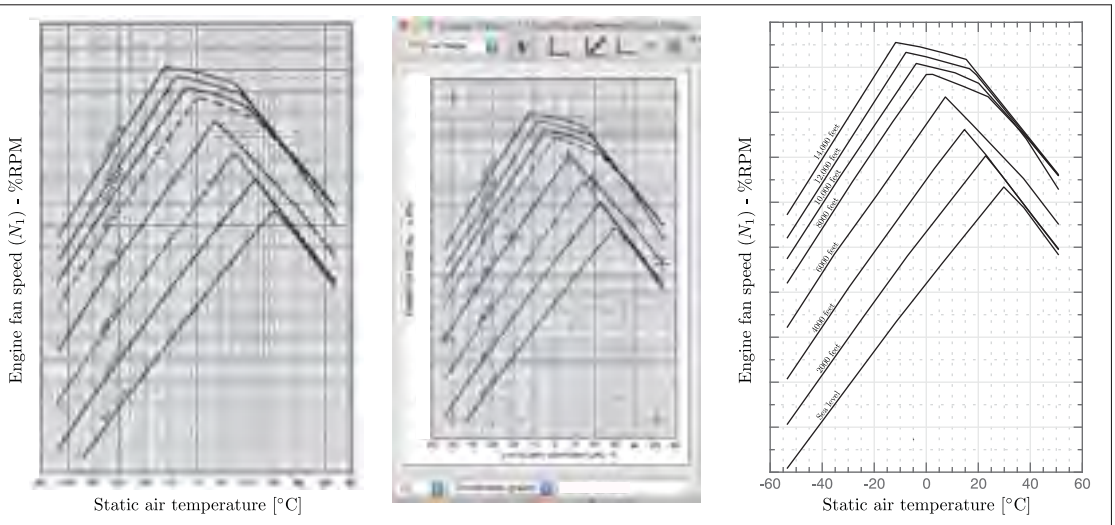

a) Original Graphic Image b) Digitalization Process c) Digitalized Graphic Image

Figure 2.6 Digitalization Process of the Fan Speed at Maximum Takeoff Thrust Setting

the user must define three reference points or coordinates. These coordinates are used by the software to map the number of pixels in a coordinate system. Afterward, the user can scan the curves by drawing over the lines or by drawing a series of points that represent well the lines. Finally, curves are rearranged using linear interpolation and extrapolation techniques to create a lookup table, which can be easily exported in a CSV format readable by any analysis program such as Matlab.

Thus, for the six chart images published in the aircraft flight manual (three thrust ratings for two anti-ice configurations), a table describing the variation of the fan speed as function of pressure altitude and the air temperature was digitized using Engauge Digitizer. These tables were next imported into Matlab in order to create a set of lookup tables and to construct a part of the engine performance database.

2.3.1.2 Performance Data Available in the Flight Crew Operating Manual

The second document used in this study to complete the engine database is the Flight Crew Operating Manual (FCOM). In addition to provide a detailed description of the aircraft propulsion

system, this document is also supplementing the AFM. Regarding the engine performance, the manual provides a number of reference profiles for climb, cruise and descent regimes which specify the aircraft performance at various gross weight, airspeed and environmental conditions. However, unlike the AFM, these data are not published graphically, but rather as tables. An example of a table provided in the FCOM that specifies the performance of the aircraft/engine for a cruise at 33,000 ft is given in Figure 2.7.

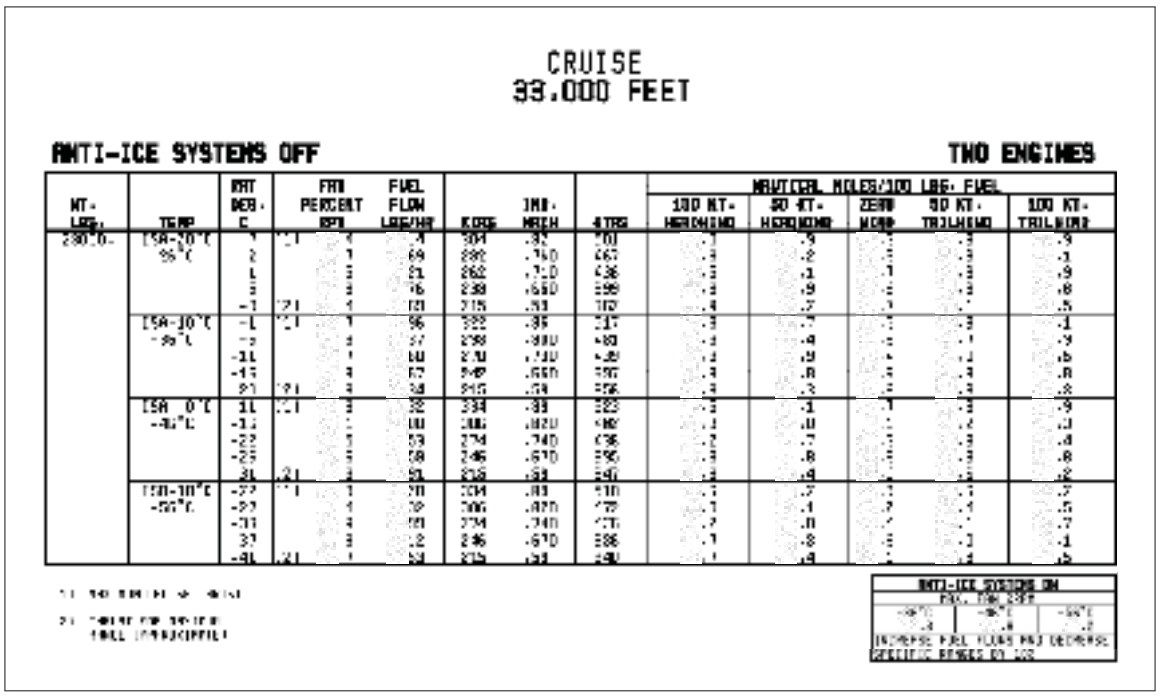

Figure 2.7 Example of Cruise Performance Data Published in the Citation X FCOM

As shown in Figure 2.7, the specific performance data are given in a table for various combinations of engine fan speeds, aircraft weights, and flight conditions expressed in terms of airspeeds, Mach numbers, and temperatures. The different fan speeds presented in the table provide the aircraft/engine performance (i.e., fuel flow and specific range) for five thrust levels between the approximate maximum range thrust and maximum cruise thrust. The first one, indexed by the number (1) in the table, represents the thrust for which the aircraft airspeed (i.e., Mach number) is the highest, while the second one, referred by the number (2), represents the thrust for which

the fuel flow is the lowest. Such a variation of the speeds allows, therefore, a good estimate of the engine performance over the aircraft range of operational speeds in cruise.

Regarding the effect of the anti-ice systems on the engine performance, the FCOM of the Cessna Citation X does not provide additional tables. Instead, the manual includes several notes such as those given on the right hand side below the main table in Figure 2.7. According to these notes, activating the anti-ice systems during a cruise at 33,000 ft will increase the fuel flow and decrease the aircraft specific range (distance the aircraft travels per unit of fuel consumed) by ten percent (10%). The maximum engine fan speed allowed for this cruise altitude is also reduced depending on the outside air temperature (or temperature deviation from a standard day, ΔISA).

The combination of all this information makes it possible to derive a model for the maximum cruise thrust, but also to obtain a model describing the variation of the fuel flow of the engine due to the anti-ice activation. Thus, for each of the 21 cruise altitudes provided in the FCOM, all the data existing in the manual were manually recopied in the same order in an excel file and saved in a CSV format. The gathered data were next imported in Matlab in order to be rearranged in a set of lookup tables, and to complete the engine performance database.

Finally, it is important to mention that the FCOM also provides performance data for the climb and descent flight phases. However, these data are not as detailed as those for the cruise since they do not include information regarding the engine fan speed. This is the reason why they were not considered in this study.

2.3.1.3 Aircraft Computerized Flight Trajectories

So far, the AFM and FCOM have allowed the collection of a large amount of data regarding the engine operating limits. However, as mentioned in the introduction of this paper, a considerable drawback of these manuals is that they do not provide any information for the engine thrust. Since the main purpose of a jet engine is to generate a thrust force that propels the aircraft forward, it is impossible to design a performance model without taking this information into

account. Thus, to overcome this problem, a third reference source based on computerized flight trajectories was used to complete the engine performance database, and is here detailed.

For the purpose of this study, the Cessna Citation X In-Flight Performance (IFP) model used to generate the required flight profiles was developed by our LARCASE research team in previous studies (Ghazi, 2014; Ghazi & Botez, 2015). This model can be used to generate any flight profiles above 1500 ft for any aircraft configuration. An example of flight parameters that can be obtained with the IFP model is shown in Table 2.1.

Table 2.1 Example of a Climb Flight Profile Generated with the Cessna Citation X IFP

Flight Profile Conditions						**Engine Parameters**			
Time [min]	Altitude [ft]	CAS [kts]	Mach	OAT [°C]	ΔISA [°C]	N_1 [%RPM]	N_2 [%RPM]	F_N [lbf]	W_F [lb/h]
00.00	1500	250	0.234	12.0	0	82.31	93.58	4,475	2,376
00.22	2274	250	0.236	10.5	0	82.63	93.56	4,430	2,342
00.45	3051	250	0.241	9.00	0	82.93	93.54	4,363	2,307
00.67	3798	250	0.243	7.50	0	83.22	93.51	4,315	2,274
⋮	⋮	⋮	⋮	⋮	⋮	⋮	⋮	⋮	⋮
18.62	43,835	250	0.559	-56.5	0	92.70	92.31	1,335	828.5
18.85	44,012	250	0.562	-56.5	0	92.64	92.30	1,320	821.6
19.07	45,000	250	0.564	-56.5	0	92.59	92.29	1,308	814.2

The sample data given in Table 2.1 specifies the time taken by the Cessna Citation X to climb from 1500 ft to a specified altitude (in this case 45,000 ft) with an initial gross weight, a climb speed schedule of 250 KCAS (kts Calibrated Airspeed) and under ISA conditions. The table also provides the evolution with respect to the time of the four main engine parameters, that are the fan speed N_1, the core speed N_2, the thrust F_N and the fuel flow W_F.

Each computerized trajectory was generated in a text file format, and then converted to CSV format to be imported and processed in Matlab. In order to obtain a model that can accurately represent the engine performance over a variety of flight conditions, a total of 12 profiles was used in this study. These profiles were chosen as follows:

- Climb trajectory data from 1500 to 45,000 ft:
  - 3 climb profiles at ISA conditions covering a range of aircraft operating speeds (150KCAS, 250 KCAS, and 340 KCAS);
  - 2 climb profiles at ISA+10°C and ISA+20°C conditions for two operating speeds (250 KCAS and 340 KCAS);
  - 2 climb profiles at ISA conditions with anti-ice systems enabled for two operating speeds (270 KCAS and 340 KCAS).
- Descent trajectory data from 45,000 to 1500 ft:
  - 3 descent profiles at ISA conditions covering a range of aircraft operating speeds (150 KCAS, 250 KCAS, and 340 KCAS);
  - 2 descent profiles at ISA conditions with anti-ice systems enabled for two arbitrary operating speeds (250 KCAS and 340 KCAS).

The climb and descent profiles at ISA conditions are used in this study to identify a model for the engine thrust and fuel flow under standard conditions. These same profiles are also used to complete the thrust rating database by taking into account the engine fan speed limitations for the maximum climb and flight idle settings.

The two climb profiles at ISA+10°C and ISA+20°C are used to estimate the flat rating temperature of the engine for the maximum climb thrust rating. Regarding the flight idle setting, this process is not necessary because the temperature of the turbines during the descent phase is generally well below the temperature limit set by the manufacturer. In this case, it is assumed that under normal operating conditions, the engine should always operate in the flat temperature region.

2.3.2 Engine Parameters Functional Relationships

Now that enough information has been collected, the second step in the identification process is to obtain a set of fundamental relationships between the engine performances (i.e., thrust and fuel flow) and parameters affecting these performances. A common way to characterize these performances is to use a set of corrected parameters derived by dimensional analysis. The

objective of this section is therefore to briefly describe the principle of dimensional analysis and derive a particular correction of the thrust as an illustrative example. This principle will be next generalized to the other parameters to propose a complete set of functional relationships describing the performance of the Cessna Citation X propulsion system.

2.3.2.1 Dimensional Analysis Description

Any physical system can be described by elaborating mathematical relationships between a set of variables in accordance with the laws of fundamental physics. However, depending on the variables selected to represent the properties of the system, these relationships may vary in complexity and ease of use. Dimensional analysis is a technique for simplifying a physical problem by using dimensional homogeneity to reduce the number of variables that are physically relevant to the problem under consideration. One of the most frequently used dimensional analysis technique in aircraft performance studies is based on the method proposed by Buckingham (1914).

To illustrate the idea behind the π-theorem, let's consider n dimensional parameters $\{x_1, \ldots, x_n\}$ that are relevant in a given physical problem, and that are inter-related by a physical unknown equation. Without any loss of generality, these parameters can be expressed by a functional relationship under the form:

$$f(x_1, x_2, \ldots, x_n) = 0 \qquad \text{or equivalently} \qquad x_1 = \phi(x_2, x_3, \ldots, x_n) \tag{2.1}$$

where f and ϕ are unknown functions. By analogy to the engine case study, the variable x_1 would represent the engine thrust, and the remaining variables $\{x_2, \ldots, x_n\}$ would represent the parameters affecting the thrust such as pressure altitude, air temperature and airspeed.

The π-theorem in its simplified form includes two parts. The first part of the theorem aims to explain what type of reduction in number of variables can be expected, and can be stated as (Buckingham, 1914):

Theorem 1 (Reduction of the problem)**.** *If a physical problem is characterized by n dimensional variables having k fundamental units (i.e., time, length, temperature or mass), then the functional relationship between the dimensional variables can be reduced into a relationship between* $(n-k)$ *dimensionless and independent quantities or* π*-group denoted by* $\{\pi_1, \pi_2, \ldots, \pi_{(n-k)}\}$*. The reduced functional relationship can be thus expressed in its compact form:*

$$F(\pi_1, \pi_2, \ldots, \pi_{(n-k)}) = 0 \qquad \textit{or equivalently} \qquad \pi_1 = \Phi(\pi_2, \pi_3, \ldots, \pi_{(n-k)}) \tag{2.2}$$

where F *and* Φ *are the compacting forms of* f *and* ϕ*.*

Because of the number of possible combinations, the definition of the π-parameters is not unique and can vary from a study to another. To help the user in defining a possible combination of parameters, the second part of the theorem aims to give a procedure to construct the π-parameters once at a time (Buckingham, 1914).

Theorem 2 (Construction of the π-parameters)**.** *To construct the set of* π*-parameters:*

i *Select* $p = (n-k)$ *reference variables* $\{xr_1, \ldots, xr_p\}$ *from the physical variables* $\{x_1, \ldots, x_n\}$*. These variables should characterize the physical problem, be dimensionally-distinct and include all the fundamental units so that the problem can be solved.*

ii *For each reference variable* xr_i*,* $i = \{1, \ldots, p\}$*, formulate the corresponding* π_i*-parameter by multiplying the remaining variables (those that were not chosen as reference variables) in turn by the reference variable; each turn raise to an unknown exponent:*

$$\pi_i = \left[x_1^{a_1} \times x_2^{a_2} \times \ldots \times x_{(n-p)}^{a_{(n-p)}}\right] \times [xr_i] \tag{2.3}$$

where the coefficients $\{a_1, a_2, \ldots, a_{(n-p)}\}$ *are constants.*

iii *Find the exponents by forcing the* π*-parameters to be dimensionless*

For each π-parameter created, a linear algebraic analysis must be performed in order to find the value of the exponents which make the product in Eq. (2.3) dimensionless. This procedure is illustrated in the following section.

2.3.2.2 Dimensionless Application Method: Engine Thrust Relationship

To illustrate how dimensional analysis was used in this study to develop the engine performance model, the dimensional analysis of the engine thrust is presented here for the case study of the Cessna Citation X turbofan. The results for the other engine parameters (i.e., fuel flow and rotational speeds) could be obtained by following a similar procedure.

Based on the description of the propulsion system provided in **Section 2.2**, and as suggested by several authors in the literature (Volponi, 1999), the main parameters which affect the performance of a typical engine should include rotational speed N_1 (or N_2), airspeed V_T, ambient temperature T, ambient pressure P, the specific air constant R_{air}, and a physical dimension of the engine such as the inlet section S_{ref}. The general expression for the thrust can be therefore expressed as:

$$F_N = f\left(N_1, V_T, T, P, R_{\text{air}}, S_{\text{ref}}\right) \tag{2.4}$$

The functional relationship in Eq. (2.4) consists of $n = 7$ variables. Each of these seven variables can be expressed in turn in terms of $k = 4$ fundamental dimensions as shown in Table 2.2, where M is the mass, L is the length, T is the time, and Θ is the temperature.

Table 2.2 Engine Thrust Dimensional Variables

Variable and Description		Physical Unit	Dimensions
Output Variable			
F_N	Thrust force	N or lbf	M.L.T^{-2}
Input Variables			
N_1	Fan speed (%RPM)	s^{-1}	T^{-1}
V_T	Aircraft airspeed	m.s^{-1}	L.T^{-1}
T	Ambient temperature	K	Θ
P	Ambient pressure	Pa	$\text{M.L}^{-1}\text{.T}^{-2}$
R_{air}	Specific air constant	$\text{J.K}^{-1}\text{.mol}^{-1}$	$\text{L}^2\text{.T}^{-2}\text{.}\Theta^{-1}$
S_{ref}	Engine inlet section	m^2	L^2

As stated in the first part of the π-theorem, the functional relationship in Eq. (2.4) can be simplified in a more compact form involving only $(n-k) = 3$ non-dimensional parameters π_1, π_2 and π_3 such that:

$$\pi_1 = \Phi(\pi_2, \pi_3) \tag{2.5}$$

Now that the reduction is defined, the next step is to determine the π-parameters using the second part of the theorem. Considering that the thrust F_N, fan speed N_1, and airspeed V_T are the most relevant physical parameters of the problem, the three non-dimensional parameters can be chosen such that:

$$\begin{aligned}
\pi_1 &= T^{a_1} P^{a_2} S_{\text{ref}}^{a_3} R_{\text{air}}^{a_4} F_N \\
\pi_2 &= T^{b_1} P^{b_2} S_{\text{ref}}^{b_3} R_{\text{air}}^{b_4} N_1 \\
\pi_3 &= T^{c_1} P^{c_2} S_{\text{ref}}^{c_3} R_{\text{air}}^{c_4} V_T
\end{aligned} \tag{2.6}$$

According to the second part of the theorem, these parameters must be dimensionless, meaning that their units must be equal to $\mathrm{M}^0\mathrm{L}^0\mathrm{T}^0\Theta^0$. Thus, replacing the physical variables with their fundamental dimensions (see. Table 2.2), yields to the following system of equations:

$$\begin{aligned}
[\pi_1] \rightarrow \left[\mathrm{M}^0\mathrm{L}^0\mathrm{T}^0\Theta^0\right] &= [\Theta]^{a_1} \left[\mathrm{ML}^{-1}\mathrm{T}^{-2}\right]^{a_2} \left[\mathrm{L}^2\right]^{a_3} \left[\mathrm{L}^2\mathrm{T}^{-2}\Theta^{-1}\right]^{a_4} \left[\mathrm{MLT}^{-2}\right] \\
[\pi_2] \rightarrow \left[\mathrm{M}^0\mathrm{L}^0\mathrm{T}^0\Theta^0\right] &= [\Theta]^{b_1} \left[\mathrm{ML}^{-1}\mathrm{T}^{-2}\right]^{b_2} \left[\mathrm{L}^2\right]^{b_3} \left[\mathrm{L}^2\mathrm{T}^{-2}\Theta^{-1}\right]^{b_4} \left[\mathrm{T}^{-1}\right] \\
[\pi_3] \rightarrow \left[\mathrm{M}^0\mathrm{L}^0\mathrm{T}^0\Theta^0\right] &= [\Theta]^{c_1} \left[\mathrm{ML}^{-1}\mathrm{T}^{-2}\right]^{c_2} \left[\mathrm{L}^2\right]^{c_3} \left[\mathrm{L}^2\mathrm{T}^{-2}\Theta^{-1}\right]^{c_4} \left[\mathrm{LT}^{-1}\right]
\end{aligned} \tag{2.7}$$

or in a more expanded form:

$$\begin{aligned}
[\pi_1] \rightarrow \left[\mathrm{M}^0\mathrm{L}^0\mathrm{T}^0\Theta^0\right] &= \mathrm{M}^{(a_2+1)}\mathrm{L}^{(-a_2+2a_3+2a_4+1)}\mathrm{T}^{(-2a_2-2a_4-2)}\Theta^{(a_1-a_4)} \\
[\pi_2] \rightarrow \left[\mathrm{M}^0\mathrm{L}^0\mathrm{T}^0\Theta^0\right] &= \mathrm{M}^{(b_2)}\mathrm{L}^{(-b_2+2b_3+2b_4)}\mathrm{T}^{(-2b_2-2b_4-1)}\Theta^{(b_1-b_4)} \\
[\pi_3] \rightarrow \left[\mathrm{M}^0\mathrm{L}^0\mathrm{T}^0\Theta^0\right] &= \mathrm{M}^{(b_2)}\mathrm{L}^{(-b_2+2b_3+2b_4)}\mathrm{T}^{(-2b_2-2b_4-1)}\Theta^{(b_1-b_4)}
\end{aligned} \tag{2.8}$$

Solving the three equations for equal exponents on both sides:

$$\begin{array}{llll} a_1 = 0 & a_2 = -1 & a_3 = -1 & a_4 = 0 \\ b_1 = -1/2 & b_2 = 0 & b_3 = 1/2 & b_4 = -1/2 \\ c_1 = -1/2 & c_2 = 0 & c_3 = 0 & c_4 = -1/2 \end{array} \tag{2.9}$$

and therefore by replacing their values given in Eq. (2.9) into Eq. (2.6), Eq. (2.10) are obtained:

$$\begin{aligned} \pi_1 &= T^0 P^{-1} S_{\text{ref}}^{-1} R_{\text{air}}^0 F_N \\ \pi_2 &= T^{-1/2} P^0 S_{\text{ref}}^{-1/2} R_{\text{air}}^{-1/2} N_1 \\ \pi_3 &= T^{-1/2} P^0 S_{\text{ref}}^0 R_{\text{air}}^{-1/2} V_T \end{aligned} \tag{2.10}$$

Thus, by the virtue of the Buckingham π-theorem, the initial relationship of the thrust in Eq. (2.4) can be rewritten in terms of the three non-dimensional parameters:

$$\pi_1 = f(\pi_2, \pi_3) \Leftrightarrow \frac{F_N}{P S_{\text{ref}}} = f\left(\frac{N_1 \sqrt{S_{\text{ref}}}}{\sqrt{R_{\text{air}} T}}, \frac{V_T}{\sqrt{R_{\text{air}} T}}\right) \tag{2.11}$$

This last result can be further simplified. Indeed, since $\sqrt{R_{\text{air}} T}$ is proportional to the speed of sound, the term $V_T / \sqrt{R_{\text{air}} T}$ in Eq. (2.11) can be replaced by the ratio of the airspeed to the speed of sound that is, the Mach number. Also, since it is more convenient to express aircraft performance using atmospheric ratios, Eq. (2.11) is rearranged as follows:

$$\frac{F_N}{\delta \left[P_0 S_{\text{ref}}\right]} = f\left(\frac{N_1 \left[\sqrt{S_{\text{ref}}}\right]}{\sqrt{\theta} \left[\sqrt{R_{\text{air}} T_0}\right]}, M\right) \tag{2.12}$$

where M is the Mach number, P_0 and T_0 are the ambient pressure and temperature at sea level respectively, and δ and θ are the ratio of pressure and temperature respectively.

Finally, noting that all the elements in brackets in Eq. (2.12) are constants, they can be eliminated without affecting the result, which gives:

$$\frac{F_N}{\delta} = f\left(\frac{N_1}{\sqrt{\theta}}, M\right) \tag{2.13}$$

This last result states that the corrected thrust (F_N/δ) is only a function of the corrected engine fan speed $(N_1/\sqrt{\theta})$ and Mach number M. The use of dimension analysis has therefore made it possible to combine the seven initial variables in Eq. (2.4) into a simpler three-variables equation.

The advantage of representing information in this way is that it significantly reduces the number and complexity of variables affecting engine performances. In addition, since the corrected parameters account for variations in temperature and pressure, the result in Eq. (2.13) can easily be generalized for any other flight conditions. Therefore a small amount of data is used to obtain a valid mathematical model throughout the entire aircraft operating envelope.

Based on these observations, it has been decided to develop the engine performance model of the Cessna Citation X using corrected parameters instead of physical parameters.

2.3.2.3 Complete Engine Performance Model Equations

By applying the Buckingham π-theorem and by following a similar linear algebraic analysis for the other engine performances, similar corrected relationships to Eq. (2.13) can be obtained for the fuel flow W_F and the engine core speed N_2. The complete functional relationships describing the corrected performance of the engine of the Cessna Citation X can be therefore summarized as follows:

$$\textbf{Corrected Thrust:} \quad \frac{F_N}{\delta} = f\left(\frac{N_1}{\sqrt{\theta}}, M\right) + \Delta F_N(h, M) \tag{2.14}$$

$$\textbf{Corrected Core Speed:} \quad \frac{N_2}{\sqrt{\theta}} = f\left(\frac{N_1}{\sqrt{\theta}}, M\right) + \Delta N_2(h, M) + \Delta N_c(h, M) \tag{2.15}$$

$$\textbf{Corrected Fuel Flow:} \quad \frac{W_F}{\delta\sqrt{\theta}} = f\left(\frac{N_2}{\sqrt{\theta}}, M\right) + \Delta W_F(h, M) \tag{2.16}$$

where $(N_2/\sqrt{\theta})$ is the corrected core speed, and $(W_F/\delta\sqrt{\theta})$ is the corrected fuel flow.

As it can be observed, several elements have been added in the proposed model. Indeed, in Eqs. (2.14) to (2.16), the parameters $\Delta F_N(h, M)$, $\Delta N_2(h, M)$, and $\Delta W_F(h, M)$ were introduced in order to model the variation of the corrected engine performance due to the activation of the anti-ice systems. Based on the description provided in the aircraft manuals, it was assumed that these variations are mainly dependent upon altitude, Mach number, and temperature. However, since the corrected parameters take into account the temperature variation, only the altitude and the Mach number have been kept in the corrected model.

Similarly, the parameter $\Delta N_c(h, M)$ shown in Eq. (2.15) was introduced in the model in order to represent the variation in engine core speed due to the compressor variable geometry vanes. According to the information provided in the aircraft manuals and based on several observations made with the computerized flight trajectories, this parameter of the engine seems to be used only during the descent, and is controlled by the FADEC depending on the altitude and Mach number.

It should be noted that the corrected model shown in Eqs. (2.14) to (2.16) does not include any functional relationship for the corrected fan speed. This may be justified by the fact that the variation of the fan speed with respect to flight conditions does not result from a physical phenomenon, but rather from design limitations determined by the engine manufacturer. In this case, it is not possible to apply the π-theorem and derive a functional relationship as it was in the case for the other engine performances. However, to remain consistent with the general structure of the proposed model, the variation of the corrected fan speed was modeled by analogy to the others parameters and according to the aircraft manuals as:

$$\textbf{Corrected Fan Speed:} \quad \frac{N_1}{\sqrt{\theta}} = f\left(h, M, \Delta\text{ISA}\right) + \Delta N_1(h, M) \tag{2.17}$$

where h is the altitude, ΔISA is the temperature deviation from a standard day, and the term ΔN_1 represents the variation in fan speed due to the activation of the anti-ice systems.

Finally, it is worth noting that there are as many functional relationships for $(N_1/\sqrt{\theta})$ as there are a number of thrust ratings. In other words, a corrected fan speed model based on Eq. (2.17) must be developed for each of the five thrust ratings presented in **Section 2.2.3.1**. The full engine model is, therefore, composed of eight equations (five equations for the thrust ratings and three equations for the engine performances), and includes a total of 17 functional relationships that need to be identified. This process is detailed in the following section.

2.3.3 Engine Mathematical Model Identification

So far, the methodology has allowed gathering sufficient data to quantify engine characteristics over a range of operating conditions. Subsequently, using dimensional analysis technique based on the Buckingham π-theorem, several functional relationships were determined to relate engine performance to flight and operating conditions. To finalize the methodology described in this paper, it is important to determine a mathematical form for each of these relationships using curve and surface fitting techniques. Since the process of curve and surface fitting has played an important historical role in the establishment of mathematical models from experimental data, this section briefly describes its principle and further presents the different fitting tools that have been used. Similar to the previous section, the theory is followed by an illustrative example showing how the methodology was applied to derive a mathematical model for the maximum climb thrust rating. This principle is then generalized to the other engine performance to create the full performance model of the AE3007C1 turbofan engine.

2.3.3.1 Curves and Surfaces Fitting using Splines

Curve (or surface) fitting is a form of mathematical regression analysis that allows researchers finding the most appropriate equation for describing the “behavior” of a set of data points. This process can be seen as a technique that provides a visual representation of the relationship

between the experimental data points that characterize a given physical phenomenon. From a mathematical point of view, a curve fitting problem can be formulated as follows: given a set of n experimental data points $\{z_1, \ldots, z_n\}$ of a dependent variable z, corresponding to n values $\{x_1, \ldots, x_n\}$ of an independent variable x, find an equation, such as $f(x)$, that approximates the set of data points. This concept can be further generalized to the studies of surfaces ("surface fitting"), the main difference being that the fitting function f is a bi-dimensional function of two independent parameters (x and y for example).

Depending on the complexity of the problem to be modeled, the fitting function $f(x, y)$ can be represented by a multitude of mathematical structures. The two most frequently used mathematical forms to describe the behavior of a set of data points are polynomials and splines. In general, polynomials are preferred by engineers and researchers because of their simplicity and ease of handling. However, performance of modern aircraft has become so complex that is difficult to describe those using simple continuous functions (Sibin *et al.*, 2010). One way to overcome this difficulty is to gradually increase the degree of the polynomial until obtaining a curve (or surface) that fits well to the data. Unfortunately, high order polynomials are often the main cause of over-fitting. This over-fitting occurs when the model structure contains too many parameters that can be justified by the data shape. In this case, the conformity of the model with the data can be questioned.

In contrast, splines are mathematical structures that are more versatile than polynomials. A typical spline is usually formed by joining several polynomials (or basic functions) together and by imposing continuity constraints at the junctions between two consecutives polynomials (or functions). A considerable advantage in using splines is that their shapes can be locally adapted without affecting the others regions of the function. In this way, the modeler can design and control the shapes of complex curves and surfaces. This is the reason why it has been decided to use splines instead of polynomials to identify the different functional relationships of the proposed engine model. Since the problem presented in this study includes curves and surfaces, two categories of spline were used: the "smoothing cubic spline" and the "thin plate spline". These splines are presented below, together with relevant comments as to their purpose.

Smoothing Cubic Spline

A cubic spline is a function defined piecewise by cubic (i.e., third-order) polynomials. The number of polynomials required to describe the spline depends upon the number of data considered. For example, if there are n independent variables $\{x_1, \ldots, x_n\}$, then the spline $f(x)$ can be expressed as follows:

$$f(x) = \begin{cases} P_1(x) & \text{if } x_1 \leq x_2 \\ P_i(x) & \text{if } x_i \leq x_{i+1} \\ \vdots & \\ P_{n-1}(x) & \text{if } x_n - 1 \leq x_n \end{cases} \tag{2.18}$$

where $P_i(x)$, for $i = \{1, \ldots, n-1\}$, is a normalized third-order polynomial. Each polynomial is connected to the next one by imposing a continuity constraint on the first derivative at the junction. A smoothing cubic spline is nothing else than a particular cubic spline that satisfies the minimization problem:

$$\min_f \left[\lambda \sum_{i=1}^{n} \{z_i - f(x_i)\}^2 + (1-\lambda) \int \left(\frac{\mathrm{d}^2 f}{\mathrm{d}x^2} \right)^2 \mathrm{d}x \right] \tag{2.19}$$

The parameter $\lambda \in [0, 1]$ is called the smoothing parameter of the spline and controls the trade-off between remaining close to the data ("closeness") and obtaining a smooth curve ("smoothness"). In the limit case where $\lambda = 0$, only the curvature of the spline defined by the second derivative of the function is minimized. In this case, the spline function $f(x)$ is reduced to a straight line which minimizes the mean squared error over the set of data points. In the opposite case, when $\lambda = 1$, only the distance between the spline and the data is minimized. In this case, the spline function $f(x)$ passes exactly through all the data points, resulting in a cubic spline interpolation.

Thin Plate Spline

Thin plate splines are very popular for the estimation of surfaces from observed data. Basically, they can be seen as an extension of smoothing cubic splines for two dimensional functions $f(x, y)$. However, rather than cubic polynomials, thin plate splines are represented by connecting a series of radial basis functions, and have the general form:

$$\begin{aligned} f(x, y) &= a_0 + a_x x + a_y y + \sum_{i=1}^{n} w_i \phi \left(\| \ (x, y) - (x_i, y_i) \ \| \right) \\ \phi(r) &= r^2 \log(r) \end{aligned} \tag{2.20}$$

where $\| \cdot \|$ denotes the Euclidian norm, and $\{a_0, a_x, a_y, w_i\}$ for $i = \{1, \ldots, n\}$, are a set of mapping coefficients defining the structure of the thin plate spline. Furthermore, since the function is now bi-dimensional, it is necessary to take into account the two independent variables in the computation of the second derivative. The minimization problem is therefore modified and reformulated as follows:

$$\min_f \left[\lambda \sum_{i=1}^{n} \{z_i - f(x_i, y_i)\}^2 + (1 - \lambda) \iint \left\{ \left(\frac{\partial^2 f}{\partial x^2} \right)^2 + \left(\frac{\partial^2 f}{\partial x \partial y} \right)^2 + \left(\frac{\partial^2 f}{\partial y^2} \right)^2 \right\} \mathrm{d}x\mathrm{d}y \right] \tag{2.21}$$

In a similar way to cubic spline, the parameter λ is a smooth factor which controls the trade-off between closeness and smoothness requirements. Typically, when λ is set to 0, only the curvature of the surface is considered. In this case, the surface is reduced to a linear plane that minimizes the mean squared error over all the data points. On the contrary, when the value of λ is equal to 1, only the closeness of the function to the data is minimized. In this case, the surface passes exactly through all the data points, resulting in a 2D interpolation technique.

2.3.3.2 Application to the Identification of the Engine Fan Speed Variation at Maximum Climb Setting

In order to better illustrate how cubic and thin plate splines were used in this study to create the engine performance model, the following sections detail the identification process for the engine

fan speed at maximum climb thrust setting. The results for the other engine parameters could be obtained by following a similar procedure.

Step 1 – Identification at ISA conditions and with anti-ice systems off

Figure 2.8 shows the corrected fan speed as function of the altitude and Mach number for the three climb profiles at ISA conditions, and with anti-ice systems off. In this figure, it is noted the drastic change of slope that occurs at $h = 38,000$ ft. Indeed, below $38,000$ ft, the corrected fan speed increases with increasing altitude, while beyond this "break altitude", the trend is completely reversed and the corrected fan speed begins to decrease as the altitude increases. Such a variation is similar to the one presented in Figure 2.3 (see **Section 2.2.3.1**), and is probably due to a design limitation imposed by the engine manufacturer to avoid overloading the fan blades in the presence of the centrifugal force.

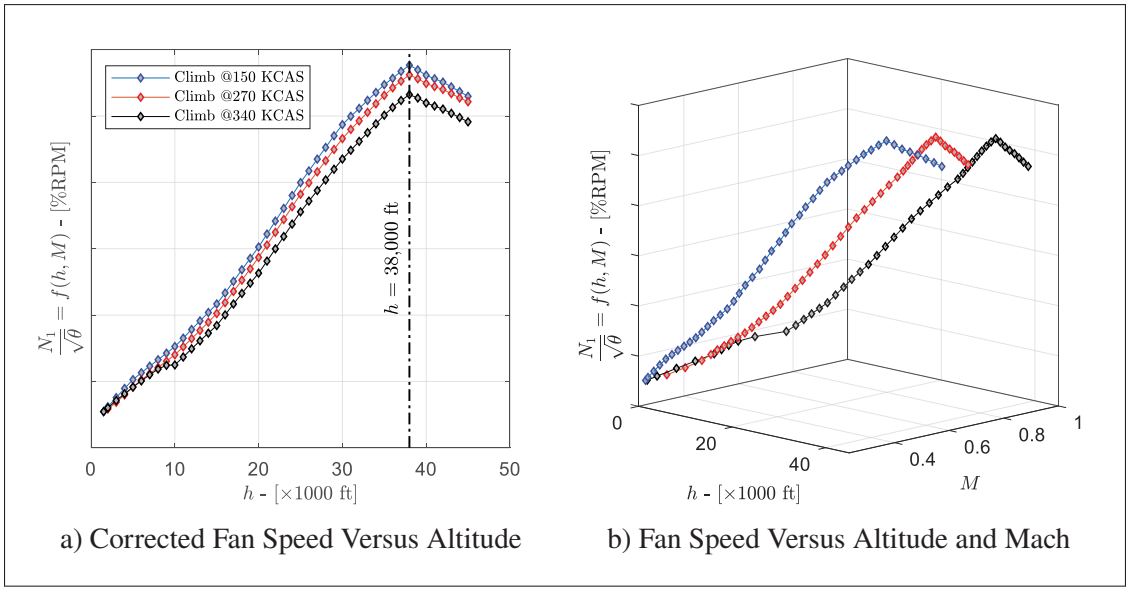

a) Corrected Fan Speed Versus Altitude

b) Fan Speed Versus Altitude and Mach

Figure 2.8 Maximum Corrected Fan Speed in Climb at ISA Conditions and Anti-Ice Systems Off

Using the functions and algorithms available in the Matlab Spline Toolbox, several thin plate splines were tested in order to find a surface that represents well the data shown in Figure 2.8. These tests were aimed at progressively increasing the smooth parameter λ from 0 to 1, and at

validating the conformity of the shape of the surface with the data. After several trials, it was found that the best compromise between data-like surface and a smooth surface was $\lambda = 0.95$. The results corresponding to this value are given in Figure 2.9.

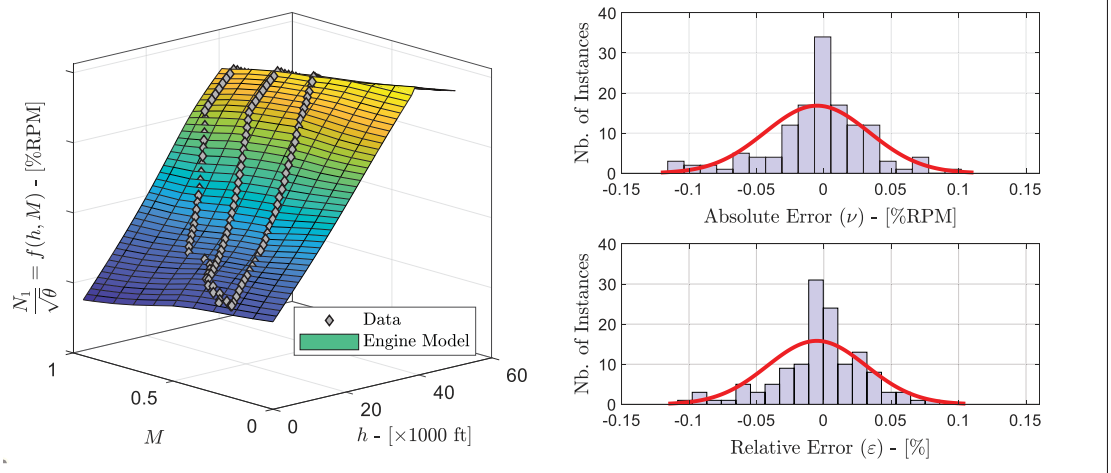

a) Maximum Corrected Fan Speed Model b) Residual and Relative Error Distribution

Figure 2.9 Identification Results for the Maximum Corrected Fan Speed at ISA Conditions

As expected, it can be seen that the resulting surface models very well the data set, and can easily handle the change in slope that occurs at $h = 38,000$ ft. Furthermore, by inspecting the two error histograms in Figure 2.9b, it can be observed that the normal distribution of the errors is symmetrical and bell-shaped around zero. According to this distribution, 100% of the identified point has a maximum relative error smaller than 0.15% and a maximum absolute residual error smaller than 0.15 %RPM.

Step 2 – Effect of the temperature deviation on the maximum fan speed

Figure 2.10a shows the corrected fan speed as a function of the altitude for the climb profile at ISA+10°C and ISA+20°C. The data in gray represents the corrected fan speed obtained from the database created in **Section 2.3.1**, whereas the data in blue represents the corrected fan speed estimated from the previous model using the same flight conditions in terms of altitudes and

Mach numbers. As expected, the temperature deviation has the effect of reducing the maximum speed of the fan. To graphically highlight this engine fan maximal speed reduction, Figure 2.10b shows the ratio δN_1 between the corrected fan speed for ΔISA = 0 and the corrected fan speed for ΔISA $\neq$ 0, as a function of ΔISA.

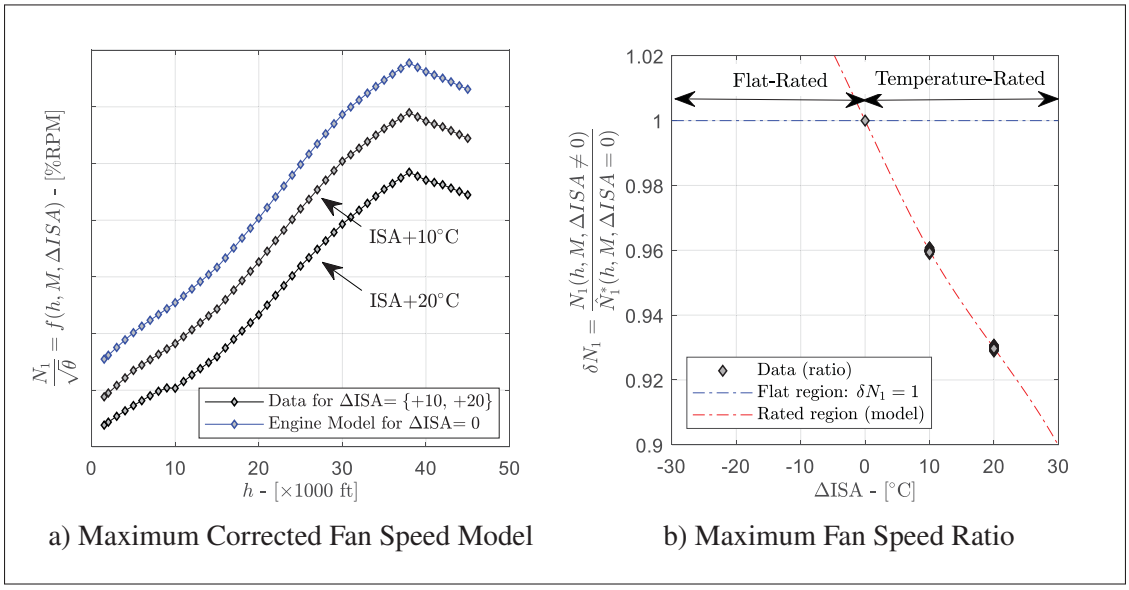

a) Maximum Corrected Fan Speed Model b) Maximum Fan Speed Ratio

Figure 2.10 Identification Results for the Maximum Corrected Fan Speed at ISA Conditions

By analyzing these results, it can be seen that two regions exist. Indeed, the blue curve delimits the flat-rated region where the ratio δN_1 is equal to 1. In this region, the maximum corrected fan speed remains constant whatever the ISA temperature deviation is. However, above the "breakpoint" temperature corresponding to ΔISA = 0°C, the ratio δN_1 computed with the engine performance database reveals that the fan speed is reduced by approximately 4% at ΔISA = 10°C, and by approximately 7% at ΔISA = 20°C. This reduction can be easily modeled by a cubic spline with a smooth factor $\lambda = 0.5$ as illustrated by the red curve in Figure 2.10b.

Step 3 - Effect of the anti-ice systems on the maximum fan speed

Finally, the third and last step of the methodology consisted in modeling the variation of the corrected fan speed due to anti-ice systems. Figure 2.11a shows the fan speed variation as a

function of the altitude for the two climb profiles with the anti-ice systems activated. The data in gray represents the corrected fan speed obtained from the database, whereas the data in blue represents the correct fan speed estimated with the model developed in **Step 1**.

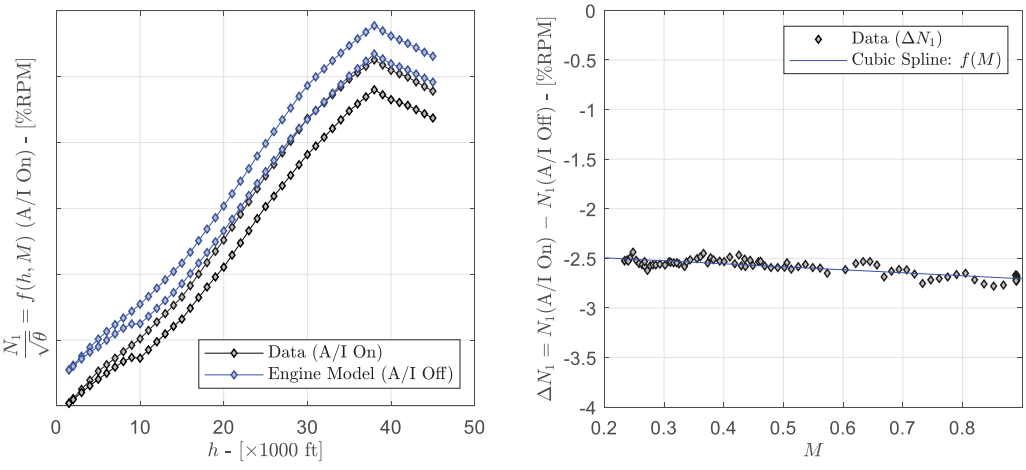

a) Effect of A/I on the Fan Speed

b) Reduction in Fan Speed due to A/I Activation

Figure 2.11 Identification Results for the Maximum Corrected Fan Speed at ISA Conditions

As it can be observed, the anti-ice systems have the effect of reducing the maximum corrected fan speed. Again, to quantify and graphically illustrate such a reduction, Figure 2.11b shows the difference ΔN_1 between the corrected fan speed with anti-ice on obtained from the database, and the corrected fan speed with anti-ice off (estimated from the previous model). Based on this graph, it seems that the activation of the anti-ice systems has the effect of reducing the maximum fan speed by approximately 2.6%RPM, and this whatever the flight condition. Such a reduction can be modeled either by a simple constant or by smoothing the cubic spline with a smooth factor $\lambda = 0$. In both cases, the average relative error is less than 3.6%, while the average absolute residual error remains below 0.1%RPM. These results can be considered as very good, and are sufficient to conclude that the complete model identified in this section represents very well the fan speed variations at maximum climb setting for all flight conditions.

2.3.3.3 Engine Performance Lookup Table Creation

Finally, once all the functional relationships describing the engine performance model were identified, the obtained results were reorganized into lookup tables in order to create the complete engine model according to the structure initially proposed in Figure 2.5. A total of eight lookup tables were generated: five for the thrust ratings, and three for the engine performance (i.e., core speed, thrust and fuel flow). Table 2.3 and Table 2.4 describe the inputs and outputs of the different lookup tables. These lookup tables can now be coupled with a linear interpolation technique to calculate the engine performances for all flight conditions in the Cessna Citation X flight envelope.

Table 2.3 Engine Performance Model Inputs and Outputs (FADEC & Thrust Ratings)

Lookup Table	**Inputs**	**Output**
Flight Idle Setting	Altitude, [ft] Mach number Anti-ice system status [0 or 1]	Corrected Fan Speed, [%RPM]
Maximum Cruise Setting	Altitude, [ft] Mach number ISA deviation temperature, [°C] Anti-ice system status [0 or 1]	Corrected Fan Speed, [%RPM]
Maximum Climb Setting	Altitude, [ft] Mach number ISA deviation temperature, [°C] Anti-ice system status [0 or 1]	Corrected Fan Speed, [%RPM]
Maximum Continuous Setting	Altitude, [ft] Mach number ISA deviation temperature, [°C] Anti-ice system status [0 or 1]	Corrected Fan Speed, [%RPM]
Maximum Takeoff Setting	Altitude, [ft] Mach number ISA deviation temperature, [°C] Anti-ice system status [0 or 1]	Corrected Fan Speed, [%RPM]

Table 2.4 Engine Performance Model Inputs and Outputs
(Engine Performance)

Lookup Table	**Inputs**	**Output**
Engine Core Speed	Corrected Fan Speed, [%RPM] Mach number Anti-ice system status [0 or 1]	Corrected Core Speed, [%RPM]
Engine Thrust	Corrected Fan Speed, [%RPM] Mach number Anti-ice system status [0 or 1]	Corrected Thrust, [lbf]
Engine Fuel Flow	Corrected Core Speed, [%RPM] Mach number Anti-ice system status [0 or 1]	Corrected Fuel Flow, [lb/h]

2.4 Model Simulation and Validation

The last section of the paper presents the results obtained for the validation of the engine performance model. To this end, a series of flight tests was performed using the Level-D Cessna Citation X Research Aircraft Flight Simulator (RAFS) available at the LARCASE laboratory. In order to cover as much as possible the entire flight envelope of the Cessna Citation X, the flight tests were regrouped into four categories: normal takeoff, climb with all engines operative, cruise at constant speed, and idle descent. In parallel, the engine parameters were also computed using the engine performance model. The engine fan speed, core speed, thrust and fuel flow were next compared for all these flight tests categories in order to conclude about the accuracy of the model.

2.4.1 Validation of the Model in Normal Takeoff

To validate the engine performance model for the takeoff, 16 flight tests were conducted in four different airports: Montreal Pierre-Elliott-Trudeau International Airport (CYUL), Mexico City International Airport (MMMX), Washington Dulles International Airport (KIAD), and Innsbruck Airport (LOWI). The reason why these airports were selected is because they all have different ground elevations. For example, CYUL has an elevation of about 100 ft above sea level,

while MMMX is located at 7000 ft above sea level. This difference of ground elevation serves to verify the robustness of the model with respect to different pressure altitudes. Moreover, since the outside air temperature has also a considerable impact on the engine performance, each flight test was realized by imposing different ISA deviations between ISA-40°C and ISA+30°C. Finally, 4 out of the 16 takeoff flight tests were realized by activating the anti-ice systems, and by simulating icing conditions.

To illustrate how each flight test was performed with the RAFS and used to validate the identified engine model, an example of takeoff from CYUL at ISA conditions is given in Figure 2.12.

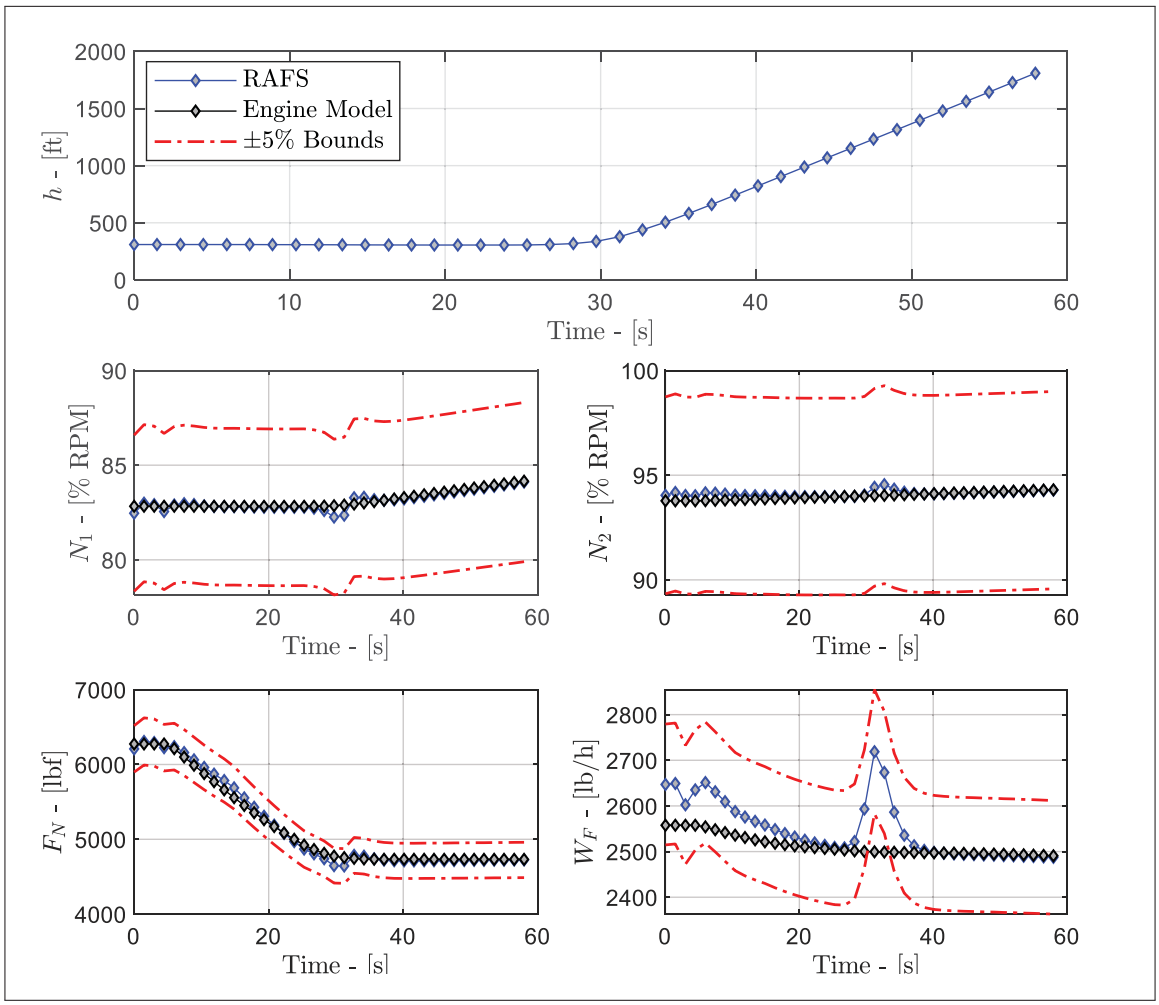

Figure 2.12 Example of Engine Performance Comparison for the Takeoff Flight Phase

In this example, the curves in blue represent the data collected during the flight test, while the gray curves represent the data estimated from the engine performance model. The ±5% tolerance in red was determined based on the Airplane Simulator Qualification Test Guide for the level-D established by the FAA (FAA, AC 120-40B).

From a general point of view, it can be seen that the four engine parameters are well predicted by the model except for a brief instant between 30 and 40 seconds. Indeed, during this interval of time, a "bump" occurs that causes the fuel flow prediction to fall outside the tolerance limits of ±5%. This phenomenon also affects the other three parameters of the engine but in a less pronounced way. Furthermore, it can be noted that this sudden variation seems to occur during the transition between the ground roll phase and takeoff phase (moment when the aircraft leaves the ground).

To understand the reason for this sudden change, it is necessary to take a closer look at the aircraft's pressurization/environment system. Indeed, according to the description provided in the FCOM, and as explained in **Section 2.2.3.2**, each engine of the Cessna Citation X has low pressure and high pressure ports from which compressor discharge air is bled off. Part of this hot and pressurized air is used by the aircraft system to supply the environmental control system and air conditioning system. When the aircraft is on the ground, both systems are supplied by the high-pressure section of the engines, whereas in flight; these systems are supplied by the low-pressure section. This transition between the low- and high-pressure sections causes a disturbance in the fuel control system, which in turn reacts by injecting more fuel into the combustion chamber to stabilize the engine fan speed. This fact can therefore explain the reason why a sudden peak of fuel flow appears during the transition from ground to air.

The comparison shown in Figure 2.12 was repeated for all the 16 takeoff flight tests. The resulting relative errors in core speed, fan speed, thrust and fuel flow are listed in Table 2.5.

As it can be observed in Table 2.5, the maximum relative errors for the fan and core speeds are smaller than 1.0%. Regarding the other two parameters, it can be seen that the average relative

Table 2.5 Engine Modeling Error in Normal Takeoff

Engine Parameter	**Average**	**Standard Deviation**	**Maximum**
Fan Speed (N_1)	0.10%	0.11%	0.95%
Core Speed (N_2)	0.17%	0.20%	0.79%
Thrust Speed (F_N)	1.24%	1.32%	4.82%
Fuel Flow (W_F)	1.28%	1.68%	8.02%

error is around 1.0%, but the maximum error is up to 4.82% for the thrust and up to 8.02% for the fuel flow. Again, these errors can be explained by the ground-to-air transition.

To prove that the fuel flow model was still good despite the maximum error of 8.02%, an additional analysis on fuel consumption was carried out. Figure 13 shows the results of comparisons between the fuel consumption obtained from flight tests conducted with the simulator and the estimated fuel consumption from the model. As it can be seen, the results are very good with a maximum relative error of 1.44% obtained for the flight test number 8. Based on the results, it is possible to conclude that the model represents very well the engine performance for the takeoff flight phase.

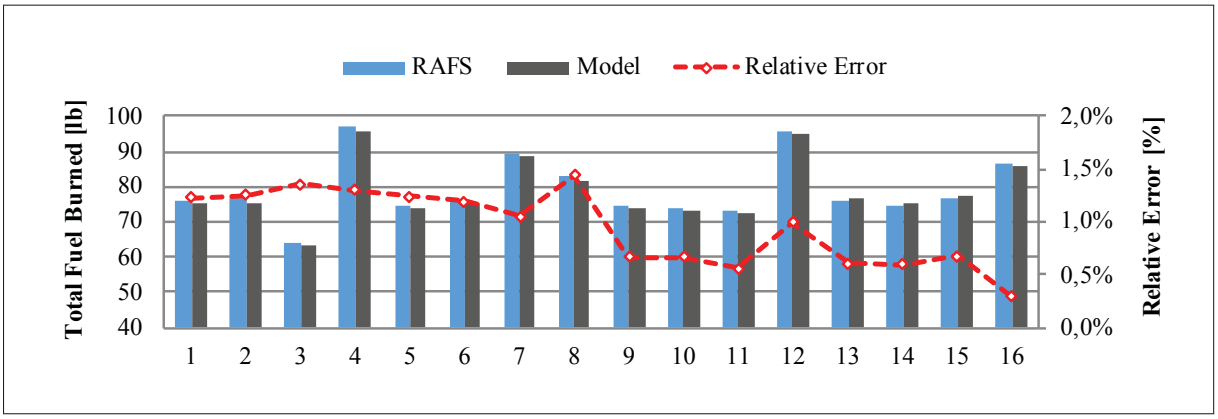

Figure 2.13 Total Fuel Burned Comparison for the Takeoff Phase

2.4.2 Validation of the Model in Climb

To validate the engine performance model in climb, 20 flight tests were performed with the Cessna Citation X flight simulator. Since climbs can be made at two different throttle settings, the flight tests were divided into two series: 10 flight tests were conducted at maximum climb setting (CLB), while the other 10 were performed at maximum continuous setting (TO/MC). In a similar way to the validation of the takeoff phase, each climb test was realized by imposing randomly different ISA temperature deviations between ISA-40°C and ISA+30°C. Finally, for 5 of the 10 flight tests for each series, the anti-ice systems were activated.

Figure 2.14 shows a comparison example for a climb test performed with the Cessna Citation X flight simulator. In this figure, the curves in blue represent the data collected during the flight test, and the gray curves represent the data estimated from the engine performance model. As it can be seen, the aircraft takes approximately 15 min (900 s) to climb from 1500 ft to 40,000 ft. The fan speed and the core speed during the climb vary slightly between 80 and 95%, while engine thrust drops considerably from 4000 lbf at the beginning of the climb to 1,500 lbf at the end of the climb. The fuel flow meanwhile passes from 2200 lb/h to 1100 lb/h, that represents a reduction of about 50%. Regarding the estimations, all the engine parameters are very well predicted with less than 5% of error.

Table 2.6 shows the relative errors obtained over the 20 climb tests for each of the four engine parameters. As it can be observed, the results are very good. Indeed, the average error on all the parameters is less than 1.0%, with a maximum average error of 0.66% for the fuel flow. Regarding the maximum error obtained on the flight tests, here again, the fuel flow has the highest value with a maximum error of 3.37%. However, this error remains acceptable, and it can be concluded that the model is representative enough of the engine performance in climb.

2.4.3 Validation of the Model in Descent

The validation of the descent phase is very similar to the climb validation process, the main difference being the throttle levers position. Indeed, during a typical descent, the pilot places

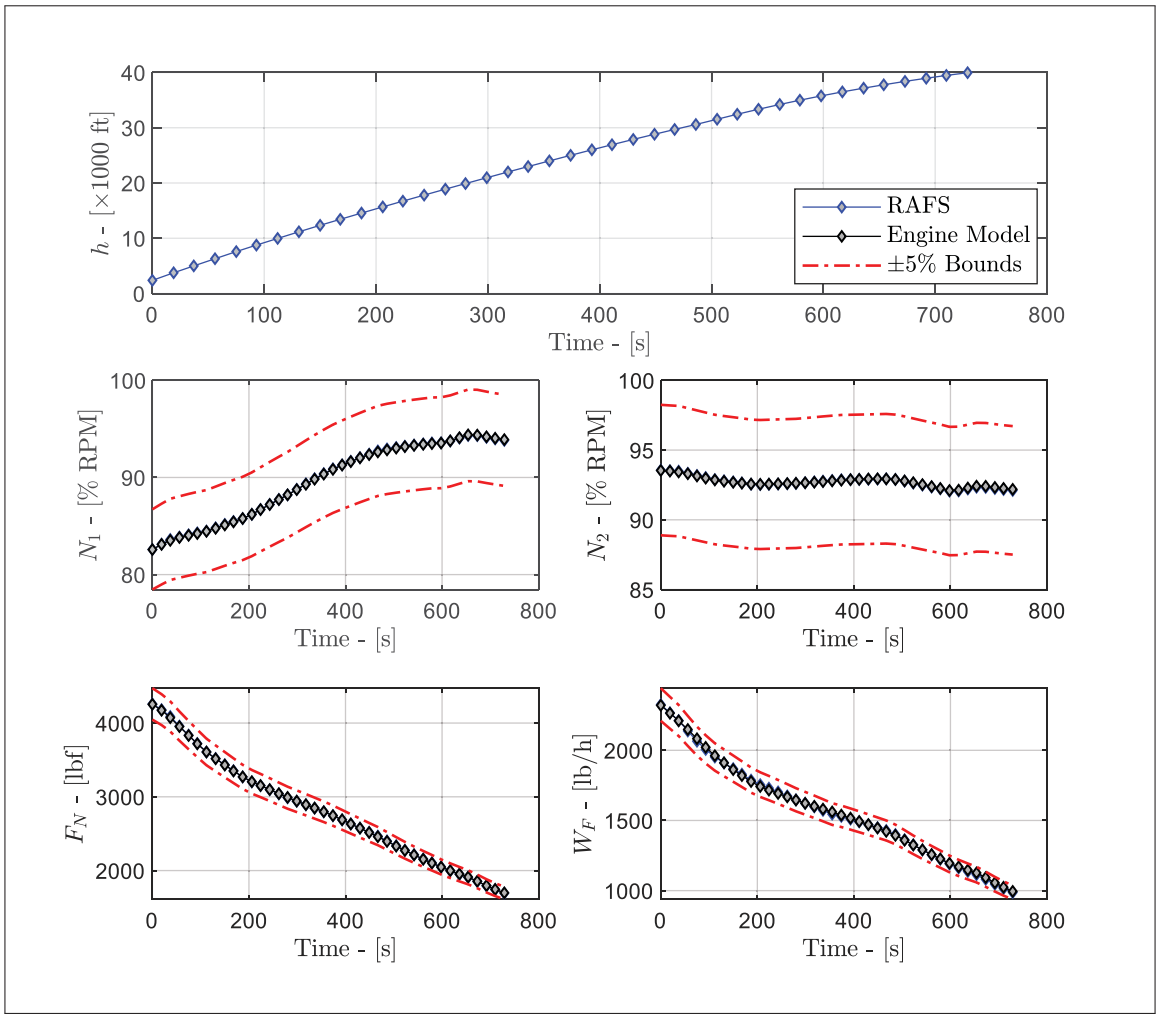

Figure 2.14 Example of Engine Performance Comparison for the Climb Phase

Table 2.6 Engine Modeling Error in Climb

Engine Parameter	**Average**	**Standard Deviation**	**Maximum**
Fan Speed (N_1)	0.03%	0.03%	0.16%
Core Speed (N_2)	0.05%	0.07%	0.41%
Thrust Speed (F_N)	0.13%	0.13%	0.90%
Fuel Flow (W_F)	0.66%	0.62%	3.37%

the thrust levers into the IDLE position. Similarly to the climb phase, the descent phase was validated for 10 flight tests for different ISA temperature deviations and two anti-ice systems

configurations (on/off). The results obtained for this flight phase are given in the following Table 2.7.

Table 2.7 Engine Modeling Error in Idle Descent

Engine Parameter	**Average**	**Standard Deviation**	**Maximum**
Fan Speed (N_1)	0.15%	0.18%	0.97%
Core Speed (N_2)	0.18%	0.17%	0.63%
Thrust Speed (F_N)	1.66%	1.97%	4.58%
Fuel Flow (W_F)	1.38%	1.15%	3.87%

As it can be seen here, the results are globally the same as the results for the climb, with the only exception that the maximum thrust error is found to be slightly higher (4.58% in descent versus 0.90% in climb). As explained in **Section 2.2.3.1**, the IDLE position represents the minimum thrust that the pilot can use during the descent. This level of thrust is established by the manufacturer in order to keep the engine running, to and provide secondary services to the aircraft such as power, hydraulic supply pressure, and cabin pressurization. For this reason, the amplitude of the thrust during the idle descent is very small, or almost zero. In this case, the relative error is not a good estimator since it can take very large values for low absolute errors. However, since all the maximum errors are smaller than 5%, it can be concluded that the model is validated for the descent flight phases.

2.4.4 Validation of the Model in Cruise

The last model validation concerns the cruise phase. To this end, a series of 30 flight tests in cruise were conducted with the flight simulator. These flight tests aimed to stabilize the aircraft at a given altitude and airspeed (i.e., Mach number) selected within the flight envelope. Once the aircraft trimmed, the flight conditions and the four engine parameters were collected for a time period of twenty seconds. The actual engine parameters were next computed by considering their average values over the period of time.

It is important to mention that from a performance point of view, the cruise is a special case where the thrust force is not computed from the engine performance model, but is rather estimated using the aerodynamic model. Indeed, to predict the fuel flow in cruise, the flight management system (or any other trajectory prediction algorithm) considers that the aircraft is always balanced along its longitudinal axis. Consequently, the thrust required to maintain the aircraft speed in cruise should be equal to the drag force, which is estimated from a"lift-to-drag" model. Then, given the required thrust to maintain the aircraft speed and altitude, the engine fan speed is computed. This last parameter becomes therefore the basis for computing the other engine parameters such as the core speed and fuel flow. For this reason, the engine thrust in cruise was assumed to be known.

Based on the engine thrust collected with the flight tests, a reverse lookup table was performed using the engine performance model in order to find the corresponding engine fan speed. Subsequently, based on the estimate of the fan speed, the engine core speed and fuel flow was next computed in a similar way to the other flight phases. Figures 2.15 to 2.16 show the results of the comparison between the engine parameters measured with the flight simulator (RAFS) and the same parameters estimated with the engine model.

Finally, Table 2.8 shows the average, standard deviation and maximum relative error for each of the three engine parameters computed over the 30 flight tests in cruise.

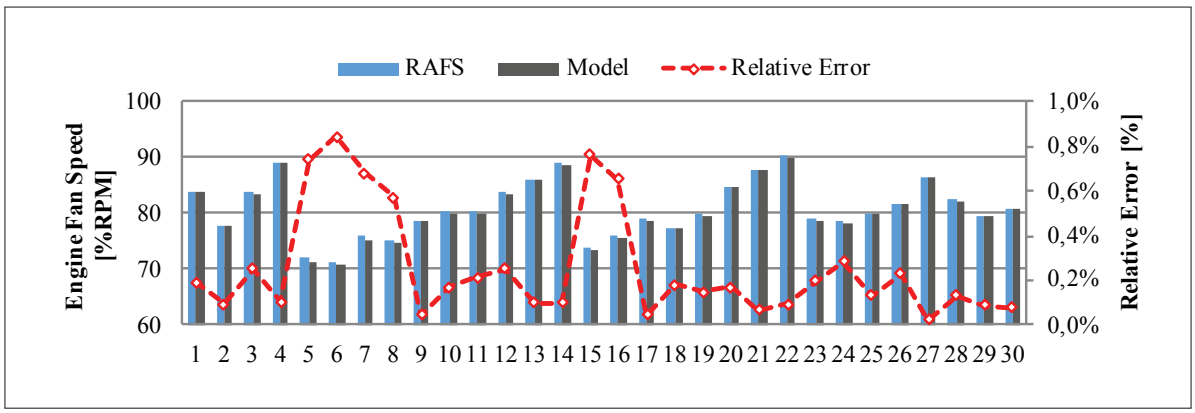

Figure 2.15 Engine Fan Speed Comparison in Cruise

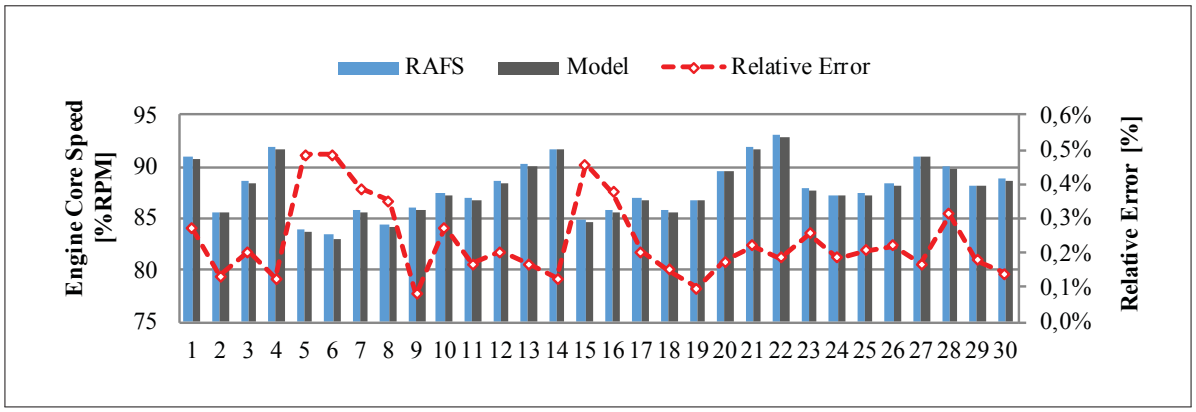

Figure 2.16 Engine Core Speed Comparison in Cruise

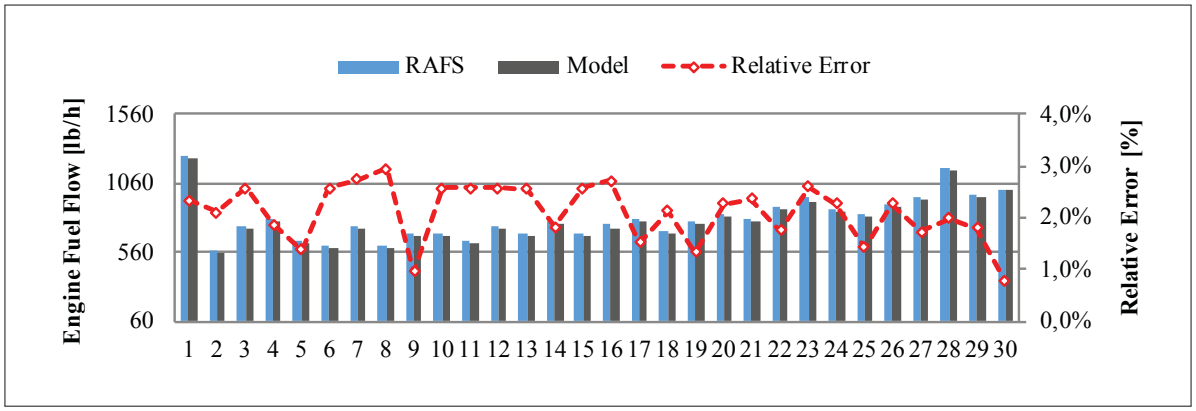

Figure 2.17 Engine Fuel Flow Comparison in Cruise

The results showed that for a given cruise condition, and by assuming that the thrust is known, the model can predict very well the engine performance. Similarly to the others flight phases, the average errors are smaller than 5% with a maximum of 2.10% obtained for the fuel flow.

Table 2.8 Engine Modeling Error in Cruise

Engine Parameter	**Average**	**Standard Deviation**	**Maximum**
Fan Speed (N_1)	0.25%	0.24%	0.84%
Core Speed (N_2)	0.23%	0.11%	0.49%
Fuel Flow (W_F)	2.10%	0.56%	2.96%

Regarding the maximum relative errors, it can be seen that the rotational speeds are predicted with less than 1.0% of error, while the fuel flow is estimated with less than 2.96% of error. These values can be explained by the fact that the fuel flow is more sensitive to a modelling error than the other two parameters. However, it can be concluded that the model remains very accurate in cruise.

2.5 Conclusion

In this paper, a complete and detailed methodology to identify an engine performance model for the Cessna Citation X business aircraft was presented. The general methodology consisted in three main steps. Firstly, an in-depth analysis of the aircraft flight manuals was realized to gather the maximum information regarding the engine propulsion system. An additional source based on computerized trajectories was also required in order to collect enough information regarding the engine thrust. Once the data were gathered, the second part of the methodology focused on the development of a set of fundamental relationships between the engine performances (i.e., core speed, thrust, and fuel flow) and parameters affecting these performances. The use of dimensional analysis technique such as the Buckingham's theorem, have allowed establishing a set of corrected relationships. As it was shown, the advantage of representing the information in this way is that it significantly reduces the number and complexity of variables affecting engine performances. Finally, the third and last part of the methodology consisted in identifying the main equations of the model using curve and surface fitting techniques.

The validation of the methodology was accomplished using data from a Level D Cessna Citation X aircraft research flight simulator designed and manufactured by CAE Inc. According to the FAA, the level-D is the highest qualification level for the flight dynamics and engine propulsion modeling. A total of 76 flight tests were conducted for different flight conditions, and flight phases. By comparing the predictions of the model with the flight tests data performed with the flight simulator, very good results were obtained. Indeed, it was shown that the model was accurate with less than 5% of error except for the takeoff phase where a maximum relative error of 8.02% was obtained for the fuel flow. However, it was demonstrated that despite this

error value, the prediction of the fuel consumption for the takeoff phase was acceptable with a maximum relative error of 1.66%. It was further concluded that the methodology proposed in this paper was adequate and could be used to model other engines.

The model developed in this paper represents the static performances of the Cessna Citation X engine. As a future work, it is desired to complete the actual model by taking into account the engine dynamics. In this way, the model would be more representative of the Cessna Citation X propulsion system, and could be further used in other studies such as aircraft stability/control or aircraft system identification.

CHAPTER 3

NEW METHODOLOGY TO IDENTIFY AN AIRCRAFT PERFORMANCE MODEL FOR FLIGHT MANAGEMENT SYSTEM APPLICATIONS

Georges Ghazi [a], Ruxandra Mihaela Botez [b] and Simon Domanti [c]

[a, b, c] Department of Automated Production Engineering, École de Technologie Supérieure, 1100 Notre-Dame West, Montréal, Québec, Canada H3C 1K3

Paper published in the *AIAA Journal of Aerospace Information Systems*, Vol. 17, No. 6, May 2020, pp. 294-310.
DOI: https://doi.org/10.2514/1.I010791

Résumé

Ce article présente les résultats de validation d'une étude menée au Laboratoire de Recherche en Commande Active en Contrôle, Avionique et AéroSevoÉlasticité (LARCASE) pour développer une technique permettant de déterminer un modèle de performance d'un avion en utilisant une quantité limitée de données. Cette technique a été appliquée au célèbre avion d'affaires à réaction, le Cessna Citation X. Toutes les données de référence utilisées pour concevoir le modèle ont été générées à l'aide d'un programme interne de performances en vol. Ces données ont ensuite été combinées avec des équations simplifiées de mécanique de vol afin d'estimer les diverses performances et caractéristiques aéro-propulsives de l'avion. Un algorithme d'identification a ensuite été développé afin de déterminer un modèle mathématique décrivant le débit de carburant, ainsi que la poussée et le coefficient de traînée de l'avion. La validation de l'étude a été réalisée en comparant des données de trajectoire prédites par le modèle avec des données de trajectoire mesurées avec un simulateur de vol pour la recherche (RAFS) du Cessna Citation X. De très bon résultats ont été obtenus pour le temps de vol, la distance au sol et la consommation de carburant.

Abstract

This paper presents the validation results of a study conducted at the Laboratory of Applied Research in Actives Controls, Avionics, and Aeroservoelasticity (LARCASE) to develop a modeling technique for determining a performance model of a particular aircraft using a limited amount of data. This technique was applied to the well-known business jet aircraft, Cessna

Citation X. All the reference data used to design the model were generated using an in-house in-flight performance program. These data were subsequently combined with simplified flight mechanics equations in order to estimate various performance and aero-propulsive characteristics of the aircraft. An original identification algorithm was next developed in order to determine a mathematical model describing the fuel flow, as well as the aircraft thrust and drag aerodynamic coefficient. Validation of the study was accomplished by comparing trajectory data predicted by the model with trajectory data measured with a research aircraft flight simulator (RAFS) of the Cessna Citation X. The results showed a very good agreement for the flight time, the ground distance traveled, and fuel consumption.

3.1 Introduction

In recent years, the aviation industry has faced many environmental problems such as climate change and greenhouse gas emissions. The impact of aircraft on the environment is mainly related to their engines. By burning fuel, aircraft engines emit various substances such as Carbone Dioxide (CO_2) or Nitrogen Oxides (NO_x), which alter the composition of the atmosphere and contribute to the acceleration of global warming (Lee *et al.*, 2009). In 2017, the aviation industry produced around 2% of global CO_2 emissions, and about 12% from all transports sources (IATA, 2018). However, since air traffic is expected to grow over the next few years, this share could increase significantly (Nygren, Aleklett & Höök, 2009).

In parallel to the environmental aspect, there is also a cost factor. Indeed, “energy is not free”, and fuel constitutes one of the major operating costs of airlines. According to IATA statistics (2018), the fuel bill of the global airline industry in 2018 was estimated at USD 180 billion, representing 23.5% of the operating expenses. Given the fact that the fuel demand is expected to increase from 1.9% to 2.6% annually until 2026, the long-term economy of the airlines could be strongly affected. As a result, any strategy to reduce fuel consumption could be a competitive advantage. In addition, by reducing fuel consumption, airlines are helping to reduce CO_2 emissions, creating a “win-win” scenario.

To address this dual ecological and economical challenge, various research programs have been initiated to develop new technologies and designs that could sustainably increase aircraft fuel efficiency. Some examples of promising solutions include the development of more efficient engine (Haselbach *et al.*, 2015; Brouckaert, Mirville, Phuah & Taferner, 2018), the use of lighter material to reduce aircraft weight (Marsh, 2012; Calado *et al.*, 2018), the design of new wing shape to improve aerodynamic efficiency (Apuleo, 2018; Segui & Botez, 2018; Segui *et al.*, 2018), the development of modern avionics systems (Ramasamy, Sabatini, Gardi & Kistan, 2014; Sabatini, Gardi, Ramasamy, Kistan & Marino, 2015; Li & Hansman, 2018), and the optimization of aircraft flight trajectories (Jensen *et al.*, 2014; Murrieta-Mendoza *et al.*, 2017a,b). It is in this last context that the study presented in this paper focuses.

3.1.1 Research Problematics and Motivations

The success of flight trajectories optimization has greatly encouraged airlines to exploit advanced flight-planning systems such as the Flight Management System (FMS). In service since the early 80's, the FMS is an avionics system whose main function is to find the most efficient route the aircraft should follow in order to minimize time and fuel costs (Walter, 2001). To accomplish this, the FMS requires various optimization algorithms as well as a mathematical definition of the aircraft performance. The word "performance" in this context refers to the motion of the aircraft in a vertical plan (i.e., altitude, distance traveled and flight time), and to the amount of fuel required to fly from take-off to landing.

The typical structure of an aircraft performance model includes two main elements; a set of differential equations used to describe the motion of the aircraft, and a performance database. The latter usually consists of a series of lookup-tables containing the engine and aerodynamic data, and is used to model the aero-propulsive characteristics of the aircraft (Sibin *et al.*, 2010). Since the reliability of the optimal trajectory calculated by the optimization algorithms is mainly based on the rationality of the performance model (Sibin *et al.*, 2010), it is therefore essential that the performance database reflects very well the actual aero-propulsive characteristics of the aircraft.

Obviously, the most reliable sources of information for creating an authentic performance database are the reports and documents produced by aircraft manufacturers. However, because of the highly competitive nature of the aviation sector, this information is generally considered as strictly confidential and, therefore is very difficult to access. These restrictions in obtaining aircraft/engine data forces FMS manufacturers to design expensive, limited or strictly licensed performance models. For this reason, studies are conducted at the Laboratory of Applied Research in Active Controls and AeroServoElasticity (LARCASE) to elaborate modeling techniques that could help manufacturers and researchers in developing aircraft performance models from a limited number of data.

3.1.2 Aircraft Performance Modelling Techniques

Currently, one of the best alternatives to access aircraft performance data is the Base of Aircraft Data (BADA, family 3). BADA is a comprehensive collection of more than 300 aircraft models developed and maintained by Eurocontrol (Nuic *et al.*, 2010). Each model in BADA is characterized by a set of aircraft-specific coefficients used for drag, lift, thrust and fuel flow calculations. According to the "BADA Performance Modelling Report" (Poles, 2009), these coefficients are derived from various information available in the aircraft flight manuals or in equivalent documents. Different climb, cruise and descent profiles data are combined with the Least Squares (LS) technique to identify the coefficients for thrust, drag and fuel flow models that satisfy the rate of climb/descent and fuel consumption data. Although widely accepted as a reference for trajectory prediction and simulation applications, studies have shown that the models of the BADA family do not robustly represent the aircraft behavior over the entire flight envelope (Nuic *et al.*, 2005, 2010).

In 2005, a new version of BADA (BADA family 4) was introduced with the objective of improving the accuracy of the previous models (Nuic *et al.*, 2005). This action was accomplished by modifying the model equations and using more detailed reference data from manufacturers. However, this version is available under strict license restrictions, which considerably limits its use.

Another alternative to estimate the aero-propulsive characteristics of an aircraft is to use empirical models. These models involve approximating the drag, thrust and specific fuel consumption of an aircraft through very simple relationships in the form of polynomials or power laws. Many of these models are readily available in various aircraft design textbooks (Ojha, 1995; Howe, 2000; Raymer, 2012). Filippone (2008), for instance, provided a very comprehensive study on the prediction of drag and lift coefficients for transport aircraft using semi-empirical models. Similarly, Bartel & Young (2008) investigated previously published empirical models to predict the thrust and fuel consumption of a modern turbofan during takeoff, climb and cruise. Ghazi *et al.* (2015c) and Botez *et al.* (2019) used different empirical equations to model the engine thrust and fuel flow of a Cessna Citation X. Camilleri *et al.* (2012) designed a lift and drag models for an Airbus A320 based on equations provided by Ojha (1995) and Asselin (1997). Researchers have also considered the possibility of combining empirical equations with open source data such as the Jane's all the Word's Aircraft Database or the ICAO Engine Emission Databank to design performance models as proposed by Metz *et al.* (2016) and Sun *et al.* (2019).

Although practical and useful, empirical equations are usually too simplified and do not accurately represent the behavior of the aircraft over its entire flight envelope. Moreover, they are not universally valid for all types of aircraft/engines, especially for modern turbofan engines exhibiting non-linear characteristics.

An aircraft performance model can also be defined in terms of excess-thrust (i.e., thrust minus drag) or excess-power. A considerable advantage of this type of model is that it can be identified from a set of known climb/descent trajectory data, without the need for information on aerodynamics or the propulsion system. However, this approach has so far been explored by very few researchers, including Ghazi *et al.* (2015b; 2015a) and Tudor (2017). This is due to the fact that performance models defined in terms of excess-thrust have limited applications because the individual values of thrust and drag are not independently known (Marshall & Schweikhard, 1973). Moreover, since the excess-thrust during cruise is by definition zero, this model cannot be extended or adapted for this portion of the flight.

The problem of separating individual variations of thrust and drag can be solved by postulating an engine model, and by deducing the drag model accordingly. Gong & Chan (2002) used this technique to determine a performance model for a Boeing 737-400 in climb. In their study, the authors used available engine data for a Pratt and Whitney PW4056 to model the thrust variation of a CFM56-3B-1. A similar approach was also considered by Cavcar & Cavcar (2004), and by Baklacioglu & Cavcar (2014) who used data of a Pratt and Whitney JT9D-7A provided by McCormick (1995) to design a model of thrust and fuel consumption for a CFM56-3B-1. The engine model was next combined with a set of climb trajectory data obtained from the flight manual to identify a drag model for a Boeing 737-400. Cavcar and Cavcar concluded that any combination of thrust/drag models that accurately reflects the rate of climb can be used to develop aircraft performance to study climb trajectories. However, Gong and Chan suggested that additional research should be conducted as attempts to apply their technique to the descent phase did not yield satisfactory results.

Most recently, researchers have developed techniques to estimate aircraft performance parameters using ADS-B (Automatic Dependent Surveillance Broadcast) data (Sun *et al.*, 2018b, 2020). This technology allows aircraft to periodically share their status parameters such as position, altitude, heading, ground speed, and vertical speed. However, the main drawback of ADS-B data is the lack of information regarding the aircraft weight and fuel consumption. Indeed, airlines consider the mass of their aircraft as a very sensitive parameter and are therefore reluctant to share this information. Although several researchers have elaborated techniques to predict the aircraft weight at takeoff (Sun, Ellerbroek & Hoekstra, 2017, 2018a), these methods do not yet allow to accurately estimate the weight of the aircraft for other phases of flight.

3.1.3 Research Objectives and Paper Organization

The objective of this paper is to propose a new modelling technique for determining a performance model for the flight envelope of an aircraft using a limited number of reference data. The originality of the proposed technique lies in the fact that no engine data or a priori model was necessary to identify the performance model. In addition, unlike studies previously mentioned,

the one presented in this paper is not limited to the climb phase, but it also considers the cruise and descent phases. The proposed technique was applied to the well-known Cessna Citation X business jet aircraft, for which a Level D Research Aircraft Flight Simulator (RAFS) was available at the LARCASE laboratory (see Figure 3.1). According to the Federal Aviation Administration (FAA), the level D corresponds to the highest qualification level for the flight dynamics and engine modeling.

Figure 3.1 Cessna Citation X Research Aircraft Flight Simulator

The remainder of this paper is structured as follows: **Section 3.2** presents the main equations considered in this study to model the behavior and the aero-propulsive characteristics of the Cessna Citation X. **Section 3.3** discusses the different steps of the proposed technique for determining a model of thrust, drag and fuel flow. **Section 3.4** is dedicated to the validation of the performance model, and to the discussion of the results. Finally, the paper ends with a conclusion and future works.

3.2 Mathematical Background and Aircraft Performance Model

The purpose of this section is to present the main equations considered in this study needed to model the performance of the Cessna Citation X. To this end, the section begins firstly with

a general presentation of the aircraft. The section then continues with the development of the equations of motion that will form the basis of the mathematical equations structure of the performance model. These equations are then supplemented by the equations of the aerodynamic model required to obtain the lift and drag forces of the aircraft. Finally, the main mathematical relationships describing the engine performance in terms of thrust and fuel flow are presented.

3.2.1 Cessna Citation X Aircraft Description

The aircraft considered in this study is the Cessna Citation X model 750, produced and manufactured by the US-American manufacturer Cessna Aircraft Company (that became a brand of Textron Aviation in 2014). The Citation X is a medium-sized business jet aircraft designed to fly at a maximum operating altitude of 51,000 ft, and at a maximum operating Mach number of 0.92. To achieve these performances, the aircraft is equipped with two high-bypass Rolls-Royce AE3007C-1 turbofan engines, installed at the rear of its fuselage. Each engine is capable of producing a maximum sea level static thrust of 6442 lbf (28.65 kN) for an average fuel consumption of 2712 lb/h (1230 kg/h). With its powerful engines and well-designed aerodynamics, the Citation X has a maximum range of 3091 nautical miles (5724 km), which allows it to fly from Montreal to Paris.

Other relevant specifications and limitations of the Cessna Citation X are given in Table 1 for the convenience of the reader (Cessna Aircraft Company, 2002). This information was considered in this study to determine the normal operating flight envelope of the aircraft, but also to define the limits of the performance model that will be identified later.

3.2.2 Simplified Aircraft Equations of Motion in a Vertical Plane

The behavior of an aircraft can be modeled using different approaches depending on the intended use. In general, for the study of flight performance, the most practical approach consists in approximating the aircraft by a variable-weight point-mass, and in restraining its motion in a vertical plane over a “flat non-rotating earth” (Ojha, 1995; Howe, 2000; Raymer, 2012). This

Table 3.1 Cessna Citation X Specifications and Limitations

Parameters	**Values**
Altitudes	
Maximum Certified Altitude	51,000 ft 15,545 m
Typical Cruise Altitudes	37,000 – 45,000 ft
Airspeed Limitations	
Maximum Operating Mach number	Mach 0.92
Maximum Operating Speed (Below 8,000 ft)	270 KCAS 500 km/h
Maximum Operating Speed (Above 8,000 ft)	350 KCAS 649 km/h
Weight Limitations	
Maximum Takeoff Weight	36,100 lb 16,375 kg
Maximum Landing Weight	31,800 lb 14,424 kg
Maximum Zero Fuel Weight	24,400 lb 11,067 kg

model, sometimes referred to as the "point-mass" model in the literature, also considers that all the forces influencing the accelerations of the aircraft are directly applied to its center of gravity.

As illustrated in Figure 3.2, the forces acting on the aircraft can be decomposed into four main components. By convention, the lift L and the drag D are the aerodynamic forces, and are defined normal and parallel to the flight path, respectively. The total thrust of the engines, denoted by F_N, is oriented in the forward direction making an angle ϕ_T relative to the aircraft fuselage. Finally, the weight W is oriented towards the center of the Earth.

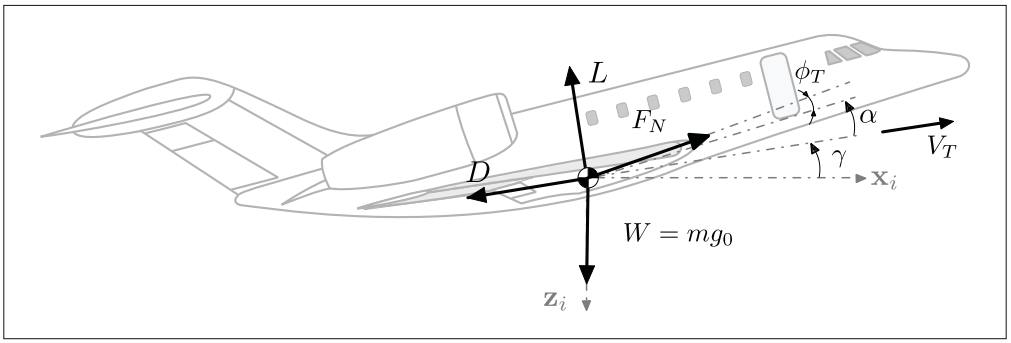

Figure 3.2 Forces Applied to the Cessna Citation X

In order to reduce the number of unknown parameters, and thus to facilitate the identification of all the coefficients that will define the aircraft performance model, several approximations can be considered for it. These approximations are listed here. The engine inclination angle with respect to the aircraft fuselage is relatively small. Similarly, the angle of attack (denoted by α in Figure 3.2) during normal operating conditions is also small in order to minimize drag, but also to prevent the aircraft from stalling. Under these conditions, the thrust direction can be assumed to be collinear with the flight speed (i.e., $\phi_T = \alpha = 0$ deg). The angular accelerations as well as the side-slip angle are neglected, and only quasi steady maneuvers in the vertical plane defined by altitude and horizontal distance are considered. Finally, the atmosphere is supposed to be at rest (i.e., no winds), and its properties are known functions of the altitude.

Thus, given all these simplifications, the equations of motion of the aircraft can be written as follows:

$$m\dot{V}_T = F_N - D - mg_0 \sin(\gamma) \tag{3.1}$$

$$L = mg_0 \cos(\gamma) \tag{3.2}$$

$$\dot{h} = V_T \sin(\gamma) \quad \text{and} \quad \dot{x} = V_T \cos(\gamma) \tag{3.3}$$

where m is the aircraft mass, V_T is the true airspeed, γ is the flight path angle, g_0 is the acceleration due to gravity, $\dot{h}$ is the vertical speed, and $\dot{x}$ is the aircraft ground speed. The last two parameters represent the aircraft velocity components in the vertical and horizontal axes, respectively. Consequently, Eq. (3.3) leads by integration to the altitude h, and to the horizontal distance traveled x (also referred to as ground distance or range).

In addition to the set of equations (3.1) to (3.3), the mass variation of the aircraft is modeled as follows:

$$\dot{m} = -W_F \Rightarrow \Delta m = \Delta F_B = W_F \times \Delta t \tag{3.4}$$

where W_F is the engines fuel flow, and ΔF_B is the fuel burned by the two engines during the time interval Δt.

3.2.3 Lift and Drag Aerodynamic Model

The lift and drag forces in Eqs. (3.1) and (3.2) constitute the two components of the aerodynamic resultant acting on the aircraft. A conventional way of expressing these two forces is to represent their variations using dimensionless aerodynamic coefficients defined as:

$$L = 0.5\rho S V_T^2 C L_s \tag{3.5}$$

$$D = 0.5\rho S V_T^2 C D_s \tag{3.6}$$

where ρ is the static air density, S is the reference wing surface of the aircraft, and CL_s and CD_s are the dimensionless lift and drag coefficients, respectively.

For subsonic flight regimes, where typical commercial aircraft are designed to fly, the drag coefficient and the lift coefficient are closely related by a fundamental equation, called the "drag polar equation". According to various references in the literature (Ojha, 1995; Howe, 2000; Raymer, 2012), the drag polar equation can be expressed in its simplest form (by neglecting the camber effect of the wing) as follows:

$$CD_s = CD_0(M) + K(M)CL_s^2 \tag{3.7}$$

where M is the Mach number, CD_0 is the zero-lift drag coefficient, and K is the lift-dependent drag coefficient factor. It must be emphasized that the drag polar model in Eq. (3.7) is generally used to represent the aerodynamic characteristics of a wing. However, by assuming that the drag of an aircraft is mainly influenced by the characteristics of its wing, this equation can be generalized to the entire aircraft.

In order to understand the influence of the Mach number, and to subsequently propose a mathematical model for CD_0 and K, typical variations of these two quantities for a Boeing 767 are shown in Figure 3.3a and Figure 3.3b , respectively McCormick (1995). As seen on these figures, the two parameters have similar variations with respect to the Mach number. Indeed, at relatively low speeds, there is no noticeable influence of the Mach number, and both parameters

seem to remain constant up to Mach 0.7. However, as the Mach number increases above Mach 0.7, both CD_0 and K begin to increase rapidly by following a power law behavior. This sudden change in trend is caused by compressibility effects and other complex aerodynamic phenomena that typically occur in the transonic region.

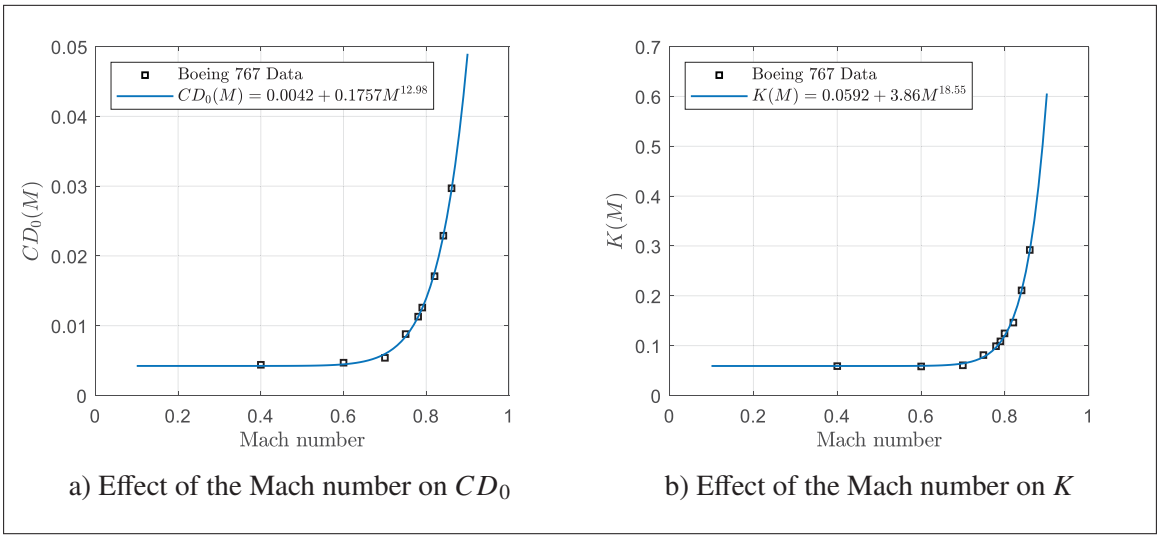

a) Effect of the Mach number on CD_0 b) Effect of the Mach number on K

Figure 3.3 Effect of Mach number on CD_0 and K for a Boeing 767

Based on these observations, it was here considered that the two parameters CD_0 and K could be approximated by two power functions, such as:

$$CD_0(M) = p_1 + p_2 M^{p_3} \tag{3.8}$$

$$K(M) = p_4 + p_5 M^{p_6} \tag{3.9}$$

where $\mathbf{p} = \{p_1, p_2, \ldots, p_6\}$ are unknown coefficients that depend on the wing and aircraft geometry. Although these two equations have been obtained semi-empirically, they nevertheless have a physical meaning. Indeed, it is easy to recognize that the two coefficients p_1 and p_4 represent the values of CD_0 and K for low Mach numbers. Conversely, the coefficients p_2 and p_5 makes it possible to model the increase of the two parameters with high Mach numbers, where compressibility and transonic effects are not negligible. Finally, the two power coefficients

p_3 and p_6 are used to adjust the "transition point" from which the compressibility and transonic effects must be considered.

To test, and then to validate the proposed models, the two relationships in Eqs. (3.8) and (3.9) are used to approximate the Boeing 767 data previously shown in Figure 3.3. The coefficients $\mathbf{p} = \{p_1, p_2, \ldots, p_6\}$ that best fit these data are estimated using the Levenberg-Marquardt algorithm available in the Matlab Optimization Toolbox. The corresponding results are represented by solid lines in Figure 3.3a and Figure 3.3b, respectively. As seen in these figures, the models match well the data at both low and high speeds. The maximum absolute error was found to be 5.52×10^{-4} for CD_0 at Mach 0.7, and 0.01 for K at Mach 0.8. In addition, the two models reflect very well the global trend of the parameters with a "flat region" up to Mach 0.6, then with an "power shape" above Mach 0.6~0.7.

Based on these results, the relationships proposed in Eqs. (3.8) and (3.9) were assumed to be sufficiently reliable to model the drag polar of the Cessna Citation X.

3.2.4 Engine Thrust and Fuel Flow Model

To complete the aircraft model that will be used in the remainder of this paper, additional relationships to describe the characteristics of an engine were required. In general, for aircraft performance analyses, the desired engine characteristics are the thrust and fuel flow. The former is used to predict the aircraft motion, while the latter is used to estimate the fuel consumption. According to several textbooks on engine performance (Torenbeek, 2013; Young, 2017), the thrust and the fuel flow of a turbofan engine can be described using the following functional relationships:

$$\frac{F_N}{\delta} = f\left(\frac{N}{\sqrt{\theta}}, M\right) \tag{3.10}$$

$$\frac{W_N}{\delta\sqrt{\theta}} = f\left(\frac{N}{\sqrt{\theta}}, M\right) \tag{3.11}$$

where δ is the relative ambient pressure ratio, and θ is the relative ambient temperature ratio. Note that the function f(x,y) in the above equations is used to simplify the general notation "a function of x and y".

The parameter $N/\sqrt{\theta}$ in Eqs. (3.10) and (3.11) is the corrected engine fan speed, defined as the ratio between the engine fan speed and the square root of the temperature ratio. This parameter reflects the engine power, and can be controlled by the pilot using the thrust levers (i.e., throttles) located in the cockpit. Basically, as the pilot advances the throttles, a signal is sent to the engine control system to increase the fan speed, resulting in greater thrust. However, to prevent engine components from operating beyond their design limits, manufacturers set thrust limits that should never be exceeded. These limits are called thrust ratings and define the maximum fan speed that the pilot can command under specific operating conditions (i.e., flight phase, altitude, Mach number and temperature) (Ghazi & Botez, 2019).

The corrected engine fan speed for a specific thrust rating can therefore be expressed in a functional form such as:

$$N_c = f(h, M) \times g(h, \Delta\text{ISA}) \tag{3.12}$$

where $N_c \equiv N/\sqrt{\theta}$ is the corrected fan speed, $f(h, M)$ describes the variation of the corrected fan speed as function of altitude and Mach number, and $g(h, \Delta\text{ISA})$ quantifies the influence of temperature on the fan speed.

The result in Eq. (3.12) can be generalized to the thrust and fuel flow in Eqs. (3.10) and (3.11) in order to obtain:

$$F_{N,c} = f(h, M) \times g(h, \Delta\text{ISA}) \tag{3.13}$$

$$W_{F,c} = f(h, M) \times g(h, \Delta\text{ISA}) \tag{3.14}$$

where $F_{N,c} \equiv F_N/\delta$ is the corrected thrust, and $W_{F,c} \equiv W_F/(\delta\sqrt{\theta})$ is the corrected fuel flow. A significant advantage of representing the engine performance in this form is that it results in an implicit functional relationship between the engine performance and flight conditions.

It is important to emphasize that the results shown in Eqs. (3.13) and (3.14) are only valid for certain flight phases in which the throttles are maintained at a fixed position (i.e., for a given thrust rating). This is typically the case for the climb and descent phases where the pilot sets the throttles to the maximum climb and idle positions, respectively. However, there are other flight phases, such as the cruise for example, where the pilot must adjust the throttles position to obtain the thrust required to maintain the flight speed. Therefore, for these particular flight phases, the thrust is generally known, and the fuel flow must be estimated accordingly by using an appropriate relationship. Such a relationship can be obtained by combining Eqs. (3.10) and (3.11), and by eliminating the parameter $N/\sqrt{\theta}$ to yield:

$$W_{F,c} = f(F_{N,c}, h) \tag{3.15}$$

Based on the analysis provided in this section, it was concluded that the model describing the engine performance of the Cessna Citation X should include a total of seven functional relationships, grouped as follows:

- Engine Performance at Idle Thrust Setting:

$$F_{N,c}^{IDL} = f_1(h, M) \times g_1(h, \Delta\text{ISA}) \tag{3.16a}$$

$$W_{F,c}^{IDL} = f_2(h, M) \times g_1(h, \Delta\text{ISA}) \tag{3.16b}$$

- Engine Performance at Maximum Climb Thrust Setting:

$$F_{N,c}^{CLB} = f_3(h, M) \times g_2(h, \Delta\text{ISA}) \tag{3.16c}$$

$$W_{F,c}^{CLB} = f_4(h, M) \times g_2(h, \Delta\text{ISA}) \tag{3.16d}$$

- Thrust-to-Fuel Model (All Flight Phase):

$$W_{F,c}^{ALL} = f_5(F_{N,c}, M) \tag{3.16e}$$

where $\{f_1, \ldots, f_5\}$ and $\{g_1, g_2\}$ are unknown mathematical functions that must be identified.

Finally, unlike for the drag polar equation, it may be difficult to propose general expressions for the functions $\{f_1, \ldots, f_5\}$ and $\{g_1, g_2\}$ without reliable engine data. This difficulty is mainly due to the complexity of turbofan engines, but also to the fact that thrust ratings are the result of optimization processes that are specific to each engine and each manufacturer. This is the reason why the study presented in this paper does not attempt to propose new empirical equations to model the thrust and fuel flow of an engine, but rather a practical methodology for identifying a model for these two quantities.

3.3 Methodology: Aircraft Performance Model Identification

Now that all the mathematical relationships defining the aircraft performance model have been introduced, the complete methodology developed at the LARCASE laboratory to identify a drag, thrust and fuel flow model for the Cessna Citation X can be presented. To this end, this section begins with a description of the tools used in this study to generate a set of trajectory data for the Cessna Citation X. The section then continues with the main part of this paper, namely the identification technique description. In order to explain well the different steps of the proposed technique, the methodology is firstly applied to the descent, then adapted to the climb and cruise phases. Finally, the identified relationships describing the aero-propulsive characteristics of the aircraft are used to create the performance database necessary for the operation of the FMS.

3.3.1 Aircraft Trajectory Data Gathering

Before launching into the details of the identification process, it was first necessary to gather a set of reference data reflecting the Cessna Citation X performance over normal operating conditions. For this purpose, an In-Flight Performance (IFP) program developed by the LARCASE research team in previous studies (Ghazi, 2014; Ghazi & Botez, 2015) was used. The IFP program is a simulation platform designed in Matlab/Simulink to evaluate the performance of the Cessna Citation X over a range of altitudes, speeds and gross weights specified by the user. This program was also designed in order to allow users to simulate the aircraft performance during various flight scenario such as climb, cruise, or descent. Moreover, each scenario can be executed with

different options. A descent, for example, can be performed at idle thrust setting, fixed rate of descent or fixed flight path angle.

In order to collect enough information to robustly represent the Cessna Citation X performance over its operating flight envelope, two categories of data were considered. The first category consisted of climb and descent trajectory data, while the second category consisted of static cruise performance data.

3.3.1.1 Climb and Descent Trajectory Data

Climb trajectories were simulated at maximum climb thrust, and at combinations of constant Calibrated Airspeed (CAS) and Mach number. Since the take-off phase was not considered in this study, the initial altitude was set at 1500 ft. However, for climb profiles where the initial climb speed was higher than 270 KCAS (kts-CAS), the initial altitude was changed to 8000 ft to comply with the speed limitation of the aircraft (see Table 3.2). Similarly, the final altitude was set to 45,000 ft, since this altitude corresponds to the highest typical cruise altitude of the Cessna Citation X.

Table 3.2 Example of Climb Flight Profile Data generated by the IFP Program

Flight Profile Definition				**Aircraft Trajectory Data**		
Altitude [ft]	ΔISA [°C]	CAS [kts]	Mach	Time [min]	Distance [n miles]	Fuel [lbs]
1500	10.0	240	0.388	0.00	0.000	0.0000
2000	10.0	240	0.391	0.15	1.090	10.340
3000	10.0	240	0.398	0.46	1.450	31.420
⋮	⋮	⋮	⋮	⋮	⋮	⋮
43,000	10.0	195	0.70	20.31	71.56	820.64
44,000	10.0	190	0.70	22.52	79.85	866.49
45,000	10.0	186	0.70	24.95	88.43	906.50

In order to obtain “sufficient” data to represent accurately the performance of the Cessna Citation X in climb and descent, 12 flight profiles were generated using the IFP program. These profiles were selected as follows:

- 3 climb profiles at ISA conditions, covering a range of operating speeds (190 KCAS, 250 KCAS / 0.70M, and 340 KCAS / 0.87M);
- 3 climb profiles for one operating speed (250 KCAS / 0.70M), and for three temperature deviation conditions (ISA-10°C, ISA+15°C and ISA+20°C);
- 3 descent profiles at ISA conditions covering a range of operating speeds (190 KCAS, 0.70M / 250 KCAS, and 0.87M / 340 KCAS);
- 3 descent profiles for one operating speed (250 KCAS / 0.70M), and for three temperature deviation conditions (ISA-10°C, ISA+15°C and ISA+20°C).

The range of operating speeds was established based on the speed limitations of the Cessna Citation X. Indeed, the lower limit of 190 KCAS corresponds to the recommended single engine enroute climb speed, while the upper limits of 340 KCAS and Mach 0.87 were determined by imposing a safety margin of 10 KCAS with respect to the maximum operating speed (i.e., 350 KCAS), and a safety margin of 5% with respect to the maximum operating Mach number (i.e., 0.92M). For the sake of simplicity, the same speed range has been applied for the descent profiles.

Finally, since the drag, thrust and fuel flow models defined in **Sections 3.2.3** and **3.2.4** were not directly related to the aircraft weight, only one medium weight configuration was considered. This weight was estimated by computing an average value between the maximum takeoff weight (i.e., 36,100 lb) and the maximum zero fuel weight (i.e., 24,400 lb), which gave approximately 30,000 lb.

3.3.1.2 Static Cruise Performance Data

Static cruise performance data provides information on the fuel flow required to operate the aircraft in level flight for a given combination of altitude, flight speed, aircraft weight and atmospheric conditions.

In order to obtain sufficient data to represent the variation of the fuel flow of the engines in cruise, a total of 45 flight conditions were considered. These flight conditions were chosen by varying the altitude from 21,000 to 45,000 ft with an increment of 3,000 ft, and by selecting five different Mach numbers for each altitude, as shown in Table 3.3. Note that the values presented in this table have been modified due to industrial confidentiality reasons, and the structure of the table has been rearranged in order to show only the essential information.

Table 3.3 Example of Static Cruise Data generated by the IFP Program

Pressure Altitude	**Atmospheric Conditions** Standard (ISA+00°C)					
21,000 [ft]	Mach	$0.58^{(1)}$	0.57	0.63	0.70	$0.76^{(2)}$
	W_F [lb/h]	1987	2109	2183	2260	2379
24,000 [ft]	Mach	$0.52^{(1)}$	0.59	0.66	0.73	$0.79^{(2)}$
	W_F [lb/h]	1701	2087	2445	2926	3452
⋮	⋮	⋮	⋮	⋮	⋮	⋮
45,000 [ft]	Mach	$0.78^{(1)}$	0.80	0.82	0.83	$0.84^{(2)}$
	W_F [lb/h]	1407	1463	1524	1601	1616

Each of the five Mach numbers corresponded to a specific thrust level between the maximum range thrust (indexed by 1 in Table 3.3) and the maximum cruise thrust (indexed by 2 in Table 3.3). The first one is the thrust level for which the fuel flow is the lowest, while the second one is the thrust level for which the aircraft flight speed is the highest. Regarding the temperature deviation, since the thrust-to-fuel model in Eq. (3.15) accounts for temperature variation, only standard atmospheric conditions (i.e., ΔISA = 0) were considered. Finally, as for the climb and descent, only one medium weight (i.e., 30,000 lb) was used for all flight conditions.

3.3.2 Corrected Fuel Flow, Corrected Thrust and Drag Coefficient Model Identification

Now that enough reference data has been collected, the methodology for determining a model for the corrected fuel flow, corrected thrust and drag coefficient can be presented. As a reminder, these three quantities are described by a total of nine functional relationships; two for the drag polar equation (CD_0 and K), five for the corrected engine performance at ISA conditions (f_1 to f_5), and two for the effects of the temperature on the engine performance (g_1 and g_2). However, to simplify the identification process, the methodology is first applied to the descent, and then adapted for the other flight phases. The descent was selected first because it readily lends itself to some simplifications that facilitate the identification of certain parameters.

3.3.2.1 Identification of a Corrected Fuel Flow Model in Descent

The first step in the identification process was to identify a model for the corrected fuel flow in the descent phase (i.e., at idle thrust setting). Since this parameter was not directly available in the reference data generated by the IFP program, it was determined by using a first-order approximation of the derivative of the fuel burned with respect to time as follows:

$$W_F[i] = \left.\frac{\mathrm{d}F_B}{\mathrm{d}t}\right|_{[i]} = \frac{F_B[i+1] - F_B[i]}{t[i+1] - t[i]}, \text{ for } i = \{1, \ldots, N-1\} \tag{3.17}$$

where F_B is the fuel burned by the engines, t is the flight time (i.e., time to climb or to descent), $i = \{1, \ldots, N-1\}$ is the discrete altitude index, and N is the number of altitudes.

It worth noticing that because of the discrete nature of Eq. (3.17), the fuel flow at the last altitude (i.e., for $i = N$) cannot be calculated. To solve this problem, the value of the fuel flow at this altitude was obtained by applying a linear regression technique to the two previous altitudes, and by extrapolating the value for the last altitude.

Then, based on the estimation of the fuel flow obtained from Eq. (3.17), the corrected fuel flow was computed using the following equation:

$$W_{F,c} = \frac{W_F[i]}{\delta[i]\sqrt{\theta[i]}} \tag{3.18}$$

where $\delta[i]$ and $\theta[i]$ are the pressure and temperature ratios calculated at the altitude $h[i]$ for the temperature deviation ΔISA corresponding to the flight profile.

This process was repeated for the six descent flight profiles to obtain a complete set of data describing the variations of the corrected fuel flow as function of altitude, Mach number, and temperature deviation. This dataset was then plotted in different graphs, as shown in Figure 3.4, to have a visual representation of the dependency between all variables.

Note that the values shown in Figure 3.4 have been normalized between 0 and 1 for reasons of confidentiality.

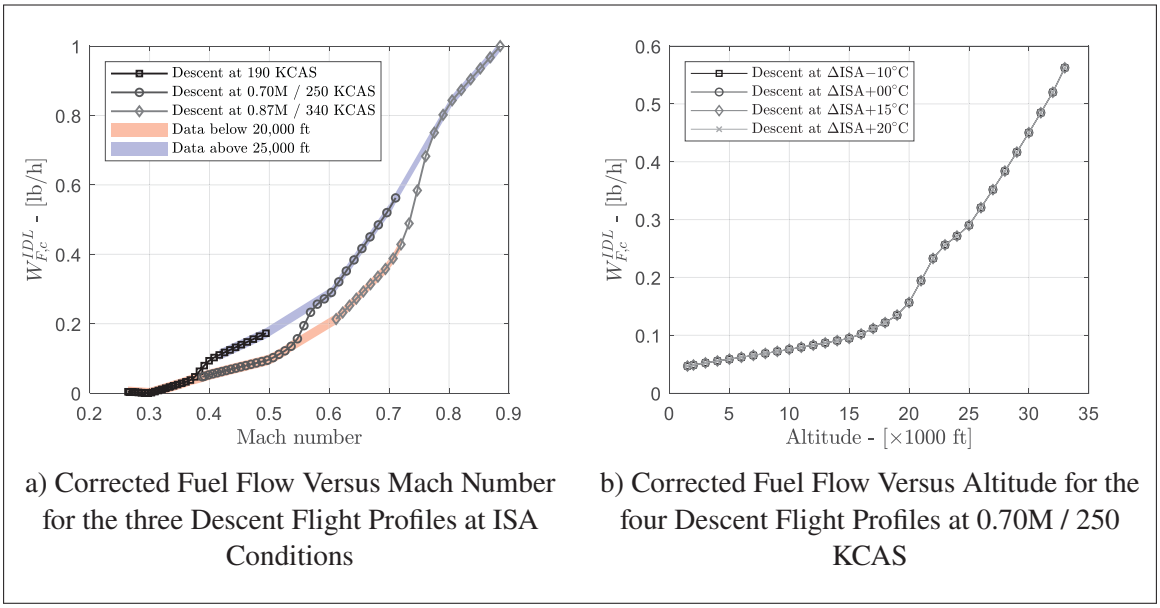

a) Corrected Fuel Flow Versus Mach Number for the three Descent Flight Profiles at ISA Conditions

b) Corrected Fuel Flow Versus Altitude for the four Descent Flight Profiles at 0.70M / 250 KCAS

Figure 3.4 Variation of the Corrected Fuel Flow in Descent

Identification of a Corrected Fuel Flow Model at ISA Conditions

Figure 3.4a shows the variation of corrected fuel flow as function of the Mach number for the three descent profiles at ISA conditions. By analyzing the data distribution, it can be seen that there is a strong correlation between the corrected fuel flow and the Mach number. Indeed, the dataset seems to be divided into two subsets that are highly dependent on the Mach number. These subsets are highlighted in Figure 3.4a by two bands of blue and red colors. Further analysis revealed that the data points in the red band corresponded to altitudes below 20,000 ft, while those in the blue band corresponded to altitudes above 25,000 ft. In addition, it was also observed that in both subsets, the corrected fuel flow followed different linear trends over various ranges of the Mach number.

Based on these observations, the functional relationship $f_2(h, M)$ was modeled in a first step as follows:

$$f_2(h, M) = \begin{cases} f_2^{(1)}(M) & \text{if } h \leq 20,000 \text{ ft} \\ f_2^{(2)}(M) & \text{if } h \geq 20,000 \text{ ft} \end{cases} \tag{3.19}$$

where $f_2^{(1)}(M)$ and $f_2^{(2)}(M)$ are two smoothing cubic splines that were identified using the Curve Fitting Toolbox available in the Matlab environment. It should be noted that attempts to model the variations of the corrected fuel flow using polynomials yielded less accurate results than splines.

To understand the transition phenomenon that occurs between 20,000 and 25,000 ft, it was necessary to analyze closely the characteristics of the engine. According to the aircraft flight manuals, the engines of the Cessna Citation X are equipped with a system of Compressor Variable Geometry (CVG) vanes. This system can be seen as a "gearbox" between the compressor stage and the turbine stage, in which the gears are replaced by a set of vanes with variable angles (i.e., geometries). This feature allows the engine control system to optimize the compressor stages conditions while maintaining the rotational speed of the turbines at its most efficient value. Thus, as the aircraft descents from 25,000 to 20,000 ft, the engine control system adjusts the angle of the compressor vanes, which results in lower fuel consumption, without affecting the thrust.

This characteristic of the engine was incorporated into the model by modifying Eq. (3.19) as follows:

$$f_2(h, M) = [1 - \phi(h)] \times f_2^{(1)}(M) + \phi(h) \times f_2^{(2)}(M) \tag{3.20}$$

where $\phi(h)$ is a sigmoid function defined such as:

$$\phi(h) = \frac{1}{1 + \exp\left[\beta_t (h - h_t)\right]} \tag{3.21}$$

where h_t and β_t are two constants that control the shape of the sigmoid. After several trials and errors, it was found that the combinations of constants that best reflect the engine behavior were $h_t = 22,500$ ft and $\beta_t = 0.0015$ ft^{-1}.

Effect of the Temperature Deviation on the Corrected Fuel Flow

Figure 3.4b shows the variation of the engine corrected fuel flow as function of the altitude for the four descent profiles at ISA-10°C, ISA+00°C, ISA+15°C and ISA+20°C. As seen in this figure, the values of the corrected fuel flow for all descent profiles are superimposed. Such a result means that the corrected fuel flow, and by extrapolation the corrected thrust, are not affected by the temperature in descent. This aspect was also confirmed by calculating the ratio between the corrected fuel flow estimated by the model in Eq. (3.20) (i.e., for ΔISA = 0) and the corrected fuel flow obtained from the reference data (i.e., for ΔISA $\neq$ 0). It was found that this ratio was always equal to one regardless of the value of the temperature deviation ΔISA. After several reflections, it was concluded that this result should be explained by the fact that the idle thrust corresponds to the minimum thrust that can be used in flight. Therefore, the turbine temperature during the descent should be lower than the temperature limit set by the manufacturer. Based on these observations, the functional relationship $g_1(h, \Delta\text{ISA})$ given by Eqs. (3.16a) and (3.16b) was assumed constant and equal to 1.

Complete Corrected Fuel Model and Results Validation

Finally, by combining the results obtained in the two previous subsections, the complete mathematical model for the corrected fuel flow in descent (i.e., at idle thrust setting) can be summarized as follows:

$$W_{F,c}^{IDL}(h, M, \Delta\text{ISA}) = [1 - \phi(h)] \times f_2^{(1)}(M) + \phi(h) \times f_2^{(2)}(M) \tag{3.22}$$

Comparison results between the corrected fuel flow obtained from the trajectory data in descent, and the corrected fuel flow predicted by the proposed model in Eq. (3.22) are shown in Figure 3.5.

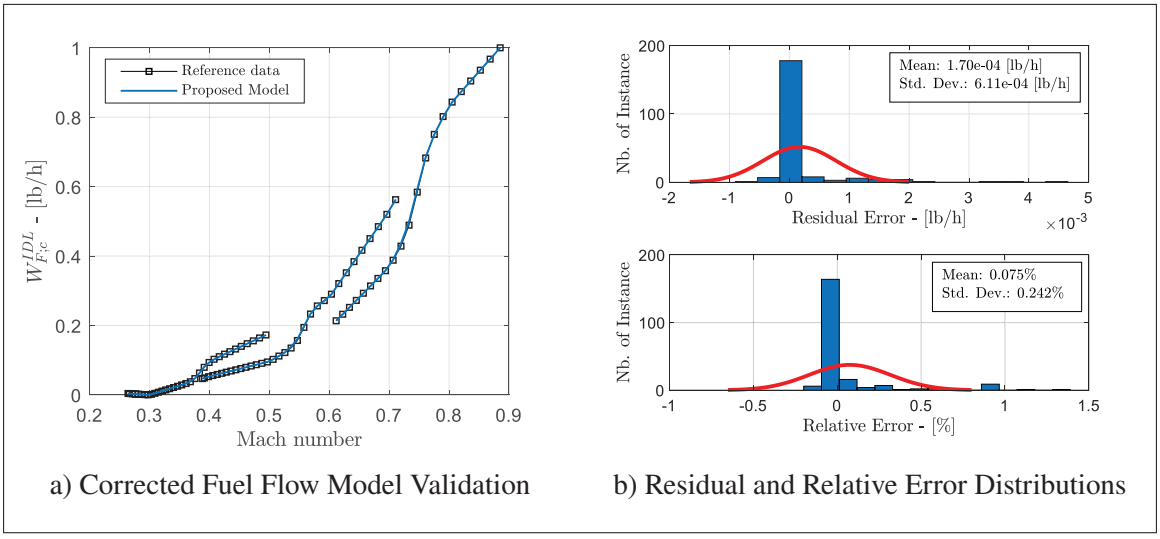

a) Corrected Fuel Flow Model Validation

b) Residual and Relative Error Distributions

Figure 3.5 dentification Results for the Corrected Fuel Flow for in Descent

As seen in Figure 3.5a, the proposed model fits the data very well, and is clearly able to account for the change in engine behavior between 20,000 ft and 25,000 ft. In addition, by observing the residual and relative errors shown in Figure 3.5b, it is possible to see that the modelling errors are very small. Indeed, the maximum relative error is less than 1.5%, while the residual error has a maximum absolute value of 10 lb/h, which is negligible.

Based on these results, it can be concluded that the model identified from the trajectory data reflects very well the variations of corrected fuel flow in descent.

3.3.2.2 Identification of the Drag Coefficient and Thrust Model in Descent

Once the corrected fuel flow model obtained, the next step in the identification process consisted in determining a model for the drag coefficient and for the corrected thrust. However, since these two quantities were not available in the reference data generated by the IFP program, they had to be deduced from the knowledge of other parameters such as the aircraft weight, flight path angle, and longitudinal acceleration, and by the use of the equations of motion. The lift coefficient was also required for the development of the drag coefficient model.

Starting from the trajectory data in descent, the aircraft weight at specific altitude $h[i]$ was calculated as follows:

$$m[i] = m[1] - F_B[i] \tag{3.23}$$

where $m[1]$ is the aircraft initial weight, and $F_B[i]$ is the fuel burned by the engines from $h[1]$ to $h[i]$.

Then, by recalling the expressions of the rate of descent and ground speed in Eq. (3.3), and by noting that:

$$\frac{\mathrm{d}h}{\mathrm{d}x} = \frac{(\mathrm{d}h/\mathrm{d}t)}{(\mathrm{d}x/\mathrm{d}t)} = \frac{\dot{h}}{\dot{x}} = \frac{V_T \sin(\gamma)}{V_T \cos(\gamma)} = \tan(\gamma) \tag{3.24}$$

the flight path angle during the descent was numerically approximated as follows:

$$\gamma[i] = \arctan\left[\frac{h[i+1] - h[i]}{x[i+1] - x[i]}\right], \text{ for } i = \{1, \ldots, N-1\} \tag{3.25}$$

where $x[i]$ is the ground distance travelled from $h[1]$ to $h[i]$. Similarly to the fuel flow defined in **Section 3.3.2.1**, the value of the flight path angle at the last altitude (i.e., for $i = N$) was obtained by applying a linear regression to the two previous altitudes, and by extrapolating the value of the flight path angle for the last altitude.

Using the estimate of the flight path angle, the aircraft longitudinal acceleration was next calculated as follows:

$$\dot{V}_T[i] = g_0 \mathrm{AF}[i] \sin(\gamma[i]) \tag{3.26}$$

where AF = $(V_T/g_0)(\mathrm{d}V_T/\mathrm{d}h)$ is the acceleration factor which depends on the climb/descent speed strategy (Young, 2017). It may be interesting to mention that this equation proved to be numerically more stable than a first-order approximation of the derivative of the true airspeed with respect to time.

Finally, based on the estimations obtained for the aircraft weight, flight path angle, and longitudinal acceleration, the difference between the thrust and the drag forces, as well as the lift coefficient were determined by rearranging the equations of motion developed in **Section 3.2.2** as follows:

$$F_N[i] - D[i] = m[i]\dot{V}_T[i] + m[i]g_0 \sin(\gamma[i]) \tag{3.27}$$

$$CL_s[i] = \frac{m[i]g_0 \cos(\gamma[i])}{0.5\rho[i]SV_T^2[i]} \tag{3.28}$$

where $\rho[i]$ is the air density corresponding to the altitude $h[i]$. This process was repeated for the three descent flight profiles at ISA conditions. It should be noted that the other flight profiles were not considered because the impact of the temperature on the engine performance was already estimated using the analysis of the corrected fuel flow.

Corrected Thrust and Drag Coefficient Model Identification Algorithm

The parameter $FD \equiv F_N - D$ in Eq. (3.27) is the "excess-thrust", and reflects the aero-propulsive performance of the aircraft. Unfortunately, due to the lack of additional information, it is impossible to go further in the development and "split" this parameter in two in order to separate the contributions of the thrust from the drag force. This is all the more difficult as the two parameters are dependent on the Mach number. The only way to solve this problem is to postulate a model of thrust, then to deduce a drag model accordingly. However, in order to ensure that the two models accurately represent the excess-thrust, it is necessary to adjust them by use of an iterative algorithm.

The following paragraphs detail the main steps of the identification algorithm developed in this study to estimate a combination of thrust and drag coefficient models that represents the best the excess-thrust data obtained from Eq. (3.27).

Step 1. Pre-Estimation of a Dataset for the Thrust. In order to start the algorithm, it is firstly necessary to estimate a set of values that more or less reflects the thrust magnitude in descent. This action can be done by relying on certain practical aspects of the descent phase. Indeed, since the idle thrust is the minimum thrust level that the engine can produce in flight, it can be considered that the thrust during the descent phase is relatively small. As a result, the magnitude of the thrust should represent only a small portion of the excess-thrust. Based on this assumption, the thrust can therefore be roughly approximated as a ratio of the excess-thrust, such as:

$$F_N[i] = r \times |FD[i]|, \text{ for } i = \{1, \ldots, N\} \tag{3.29}$$

where the ratio r must be defined so that $0 < r < 0.5$. The lower limit $r = 0$ corresponds to the particular case of a gliding flight for which the thrust is by definition zero. The upper limit $r = 0.5$ means that the thrust is equal to the drag force, which corresponds to a level flight. For the Cessna Citation X, this ratio was assumed equal to 0.10, which means that the thrust represents only 10% of the excess-thrust, while the remaining 90% are allocated to the drag force.

Clearly, this first approximation of the thrust is not "perfect". However, it remains sufficient to start the algorithm, and the thrust estimation will be refined to a better approximation throughout the iterations.

Step 2. Identification of a Corrected Thrust Model. Using the current estimation of the thrust, the corrected thrust is computed as follows:

$$F_{N,c}[i] = \frac{F_N[i]}{\delta[i]}, \text{ for } i = \{1, \ldots, N\} \tag{3.30}$$

where $\delta[i]$ is the pressure ratio calculated at the altitude $h[i]$.

The obtained values are then used to identify a model for the corrected thrust, that is for $f_1(h, M)$. The mathematical structure to be considered for $f_1(h, M)$ must be identical to that used for the corrected fuel flow model. Nevertheless, some adjustments can be applied if necessary. Indeed, for the Cessna Citation X case study, the corrected fuel flow was modeled by using two smoothing splines connected by a sigmoid function to take into account the effects of the CVG vanes. However, since this system affects the fuel flow independently of the thrust, it was assumed that the corrected thrust should be modeled by only one smoothing spline that is solely a function of the Mach number. Based on this assumption, an identification is realized using the Curve Fitting Toolbox available in Matlab to find a smoothing cubic spline that best fitted the corrected thrust values.

Step 3. Identification of a Drag Model. Using the current idle thrust model, the algorithm next computes the drag coefficient as follows:

$$CD_s[i] = \frac{f_1\left(h[i], M[i]\right)\delta[i] - FD[i]}{0.5\rho[i]SV_T^2[i]}, \text{ for } i = \{1, \ldots, N\} \tag{3.31}$$

where $f_1(h, M)$ is the corrected thrust model identified in **Step 2**.

The obtained values for the drag coefficient are subsequently used to determine the coefficients of the drag polar equation $\mathbf{p} = \{p_1, p_2, \ldots, p_6\}$ that minimize the Mean Squared Errors (MSE) between the estimated values and the predicted values. This minimization process is performed by using the Levenberg-Marquardt (LM) algorithm available in the Matlab environment. It is important to mention that the LM algorithm requires an initial point p_0 to converge to an optimal solution. Thus, for the first iteration, the initial point is set to $\mathbf{p}_0^{(1)} = \{p_1^*, 0, 0, p_4^*, 0, 0\}$, where $\{p_1^*, p_4^*\}$ are determined using a Least Square Method (LSM). However, for the next iterations, this initial point must be defined according to the results obtained during the previous iteration, that is $\mathbf{p}_0^{(k)} = \mathbf{p}_0^{(k-1)}$ where k is the number of iterations.

Step 4. Convergence Test. Finally, using the two models identified for the corrected thrust and for the drag coefficient, the algorithm computes the excess-thrust according to Eq. (3.27). The predicted values are then compared to the excess-thrust values calculated from the trajectory

data. If more than 95% of the data are estimated with a relative error of less than 2%, then the algorithm considers that both models are well adjusted, and returns them as output. Otherwise, it is necessary to refine the models. In this case, the algorithm recalculates a new estimate of the thrust using the last identified drag coefficient model as follows:

$$F_N[i] = FD[i] + 0.5\rho[i]SV_T^2[i]CD_s[i], \text{ for } i = \{1, \ldots, N\} \tag{3.32}$$

and repeats the **Steps 2** to **4** until the error criterion is satisfied, when or the number of iterations exceeds 250.

It should be emphasized that the two models returned by the algorithm do not necessary represent the actual thrust and drag coefficient of the aircraft, but they rather represent two models that, when combined, allow a prediction of the excess-thrust that matches the data obtained from the IFP program. Consequently, the models obtained can be "shifted" with respect to the actual aero-propulsive performance of the aircraft. For example, the thrust can be overestimated, while the drag is underestimated.

In addition, it should also be noted that the quality of the models depends on the choice of the ratio r. By performing several tests with the Cessna Citation X data, it has been observed that a ratio r close to 0 led generally to a corrected thrust model with negative values, while a ratio r close to 0.5 led to a drag coefficient model with relatively large values. It is therefore necessary to test several values for the ratio r, and then to select the value that gives the most appropriate results in terms of thrust and drag coefficient models.

Results Validation of the Proposed Model Identification Algorithm

The results of the identification algorithm are shown in Figure 3.6. The first remark that can be made by observing these results is that the algorithm has considerably improved the models over the iterations. Indeed, it can be seen in Figure 3.6a that the maximum and average relative errors for the excess-thrust decrease with the number of iterations. The maximum relative error was reduced from 17.68% at the first iteration to 3.9% at the tenth iteration. Similarly, the average

relative error was reduced from 3.4% to 0.5%. This result demonstrates that the algorithm has adjusted the two models at each iteration in order to find a combination that provides a good estimate of the excess-thrust.

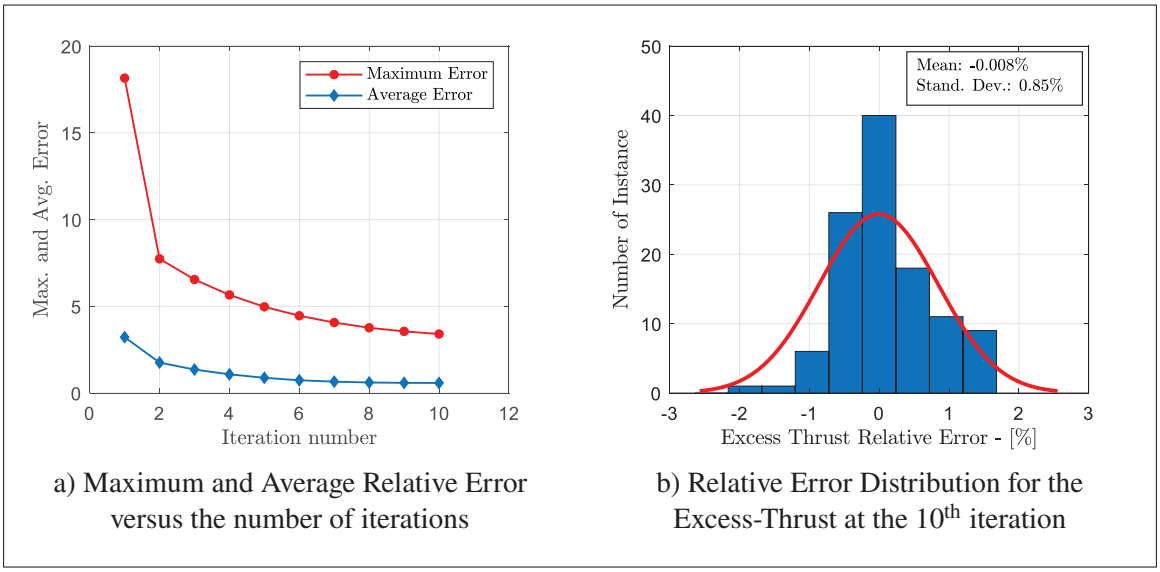

a) Maximum and Average Relative Error versus the number of iterations

b) Relative Error Distribution for the Excess-Thrust at the 10^{th} iteration

Figure 3.6 Validation Results for the Proposed Model Identification Algorithm

In view of these results, it can be concluded that the algorithm developed in this study was able to find a combination of models for the corrected thrust and drag coefficient that reflect the excess-thrust reference data very well. These two models are illustrated in Figure 3.7a and Figure 3.7b, respectively, for the convenience of the reader. Note that the values in these figures are normalized between 0 and 1 for reasons of confidentiality.

It is interesting to see that the results obtained for the corrected thrust in Figure 3.7a satisfies the assumption made in the **Step 2** of the identification algorithm, namely that the corrected thrust model should have a similar mathematical structure as the corrected fuel flow model. Indeed, the data distribution clearly reveals that there is a strong correlation between the corrected thrust and the Mach number. In addition, the data follows different linear trends over different regions of the Mach number. These two characteristics are exactly similar to those observed when analyzing the data for the corrected fuel flow in **Section 3.3.2**. This result therefore reinforces the idea that

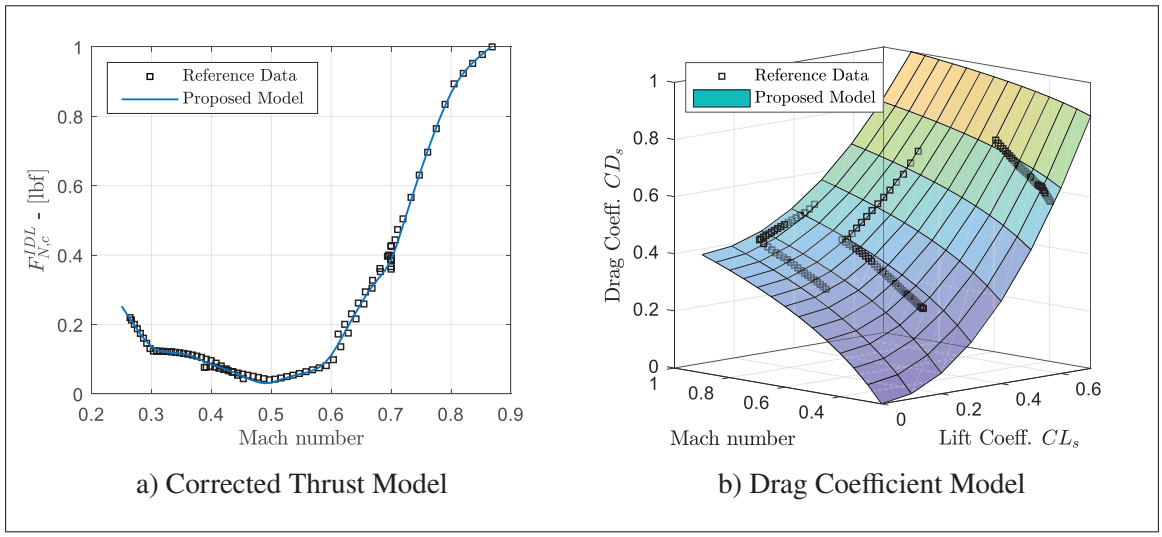

a) Corrected Thrust Model b) Drag Coefficient Model

Figure 3.7 Corrected Thrust and Drag Coefficient Models Representation

the analysis of the corrected fuel flow can be used to predict a mathematical structure for the corrected thrust model.

3.3.2.3 Adaptation of the Methodology to the Climb Phase

The three functional relationships describing the performance of the engine at maximum climb thrust setting (i.e., f_3, f_4 and g_2) can be determined by following the same procedure as for the descent phase. However, by taking advantage of the results obtained for the descent phase, several simplifications can be considered. Indeed, instead of using an iterative algorithm, it was assumed that the drag coefficient model for the descent phase should also be valid for the other flight phases. Consequently, the thrust in climb was estimated according to the following equation:

$$F_N = FD + 0.5\rho S V_T^2 CD_s \tag{3.33}$$

where the excess-thrust FD was determined from the climb trajectory data, and the drag coefficient CD_s was calculated based on the model previously identified.

The results obtained for the corrected fuel flow and corrected thrust at ISA conditions are shown in Figure 3.8a and Figure 3.8b, respectively. From a general point of view, it can be seen that the

two identified models reflect very well the reference data, and can handle the change in their behavior that occurs at 38,000 ft. This characteristic of the engine is probably due to a design limitation imposed by the engine manufacturer, either to limit the pressure at the inlet of the combustion chamber, or to avoid overloading the fan blades with centrifugal force. Regarding the modelling errors, it was found that the maximum relative error for both models was less than 1.5%.

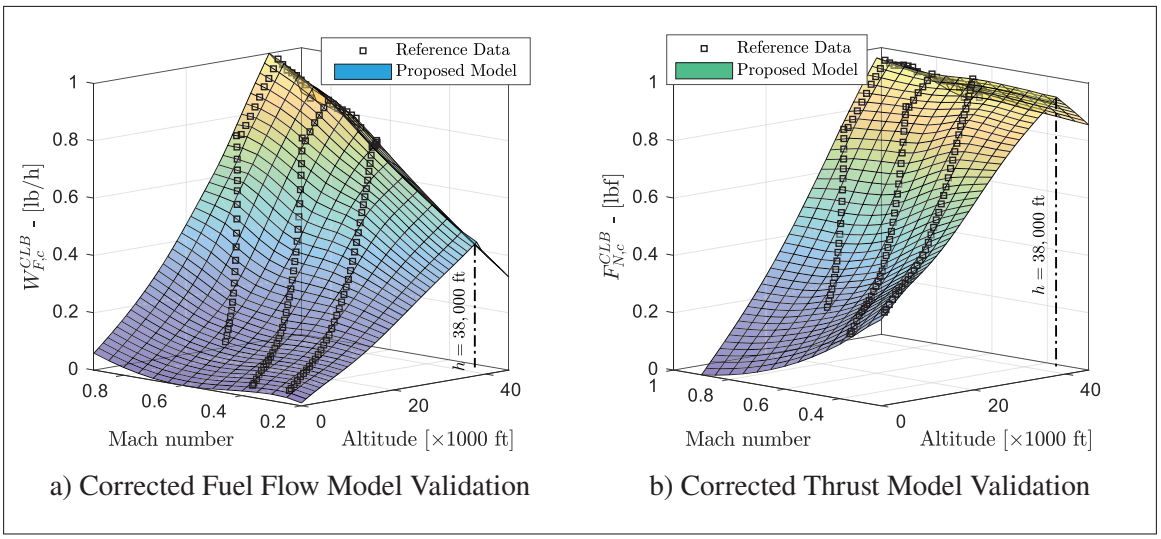

a) Corrected Fuel Flow Model Validation

b) Corrected Thrust Model Validation

Figure 3.8 Results for Identified Corrected Fuel Flow and Thrust Models in Climb at ISA Conditions

3.3.2.4 Identification of a Corrected Thrust-to-Fuel Model

The final step in the identification process consisted in determining a model for the function $f_5(F_{N,c}, M)$. As a reminder, this function makes it possible to predict the corrected fuel flow from the knowledge of the corrected thrust and the Mach number, and can be used for any flight phase. Thus, before identifying a model for $f_5(F_{N,c}, M)$, it was necessary to supplement the data obtained for the climb and descent with those for the cruise.

Since the cruise is a particular phase in which the flight path angle is by definition zero, the aerodynamic lift coefficient of the aircraft was estimated by imposing $\gamma = 0$ in Eq. (3.2), which

gives:

$$CL_s = \frac{L}{0.5\rho S V_T^2} = \frac{mg_0}{0.5\rho S V_T^2} \tag{3.34}$$

Then, by recalling that the data generated by the IFP program are obtained for level-flight conditions at constant speed (i.e., no acceleration), the thrust required to balance the aircraft was equalized to the drag force to obtain:

$$F_N = D = 0.5\rho S V_T^2 CD_s(CL_s, M) \tag{3.35}$$

where the drag coefficient $CD_s(CL_s, M)$ was calculated using the model obtained in descent.

Based on this last result, the corrected thrust in cruise was then computed by dividing the thrust value by the ambient pressure ratio. Similarly, the corrected fuel flow in cruise was also determined by diving the fuel flow value by the ambient pressure ratio times the square root of the ambient temperature ratio.

Finally, this process was applied to all the flight conditions available in Table 3.3, and the results were next combined with those obtained previously for the climb and descent phases. This make it possible to obtain a complete set of data describing the variation of the corrected fuel flow as function of the corrected thrust and the Mach number for the three flight phases. The resulting data set was subsequently used to identify a model for the function $f_5(F_{N,c}, M)$. Once again, this model identification was realized by using the Curve Fitting Toolbox available in the Matlab environment, and by testing several mathematical structures to find the one that best describes the data. After several trials and errors, the mathematical structure that offered the best results, was a thin-plate spline.

Comparison results between the corrected fuel flow obtained from the reference data and the corrected fuel flow predicted by the proposed model are presented in Figure 3.9.

As shown in Figure 3.9a, the model matches the reference data very well for the three flight phases. In addition, by analyzing the error distributions in Figure 3.9b, it is possible to see that the modelling errors are relatively small, with a maximum relative error less than 4%. Regarding

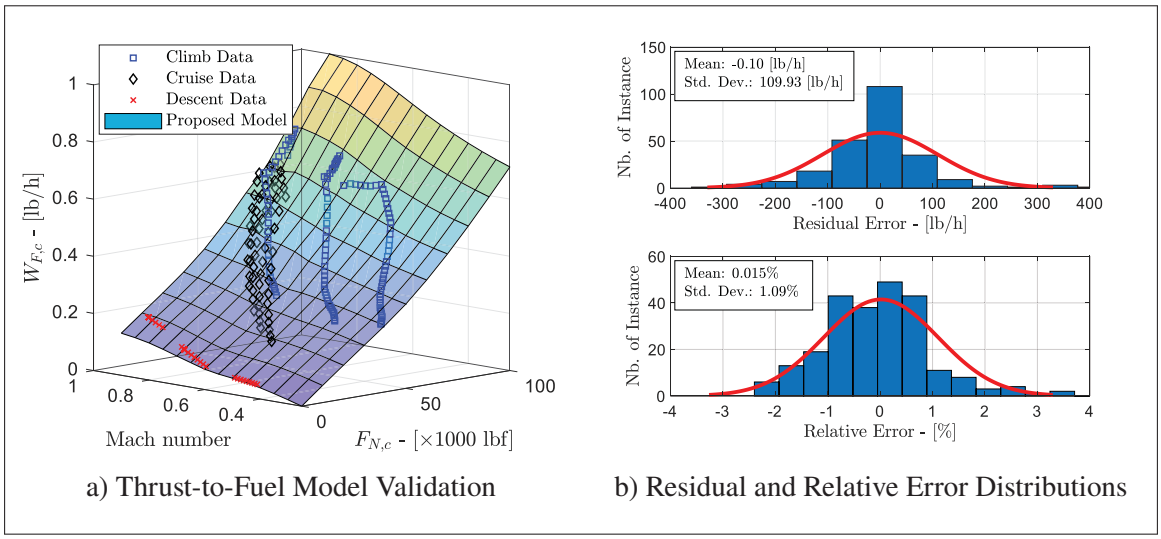

a) Thrust-to-Fuel Model Validation

b) Residual and Relative Error Distributions

Figure 3.9 Identification Results for the Thrust-to-Fuel Model

the residual error, it should be noted that the data distribution varies between ±400 lb/h. This interval size can be explained by the fact that the corrected fuel flow is obtained by dividing the fuel flow values by the product of two ratios that are smaller than one. Therefore, the magnitude of this parameter is very large, and the associated values are of the order of 10^4. Thus, a residual error of 400 lb/h is actually very small and can be neglected.

3.3.3 Aircraft Performance Database Generation

Once the model describing the aero-propulsive characteristics of the Cessna Citation X was identified, the results obtained were used to create the performance database necessary for the operation of the FMS. The performance database considered in this study was divided into four sub-databases, as shown in Table 3.4.

The first sub-database represents the drag polar equation of the aircraft. The inputs for this sub-database are the lift coefficient and Mach number, and the output is the drag coefficient. The second and third sub-databases correspond to the engine thrust, and to the fuel flow in climb and descent, respectively. The inputs of these two sub-databases are the altitude, Mach number and temperature deviation from standard atmospheric conditions, while the outputs are the corrected

Table 3.4 Aircraft Performance Databases Inputs and Outputs

Sub-Database	**Flight Phase**	**Inputs**	**Output(s)**
Aerodynamic Drag Polar	Climb, Cruise, and Descent	Lift Coefficient Mach number	Drag Coefficient
Engine Performance at Maximum Climb Thrust Seeting	Climb	Altitude [ft] Mach number ISA deviation	Corrected Thrust [lbf] Corrected Fuel Flow [lb/h]
Engine Performance at Idle Thrust Setting	Descent	Altitude [ft] Mach number ISA deviation	Corrected Thrust [lbf] Corrected Fuel Flow [lb/h]
Engine Thrust-to-Fuel Performance	Climb, Cruise, and Descent	Mach number Corr. Thrust [lbf]	Drag Coefficient Corrected Fuel Flow [lb/h]

engine thrust and corrected fuel flow in descent and climb. Finally, the last sub-database gives the engine corrected fuel flow in cruise as function of the corrected thrust and the Mach number.

3.4 Results and Validation of the Aircraft Performance Model

The last section of this paper presents the results obtained for the validation of the aircraft performance model. For this purpose, a series of flight tests was conducted with the Cessna Citation X Research Aircraft Flight Simulator (RAFS) available at the LARCASE laboratory. In order to evaluate the validity of the aircraft performance model over a wide range of operating conditions, three categories of flight tests were considered: climb at constant CAS/Mach, level flight at constant speed, and idle descent at constant Mach/CAS. In parallel, the performance database in Table 3.4 was implemented into a modified version of the IFP program in order to integrate the simplified equations of motion developed in **Section 3.2.2**, and thus to predict the aircraft performances.

Validation of the model was accomplished by comparing the aircraft performance measured from the flight simulator (RAFS) with those computed by the modified IFP program (A/C Model).

3.4.1 Validation of the Aircraft Performance Model for the Climb Phase

To validate the model for the climb phase, a first series of 60 flight tests was conducted with the Cessna Citation X flight simulator. These flight tests aimed to reproduce normal climb procedures at constant CAS/Mach from an initial altitude of 1500 ft to a predetermined Top-of-Climb (T/C, transition point between the climb phase and the cruise phase). For the sake of simplicity, the T/C was imposed at 45,000 ft for all flight tests. This altitude was chosen because it corresponds to the highest typical cruise altitude of the Cessna Citation X (see Table 3.1). Similarly, to facilitate the completion of all flight tests, it was decided to define 20 different climb scenarios, and to reproduce these scenarios for three different aircraft weight configurations: light (26,000 lb), medium (30,000 lb) and heavy (36,000 lb).

Each of the 20 climb scenarios was carried out with the assistance of the autopilot to be consistent with current piloting procedures, and by following the steps describe below:

1. Climb at constant CAS_1 from 1500 ft until 10,000 ft;
2. At 10,000 ft, accelerate from CAS_1 to a desired CAS_2;
3. Proceed climb at constant CAS_2 until the crossover altitude of 30,000 ft;
4. At the crossover altitude, change climb speed strategy to constant Mach M_{CLB};
5. Proceed climb at constant Mach M_{CLB} until the T/C point, defined at 45,000 ft.

Starting from this “standardized procedure”, the 20 nominal climb scenarios were established by selecting different initial speeds CAS_1 in the range of 200 to 250 KCAS, and different speeds CAS_2 in the range of 270 to 340 KCAS. Finally, to verify the validity of the engine model, 5 of the 20 nominal climb scenarios were realized by arbitrarily imposing a temperature deviation between ISA-20°C and ISA+20°C.

After each flight test, the aircraft performance in terms of time-to-climb, ground distance traveled, and fuel burned collected during the simulation were saved and exported into an Excel file. In parallel, the modified version of the IFP program was used to compute these three parameters for the same operating conditions.

Figure 3.10 shows an example of results comparison for a given climb scenario conducted with CAS_1 = 250 KCAS and CAS_2 = 320 KCAS, and for the three aircraft weight configurations. Note that the initial conditions for the medium and heavy configurations have been shifted for better visualization of the results. As shown in this figure, there is a very good agreement between the performance measured with the RAFS and the performance predicted by the model. The largest errors were obtained for the heavy configuration (in red color). It was found that, for this configuration, the error for the time-to-climb at the T/C was approximately 1.26% (0.39 min), while the errors for the ground distance and fuel burned were about 0.69% (1.45 n miles) and -1.35% (-23.01 lb), respectively. The negative sign means that the model overestimated the fuel burned.

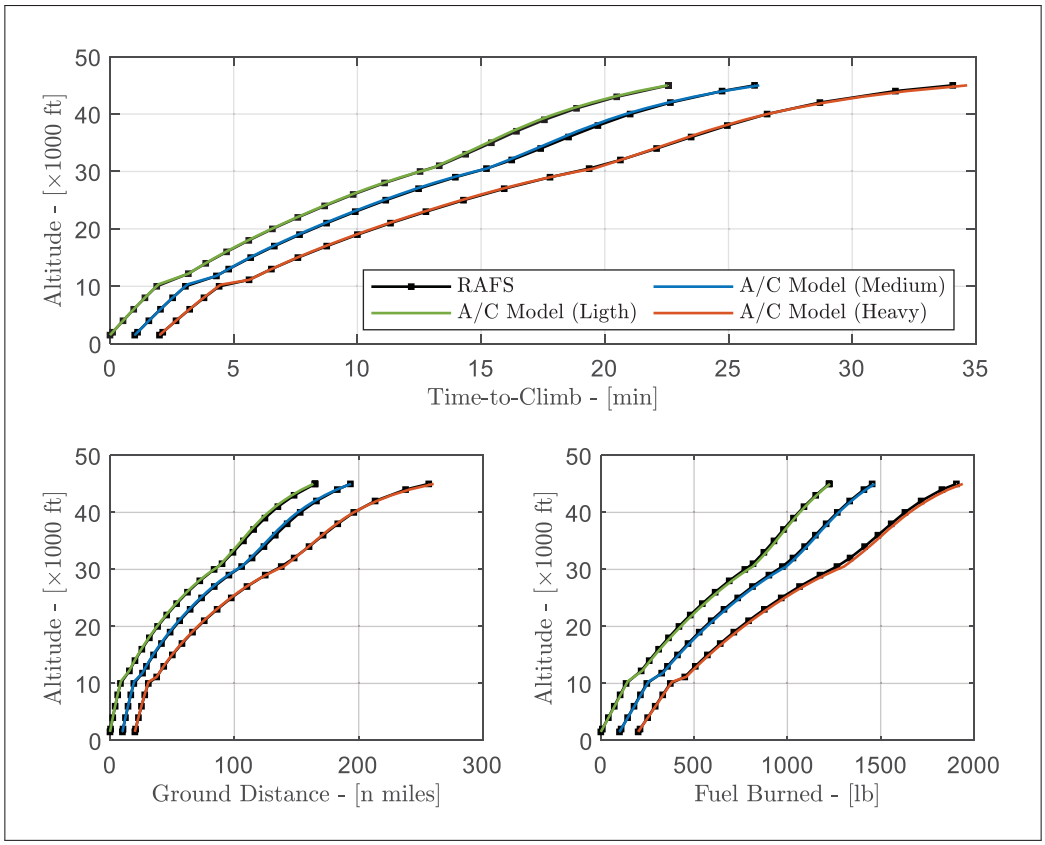

Figure 3.10 Example of Aircraft Performance Comparison for the Climb Phase

The comparison illustrated in Figure 3.10 was repeated for all 60 climb tests. The relative errors obtained for the time-to-climb, ground distance, and fuel burned are presented in Figure 3.11.

These errors were calculated by comparing the performance measured with the RAFS to the performance predicted by the model every 500 ft.

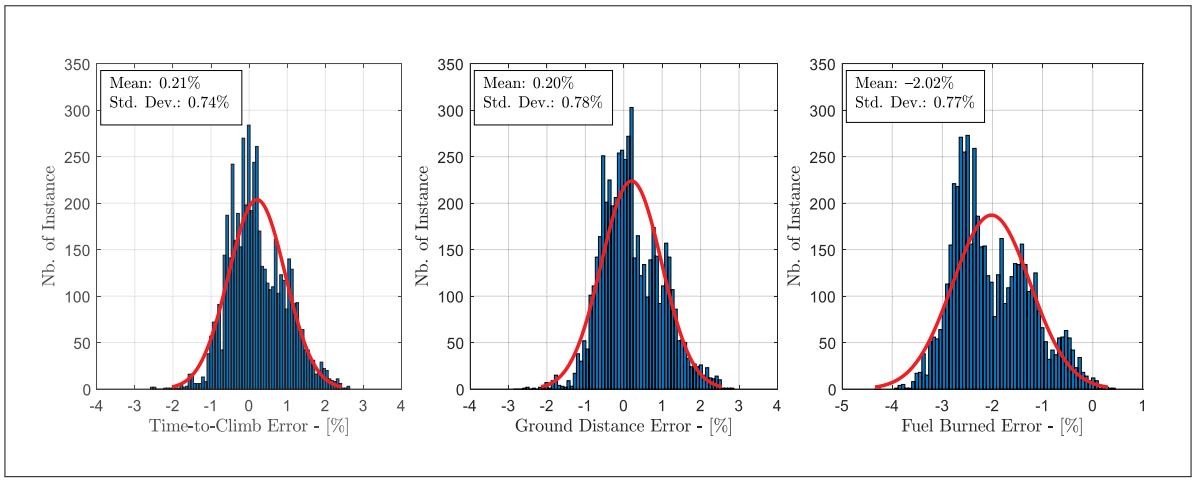

Figure 3.11 Time-to-Climb, Ground Distance, and Fuel Burned Distribution Errors for the Climb Phase

From a general point of view, the results obtained for the three parameters are very good. Indeed, by analyzing the first two graphs of Figure 3.11, it can be seen that the time-to-climb and ground distance are very well predicted with less than 3% of error. In addition, the relative errors for these two parameters are normally distributed with a mean value close to zero, and a standard deviation of the order of 0.75%. Regarding the fuel burned, this parameter is also well estimated with less than 4% of relative error. However, it is interesting to note that, unlike the time-to-climb and the ground distance for which the errors are centered around zero, the errors distribution for the fuel burned is shifted to the left with an average value of -2.02%. Moreover, it can also be noted that the majority of the relative errors are negative. These results indicate that the model tends to overestimate the aircraft fuel consumption by 2.02% on average. In a way, this aspect can be considered positive because it is preferable that a flight planning system such as the FMS overestimates fuel consumption rather than the other way around.

Based on the results provided in this section, it can be concluded that the model identified in this study reflects very well the performance of the Cessna Citation X for the climb phase throughout its operating flight envelope.

3.4.2 Validation of the Aircraft Performance Model for the Cruise Phase

The validation of the performance model continues with the cruise phase. As the basis for evaluation of the accuracy of the model, 20 cruise scenarios were established by selecting four different altitudes in the range of 30,000 to 45,000 ft, and five different Mach numbers in the range of 0.60 to 0.87. Once again, these flight conditions were chosen because they are representative of the typical cruising conditions of the Cessna Citation X. In addition, as for the climb phase, the scenarios were reproduced for three aircraft weight configurations; light (27,000 lb), medium (30,000 lb), and heavy (35,000 lb). Finally, to verify the robustness of the thrust-to-fuel model, 5 of the 20 of cruise scenarios were realized by arbitrarily imposing different temperature deviations between ISA-20°C and ISA+20°C.

Figure 3.12 to Figure 3.14 show the results of comparisons between the fuel burned measured with the RAFS, and the fuel burned predicted by the model. Each figure corresponds to one of the three aircraft weight configurations.

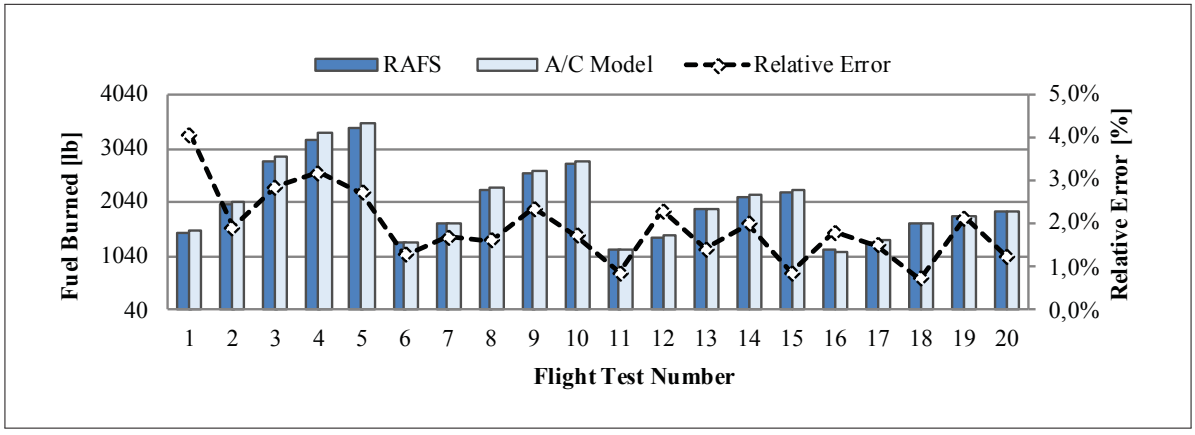

Figure 3.12 Aircraft Fuel Burned Comparison for the Lightweight Configuration

From a general point of view, the results show that for a given cruise condition, the performance model was able to predict very well the fuel consumption of the aircraft. Indeed, it can be seen from the three figures that the maximum absolute relative error is always smaller than 4.5%. Moreover, it can be noted that fuel burned estimated by the model is in general higher than its

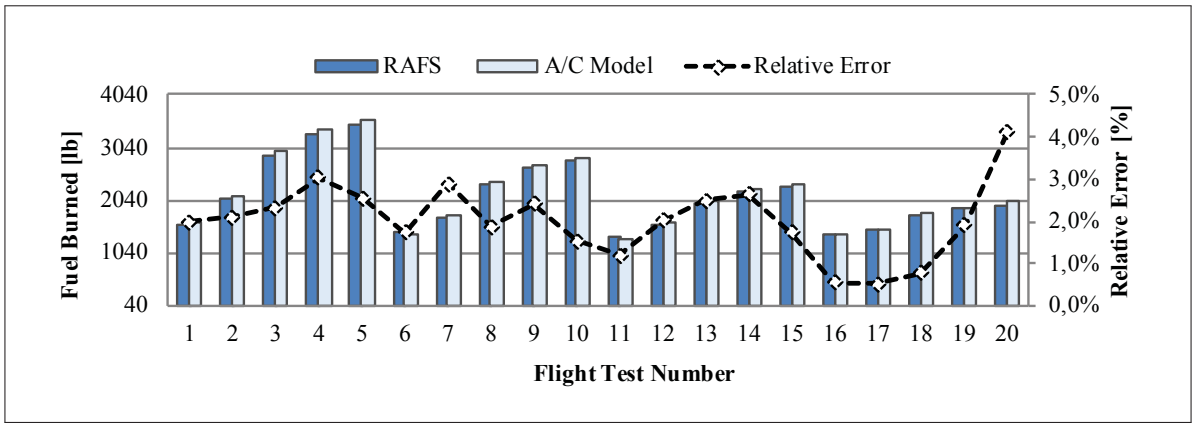

Figure 3.13 Aircraft Fuel Burned Comparison for the Medium Weight Configuration

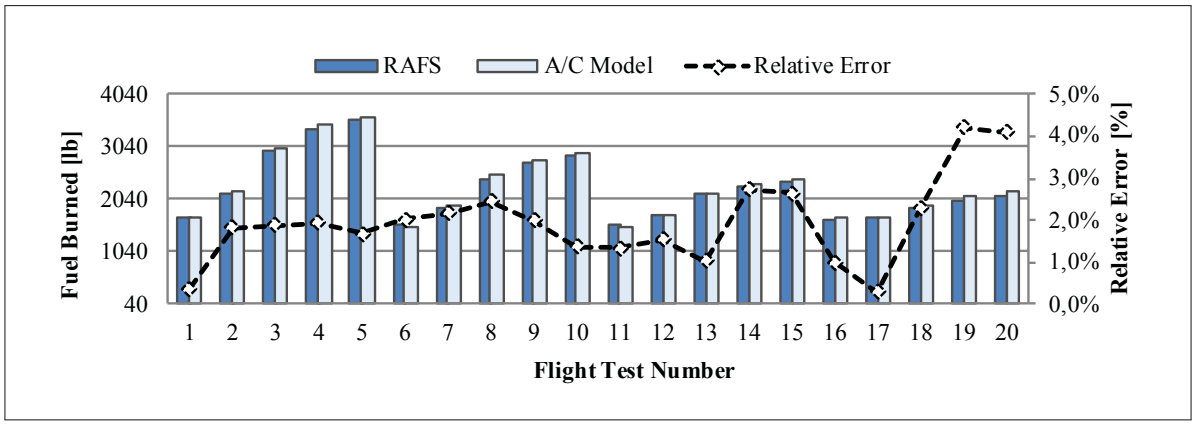

Figure 3.14 Aircraft Fuel Burned Comparison for the Heavy Weight Configuration

value measured with the RAFS. This aspect was corroborated by the calculation of the average relative error of the 60 flight tests, which turned out to be approximately -1.94%. Such results are consistent with those obtained for the climb phase, and indicate that the model tends to overestimate the fuel consumption of the aircraft.

In the light of the results presented in this section, it can be concluded that the thrust-to-fuel model identified in this study reflects very well the fuel consumption of the Cessna Citation X for the cruise phase. Moreover, since the thrust required to compute the fuel flow in cruise was estimated from the drag model, the results presented in this section allow also to validate the aerodynamic model.

3.4.3 Validation of the Aircraft Performance Model for the Descent Phase

Finally, the last flight phase to be validated is the descent phase. For this purpose, 60 additional flight tests were conducted with the Cessna Citation X flight simulator. As in the case of the climb phase, these flight tests aimed to reproduce normal descent procedures from a predefined Top-of-Descent (T/D, transition point between the cruise phase and the descent phase) to a final altitude of 2000 ft. For the sake of simplicity, the T/D was considered to be same as the T/C, i.e,. 45,000 ft. Moreover, to facilitate the completion of the flight tests, 20 nominal descent scenarios were defined, and were further repeated for three aircraft weight configurations: light (26,000 lb), medium (29,000 lb) and heavy (32,000 lb).

Each of the 20 descent scenarios was carried out with the assistance of the autopilot to be consistent with current piloting procedures, and by following the steps describe below:

1. Descent at constant Mach M_{des} from the T/D to the crossover altitude of 30,000 ft;
2. At the crossover altitude, change climb speed strategy to constant CAS_1;
3. Proceed descent at constant CAS_1 until the meter fix altitude of 10,000 ft;
4. At 10,000 ft, decelerate from CAS_1 to a desired CAS_2;
5. Proceed descent at constant CAS_2 until 2000 ft.

Thus, starting from this "standardized procedure", the 20 nominal descent scenarios were established by selecting different Mach number M_{des} in the range of 0.60 to 0.87, and different speeds CAS_2 in the range of 200 to 250 KCAS. Finally, to verify the reliability of the engine performance model, 5 of the 20 descent scenarios were realized by arbitrarily imposing a temperature deviation between ISA-20°C and ISA+20°C.

Figure 3.15 shows an example of results comparison for a descent scenario realized with $M_{des} = 0.84$ and $CAS_2 = 250$ KCAS, and for the three aircraft weight configurations. Note that the initial conditions for the medium and heavy weight configurations have been shifted to facilitate the visualization of the results. As it can be seen in this figure, the aircraft performance predicted by the model is almost superimposed to the aircraft performance measured with the RAFS. The largest errors were obtained for the heavy configuration (in red color). It was found

that, for this configuration, the time-to-descent error at 2000 ft was approximately 1.52% (0.31 min), while the relative errors for the ground distance error and fuel burned were about 0.22% (0.28 n mile), and -3.11% (-8.51 lb), respectively.

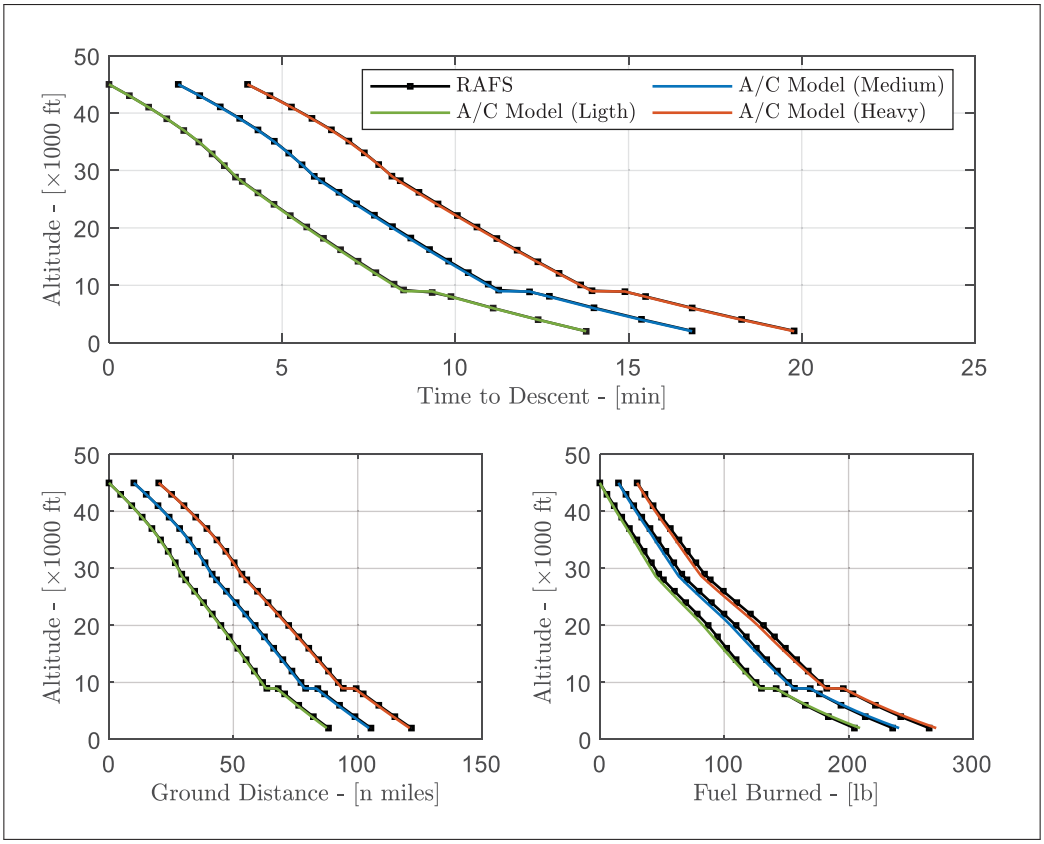

Figure 3.15 Example of Aircraft Performance Comparison for the Climb Phase

The comparison illustrated in Figure 3.15 was repeated for all the 60 descent flight tests. The resulting relative errors for the time-to-descent, ground distance, and fuel burned are presented in Figure 3.16. These errors were calculated by comparing the aircraft performance measured with the RAFS to those predicted by the model at each 500 ft.

As shown in Figure 3.16, the results obtained for the descent phase are globally similar to those obtained for the climb phase. Indeed, it can be seen from the two first graphs that the time-to-descent and the ground distance are once again very well predicted with less than 4 and 3% of relative errors, respectively. However, it is worth noting that the errors distribution for the

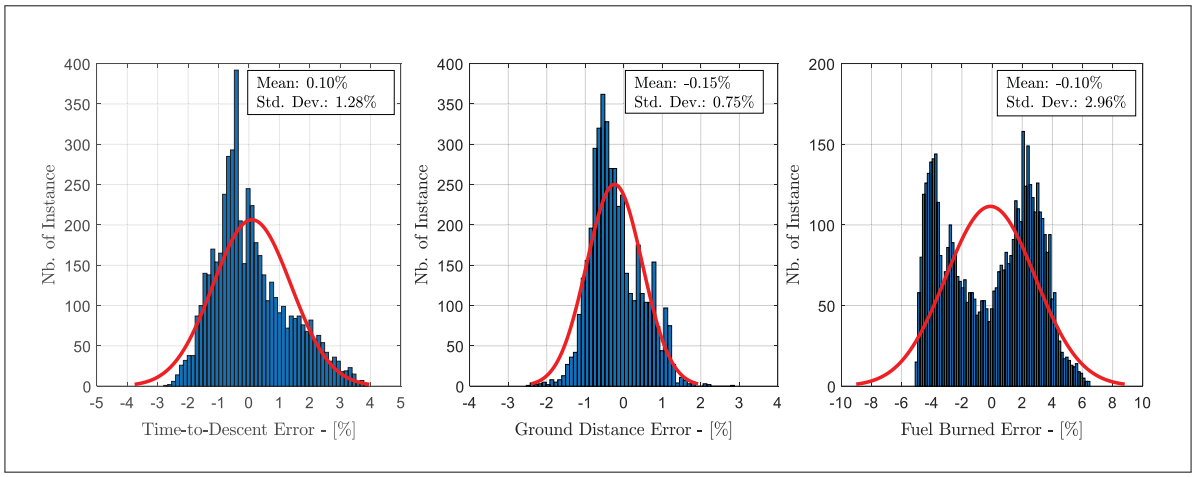

Figure 3.16 Example of Aircraft Performance Comparison for the Descent Phase

time-to-descent is slightly narrower than that of the ground distance. This aspect can also be observed by comparing the standard deviation obtained for these two parameters; the standard deviation is slightly higher for the time-to-descent. These results mean that the model tends to better estimate the ground distance than the time-to-descent. Regarding the fuel burned, it can be seen that its relative errors vary in a relatively wide range from -6 to +7%. This aspect was not expected in view of the results obtained during the identification process in **Section 3.3.2.1**.

To understand the reason of these relatively large errors, it was necessary to analyze their variations over the flight envelope of the aircraft. For this purpose, Figure 3.17 shows the average relative, and the residual errors for the fuel burned as function of altitude and Mach number. These relative errors were calculated from the flight data at ISA conditions, and for the three aircraft weights. The color bar to the right of each graph indicates the absolute value of the error with a color gradient from blue for the minimum error to red for the maximum error.

As shown in Figure 3.17a, the flight conditions for which the relative errors are the highest are located in the upper right corner of the flight envelope. These conditions correspond to the beginning of the descent, where the fuel burned is close to zero. This fact means therefore that the relative error is not representative of the accuracy of the model in descent because it may take high values for low absolute errors. This aspect was corroborated by observing the results

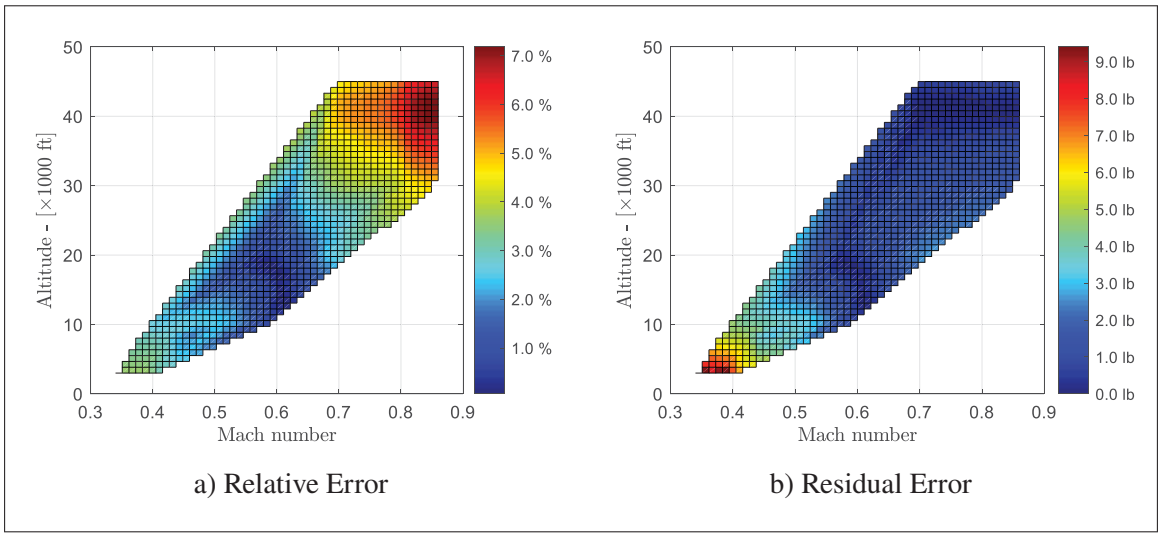

a) Relative Error b) Residual Error

Figure 3.17 Variation of the Fuel Burned Errors over the Flight Envelope in Descent

in Figure 3.17b. Indeed, it can be seen that for the same flight conditions, the residual errors are smaller than 2 lb, while the maximum residual error over the entire flight envelope is less than 10 lb. Compared to the other flight phases, it is evident that a difference of 10 lb can be considered negligible. Thus, despite the large values of the relative errors, it can be concluded that the model represents very well the aircraft performance, and the fuel consumption in descent.

Finally, it is also interesting to note the particular "M" shape of the error distribution for the fuel burned in Figure 3.16. Indeed, the errors distribution seem to be divided into two sub-distributions: a first sub-distribution centered around -4% and a second one more centered around +3%. By analyzing more closely the results, it was found that the errors corresponding to the first sub-distribution were obtained for altitudes between 20,000 and 45,000 ft, while the errors corresponding to the second sub-distribution were obtained for altitudes below 20,000 ft. This result means that the model tends to underestimate the fuel consumption above 20,000 ft, and then to overestimate the fuel consumption below 20,000 ft. Once again, this observation is consistent with the observations previously made for the climb and cruise phases.

Based on the analysis presented in this section, it can be concluded that the model identified in this study reflects very well the performance of the Cessna Citation X in the descent phase.

3.5 Conclusion

In this paper, a new original technique for identifying an aircraft performance model in climb, cruise and descent was developed. The technique was successfully applied to the well-known Cessna Citation X business jet aircraft, for which an In-Flight Performance (IFP) program and a Cessna Citation X Research Aircraft Flight Simulator (RAFS) were available.

Starting from a set of known trajectory data, the identification technique consisted, in the first step, in estimating a model for the engine fuel flow in descent. It was shown that the advantage of beginning with the model estimation for the fuel flow is that the mathematical structure obtained for this parameter could be used to predict valuable information for the engine thrust. Once the fuel flow model obtained, the second step was to identify a model for the thrust and drag coefficient of the aircraft. This step was accomplished by the use of an iterative algorithm whose role was to find a combination of thrust and drag coefficient models that best reflected the excess-thrust of the aircraft in descent. The identification results showed that the proposed algorithm allowed both models to be adjusted throughout the iterations, and to find a very good solution after only 10 iterations. Finally, the identification technique was applied to the climb and cruise phase.

Validation of the methodology was accomplished by comparing the performance data predicted by the identified model with performance data measured with the RAFS. A total of 180 flight tests were conducted for different flight scenarios, and flight conditions. These conditions were selected in order to cover as much a possible the entire operating envelope of the aircraft. Results comparison showed that the identified model was able to predict the aircraft performance with less than 5% of error, except for the descent phase. It was observed that the fuel consumption in descent was estimated with a maximum relative error of 8%. However, after analyzing more closely the results, it was found that this error was acceptable since it corresponded to a residual error of only 10 lb, which can be neglected in comparison to the total aircraft weight.

Following the analyses of different results, it has been concluded that the technique proposed in this paper was adequate, and could be further used to identify a performance model for other types of aircraft.

The identification technique developed in this paper allows to estimate a combination of thrust/drag model that reflects well the excess-thrust of the aircraft. However, as explained in **Section 3.3.2**, the results of the identification algorithm are fundamentally influenced by the choice of the ratio r. As future work, it is desired to take the study a step further by determining a better way of estimating the value of the ratio r on the basis of the trajectory data or the information available in the aircraft flight manuals.

CHAPTER 4

CESSNA CITATION X TAKEOFF AND DEPARTURE TRAJECTORIES PREDICTION IN PRESENCE OF WINDS

Georges Ghazi [a], Ruxandra Mihaela Botez [b] and Nicolas Maniette [c]

[a, b, c] Department of Automated Production Engineering, École de Technologie Supérieure, 1100 Notre-Dame West, Montréal, Québec, Canada H3C 1K3

Paper published in the *AIAA Journal of Aerospace Information Systems* on October 2020.
DOI: https://doi.org/10.2514/1.I010854

Résumé

L'objectif de cet article est de présenter une méthode pratique développée au Laboratoire de Recherche en Commande Active en Contrôle, Avionique et AéroSevoÉlasticité (LARCASE) pour calculer les trajectoires de décollage et de départ de l'avion Cessna Citation X. La méthode consistait à intégrer numériquement les équations de mouvement de l'avion pour chaque segment composant un profil type de décollage et de départ. À cette fin, la trajectoire complète de l'avion a été divisée en cinq segments typiques, dont l'accélération au sol, la rotation, la transition, la montée à vitesse constante et l'accélération en montée. Pour chaque segment, des algorithmes détaillés ont été conçus pour résoudre et intégrer les équations de mouvement en utilisant la méthode d'Euler. La trajectoire complète de l'avion a été obtenue en combinant ces segments dans un ordre précis en fonction de la procédure de départ. La validation de la méthodologie a été évaluée avec un simulateur de vol de recherche du Cessna Citation X. Un total de 38 tests ont été effectués avec le simulateur dans une large gamme de conditions d'opération. Les résultats obtenus ont montré que les données de trajectoire prédites par les différents algorithmes correspondaient aux données de trajectoire obtenues à partir du simulateur avec moins de 5% d'erreur relative.

Abstract

The objective of this paper is to present a practical method developed at the Laboratory of Applied Research in Actives Controls, Avionics, and AeroServoElasticity (LARCASE) for

calculating takeoff and departure trajectories of a Cessna Citation X. The method consisted in numerically integrating the aircraft equations of motion for each segment that composed a typical takeoff and departure profile. For this purpose, the complete aircraft trajectory was divided into five typical segments, including ground acceleration, rotation, transition, climb at constant speed, and climb acceleration. For each segment, detailed algorithms to solve and integrate the equations of motion using an Euler scheme were designed. The complete aircraft trajectory was obtained by combining these segments in a specified order depending on the departure procedure profile. The validation of the methodology was evaluated with a qualified Research Aircraft flight Simulator (RAFS) of the Cessna Citation X. A total of 38 tests were carried out with the RAFS over a wide range of operational conditions. Comparison results showed that the trajectory data predicted by the different algorithms matched the trajectory data obtained from the RAFS with less than 5% of relative error.

4.1 Introduction

In recent years, the impact of aircraft on the environment has become one of the major concerns of the aviation industry. By burning fuel, aircraft engines produce carbon dioxide (CO_2), which contributes to global warming, but also pollutants such as nitrogen oxide (NO_x) and oxides of sulfur (SO_x), which are considered harmful to human health (Lee *et al.*, 2009). In 2018, the International Air Transport Association (IATA) estimated that the aviation industry was responsible for only 2 to 3% of global CO_2 emissions (IATA, 2018). This percentage, although relatively low, could nevertheless increase considerably in the coming years as the number of passengers is expected to double to 8.2 billion by 2037 (IATA, 2020).

In addition to emissions, the noise produced by commercial aircraft during takeoff operations has a high impact on the quality of life of people living in the vicinity of airports. Indeed, studies have shown that aircraft noise is not only a source of discomfort, but can also cause stress, anxiety, sleep disorders and cardiovascular disease (Correia *et al.*, 2013; Basner *et al.*, 2017).

Aware of its impact on the environment, the aviation industry has set several ambitious goals, including those of halving its net emissions by 2050 compared to 2005 levels and reducing its noise footprint by 50% (IATA, 2018). To achieve these objectives, many technologies are developed and implemented by aviation stakeholders. Current promising solutions include the development of more efficient and quieter engines (Haselbach *et al.*, 2015; Brouckaert *et al.*, 2018), the use of lighter materials to reduce aircraft weight (Marsh, 2012; Calado *et al.*, 2018), and the design of new wing shapes (Segui & Botez, 2018; Segui *et al.*, 2018, 2019). Another effective solution, more suitable in the short term, is based on the optimization of flight trajectories (Patrón *et al.*, 2014; Murrieta-Mendoza *et al.*, 2017a,b) and departure procedures (Roberson & Johns, 2007; Prats *et al.*, 2011).

4.1.1 Research Problems and Motivations

Defining an efficient departure procedure to mitigate noise and emissions is a complex process which requires the use of modern guidance and navigation technologies such as the Flight Management System (FMS). The FMS is an avionics computer which, among its many functions, can predict the takeoff performance of an aircraft, and provide the crew with vertical guidance to follow a predefined departure procedure [19,20]. In some cases, the FMS can also assist the crew in determining the most appropriate takeoff thrust to reduce fuel consumption while ensuring the safety of the flight. To accomplish these functions, the FMS requires a detailed takeoff performance model.

The typical structure of takeoff performance models encoded in most modern FMSs consists of a set of databases, called “performance databases” (Walter, 2001; Murrieta-Mendoza, Demange, George & Botez, 2015) These databases can be seen as multidimensional lookup tables containing relevant information on the aircraft performance and limitations. The word “performance” in this context refers to the ground distance traveled by the aircraft, and to the amount of fuel burned to perform a specific maneuver (i.e., takeoff, climb, acceleration). Using linear interpolation techniques and mathematical equations, the FMS can determine the aircraft vertical trajectory along a given lateral flight path (Liden, 1994; Murrieta-Mendoza & Botez, 2015).

Although very practical, takeoff performance models using databases have some drawbacks. Indeed, the databases are generally obtained from the various charts and tables published in aircraft flight manuals. All this information must therefore be extracted and post-processed manually before it can be encoded in the FMS memory. Such a process is time-consuming and can especially lead to uncertainties due to transcription errors. Another drawback is that data published in the flight manuals are usually generated according to standard procedures. As a result, it is not possible to generalize this data to other types of procedures, which greatly limits the capabilities of the FMS.

Faced with these drawbacks, FMS manufacturers are looking for new calculation tools to assess the performance of an aircraft during the takeoff and initial-climb phases. For this reason, studies are being conducted at the Laboratory of Applied Research in Active Controls, Avionics and AeroServoElasticity (LARCASE) to help researchers and avionics manufacturers to develop new modeling techniques to predict aircraft flight trajectories.

4.1.2 Methods for Calculating Aircraft Takeoff and Initial-Climb Trajectories

Currently, one of the best alternatives for FMS manufacturers to perform takeoff and climb performance analysis is to use proprietary applications developed by commercial aircraft manufacturers, such as Boeing (Blake, 2009) or Airbus (Airbus, 2002b). These applications were designed to help airline engineers perform detailed aircraft performance analyzes and effectively manage flight planning. They usually contain a wide range of tools and include very accurate aircraft performance models developed from flight test data. Unfortunately, these applications are very expensive and are only available under strict license agreements. Moreover, due to intellectual properties, they are often designed as black boxes, which means that the details of internal operations are not disclosed.

There are other more affordable commercial aviation programs that can be used to perform a variety of aircraft performance calculations. A comprehensive list of these programs can be found in (Filippone, 2008). However, because of their commercial nature, the details of the

models and of their internal operations are also not disclosed. In addition, it should be noted that most of these programs are based on simplified models, and there are no technical publications available.

The design of a flexible tool for the study of takeoff and departure procedures requires techniques and algorithms adapted to calculate aircraft trajectories. One of the most direct approach to do this is to solve and integrate a set of ordinary differential equations (also known as equations of motion) assuming initial conditions and constraints. This approach has notably been used by several researchers to optimize aircraft departure procedures for minimum noise impact (Erzberger & Lee, 1969; Visser & Wijnen, 2001; Prats *et al.*, 2011; McEnteggart & Whidborne, 2018). However, most of these studies have mainly focused on the optimization process, while the technique used to calculate the aircraft trajectory was either briefly introduced or omitted. In fact, the number of technical publications in the literature detailing methods for calculating aircraft takeoff and initial-climb trajectories was found to be very limited.

Quanbeck (1982) [33], for example, described a method for generating three-dimensional aircraft trajectories. The method consisted of using a Newton-Raphson optimization algorithm to solve the aircraft equations of motion, and a fourth-order Runge-Kutta scheme to integrate them. Unfortunately, the author did not apply his method to the takeoff and initial-climb phases, and no validation results were provided to demonstrate the reliability of the proposed method. A similar approach was considered by Filippone (2008) to evaluate the takeoff balanced field of a Boeing 777-200/300, and by Zhu *et al.* (2016) to compute the takeoff distance for a four-engine commercial aircraft. In both studies, the authors mentioned the use of a fourth-order Runge-Kutta scheme to integrate the aircraft equations of motion, but did not describe the technique used to solve them. In addition, Zhu *et al.* (2016) used a linear approximation to estimate the ground distance and time during the rotation phase, while Filippone (2008) did not considered this portion of the takeoff. In another study, Lambrecht & Slater (1999) presented a simplified method to integrate the equation of motion based on a modified Euler algorithm; their method was applied to the study of departure trajectories without considering the takeoff phase. Van Bavel (2014) proposed a technique to compute the takeoff performance of a Diamond D-JET

single engine turbofan aircraft. However, as in the previously cited studies, the influence of the wind and of the runway slope on the aircraft performance was not considered, and the method used to solve the motion equations was not detailed.

One reference that have been found particularly relevant to the study presented in this paper is provided by Blake (2009). In this report, the author described a step-by-step integration process used at Boeing to calculate the ground acceleration distance of an aircraft. Blake also provided a comprehensive technique for solving and integrating the equations of motion during a climb at constant speed. However, the scope of the report was limited to these two flight phases, and no solution was proposed for the other segments of the takeoff or for the climb-acceleration phase. Moreover, the author did not implement the influence of the wind on its proposed methodology.

Another approach to evaluate the takeoff and initial-climb trajectory of an aircraft is to use empirical or semi-empirical models. These models are closed-form solutions of the equations of motion, and can be found at different levels of details in various aircraft design manuals (Filippone, 2006; Raymer, 2012; Young, 2017). DARcoporation, for instance, used the theory described in Roskam's books (Roskam, 1985) to develop the Aircraft Performance Program (APP) (DARcoporation, 2019) for the study of aircraft performance for all phases of flight, including takeoff. Similarly, the Federal Aviation Administration (FAA) used the model equations proposed in SAE-AIR-1845 1998 to design the Aviation Environmental Design Tool (AEDT), and to model aircraft performance from takeoff to landing. Zammit-Mangion & Eshelby (2008) combined empirical equations based on flight tests data to model the performance of an aircraft during rotation and transition phases. Angeiras (2015) conducted a study to calculate the balanced field length of jet-engine aircraft using different semi-empirical models. The authors showed that the accuracy of the models considered in their study varied between 6.1 and 13.3%.

Although very practical, empirical models are generally too simplified and have a limited range of validity. These models are therefore useful for investigation of takeoff performance in early design phases, but they are not suitable for accurate analysis of takeoff and departure trajectories.

4.1.3 Research Objective and Paper Organization

The analysis presented in the previous section revealed that there is a lack of publications in the literature dealing with detailed methods for calculating aircraft takeoff and initial-climb trajectories. In addition, it has been found that in most studies, the equations used to describe the behavior of the aircraft have been simplified by neglecting various parameters such as the wind acceleration and the runway slope. Finally, all the studies except that proposed by Bavel Van Bavel (2014), did not consider the equation of moments. Yet, this equation is necessary in order to estimate the deflection of the control surfaces and to model the influence of the center of gravity on the performance of the aircraft.

The objective of this paper is therefore to propose a complete and flexible method for calculating the takeoff and departure trajectories of an aircraft, and for estimating a maximum number of flight parameters in order to allow any user to complete detailed performance analyses. The method aims to provide different algorithms to solve the equations of motion in order to trim the aircraft under various operating conditions, and to integrate them to predict the aircraft trajectory. These algorithms take into account the effects of non-constant winds and the runway slope on the aircraft performance, and can also be used to predict various flight parameters, such as the angle attack, the flight path angle and control surface deflections. Various methodologies are also proposed to model piloting techniques and reduced thrust operations. Finally, another originality of the proposed algorithms relied on the inclusion of the moment equation to accurately model the aircraft performance as a function of its position of the center of gravity.

Finally, the method was applied to the business jet aircraft Cessna Citation X for which a Research Aircraft Flight Simulator (RAFS) was available (see Figure 4.1). This RAFS was designed and built by CAE Inc. based on flight-test data provided by Textron Aviation. The flight dynamics and propulsion models encoded in the RAFS satisfy the criteria imposed by the Federal Aviation Administration (FAA) for the level-D (highest level of certification). The RAFS was therefore considered as a very good reference to evaluate the validity of the proposed method.

Figure 4.1 Cessna Citation X Research Aircraft Flight Simulator

The rest of the paper is structured as follows. **Section 4.2** introduces the mathematical equations used in this study to model the aircraft flight dynamics and aero-propulsive characteristics. **Section 4.3** deals with the complete methodology needed to predict the aircraft trajectory. **Section 4.4** presents the comparison and validation results. Finally, the paper ends with conclusions and remarks concerning future possible research.

4.2 Conventional Departure Procedure and Aircraft Mathematical Model

Before presenting the methodology to calculate the Cessna Citation X takeoff and initial-climb trajectories, it may be useful to introduce several notations and mathematical equations needed to model the aircraft behavior during these two flight phases. From this perspective, this section begins with a brief introduction to the Cessna Citation X, as well as with a description of the different segments that compose a typical departure procedure. The section then details the development of the aircraft mathematical model, which includes the equations of motion, the aero-propulsive model equations, and the environment model equations.

4.2.1 Cessna Citation X Aircraft Description

The aircraft considered in this study is the well-known Cessna Citation X (Model 750), produced and manufactured by Cessna Aircraft Company (became a brand of Textron Aviation in 2014). Introduced to the aviation market in 1996, the Citation X is a medium-sized business jet designed to accommodate 12 passengers, and to fly at a maximum altitude of 51,000 ft (15.5 km), and at a maximum speed equivalent to Mach 0.92. The aircraft propulsion system consists of two high-bypass Rolls-Royce AE3007C-1 turbofans. Each engine is capable of producing a maximum sea level static-thrust of approximately 6442 lbf (28.65 kN) for an average fuel consumption of 2712 lb/h (1230 kg/h). The Cessna Citation X has a maximum range of 3091 n miles (5725 km).

Other relevant takeoff specifications and limitations of the aircraft are given in Table 4.1. This information was obtained from the aircraft flight manuals and was used to define the limits of the aircraft operating envelope.

Table 4.1 Cessna Citation X Takeoff Specifications and Limitations

Parameters	**Values**	
Performance Limitations		
Maximum Takeoff Altitude	14,000 ft	4267 m
Maximum Tailwind Component	10 kts	18.52 km/h
Maximum Ambient Temperature	ISA+35°C	
Weight Limitations		
Maximum Takeoff Weight	36,100 lb	16,375 kg
Maximum Zero Fuel Weight	24,400 lb	11,067 kg
Initial-Climb Speed Limitations (Indicated Airspeed)		
Maximum Speed (Flaps 15°)	210 kts	389 km/h
Maximum Speed (Flaps 05°)	250 kts	463 km/h
Maximum Speed (Flaps 00°)	270 kts	500 km/h

4.2.2 Aircraft Departure Procedure and Flight Segments Definition

The portion of the flight considered in this paper is a normal departure procedure, which includes the takeoff phase and the initial-climb phase to 3000 ft above ground level (AGL). However, due to several aspects, such as terrain topography, noise restriction or aircraft performance, departure procedures may slightly vary from one airport/aircraft to another (ICAO, 2010). Thus, for the sake of simplicity, it is assumed that the aircraft always takes off by following one of the two standard Noise Abatement Departure Procedures (NADPs) illustrated in Figure 4.2.

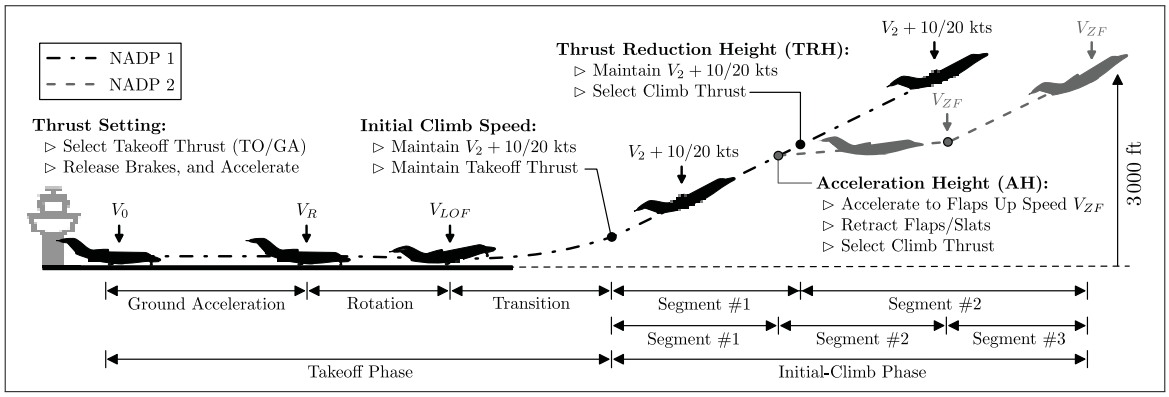

Figure 4.2 Noise Abatement Departure Procedures Illustration (NADP 1 and 2)

As shown in Figure 4.2, the aircraft vertical trajectory can be divided into four main segments: 1) the ground acceleration, 2) the rotation, 3) the transition, and 4) the initial-climb. The latter is itself composed of two or three segments depending on the selected departure procedure (NADP 1 or 2). A description together with relevant comments of these segments are given in the following sections.

4.2.2.1 Ground Acceleration from V_0 to V_R

The ground acceleration marks the beginning of the takeoff phase. This segment is initiated when the crew applies the maximum takeoff thrust by progressively advancing the thrust levers from the IDLE position to the Take-Off/Go-Around (TO/GA) position. In some cases, when the aircraft configuration and runway conditions allow, takeoff may be accomplished by using a

lower thrust than the maximum thrust. This procedure is commonly used by airlines because it preserves engine wear, and it reduces fuel consumption at the expense of the takeoff distance.

There are two methods to safely reduce engine thrust during takeoff: the assumed temperature method, and the derate method. In the first method, the thrust reduction is obtained by controlling the engines to produce a thrust assuming that the outside temperature is equal to a "fictitious" temperature, also called flexible temperature (FLEX). This temperature is specified by the crew in the FMS, and must be higher than the outside temperature. In the second method, the thrust reduction is obtained by preselecting in the FMS a certified takeoff thrust rating that is lower than the maximum rated takeoff thrust (i.e., TO/GA). The default thrust reduction level is TO/GA-10% or -20%, but for some aircraft, this percentage can be modified by the airline.

Once the brakes are released and the thrust is established, the aircraft begins to accelerate from an initial speed V_0 to a predetermined calibrated airspeed V_R, called the rotation speed.

4.2.2.2 Rotation from V_R to V_{LOF}

At the rotation speed V_R, the pilot pulls the yoke/stick back to move the elevators upward, and to initiate the rotation segment. The rate at which the aircraft pivots around its main landing gear depends on the aircraft weight and center of gravity location, but also on the pilot technique. In general, aircraft manufacturers recommend a rotation rate of approximately 3 to 5°/s in order to ensure adequate takeoff performance and avoid a tail strike. However, for aircraft such as the Cessna Citation X, this value may be higher due to relatively small inertia (Young, 2017).

The nose-up motion of the aircraft causes an increase in the angle of attack, which results in a progressive increase in the lift force. When the lift exceeds the aircraft weight, the main landing gear leaves the ground and the aircraft takes off. The speed at which the aircraft takes off is called the lift-off speed and is denoted by V_{LOF}.

4.2.2.3 Transition from V_{LOF} to $V_2 + \Delta V_2$

After the lift-off, the pilot continues to adjust the aircraft attitude by using the elevators to capture a predetermined calibrated airspeed of $V_2 + \Delta V_2$. The speed V_2 is called the takeoff safety speed; it is established by the aircraft manufacturer as the minimum speed at which the aircraft may climb in case of engine failure. Under normal operating conditions (i.e., with all engines operative), a speed of V_2+10/20 kts is preferred as it offers better climb performance in terms of gain in altitude over a given amount of time.

During the transition segment, the landing gear must be retracted when a positive climb rate has been established or at a given altitude. The thrust and the flaps, however, remain in their initial configurations.

4.2.2.4 Initial-Climb and Departure Profile

Once the speed of V_2+10/20 kts is captured, the pilot can then begin the initial-climb phase by conforming to one of the two noise abatement procedures illustrated in Figure 4.2.

For the NADP 1, the pilot is expected to climb at V_2+10/20 kts until the Thrust Reduction Height (TRH), which typically ranges from 800 to 1500 ft. At this altitude, the thrust must be reduced to climb thrust by placing the thrust levers in the climb detent (CLB). The pilot then continues to climb at V_2+10/20 kts to 3000 ft AGL while maintaining the flaps in their initial takeoff configuration.

For the NADP 2, the pilot is expected to climb at V_2+10/20 kts until the Acceleration Height (AH), which typically ranges from 800 to 1000 ft. At this altitude, the pilot accelerates the aircraft to the flaps up speed V_{ZF} by reducing the aircraft pitch attitude. During the acceleration, the flaps must be progressively retracted, and the thrust reduction must be performed either at the beginning of the first flaps retraction, or when the flaps are fully retracted. After the acceleration phase, the pilot then continues to climb at V_{ZF} to 3000 ft AGL.

4.2.3 Aircraft Mathematical Equations and Flight Model

For the purposes of this study, the aircraft is modeled as a rigid body, and its motion is strictly confined in a vertical plane on a non-rotating, flat earth (Young, 2017). All engines are supposed to be operational, and there is no asymmetric thrust. In addition, it is assumed that the aircraft accelerates along a runway which has a slope angle of γ_R as shown in Figure 4.3. Finally, the wind is reduced to its longitudinal component that is altitude-dependent.

4.2.3.1 Aircraft Equations of Motion

The forces acting on the aircraft during takeoff are illustrated in Figure 4.3.

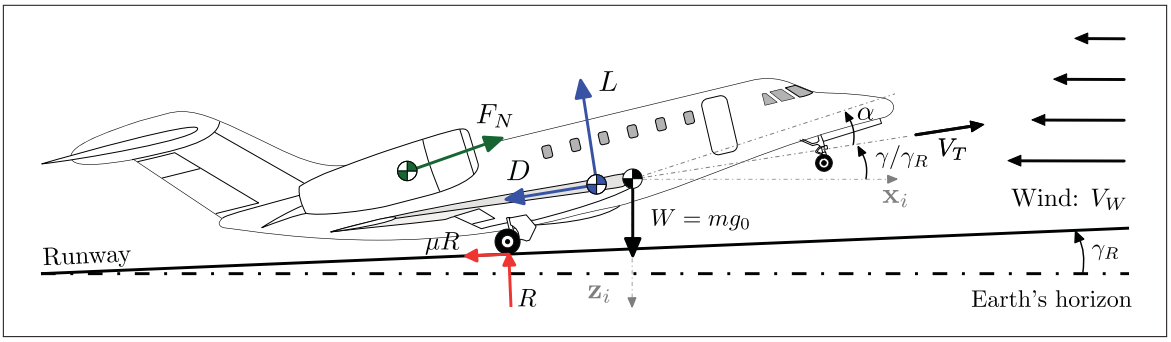

Figure 4.3 Forces Applied to the Cessna Citation X during Takeoff

The lift L and the drag D are the aerodynamic forces, and they are defined to be normal and parallel to the aircraft airspeed. The total thrust of the engines, denoted by F_N, is oriented in the forward direction making an angle ϕ_T relative to the aircraft fuselage. The reaction force acting on each landing gear (i.e., main and nose) is decomposed into a normal force R, and a friction force μR, where μ is the friction coefficient. Finally, the weight W is oriented towards the center of the Earth.

By summing the forces along and parallel to the flight path, it can be shown that the pertinent equations describing the motion of the aircraft are:

$$m\dot{V}_T = F_N \cos(\alpha + \phi_T) - D - \mu(R_M + R_N) - mg_0 \sin(\gamma) - m\dot{V}_W \cos(\gamma) \tag{4.1}$$

$$m\dot{\gamma}V_T = F_N \sin(\alpha + \phi_T) + L + R_M + R_N - mg_0 \cos(\gamma) + m\dot{V}_W \sin(\gamma) \tag{4.2}$$

$$\dot{h} = V_T \sin(\gamma) \quad \text{and} \quad \dot{x} = V_T \cos(\gamma) + V_W \tag{4.3}$$

where m is the aircraft mass, V_T is the true airspeed, V_W is the horizontal wind speed component, α is the angle of attack, γ is the flight path angle, g_0 is the acceleration of gravity, and R_M and R_N are the ground reaction forces acting on the main and nose landing gear, respectively.

The two parameters $\dot{h}$ and $\dot{x}$ in Eq. (4.3) represent the components of aircraft velocity in the vertical and horizontal directions. These parameters lead therefore by integration to the aircraft altitude h, and to the ground distance x.

In addition to the force equations (4.1) and (4.2), the moment equation can be also obtained by resolving the moments applied about the aircraft center of gravity. By assuming that the angular acceleration of the aircraft is either zero or very small, the following equation can be written:

$$\begin{aligned} 0 = {} & M_y + (\Delta\bar{x}_{CT} - \Delta\bar{x}_{CG})\, F_N \sin(\alpha + \phi_T) + (\Delta\bar{z}_{CT} - \Delta\bar{z}_{CG})\, F_N \cos(\alpha + \phi_T) - \cdots \\ & \cdots - \Delta\bar{x}_{CG} L + \Delta\bar{z}_{CG} D + (\Delta\bar{x}_M - \Delta\bar{x}_{CG})\, R_M - (\Delta\bar{z}_M - \Delta\bar{z}_{CG})\, \mu R_M + \cdots \\ & \cdots + (\Delta\bar{x}_N - \Delta\bar{x}_{CG})\, R_N - (\Delta\bar{z}_N - \Delta\bar{z}_{CG})\, \mu R_N \end{aligned} \tag{4.4}$$

where M_y is the aerodynamic pitching moment, and $\{\Delta\bar{x}, \Delta\bar{z}\}$ are the distances of the center of gravity (CG), center of thrust (CT), and landing gear contact points (noise: N, main: M) relative to the wing aerodynamic center. Note that these distances are expressed along, and perpendicular to the airspeed direction to be consistent with Eqs. (4.1) and (4.2).

It should also be noted that Eq. (4.4) is only necessary when the elevator deflection or the horizontal stabilizer position required to hold a given pitch attitude has to be calculated. This equation is also used to model the influence of the center of gravity location on the aircraft

performance by calculating the "trim drag" generated by the two control surfaces. However, if the elevator deflection and the horizontal stabilizer position are not explicitly considered in the mathematical model of the aircraft, Eq. (4.4) can be ignored, and the methodology can still be applied.

Finally, the aircraft mass variation due to fuel consumption is modeled as follows:

$$\dot{m} = -W_F \Rightarrow \Delta m = \Delta F_B = W_F \times \Delta t \tag{4.5}$$

where W_F is the engines fuel flow, and ΔF_B is the fuel burned during a given time interval Δt.

4.2.3.2 Aerodynamic Coefficients Model

The lift, drag and pitching moment in Eqs. (4.1), (4.2) and (4.4) are the three components of the aerodynamic resultant acting on the aircraft. These components are represented using non-dimensional coefficients, such as:

$$L = 0.5\rho S V_T^2 C L_s \tag{4.6}$$

$$D = 0.5\rho S V_T^2 C D_s \tag{4.7}$$

$$M_y = 0.5\rho S \bar{c} V_T^2 C m_s \tag{4.8}$$

where ρ is the air density, S is the aircraft wing reference area, $\bar{c}$ is the wing mean aerodynamic chord, and CL_s, CD_s and Cm_s are the lift, drag and pitching moment aerodynamic coefficients, respectively.

The model used in this study to evaluate the aerodynamic coefficients was generated in-house by the LARCASE team based on the data encoded in the RAFS. The model consists of a set of lookup tables describing the variations of each coefficient as function of the angle of attack α, the Mach number M, the flaps setting δ_f, the landing gear position δ_g, the horizontal stabilizer position δ_s, the elevators deflection δ_e, and the aircraft height $\bar{h}$.

Mathematically, these coefficients are expressed as follows:

$$CL_s = CL_{WB}(\alpha, M, \delta_f) + \Delta CL_{GR}(\alpha, M, \delta_g) + \Delta CL_{HT}(\alpha, M, \delta_e, \delta_s) + \Delta CL_{GE}(\alpha, M, \bar{h}) \tag{4.9}$$

$$CD_s = CD_{WB}(\alpha, M, \delta_f) + \Delta CD_{GR}(\alpha, M, \delta_g) + \Delta CD_{HT}(\alpha, M, \delta_e, \delta_s) + \Delta CD_{GE}(\alpha, M, \bar{h}) \tag{4.10}$$

$$Cm_s = Cm_{WB}(\alpha, M, \delta_f) + \Delta Cm_{GR}(\alpha, M, \delta_g) + \Delta Cm_{HT}(\alpha, M, \delta_e, \delta_s) + \Delta Cm_{GE}(\alpha, M, \bar{h}) \tag{4.11}$$

where each element in the above equations (i.e., CL_{WB}, ΔCL_{GR}, ΔCL_{HT}, etc.) is a three- or four-dimensional lookup table. Each lookup table is interpolated individually by using a linear interpolation technique. The total coefficients of the aircraft are then obtained by summing their contributions corresponding to the wing-body (CX_{WB}), the landing gear (ΔCX_{GR}), the horizontal stabilizer (ΔCX_{HT}), and the ground effect (ΔCX_{GE}).

4.2.3.3 Thrust and Fuel Flow Models

In the same way as for the aerodynamic coefficients, the engine model is also composed of a set of four-dimensional lookup tables describing the variation of the thrust and fuel flow as function of the altitude h, the Mach number M, and temperature conditions. These lookup tables were developed and validated by the authors in a previous study using data from the RAFS (Ghazi *et al.*, 2015c; Ghazi & Botez, 2019) - [see **Chapter 2**].

Mathematically, the thrust and fuel flow are expressed as follows:

$$F_N = F_N(N_1, h, M, \Delta\text{ISA}) \tag{4.12}$$

$$W_F = W_F(N_1, h, M, \Delta\text{ISA}) \tag{4.13}$$

where N_1 is the engine fan speed, and ΔISA is the temperature deviation from a standard day value.

The engine fan speed N_1 is also described by a four-dimensional lookup table, and is mathematically expressed as follows:

$$N_1 = N_1(h, M, \Delta\text{ISA}, TRP) - \Delta N_1 \tag{4.14}$$

where TRP is the Thrust Rating Parameter (i.e., IDLE, CLB, or TO/GA), and ΔN_1 is a factor that quantifies the thrust reduction in the case of a derated thrust. For the assumed temperature method, the fan speed N_1 is interpolated using a temperature deviation ΔISA calculated from a FLEX temperature rather than from the actual temperature.

4.2.4 Environment Model and Airspeed Conversions

The mathematical model used in this paper to evaluate the atmosphere properties around the airport is based on the International Standard Atmosphere (ISA). Thus, the temperature at a specific altitude is calculated by assuming a linear distribution with a temperature offset ΔISA, such as:

$$T = T_0 - T'h + \Delta\text{ISA} \tag{4.15}$$

where T_0 is the standard sea level temperature, and T' is the temperature gradient. From the temperature distribution law defined in Eq. (4.15), the pressure and density are computed according to the two following relationships:

$$P = P_0 \left[1 - T'h/T_0\right]^{g_0/(R_{\text{air}}T')} \tag{4.16}$$

$$\rho = \rho_0 \left(\delta/\theta\right) \tag{4.17}$$

where P_0 and ρ_0 are the standard sea level pressure and density, respectively, R_{air} is the air gas constant, $\delta = P/P_0$ is pressure ratio, and $\theta = T/T_0$ is temperature ratio.

Similar to the temperature, the wind speed is modeled as function of altitude according to the following equation:

$$V_W = V_{W,0} + V'_W(h - h_0) \tag{4.18}$$

where $V_{W,0}$ is the wind speed at the airport, h_0 is the airport altitude, and V'_W is the wind gradient assumed to be constant. It should be noted that the sign convention for the wind speed is such that a tailwind is positive, while a headwind is negative.

Finally, the results of Eqs. (4.15) to (4.17) are also used in converting airspeed between calibrated airspeed (V_C), true airspeed (V_T), and Mach number (M). Typically, when V_C is known, the Mach number is first calculated as follows:

$$M = \sqrt{5\left\{\left[\frac{1}{\delta}\left\{\left[1+0.2\left(\frac{V_C}{a_0}\right)^2\right]^{3.5}-1\right\}+1\right]^{1/3.5}-1\right\}} \tag{4.19}$$

and V_T is then obtained using the following equation:

$$V_T = a_0 M\sqrt{\theta} \tag{4.20}$$

Conversely, when V_T is known, the Mach number is first calculated from Eq. (4.20), and V_C is then obtained as follows:

$$V_C = a_0\sqrt{5\left\{\left[\delta\left\{\left(1+0.2M^2\right)^{3.5}-1\right\}+1\right]^{1/3.5}-1\right\}} \tag{4.21}$$

where a_0 is the sea level speed of sound.

4.3 Aircraft Takeoff and Departure Trajectory Prediction Algorithm

The methodology to calculate the Cessna Citation X takeoff and initial-climb trajectory consists in numerically integrating the aircraft equations of motion presented in **Section 4.2.3** from an initial state (i.e. weight, speed, altitude, etc.) and by assuming environment conditions (i.e., temperature, pressure, density and wind). For the sake of calculations, the aircraft trajectory is divided into five types of segments: ground acceleration, rotation, transition, climb at constant calibrated speed, and climb acceleration. The complete aircraft trajectory is obtained by combining these segments in a specified order depending on the departure procedure profile.

4.3.1 Evaluation of the Aircraft Trajectory for the Ground Acceleration Segment

The aircraft trajectory during the ground acceleration is calculated by numerically integrating the aircraft equations of motion from an initial airspeed $V_{T[0]}$ to a predetermined airspeed $V_{T[N]}$. For this purpose, the ground acceleration segment is divided into N airspeed intervals (or sub-segments) as illustrated in Figure 4.4.

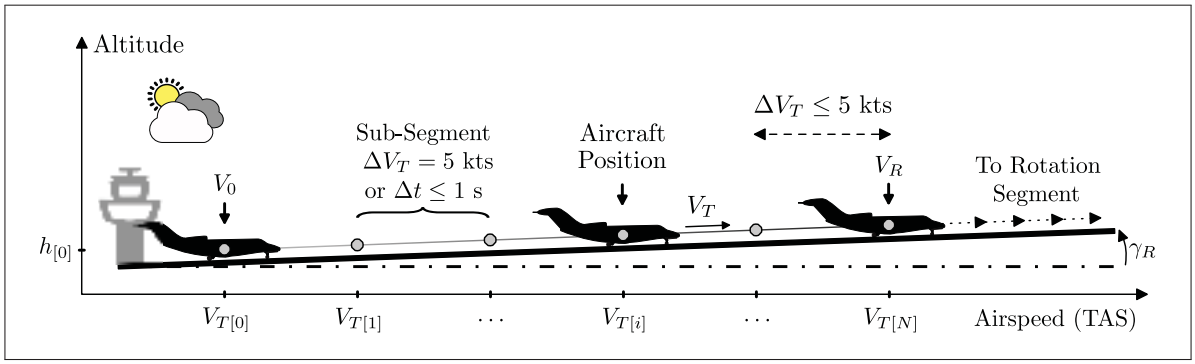

Figure 4.4 Illustration of the Calculation Procedure for the Ground Acceleration Segment

The step size for the airspeed is arbitrary. As general rule, a large step size will reduce the computation time to the detriment of the results accuracy, while a small step size will provide a slight gain in accuracy at the expense of additional computational effort. A suggested size is between 5 and 10 kts (see **Section 4.3.1.3** for more details). However, in order to improve the efficiency of the algorithm the time step should not exceed 1.0 s, especially in the beginning of the acceleration phase. In addition, to ensure a good capture of the final airspeed, it is necessary to reduce the size of the last sub-segment.

4.3.1.1 Aircraft Equations of Motion Simplification and Model Parameterization

To simplify the calculations, several simplifications can be applied. As shown in Figure 4.4, the aircraft trajectory during the ground acceleration phase remains parallel to the runway. Therefore, the flight path angle γ is constant (i.e., $\dot{\gamma} = 0$), and equal to the runway inclination (i.e.,$\gamma = \gamma_R$). In addition, the variation of the aircraft attitude during the acceleration phase can only result from the extension of the nose landing gear because of the lift force which increases

as the aircraft gains speed. However, the magnitude of this variation is in general small, and to a good approximation can be neglected. Consequently, the aircraft angle of attack can be assumed constant. Finally, by neglecting the altitude variation due to the runway slope, the wind speed can also be assumed constant.

By implementing these simplifications into Eqs. (4.1) to (4.3), the equations describing the motion of the aircraft within the ground acceleration segment can be stated as follows:

$$R = mg_0 \cos(\gamma_R) - F_N \sin(\alpha_0 + \phi_T) - L \tag{4.22}$$

$$\dot{V}_T = m^{-1} \left[F_N \cos(\alpha_0 + \phi_T) - D - \mu R - mg_0 \sin(\gamma_R) \right] \tag{4.23}$$

$$\dot{h} = V_T \sin(\gamma_R) \quad \text{and} \quad \dot{x} = V_T \cos(\gamma_R) + V_{W,0} \tag{4.24}$$

where $R = (R_M + R_N)$ is the total ground reaction force, and α_0 is the aircraft angle of attack on the ground.

In the beginning of the acceleration, the engine thrust increases from IDLE to TO/GA. To avoid asymmetry thrust, pilots do not directly apply full thrust, but rather use a "two-step stabilization" procedure which consists of first advancing the thrust levers about halfway between IDLE and TO/GA, and then advancing them directly to TO/GA once the engines have stabilized. To model this aspect, a series of acceleration tests was conducted with the Cessna Citation X RAFS. These tests aimed to accelerate using a "two-step stabilization" procedure, and to collect the engine fan speed over a period of 20 seconds. The results obtained for all the tests are shown in Figure 4.5.

Based on the data shown in Figure 4.5, the engine acceleration was approximated using a sigmoid function as follows:

$$N_1 = N_1^{IDLE} + \frac{\left(N_1^{TO/GA} - N_1^{IDLE} \right)}{1 + \exp\left[-(t - t_d).\tau^{-1} \right]} \tag{4.25}$$

where N_1^{IDLE} and $N_1^{TO/GA}$ are the engine fan speeds corresponding to the IDLE and TO/GA regimes, $\tau = 0.67$ s represents the time constant, and $t_d = 8.5$ s is the time delay.

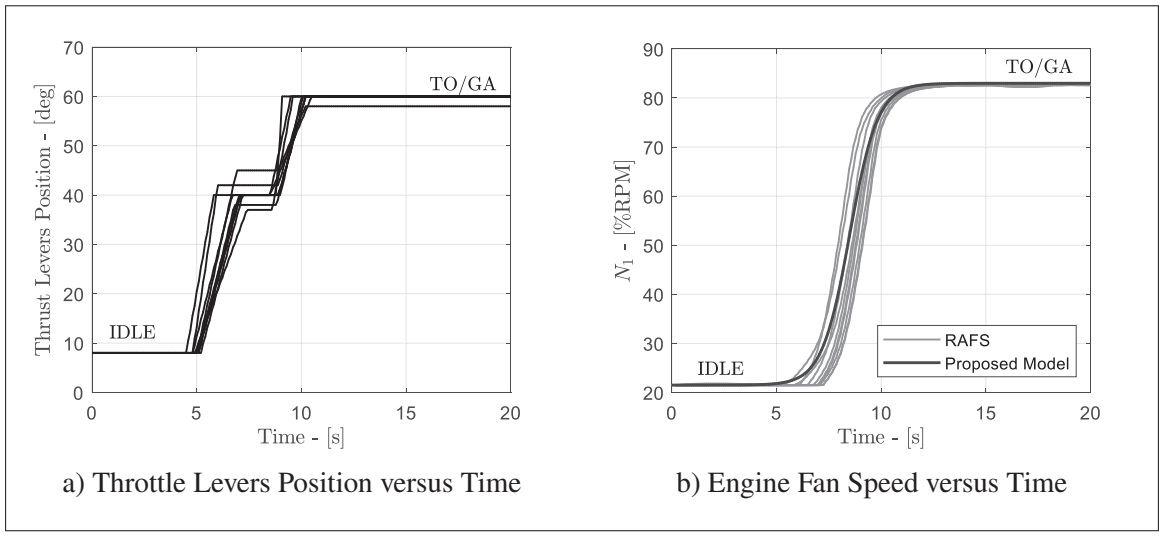

a) Throttle Levers Position versus Time

b) Engine Fan Speed versus Time

Figure 4.5 Engine Acceleration from IDLE to TO/GA using a "Two-Step Stabilization" Procedure

Another important parameter to be determined is the friction coefficient which depends on the runway surface condition. To accurately model this parameter, another series of ground acceleration test was conducted with the RAFS for various aircraft weights and runway conditions. The data collected during the tests were used to calculate the aero-propulsive forces (i.e., lift, drag and thrust), and then to estimate the aircraft acceleration based on Eqs. (4.22) and (4.23) for different friction coefficients ranging from 0 to 0.06. For each friction coefficient value, the average absolute error between the measured and the estimated acceleration was calculated. The errors were finally inversely normalized by mapping the highest value to 0 and the lowest value to 1.

The results obtained are shown in Figure 4.6, where each graph is traced for each different runway condition; dry, wet with a water depth of 5 mm, and wet with a water depth of 12 mm.

By approximating the error distributions in Figure 4.6 with a first-order Gaussian curve, the friction coefficient was determined to be 0.018 for a dry runway, 0.027 for a wet runway with a water depth of 5 mm, and finally 0.038 for a runway with a water depth of 12 mm. Note that in

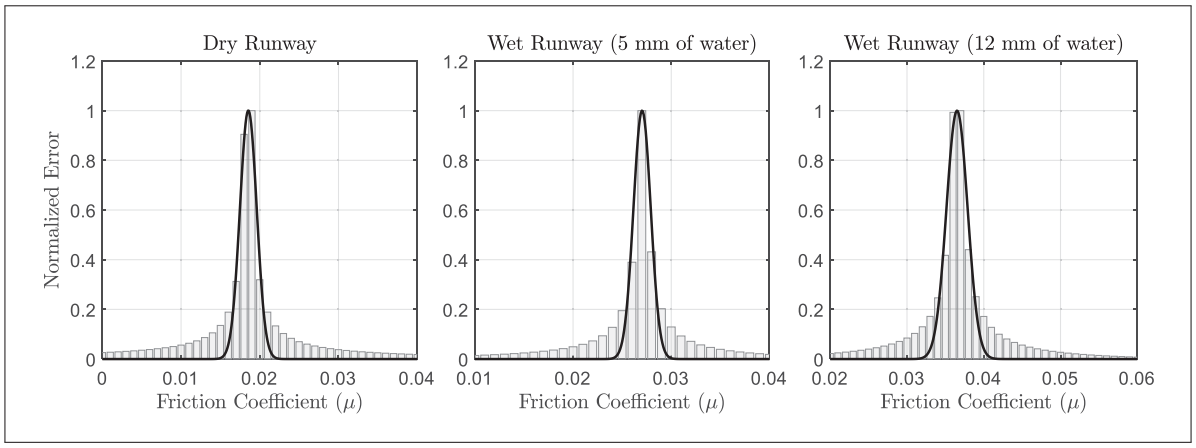

Figure 4.6 Friction Coefficient Determination for a Dry and Wet Runway

the absence of accurate information to determine the value of the friction coefficient, empirical values available in references (Raymer, 2012; Young, 2017) can be considered.

Finally, the aircraft angle of attack on the ground α_0 was estimated to be around -1.28° based on a three-view diagram of the Cessna Citation X.

4.3.1.2 Elevators Deflection and Horizontal Stabilizer Position Determination

To evaluate the lift and drag forces in Eqs. (4.22) and (4.23), it is necessary to know the elevators deflection and the horizontal stabilizer position. In general, during ground acceleration, pilots are not expected to use the elevators. Therefore, the elevators can be assumed to have zero deflection. The horizontal stabilizer, however, must be configured according to the flight manual recommendations. In the Cessna Citation X case, the stabilizer position for takeoff is given as function of the center of gravity position and flap setting (5° or 15°).

Under this particular condition, Eq. (4.4) can be used to decompose the total ground reaction force and determine the contributions of the main and nose landing gears. By introducing the ratio $\delta_R = R_M/(R_M + R_N)$, and recalling that $R = (R_M + R_N)$, it can be shown from Eq. (4.4) that:

$$\delta_R = -\frac{\Sigma M_{OG} + R\left(\Delta\bar{x}_N - \Delta\bar{x}_{CG}\right) - \mu R\left(\Delta\bar{z}_N - \Delta\bar{z}_{CG}\right)}{R\left(\Delta\bar{x}_M - \Delta\bar{x}_N\right) - \mu R\left(\Delta\bar{z}_M - \Delta\bar{z}_N\right)} \tag{4.26}$$

where ΣM_{OG} is the "out-of-ground" moment defined such as:

$$\begin{aligned}\Sigma M_{OG} = M_y - \Delta\bar{x}_{CG}L + \Delta\bar{z}_{CG}D + \left(\Delta\bar{x}_{CT} - \Delta\bar{x}_{CG}\right)F_N\sin(\alpha_0 + \phi_T) + \cdots \\ \cdots + \left(\Delta\bar{z}_{CT} - \Delta\bar{z}_{CG}\right)F_N\cos(\alpha_0 + \phi_T)\end{aligned} \tag{4.27}$$

Finally, the reaction force applied to each landing gear can be calculated as follows:

$$\begin{aligned}R_M &= \delta_R R \\ R_N &= (1 - \delta_R)R\end{aligned} \tag{4.28}$$

where R is obtained from Eq. (4.22).

4.3.1.3 Complete Calculation Process

Equations (4.22) to (4.28) are the main equations describing the aircraft performance during the ground acceleration phase. The complete procedure proposed to integrate these equations, and to compute the aircraft trajectory for this type of segment is described in Algorithm 4.1. Note that the rotation speed V_R is assumed to be known from the takeoff performance data published in the aircraft flight manuals.

The method used to integrate the equations of the aircraft was based on the Euler method. This method was chosen for its simplicity, but also because of the fact that it offers a good compromise between results accuracy and computation time depending on the integration step size. Figure 4.7a shows the precision of the algorithm for various values of the airspeed step size. The relative errors shown in this figure were obtained by comparing the data estimated by the algorithm with those measured with the RAFS for 10 ground acceleration tests. Figure 4.7b, on the other hand, shows the influence of the airspeed step size on the computation time.

Algorithm 4.1 Calculation Procedure for the Ground Acceleration Segment

0. Initialization: Initialise the aircraft states; mass $m_{[0]}$, altitudes $h_{[0]}$ and $\bar{h}_{[0]}$, and true airspeed $V_{T[0]} = -V_{W,0}$, and then set the time $t_{[0]}$, ground distance $x_{[0]}$, and fuel burned $F_{B[0]}$ to zero.

1. Aircraft Configuration and Rotation Speed Definition: Select the aircraft flap setting and center of gravity location. Determine the horizontal stabilizer position δ_s and the rotation speed V_R as recommended in the aircraft flight manuals. Set δ_e to zero.

2. Integration and Model Parameters Definition: Define the maximum airspeed step $\Delta V_T^{MAX} = 5$ kts, and compute the target airspeed $V_{T,R}$ by converting the rotation speed V_R from CAS to TAS. Define the runway parameters: μ and γ_R. Set i to 0.

3. Main Loop: repeat

a) Based on the atmosphere model, compute the parameters: air density ρ, temperature ratio θ, pressure ratio δ, and Mach number M from $V_{T[i]}$.

b) Based on the engine model and flight conditions, compute the thrust F_N and fuel flow W_F by assuming TO/GA, derate or FLEX setting.

c) By considering a constant angle of attack α_0, and based on the aircraft configuration, interpolate the three aerodynamic coefficients: CL_s, CD_s, and Cm_s.

d) Compute the total ground reaction:

$$R = m_{[i]} g_0 \cos(\gamma_R) - F_N \sin(\alpha_0 + \phi_T) - L$$

e) Knowing the total ground reaction, compute the aircraft acceleration:

$$\dot{V}_T = m_{[i]}^{-1} \left[F_N \cos(\alpha_0 + \phi_T) - D - \mu R - m_{[i]} g_0 \sin(\gamma_R) \right]$$

f) Decompose the ground reaction for each landing gear using Eqs. (4.26) to (4.28).

g) Adjust the time step for the current sub-segment:

$$\Delta t = \min \left\{ 1, \Delta V_T^{MAX} / \dot{V}_T, \left(V_{T,R} - V_{T[i]} \right) / \dot{V}_T \right\}$$

h) Compute the speed, altitude, distance, and mass variations for the current sub-segment:

$$\Delta V_T = \dot{V}_T \Delta t \quad \Delta h = V_{T[i]} \sin(\gamma_R) \Delta t \quad \Delta x = \left[V_{T[i]} \cos(\gamma_R) + V_{W,0} \right] \Delta t \quad \Delta m = W_F \Delta t$$

i) Update the aircraft states, and the number of iterations:

$$h_{[i+1]} = h_{[i]} + \Delta h \quad t_{[i+1]} = t_{[i]} + \Delta t \quad V_{T[i+1]} = V_{T[i]} + \Delta V_T \quad \bar{h}_{[i+1]} = 0$$
$$x_{[i+1]} = x_{[i]} + \Delta x \quad m_{[i+1]} = m_{[i]} - \Delta m \quad F_{B[i+1]} = F_{B[i]} + \Delta m \quad i = i + 1$$

while $\left(V_{T[i]} < V_{T,R} \right)$;

4. Return all flight parameters, including altitude, distance, time and fuel burned.

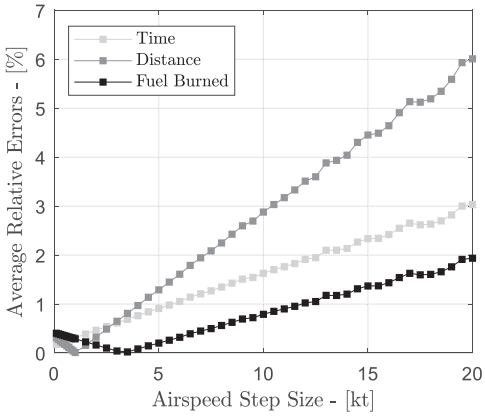

a) Distance, Fuel Burned, and Time Average Relative Errors versus Airspeed Step Size

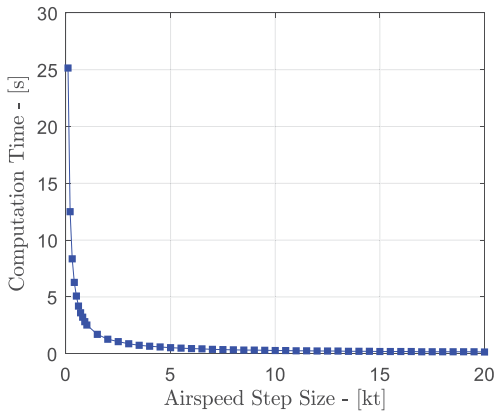

b) Computation Time versus Airspeed Step Size

Figure 4.7 Airspeed Step Size Influence

Typically, a step size smaller than 5 kt provides very good estimates, with relative errors of less than 1.5%. However, the computation time is relatively large, ranging from 25 to 0.5 seconds. Conversely, a step size higher than 10 kts allows the computation time to be reduced to 0.28 seconds, but the absolute relative errors increase up to 3%. In addition, the gain in terms of computation time reduction above 10 kts is almost negligible. Consequently, a good compromise would be the choice of a step size between 5 and 10 kt, which enables relative errors between 1.5 and 3%, and a computation time between 0.5 and 0.28 seconds.

4.3.2 Evaluation of the Aircraft Trajectory for the Rotation Segment

The aircraft trajectory from the beginning of the rotation to the lift-off is calculated by following a procedure similar to that used for the ground acceleration. However, since the lift-off speed cannot be determined from the data published in the aircraft flight manuals, the equations of motion need to be integrated in time. Moreover, the only way to detect if the aircraft has reached the lift-off speed is to compute the ground reaction and check whenever it is zero. This fact means that the calculations must be repeated as long as the ground reaction is positive. Such a concept is schematically illustrated in Figure 4.8.

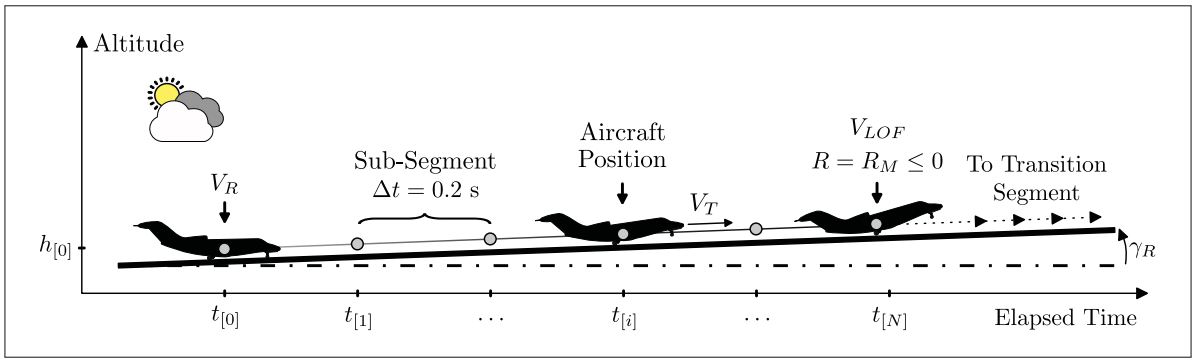

Figure 4.8 Illustration of the Calculation Procedure for the Rotation Segment

The step size for the calculations is arbitrary. However, since the time to rotate the aircraft is relatively small in practice, it is preferable to use a small step time. This will also lead to a greater accuracy in the prediction of the lift-off speed. A suggested time step for the rotation calculations is between 0.2 and 0.5 s.

4.3.2.1 Aircraft Equations of Motion Simplification and Model Parameterization

As for the ground acceleration, several simplifications can be applied to simplify the calculation process. Indeed, during the rotation, the aircraft pivots around its main landing gear at a quasi-constant rate, while it continues to accelerate down the runway. This fact implies that the flight path angle remains constant and equal to the runway inclination, and that the variation of the angle of attack can be approximated by:

$$\alpha = \min\left[\alpha_0 + \dot{\alpha}_R \times t, \alpha_{TS}\right] \tag{4.29}$$

where $\dot{\alpha_R}$ is the aircraft rotation rate, and α_{TS} is the maximum allowed angle of attack to prevent a tail strike.

By following a procedure similar to that used for the friction coefficient in **Section 4.3.1.1**, the rotation rate $\dot{\alpha}_R$ was estimated in average at 6.5°/s, while the maximum angle of attack $\alpha_{TS} = 17°$ was geometrically determined from a three-view diagram of the Cessna Citation X.

Another simplification that can be considered to reduce the complexity of the equations relies on the fact that from the beginning of the rotation to the lift-off moment, the nose landing gear is not in contact with the ground. This means that the ground reaction force R_N is zero, and that the apparent aircraft weight (i.e., weight minus the lift and thrust components) is supported only by the main landing gear.

Thus, by combining these observations with Eqs. (4.1) to (4.3), the pertinent equations describing the motion of the aircraft during the rotation can be stated as follows:

$$R_M = mg_0 \cos(\gamma_R) - F_N \sin(\alpha + \phi_T) - L \quad \text{and} \quad R_N = 0 \tag{4.30}$$

$$\dot{V}_T = m^{-1} \left[F_N \cos(\alpha + \phi_T) - D - \mu R_M - mg_0 \sin(\gamma_R) \right] \tag{4.31}$$

$$\dot{h} = V_T \sin(\gamma_R) \quad \text{and} \quad \dot{x} = V_T \cos(\gamma_R) + V_{W,0} \tag{4.32}$$

4.3.2.2 Elevators Deflection and Horizontal Stabilizer Position Determination

To complete the calculation procedure, it is necessary to determine the elevators deflection that the pilot must apply to rotate the aircraft (the horizontal stabilizer is supposed to remain in its initial configuration). A practical approach to do this is to assume that the aircraft is in quasi-static equilibrium within each sub-segment of the rotation segment.

Mathematically, this aspect implies:

$$\begin{aligned} \Sigma M(\delta_e) = {} & M_y(\delta_e) - \Delta\bar{x}_{CG} L(\delta_e) + \Delta\bar{z}_{CG} D(\delta_e) + (\Delta\bar{x}_{CT} - \Delta\bar{x}_{CG})\, F_N \sin(\alpha + \phi_T) + \cdots \\ & \cdots + (\Delta\bar{z}_{CT} - \Delta\bar{z}_{CG})\, F_N \cos(\alpha + \phi_T) + (\Delta\bar{x}_M - \Delta\bar{x}_{CG})\, R_M - \cdots \\ & \cdots - (\Delta\bar{z}_M - \Delta\bar{z}_{CG})\, \mu R_M = 0 \end{aligned} \tag{4.33}$$

The technique proposed in this study to solve this equation is called “reverse lookup table”, and is illustrated in Figure 4.9 for the convenience of the reader.

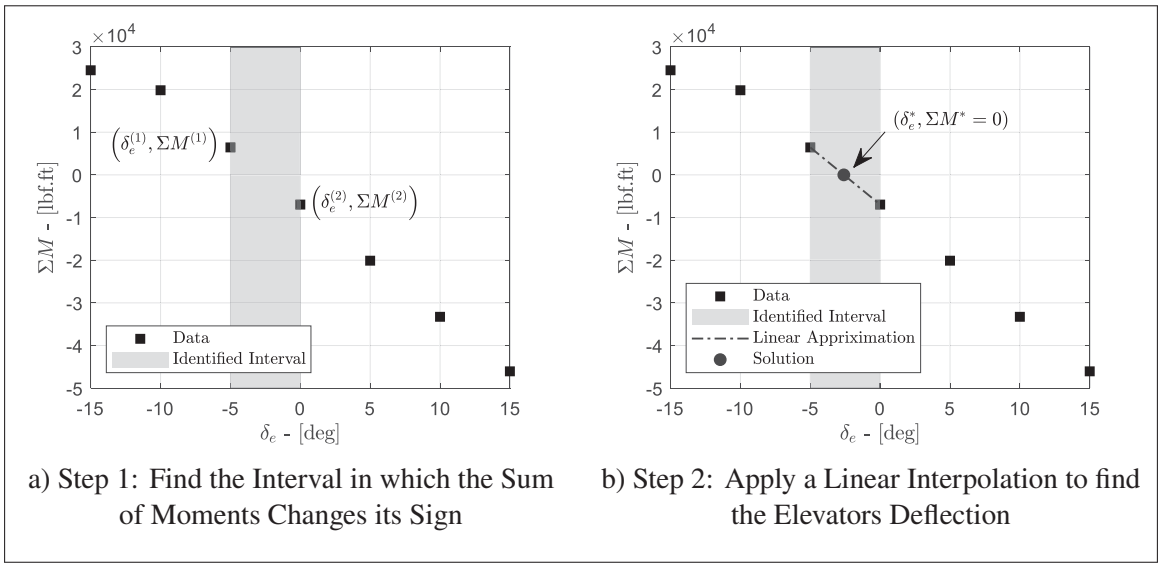

a) Step 1: Find the Interval in which the Sum of Moments Changes its Sign

b) Step 2: Apply a Linear Interpolation to find the Elevators Deflection

Figure 4.9 Illustration of the "Reverse Lookup Table" Technique

As shown in Figure 4.9a, the technique consists first in evaluating the sum of moments for several elevators positions, and in finding the interval $[\delta_e^{(1)}, \delta_e^{(2)}]$ in which the sum changes its sign. Once this interval is identified, a linear interpolation is then applied, as shown in Figure 4.9b to determine the elevators deflection δ_e^* leading to $\Sigma M(\delta_e) = 0$. The result of this interpolation can be mathematically written as follows:

$$\delta_e^* = \delta_e^{(1)} + \frac{\delta_e^{(2)} - \delta_e^{(1)}}{\Sigma M^{(2)} - \Sigma M^{(1)}} \Sigma M^{(1)} \tag{4.34}$$

where $\Sigma M^{(1)}$ and $\Sigma M^{(2)}$ are the sum of moments evaluated at $\delta_e^{(1)}$ and $\delta_e^{(2)}$, respectively.

4.3.2.3 Complete Calculation Process

Equations (4.29) to (4.33) are the main equations describing the aircraft performance during the rotation segment. The complete procedure proposed to integrate these equations and compute the aircraft trajectory for this type of segment is described in Algorithm 4.2.

Algorithm 4.2 Calculation Procedure for the Rotation Segment

0. Initialization: From the results of Algorithm 4.1, initialise the aircraft states; mass $m_{[0]}$, altitudes $h_{[0]}$ and $\bar{h}_{[0]}$, true airspeed $V_{T[0]}$, time $t_{[0]}$, ground distance $x_{[0]}$, and fuel burned $F_{B[0]}$.

1. Integration and Model Parameters Definition: Set the time step Δt. Set the rotation rate $\dot{\alpha}_R$, and the tail strike angle α_{TS}. Set i to 0.

2. Main Loop: repeat

a) Based on the atmosphere model, compute the parameters: air density ρ, temperature ratio θ, pressure ratio δ, and Mach number M from $V_{T[i]}$.

b) Based on the engine model and flight conditions, compute the thrust F_N and fuel flow W_F by assuming TO/GA, derate or FLEX setting.

c) Compute the current angle of attack:

$$\alpha = \min\left[\alpha_0 + \dot{\alpha}_R \times (t_{[i]} - t_{[0]}), \alpha_{TS}\right]$$

d) Based on the aircraft configuration, perform a reverse lookup table to find the elevators deflection δ_e required to cancel the sum of moments.

e) From the knowledge of α and δ_e, interpolate the two aerodynamic coefficients: CL_s, and CD_s.

f) Compute the ground reaction applied to the main landing gear ($R_N = 0$):

$$R_M = \max\left[0, m_{[i]} g_0 \cos(\gamma_R) - F_N \sin(\alpha + \phi_T) - L\right]$$

g) Knowing the ground reaction, compute the aircraft acceleration:

$$\dot{V}_T = m_{[i]}^{-1}\left[F_N \cos(\alpha + \phi_T) - D - \mu R_M - m_{[i]} g_0 \sin(\gamma_R)\right]$$

h) Compute the speed, altitude, distance, and mass variations for the current sub-segment:

$$\Delta V_T = \dot{V}_T \Delta t \quad \Delta h = V_{T[i]} \sin(\gamma_R)\Delta t \quad \Delta x = \left[V_{T[i]} \cos(\gamma_R) + V_{W,0}\right]\Delta t \quad \Delta m = W_F \Delta t$$

i) Update the aircraft states, and the number of iterations:

$$h_{[i+1]} = h_{[i]} + \Delta h \quad t_{[i+1]} = t_{[i]} + \Delta t \quad V_{T[i+1]} = V_{T[i]} + \Delta V_T \quad \bar{h}_{[i+1]} = 0$$
$$x_{[i+1]} = x_{[i]} + \Delta x \quad m_{[i+1]} = m_{[i]} - \Delta m \quad F_{B[i+1]} = F_{B[i]} + \Delta m \quad i = i + 1$$

while $(R_M > 0)$;

3. Return all flight parameters, including altitude, distance, time and fuel burned.

4.3.3 Evaluation of the Aircraft Trajectory for the Transition Segment

The trajectory of the aircraft during the transition phase is calculated by numerically integrating the aircraft equations of motion from the lift-off speed V_{LOF} to a given initial climb speed $V_2 + \Delta V_2$. Note that the takeoff safety speed V_2 is assumed to be known since this information is available in the aircraft flight manuals. The speed increment ΔV_2, on the other hand, is a user-defined input which can be chosen arbitrarily in the range of 10 to 20 kts.

Although the transition segment is delimited in terms of speed, it is more convenient to integrate the aircraft equations as function of time rather than as function of airspeed. For this purpose, the transition segment is divided into N time intervals (or sub-segments) as illustrated in Figure 4.10. The suggested size for the time step is the same as that used for the rotation segment, i.e., between 0.2 and 0.5 s.

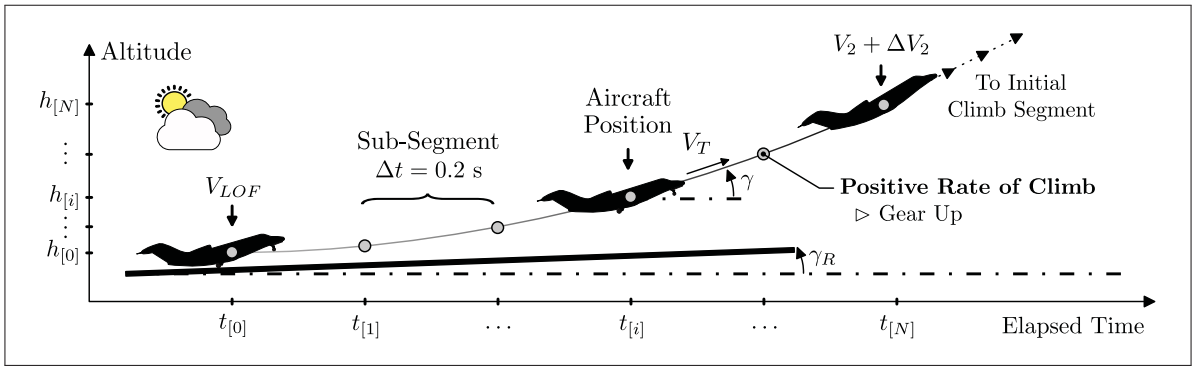

Figure 4.10 Illustration of the Calculation Procedure for the Transition Segment

4.3.3.1 Aircraft Equations of Motion Simplification and Model Parameterization

During the transition segment, the aircraft is expected to continue to accelerate along a curved trajectory, which implies that its flight path angle increases from γ_R to a specific unknown value. For the sake of simplicity, the flight path angle is assumed to increase linearly with time, such as:

$$\gamma = \gamma_R + \dot{\gamma} \times t \tag{4.35}$$

The rate of flight path angle $\dot{\gamma}$ in Eq. (4.35) depends on several factors such as the aircraft weight, the center of gravity position, and the pilot technique. According to several references (Van Bavel, 2014; Young, 2017), a practical approach for the modelling of this parameter is to consider that the pilots maintains a constant load factor $n_z = L/W$ (i.e., the ratio of the lift force to the aircraft weight). Under this condition, Eq. (4.2) can be rewritten as follows:

$$\dot{\gamma} = \frac{g_0}{V_T}\left[\frac{F_N \sin(\alpha + \phi_T)}{W} + n_z - \cos(\gamma) + \frac{\dot{V}_W \sin(\gamma)}{g_0}\right] \tag{4.36}$$

or in a more simplified form by assuming that α and γ are small quantities:

$$\dot{\gamma} = \frac{g_0\,[n_z - 1]}{V_T} \tag{4.37}$$

Following several tests performed with the RAFS, it was found that the load factor varied between 1.10 and 1.28 depending on the aircraft takeoff weight. Based on this observation, it was decided to approximate the load factor by the following polynomial:

$$n_z = p_0 + p_1 W_{TO} + p_2 W_{TO}^2 \tag{4.38}$$

where W_{TO} is the takeoff weight, and the coefficients $\{p_0, p_1, p_2\}$ were estimated using the least-squares method. Note that in the absence of accurate information for the modeling of the variation of the load factor, an empirical value of 1.15 as proposed in references (Raymer, 2012; Young, 2017) can be considered.

Another important parameter to be considered in the calculations process is the wind. Indeed, even if the altitude variation during the transition segment is relatively small, the resulting change in wind speed due to a non-zero wind gradient may impact the acceleration of the aircraft. For this reason, the wind is no longer assumed to be constant, and the time rate of change of the wind speed is approximated using the following chain of rules:

$$\dot{V}_W = \mathrm{d}V_W/\mathrm{d}t = \underbrace{(\mathrm{d}V_W/\mathrm{d}h)}_{V'_W} \times \underbrace{(\mathrm{d}h/\mathrm{d}t)}_{V_T \sin(\gamma)} = V'_W V_T \sin(\gamma) \tag{4.39}$$

Finally, since the aircraft has become airborne, it is evident that all the landing gears are no longer in contact with the ground. Consequently, the reaction forces R_M and R_N are set to zero.

Thus, by introducing all these simplifications in Eqs. (4.1) to (4.3), the pertinent equations describing the motion of the aircraft during the transition segment can be stated as follows:

$$L = m\dot{\gamma}V_T + mg_0\cos(\gamma) - F_N\sin(\alpha + \phi_T) - mV'_W V_T\sin(\gamma)^2 \tag{4.40}$$

$$\dot{V}_T = m^{-1}\left[F_N\cos(\alpha + \phi_T) - D - mg_0\sin(\gamma)\right] - V'_W V_T\sin(\gamma)\cos(\gamma) \tag{4.41}$$

$$\dot{h} = V_T\sin(\gamma) \quad \text{and} \quad \dot{x} = V_T\cos(\gamma) + V_W \tag{4.42}$$

It should be noted that during the transition, the landing gear must be retracted as soon as a positive rate of climb has been established. In this study, the landing gear retraction is initiated when the rate of climb exceeds 500 ft/min, and the landing gear position is decreased linearly from 1 (extended) to 0 (retracted) in 2 seconds.

4.3.3.2 Elevators Deflection, Horizontal Stabilizer Position and Angle of Attack Determination

In order to evaluate the lift and drag forces in Eqs. (4.40) and (4.41), it is necessary to determine the elevators deflection (note that the horizontal stabilizer is still considered to remain in its initial configuration), but also the angle of attack which is now an unknown parameter. Once again, these two parameters can be calculated by assuming that the aircraft is in quasi-static equilibrium, and by trimming the aircraft in each sub-segment of the transition segment.

The technique proposed in this study to trim the aircraft is summarized in Algorithm 4.3. This technique consists in iteratively searching for a combination of angle of attack and elevators deflection that satisfies the equilibrium of the aircraft. For this purpose, the algorithm starts with an initial estimate of the angle of attack and elevators deflection, denoted by $\{\alpha^{k-1}, \delta_e^{k-1}\}$. Based on these two estimates, the algorithm computes the lift coefficient required to balance the aircraft along the vertical axis by using Eq. (4.40). The algorithm then applies a "reverse lookup technique", similar to the technique illustrated in Figure 4.9, in order to obtain a new

estimation of the angle of attack α^k that is further used to obtain the required lift coefficient. Finally, by using the new estimate of the angle of attack, the algorithm applies a second "reverse lookup technique" to find the elevators position δ_e^k that cancels the sum of the moments:

$$\begin{aligned}\Sigma M(\delta_e) = M_y(\delta_e) - \Delta\bar{x}_{CG} L(\alpha^k, \delta_e) + \Delta\bar{z}_{CG} D(\alpha^k, \delta_e) + \cdots \\ \cdots + (\Delta\bar{x}_{CT} - \Delta\bar{x}_{CG})\, F_N \sin(\alpha^k + \phi_T) + (\Delta\bar{z}_{CT} - \Delta\bar{z}_{CG})\, F_N \cos(\alpha^k + \phi_T)\end{aligned} \tag{4.43}$$

Because of the inaccuracy of the first iteration, it is necessary to redo the calculations by replacing the initial estimates $\{\alpha^{k-1}, \delta_e^{k-1}\}$ with their new estimates $\{\alpha^k, \delta_e^k\}$. This process is repeated until the values of the angle of attack and the elevators deflection between two consecutive iterations are acceptably close.

Algorithm 4.3 Aircraft Trim Procedure for the Transition Segment

0. Initialization: For the trim algorithm, it is assumed that all aircraft parameters are known except the angle of attack α, and the elevators deflection δ_e.

1. Define Initial Estimates: Set $\alpha^{[0]} = 0$, and $\delta_e^{[0]} = 0$. Note that in order to accelerate the convergence of the algorithm, these two parameters can be initialized based on the results obtained for the previous sub-segment. Set the number of iterations $k = 0$.

2. Main Loop: repeat

a) Update the number of iterations: $k = k + 1$.

b) From the current estimate of the angle of attack $\alpha^{[k-1]}$, compute the lift force required to balance the aircraft along the vertical axis:

$$L^* = m\dot{\gamma}V_T + mg_0\cos(\gamma) - F_N \sin(\alpha^{[k-1]} + \phi_T) - mV'_W V_T \sin(\gamma)^2$$

c) Compute the corresponding lift coefficient CL_s^*:

$$CL_s^* = L^*/0.5\rho S V_T^2$$

d) Assuming $\delta_e^{[k-1]}$, perform a reverse lookup table to find the new estimate for the angle of attack $\alpha^{[k]}$ which leads to the lift coefficient CL_s^*.

e) From the knowledge of $\alpha^{[k]}$, perform a "reverse lookup table" to find the new estimate $\delta_e^{[k]}$ which cancels the sum of moments.

while $|\alpha^{[k]} - \alpha^{[k-1]}| \geq 0.1$ ***OR*** $|\delta_e^{[k]} - \delta_e^{[k-1]}| \geq 0.1$, ***AND*** $k \leq 25$;

3. Return the last trim parameters: $\alpha^{[k]}$ **and** $\delta_e^{[k]}$**.**

4.3.3.3 Complete Calculation Process

Equations (4.29) to (4.33) are the main equations describing the aircraft performance during the transition segment. The complete procedure proposed to integrate these equations, and to compute the aircraft trajectory for this type of segment is described in Algorithm 4.4.

It is important to mention that overestimating the load factor can cause the flight path angle to increase too rapidly, which can lead to a negative acceleration. If this happens, the speed will begin to decrease, and the aircraft will never reach the desired initial climb speed. This is the reason why it is necessary to stop the calculation process when the aircraft acceleration becomes negative or zero, otherwise the algorithm will never stop.

4.3.4 Evaluation of the Aircraft Trajectory for a Climb at Constant CAS Segment

The aircraft trajectory for a climb at constant CAS segment is calculated by numerically integrating the aircraft equations of motion from an initial altitude $h_{[0]}$ to a final altitude $h_{[N]}$. For this purpose, the aircraft trajectory is divided into N altitude sub-segments, as illustrated in Figure 4.11.

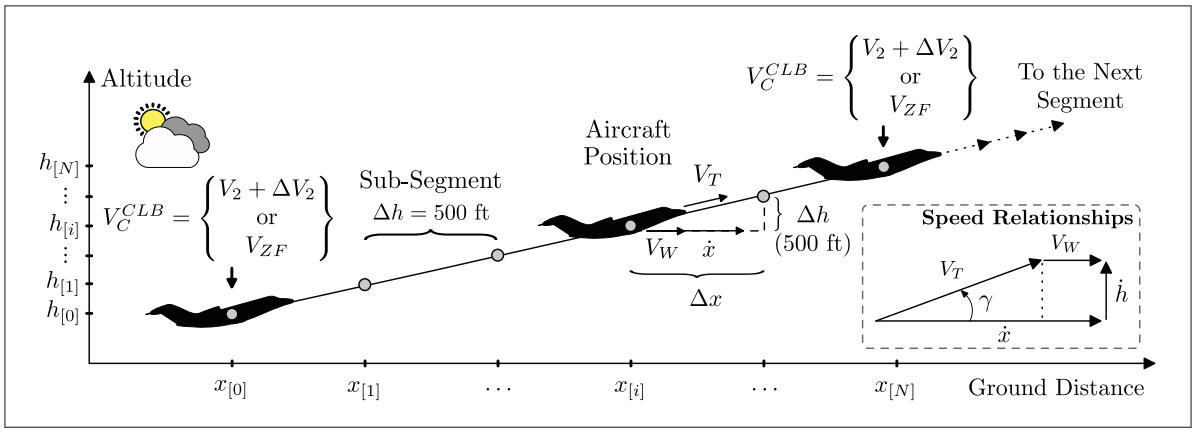

Figure 4.11 Illustration of the Calculation Procedure for a Climb at Constant CAS Segment

Algorithm 4.4 Calculation Procedure for the Transition Segment

0. Initialization: From the results of Algorithm 4.2, initialise the aircraft states; mass $m_{[0]}$, altitudes $h_{[0]}$ and $\bar{h}_{[0]}$, true airspeed $V_{T[0]}$, time $t_{[0]}$, ground distance $x_{[0]}$, and fuel burned $F_{B[0]}$.

1. Integration and Model Parameters Definition: Set the time step Δt. Compute the CAS $V_{C[0]}$ from the TAS $V_{T[0]}$. Select the takeoff safety speed V_2, and the speed increment ΔV_2. Find the load factor n_z using Eq. (4.38). Set i to 0.

2. Main Loop: repeat

a) Based on the atmosphere model, compute the parameters: air density ρ, temperature ratio θ, pressure ratio δ, Mach number M from $V_{T[i]}$, and wind speed V_W.

b) Based on the engine model and flight conditions, compute the thrust F_N and fuel flow W_F by assuming TO/GA, derate or FLEX setting.

c) Fom the knowledge of the load factor n_z, compute the flight path angle:

$$\gamma = \gamma_R + \dot{\gamma}(t_{[i]} - t_{[0]}), \text{ where } \dot{\gamma} = g_0 \left(n_z - 1\right) / V_{T[i]}$$

d) If $\dot{h} = V_{T[i]} \sin(\gamma) \geq 500$ ft/min, retract gears.

e) Use Algorithm 4.3 to trim the aircraft for the current flight condition, and to determine the angle of attack α, and the elevators deflection δ_e.

f) For the current condition, compute the aircraft acceleration:

$$\dot{V}_T = m_{[i]}^{-1} \left[F_N \cos(\alpha + \phi_T) - D - m_{[i]} g_0 \sin(\gamma)\right] - V'_W V_{T[i]} \sin(\gamma) \cos(\gamma)$$

g) Compute the speed, altitude, distance, and mass variations for the current sub-segment:

$$\Delta V_T = \dot{V}_T \Delta t \quad \Delta h = V_{T[i]} \sin(\gamma) \Delta t \quad \Delta x = \left[V_{T[i]} \cos(\gamma) + V_W\right] \Delta t \quad \Delta m = W_F \Delta t$$

h) Update the aircraft states:

$$h_{[i+1]} = h_{[i]} + \Delta h \qquad t_{[i+1]} = t_{[i]} + \Delta t \qquad V_{T[i+1]} = V_{T[i]} + \Delta V_T \qquad \bar{h}_{[i+1]} = \bar{h}_{[i]} + \Delta h$$
$$x_{[i+1]} = x_{[i]} + \Delta x \quad m_{[i+1]} = m_{[i]} - \Delta m \quad F_{B[i+1]} = F_{B[i]} + \Delta m$$

i) Compute the new CAS $V_{C[i+1]}$ from the TAS $V_{T[i+1]}$, and update the number of iterations: $i = i + 1$.

while $\left(V_{C[i]} < V_2 + \Delta V_2\right)$ ***AND*** $\left(\dot{V}_T > 0\right)$;

3. Return all flight parameters, including altitude, distance, time and fuel burned.

Note that depending on the climb segment (see Figure 4.2), the final altitude may be equal to the thrust reduction height (TRH), acceleration height (AH) or 3000 ft AGL. The initial altitude, on the other hand, is always defined according to the final altitude of the previous segment.

As for the other segments, the altitude step size for the integration process is arbitrary. A suggested altitude step size that provides a good compromise between precision and computation effort is between 500 and 1000 ft (Blake, 2009). Therefore, since the initial and final altitudes are not necessarily multiples of the step size, the size of the first and last sub-segment may be smaller than the step size.

4.3.4.1 Aircraft Equations of Motion Simplification and Model Parameterization

The aircraft trajectory during a climb at constant CAS segment is not exactly straight but is rather slightly curved. However, at low altitudes, and for climb segments of 500 to 1000 ft, this curvature is relatively small, and to a good approximation can be neglected. Under this condition, the flight path angle within a given sub-segment can be considered constant, and the rate of change of climb angle with respect to time can be assumed to be zero (i.e., $\dot{\gamma} = 0$).

In addition, given the fact that the aircraft is climbing at constant CAS, Eq. (4.2) can be modified to facilitate calculations. Indeed, by noticing that:

$$\dot{V}_T = \frac{\mathrm{d}V_T}{\mathrm{d}t} = \frac{\mathrm{d}V_T}{\mathrm{d}h} \times \frac{\mathrm{d}h}{\mathrm{d}t} = \frac{\mathrm{d}V_T}{\mathrm{d}h} V_T \sin(\gamma) \tag{4.44}$$

and by recalling that $\dot{V}_W = V'_W V_T \sin(\gamma)$ and that $R_M = R_N = 0$, Eq. (4.2) can be rearranged as follows:

$$\frac{F_N \cos(\alpha + \phi_T) - D}{m g_0} - \frac{V'_W V_T \sin(\gamma)\cos(\gamma)}{g_0} = \left(1 + \frac{V_T}{g_0}\frac{\mathrm{d}V_T}{\mathrm{d}h}\right)\sin(\gamma) \tag{4.45}$$

Then, by isolating the sine of the flight path angle on the right-hand side of Eq. (4.45), it can be shown that:

$$\sin(\gamma) = \frac{F_N \cos(\alpha + \phi_T) - D}{m g_0 \left(1 + \dfrac{V_T}{g_0} \dfrac{\mathrm{d}V_T}{\mathrm{d}h}\right)} - \frac{V'_W V_T \sin(\gamma) \cos(\gamma)}{g_0 \left(1 + \dfrac{V_T}{g_0} \dfrac{\mathrm{d}V_T}{\mathrm{d}h}\right)} \tag{4.46}$$

Finally, by introducing the notation:

$$\mathrm{AF} = \frac{V_T}{g_0} \frac{\mathrm{d}V_T}{\mathrm{d}h} \tag{4.47}$$

Eq. (4.46) can be rewritten in a more compact form as follows:

$$\sin(\gamma) = \frac{F_N \cos(\alpha + \phi_T) - D}{m g_0 (1 + \mathrm{AF})} - \frac{V'_W V_T \sin(\gamma) \cos(\gamma)}{g_0 (1 + \mathrm{AF})} \tag{4.48}$$

The parameter AF in Eq. (4.47) is called the "acceleration factor". This parameter is a factor which corrects for the fact that below the tropopause, the aircraft true airspeed for a given calibrated airspeed increases with an increase in altitude.

According to Blake (2009), the acceleration factor for a climb at constant CAS below the tropopause can be computed as follows:

$$\mathrm{AF} = 0.7 M^2 \left[\frac{\left(1 + 0.2 M^2\right)^{3.5} - 1}{0.7 M^2 \left(1 + 0.2 M^2\right)^{2.5}} - 0.190263 \frac{T_{\mathrm{ISA}}}{T} \right] \tag{4.49}$$

where T_{ISA} is the standard day temperature (i.e., for $\Delta\mathrm{ISA} = 0$).

Thus, by combining all the simplifications introduced in this section with Eqs. (4.1) to (4.3) the pertinent equations describing the aircraft motion for a climb at constant CAS segment can be stated as follows:

$$L = m g_0 \cos(\gamma) - F_N \sin(\alpha + \phi_T) - m V'_W V_T \sin(\gamma)^2 \tag{4.50}$$

$$\gamma = \arcsin \left[\frac{F_N \cos(\alpha + \phi_T) - D}{m g_0 (1 + \mathrm{AF})} - \frac{V'_W V_T \sin(\gamma) \cos(\gamma)}{g_0 (1 + \mathrm{AF})} \right] \tag{4.51}$$

$$\dot{h} = V_T \sin(\gamma) \quad \text{and} \quad \dot{x} = V_T \cos(\gamma) + V_W \tag{4.52}$$

where AF is calculated from Eq. (4.49).

4.3.4.2 Elevators Deflection, Horizontal Stabilizer Position, and Aerodynamic Angles Determination

To complete the calculation procedure, it is necessary to determine the angle of attack, flight path angle, elevators deflection, and horizontal stabilizer position required to compute the lift and drag forces in Eqs. (4.50) and (4.51). However, since there are not enough equations to determine these four unknown parameters, the problem needs to be simplified by eliminating one of the two control surfaces. Therefore, if the elevators are chosen to control the aircraft attitude, the configuration of the horizontal stabilizer can be considered as identical to that of the previous segment. Conversely, if the horizontal stabilizer is chosen to control the aircraft attitude, the elevators must be set to zero.

The technique proposed in this study to predict the angle of attack, flight path angle, and elevators deflection (or horizontal stabilizer position) consists in trimming the aircraft in each sub-segment of the climb trajectory. For this purpose, the iterative process shown in Algorithm 4.3 can be re-used after several modifications. Indeed, since the flight path angle is unknown, and because of the non-linearity of Eq. (4.51), it is necessary to add a new convergence loop. For this loop, the algorithm uses Eq. (4.51) to obtain a new estimate of the flight path angle at each iteration.

This process is repeated until the estimate of the flight path angle between two consecutive iterations are close. The modified trim procedure for a climb a constant calibrated airspeed is given in Algorithm 4.5.

It should be noted that Algorithm 4.5 can be similarly developed if the horizontal stabilizer is used for trimming purposes. In this case, the elevators are set to zero, and the variable δ_e is replaced by δ_s. All the other steps of the algorithm remain exactly the same.

Algorithm 4.5 Aircraft Trim Procedure for a Climb at Constant CAS Segment

0. Initialization: For the trim algorithm, it is assumed that all aircraft parameters are known except the angle of attack α, the flight path angle γ, and the elevators position δ_e.

1. Define Initial Estimates: Set $\alpha^{[0]} = 0$, $\gamma^{[0]} = 0$, and $\delta_e^{[0]} = 0$. Note that in order to accelerate the convergence of the algorithm, these two parameters can be initialized based on the results obtained for the previous sub-segment. Set $k = 0$.

2. Main Loop: repeat

a) Update the number of iterations: $k = k + 1$.

b) From the current estimate of the angle of attack $\alpha^{[k-1]}$ and flight path angle $\gamma^{[k-1]}$, compute the lift force required to balance the aircraft along the vertical axis:

$$L^* = mg_0 \cos(\gamma^{[k-1]}) - F_N \sin(\alpha^{[k-1]} + \phi_T) - mV'_W V_T \sin(\gamma^{[k-1]})^2$$

c) Compute the corresponding lift coefficient CL_s^*:

$$CL_s^* = L^*/0.5\rho S V_T^2$$

d) Assuming $\delta_e^{[k-1]}$, perform a reverse lookup table to find the new estimate for the angle of attack $\alpha^{[k]}$ which leads to the lift coefficient CL_s^*.

e) Based on $\alpha^{[k]}$ and $\delta_e^{[k-1]}$, interpolate the drag coefficient CD_s, and compute the drag force $D = 0.5\rho S V_T^2 CD_s$.

f) From the knowledge of $\alpha^{[k]}$ and $\gamma^{[k-1]}$, compute a new estimate for the flight path angle $\gamma^{[k]}$:

$$\gamma^{[k]} = \arcsin\left[\frac{F_N \cos(\alpha^{[k]} + \phi_T) - D}{mg_0(1 + \text{AF})} - \frac{V'_W V_T \sin(\gamma^{[k-1]}) \cos(\gamma^{[k-1]})}{g_0(1 + \text{AF})}\right]$$

g) Assuming $\alpha^{[k]}$, perform a "reverse lookup table" to find the new estimate $\delta_e^{[k]}$ which cancels the sum of moments.

while $|\alpha^{[k]} - \alpha^{[k-1]}| \geq 0.1$ ***OR*** $|\gamma^{[k]} - \gamma^{[k-1]}| \geq 0.1$ ***OR*** $|\delta_e^{[k]} - \delta_e^{[k-1]}| \geq 0.1$, ***AND*** $k \leq 25$;

3. Return the last trim parameters: $\alpha^{[k]}$**,** $\gamma^{[k]}$ **and** $\delta_e^{[k]}$**.**

4.3.4.3 Complete Calculation Procedure

Equations (4.50) to (4.52) are the main equations describing the aircraft performance for a climb at constant CAS segment. The complete procedure proposed to integrate these equations, and to compute the aircraft trajectory for this type of segment is described in Algorithm 4.6.

Algorithm 4.6 Calculation Procedure for a Climb at Constant CAS Segment

0. Initialization: Set the aircraft initial states from the results of the previous segment; mass $m_{[0]}$, altitudes $h_{[0]}$ and $\bar{h}_{[0]}$, true airspeed $V_{T[0]}$, time $t_{[0]}$, ground distance $x_{[0]}$, and fuel burned $F_{B[0]}$.

1. Integration and Model Parameters Definition: Depending on the climb segment, set the aircraft calibrated airspeed V_C^{CLB}. Define the final altitude $h_{[N]}$ = {TRH, AH,or 3000}. Set the integration step Δh and divide the climb segment into N sub-intervals.

2. Main Loop: for $i = 0$ *to* $(N-1)$ **do**

a) Based on the atmosphere model, compute the parameters: air density ρ, temperature ratio θ, pressure ratio δ, Mach number M from $V_{T[i]}$, and wind speed V_W.

b) From the selected CAS V_C^{CLB}, calculate the TAS $V_{T[i]}$, and Mach number M.

c) From the knowledge of the Mach number M and temperature, compute the acceleration factor AF.

d) Based on the engine model and flight conditions, compute the thrust F_N and fuel flow W_F by assuming TO/GA, derate or FLEX setting.

e) Use Algorithm 4.5 to trim the aircraft for the current flight condition, and to determine the angle of attack α, the flight path angle γ, the elevators deflection δ_e, and stabilizer position δ_s.

f) Compute the altitude, distance, and mass variations for the current sub-segment:

$$\Delta h = V_{T[i]} \sin(\gamma)\Delta t \quad \Delta x = \left[V_{T[i]} \cos(\gamma) + V_W\right] \Delta t \quad \Delta m = W_F \Delta t$$

g) Update aircraft states :

$$h_{[i+1]} = h_{[i]} + \Delta h \quad x_{[i+1]} = x_{[i]} + \Delta x \quad m_{[i+1]} = m_{[i]} - \Delta m$$
$$\bar{h}_{[i+1]} = \bar{h}_{[i]} + \Delta h \quad t_{[i+1]} = t_{[i]} + \Delta t \quad F_{B[i+1]} = F_{B[i]} + \Delta m$$

end for

3. Return all flight parameters, including altitude, distance, time and fuel burned.

4.3.5 Evaluation of the Aircraft Trajectory during a Climb Acceleration Segment

The aircraft trajectory during a climb acceleration from the initial climb speed $V_2 + \Delta V_2$ to a user-defined flaps up speed V_{ZF} is calculated by following a procedure similar to that used for the transition segment. For this purpose, the aircraft trajectory is divided into N time sub-segments as illustrated in Figure 4.12.

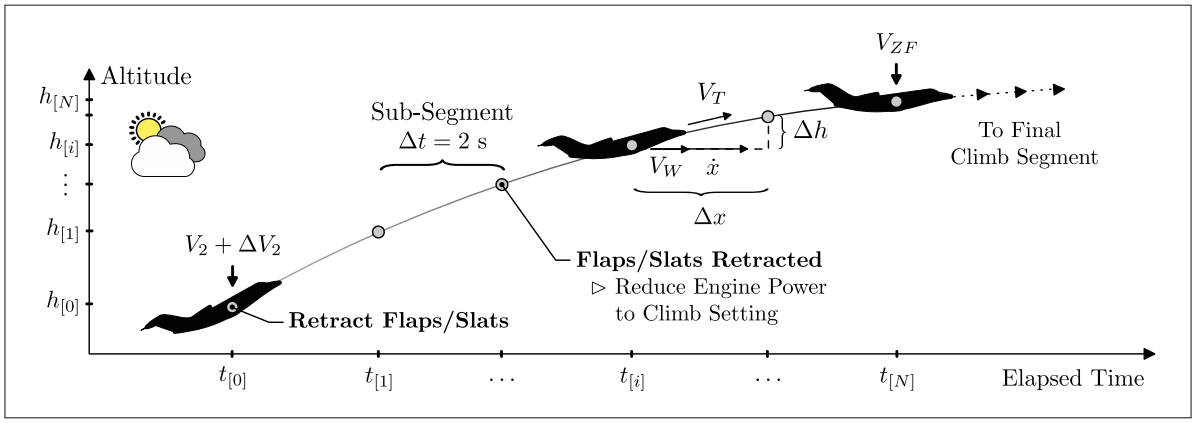

Figure 4.12 Illustration of the Calculation Procedure for a Climb Acceleration Segment

Once again, the time step size for the calculation is arbitrary. A suggested size for the climb acceleration is between 1 and 2 seconds. However, the step size can be adjusted depending on the speed increment between $V_2 + \Delta V_2$ and V_{ZF} in order to improve the results accuracy.

4.3.5.1 Aircraft Equations of Motion Simplification and Model Parameterization

The way in which an aircraft accelerates in climb is strongly dependent upon the autopilot flight control laws. In general, most of commercial aircraft accelerates by either maintaining a constant climb gradient, or a constant rate of climb. However, following several simulations with the RAFS, it was found that the logic that reflected best the behavior of the Cessna Citation X was an acceleration at a constant rate of true airspeed (TAS). In addition, based on the data collected during the simulations, the average acceleration was estimated at approximately 3.11 ft/s^2.

Under this condition, Eq. (4.1) can be rewritten as follows:

$$\sin(\gamma) = \frac{F_N \cos(\alpha + \phi_T) - D}{m g_0} - \frac{\dot{V}_T^{ACC} V_W' V_T \sin(\gamma) \cos(\gamma)}{g_0} \tag{4.53}$$

where $\dot{V}_T^{ACC}$ is the desired rate of TAS.

By analyzing the simulation data obtained from the RAFS, it was also noted that the flight path angle decreased as the aircraft gained speed. However, this variation was proved to be very slow and, because of this fact, it was decided to neglect the time rate of change of the flight path angle (i.e., $\dot{\gamma} = 0$).

Thus, by combining these simplifications with Eqs. (4.1) to (4.3), the pertinent equations describing the motion of the aircraft during a climb acceleration segment can be stated as follows:

$$L = m g_0 \cos(\gamma) - F_N \sin(\alpha + \phi_T) - m V_W' V_T \sin(\gamma)^2 \tag{4.54}$$

$$\gamma = \arcsin \left[\frac{F_N \cos(\alpha + \phi_T) - D}{m g_0} - \frac{\dot{V}_T^{ACC} + V_W' V_T \sin(\gamma) \cos(\gamma)}{g_0} \right] \tag{4.55}$$

$$\dot{h} = V_T \sin(\gamma) \quad \text{and} \quad \dot{x} = V_T \cos(\gamma) + V_W \tag{4.56}$$

It is worth mentioning that during the climb acceleration phase, flaps should be retracted gradually at an adequate airspeed. Similarly, depending on the airline/airport policy, engine thrust should be reduced to climb setting either at the same time as flaps retraction or once the flaps are fully retracted. For the sake of simplicity, it was assumed in this study that the flaps retraction was always initiated at the beginning of the acceleration phase, and that the flaps were retracted linearly from their initial position (e.g., 15° or 5°) to 0° (i.e., fully retracted) at a rate of -1.29°/s.

Regarding the thrust, it was decided to initiate the engine power reduction from TO/GA to CLB once the flaps were fully retracted. In addition, the reduction is applied on the fan speed N_1 by using a technique similar to that used for the acceleration in **Section 4.3.1.1** [see Eq. (4.25)].

4.3.5.2 Elevators Deflection, Horizontal Stabilizer Position, and Aerodynamic Angles Determination

To complete the calculation procedure, it is necessary to determine the angle of attack, flight path angle, elevators deflection, and horizontal stabilizer position required to compute the lift and drag forces in Eqs. (4.54) and (4.55). The technique used to estimate these parameters is quasi similar to the one used for a climb at constant calibrated airspeed (CAS), with the difference that the flight path angle is updated using the results in Eqs. (4.55). All the other steps remain exactly the same.

Algorithm 4.7 illustrates the trim procedure for the convenience of the reader.

In case when the aircraft accelerates at constant climb gradient or at constant rate of climb, Algorithm 7 can be used by removing the Step f), and by computing the flight path angle as follows:

$$\gamma = \arcsin\left[\frac{V/S}{V_T}\right] \quad \text{or} \quad \gamma = \arctan\left[\frac{C\%}{100}\right] \tag{4.57}$$

where V/S is the rate of climb (e.g., 500 or 1000 ft/min), and $C\%$ is the climb gradient expressed in percentage. Similarly, the case of a level-off acceleration can be obtained by simply imposing zero flight path angle (i.e., $\gamma = 0$).

4.3.5.3 Complete Calculation Process

Equations (4.54) to (4.56) are the main equations describing the aircraft performance for a climb acceleration segment. The complete procedure proposed to integrate these equations and compute the aircraft trajectory for this type of segment is described in Algorithm 4.8.

Algorithm 4.7 Aircraft Trim Procedure for a Climb Acceleration Segment

0. Initialization: For the trim algorithm, it is assumed that all aircraft parameters are known except the angle of attack α, the flight path angle γ, and the elevators position δ_e.

1. Define Initial Estimates: Set $\alpha^{[0]} = 0$, $\gamma^{[0]} = 0$, and $\delta_e^{[0]} = 0$. Note that in order to accelerate the convergence of the algorithm, these two parameters can be initialized based on the results obtained for the previous sub-segment. Set $k = 0$.

2. Main Loop: repeat

a) Update the number of iterations: $k = k + 1$.

b) From the current estimate of the angle of attack $\alpha^{[k-1]}$ and flight path angle $\gamma^{[k-1]}$, compute the lift force required to balance the aircraft along the vertical axis:

$$L^* = mg_0 \cos(\gamma^{[k-1]}) - F_N \sin(\alpha^{[k-1]} + \phi_T) - mV'_W V_T \sin(\gamma^{[k-1]})^2$$

c) Compute the corresponding lift coefficient CL_s^*:

$$CL_s^* = L^*/0.5\rho S V_T^2$$

d) Assuming $\delta_e^{[k-1]}$, perform a reverse lookup table to find the new estimate for the angle of attack $\alpha^{[k]}$ which leads to the lift coefficient CL_s^*.

e) Based on$\alpha^{[k]}$ and $\delta_e^{[k-1]}$, interpolate the drag coefficient CD_s, and compute the drag force $D = 0.5\rho S V_T^2 CD_s$.

f) From the knowledge of $\alpha^{[k]}$ and $\gamma^{[k-1]}$, compute a new estimate for the flight path angle $\gamma^{[k]}$:

$$\gamma^{[k]} = \arcsin\left[\frac{F_N \cos(\alpha^{[k]} + \phi_T) - D}{mg_0} - \frac{\dot{V}_T^{ACC} V'_W V_T \sin(\gamma^{[k-1]}) \cos(\gamma^{[k-1]})}{g_0}\right]$$

g) Assuming $\alpha^{[k]}$, perform a "reverse lookup table" to find the new estimate $\delta_e^{[k]}$ which cancels the sum of moments.

while $|\alpha^{[k]} - \alpha^{[k-1]}| \geq 0.1$ ***OR*** $|\gamma^{[k]} - \gamma^{[k-1]}| \geq 0.1$ ***OR*** $|\delta_e^{[k]} - \delta_e^{[k-1]}| \geq 0.1$, ***AND*** $k \leq 25$;

3. Return the last trim parameters: $\alpha^{[k]}$, $\gamma^{[k]}$ **and** $\delta_e^{[k]}$.

4.4 Simulation and Validation Results

The last section of this paper presents the simulation results obtained for the validation of the proposed methodology. For this purpose, a series of tests were conducted with the Cessna

Algorithm 4.8 Calculation Procedure for a Climb Acceleration Segment

0. Initialization: Set the aircraft initial states from the results of the previous segment; mass $m_{[0]}$, altitudes $h_{[0]}$ and $\bar{h}_{[0]}$, true airspeed $V_{T[0]}$, time $t_{[0]}$, ground distance $x_{[0]}$, and fuel burned $F_{B[0]}$.

1. Integration and Model Parameters Definition: Set the time step Δt, and the number of iterations i to zero. Compute the CAS $V_{C[0]}$ from the initial TAS $V_{T[0]}$. Select the desired CAS $V_{ZF} \leq 250$ kts.

2. Main Loop: repeat

a) Based on the atmosphere model, compute the parameters: air density ρ, temperature ratio θ, pressure ratio δ, Mach number M from $V_{T[i]}$, and wind speed V_W.

b) Retract flaps by assuming a linear variation from 15° (or 5°) to 0° at -1.29°/s.

c) Based on the engine model and flight conditions, compute the thrust F_N and fuel flow W_F by assuming by assuming a N_1 reduction from TO/GA to CLB.

d) Use Algorithm 4.7 to trim the aircraft for the current flight condition, and to determine the angle of attack α, the flight path angle γ, the elevators deflection δ_e, and stabilizer position δ_s.

e) For a climb acceleration at constant rate of TAS, set $\dot{V}_T = \dot{V}_T^{ACC}$. For a climb acceleration at constant climb gradient, constant rate of climb or level-off, compute the aircraft acceleration using the following equation:

$$\dot{V}_T = m_{[i]}^{-1}\left[F_N \cos(\alpha + \phi_T) - D - m_{[i]} g_0 \sin(\gamma)\right] - V'_W V_{T[i]} \sin(\gamma)\cos(\gamma)$$

f) Compute the altitude, distance, speed, and mass variations for the current sub-segment:

$$\Delta h = V_{T[i]} \sin(\gamma)\Delta t \quad \Delta x = \left[V_{T[i]} \cos(\gamma) + V_W\right]\Delta t \quad \Delta V_T = \dot{V}_T \Delta t \quad \Delta m = W_F \Delta t$$

g) Update the aircraft states, and the number of iterations:

$$h_{[i+1]} = h_{[i]} + \Delta h \qquad t_{[i+1]} = t_{[i]} + \Delta t \qquad V_{T[i+1]} = V_{T[i]} + \Delta V_T \qquad \bar{h}_{[i+1]} = \bar{h}_{[i]} + \Delta h$$
$$x_{[i+1]} = x_{[i]} + \Delta x \qquad m_{[i+1]} = m_{[i]} - \Delta m \qquad F_{B[i+1]} = F_{B[i]} + \Delta m$$

h) Compute the new CAS $V_{C[i+1]}$ from the TAS $V_{T[i+1]}$, and update the number of iterations: $i = i + 1$.

while $\left(V_{C[i]} < V_{ZF}\right)$;

3. Return all flight parameters, including altitude, distance, time and fuel burned.

Citation X RAFS. In order to evaluate the validity of the methodology over a wide range of operating conditions, two categories of tests were considered: (1) normal takeoff, and (2) normal takeoff with initial-climb. In parallel, the algorithms developed in **Section 4.3** were used to calculate the aircraft performance and trajectory for the same simulation conditions.

The validation of the results was accomplished by comparing the aircraft performance data measured from the RAFS with those calculated by the algorithms. The criterion established to validate the model was that the model and the measured data agree within 5%, as recommended by the FAA (1991) for the qualification of flight simulator.

4.4.1 Simulation Results for the Takeoff Phase

The validation process begins with the takeoff phase which includes the ground acceleration, the rotation, and the transition. To this end, a first series of 20 takeoff tests was conducted with the Cessna Citation X RAFS.

The approach adopted to choose the tests, and to evaluate the accuracy of the algorithms over a wide range of flight conditions was to establish a reference takeoff test and to reproduce it several times by modifying each time a specific parameter, such as the aircraft weight, the temperature deviation, or the runway surface condition. In addition, in order to analyze the influence of runway elevation on the aircraft performance, the tests were conducted at different airports, including Montreal Pierre Elliott Trudeau Airport (CUYL, 96 ft), Washington Dulles International Airport (KIAD, 303 ft), Innsbruck International Airport (LOWI, 1904 ft), and Mexico City International Airport (MMMX, 7294 ft). Finally, for a better comparison of these data, all takeoff tests were simulated up to 100 ft AGL. Therefore, the stopping criterion for the transition segment was changed to 100 ft AGL in Algorithm 4.4.

Table 4.2 summarizes the list of tests retained. The reference test is the tesr number 3, which corresponds to a takeoff at CYUL on a dry runway for an aircraft weight of 33,000 lb, under ISA conditions and in the absence of winds.

Table 4.2 List of Flight Tests for the Validation of the Takeoff Phase.

Aircraft/Flight Parameter	Parameter Range	Test No
Takeoff Weight [×1000 lb]	26 / 28 / 30 / 33 / 35	1, 2, 3, 4, 5
Runway Elevation [ft]	303 / 1904 / 7294	6, 7, 8
Temperature Deviation [°C]	-25 / -10 / +10 / +25	9, 10, 11, 12
Wind Speed [kts]	+10 / -10 / -20 / -30	13, 14, 15, 16
Runway Surface Condition	Wet + 5 / Wet + 12	17, 18
Reduced Takeoff Thrust	TOGA-10% / FLEX (+40)	19, 20

4.4.1.1 Trajectory Comparison for the Reference Takeoff Test

In order to illustrate how each test was validated, an example of results obtained for the reference test (i.e., no 3) is given in Figure 4.13. In this figure, the data measured with the RAFS are represented by the black curves, while those predicted by the algorithms are represented by the blue curves. The red band delimited by the two dotted lines indicates the region of 5% in which the predictions should be considered for a good match.

From an overall point of view, it can be seen that there is a good agreement between the measured and predicted data. Indeed, the takeoff distance, and the time-to-takeoff are both very well estimated, and the predictions are always found within the region of 5%. In addition, it can be seen that the aircraft trajectory during the transition phase is very well modeled by the algorithm. This aspect allows to validate the load factor model expressed in Eq. (4.38) as well as the technique proposed to describe the flight path variation during the transition phase.

Regarding the fuel burned, the results obtained are also very good, despite the fact that their estimates were found to be slightly outside the region of 5% during the first ten seconds. This deviation is mainly explained by the difficulty of modeling the thrust management, and the engine dynamics in the beginning of the acceleration segment. However, after 10 seconds, the estimate returns inside the region of 5%, which validates the results.

Finally, by comparing the trajectory data at the end of the takeoff phase, it was found that the relative errors were approximately 0.60% (20.5 ft) for the ground distance, 1.18% (0.42 s) for

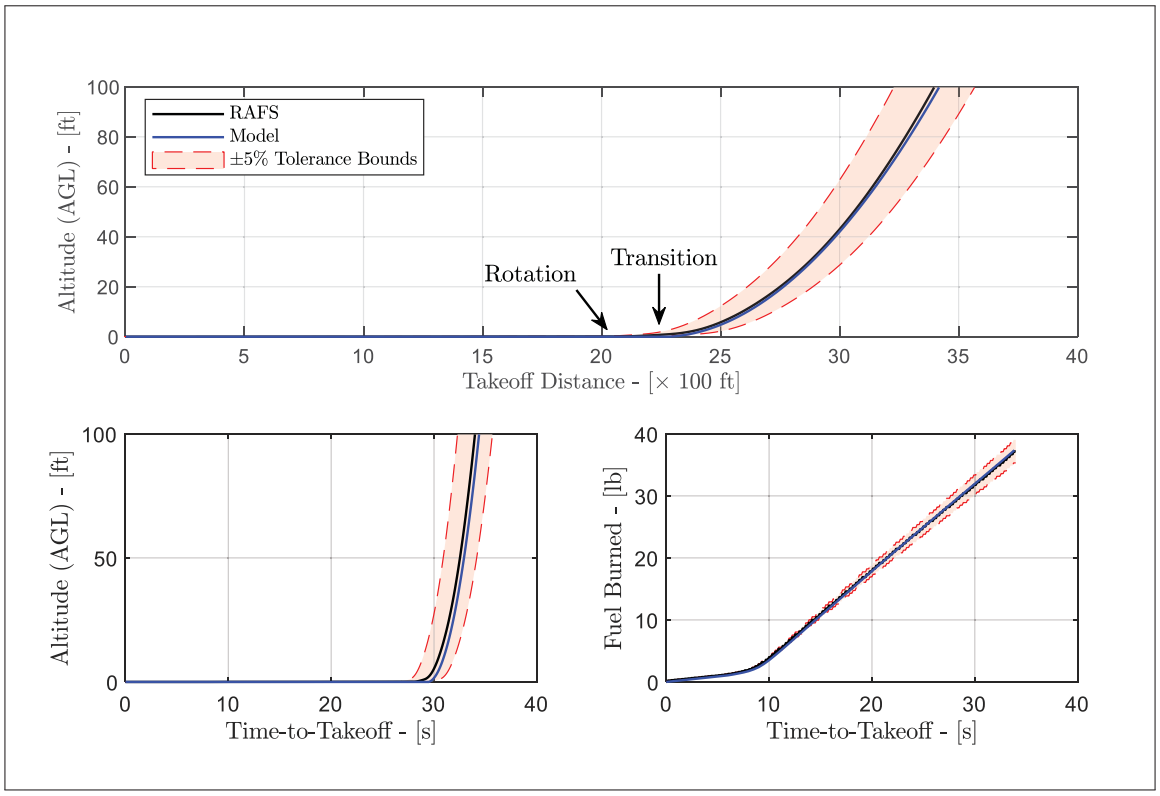

Figure 4.13 Aircraft Trajectory and Fuel Burned Comparison for the Reference Test (No 3)

the time-to-takeoff, and 0.45% (0.17 lb) for the fuel burned. These differences are negligible, and it can be concluded that the algorithms predicted very well the aircraft trajectory, and the fuel consumption for the reference test.

4.4.1.2 Trim Parameters Comparison for the Reference Takeoff Test

To further evaluate the efficiency of the algorithms, another comparison was made for the aircraft trim parameters. For this purpose, Figure 4.14 shows the variations of the engine parameters (i.e., fan speed and fuel flow), ground reaction forces (i.e., R_N and R_M), angle of attack and elevators deflection with respect to time.

By analyzing the first two graphs shown in Figure 4.14, it can be seen that the engine fan speed and fuel flow, especially in the beginning of the acceleration phase, are very well estimated by

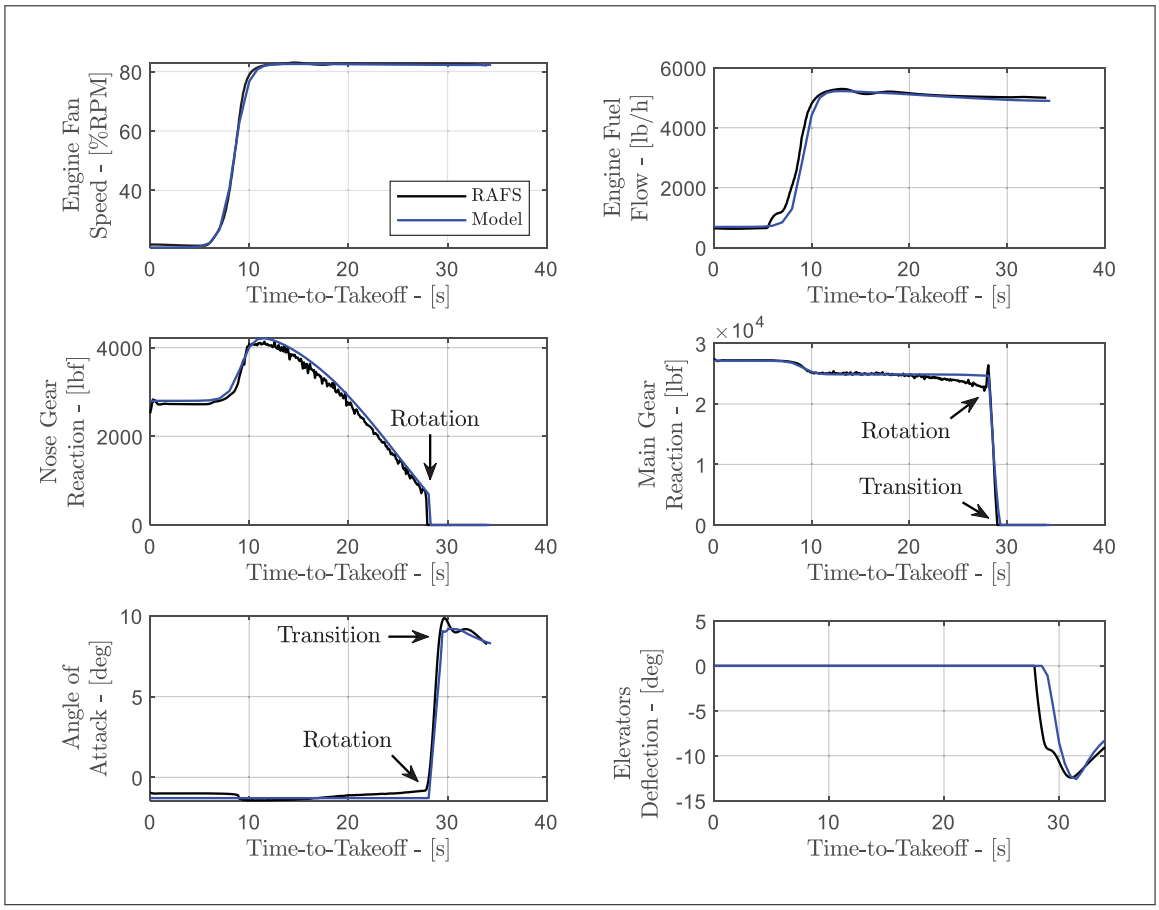

Figure 4.14 Aircraft Trim Parameters Comparison for the Reference Test (No 3)

the algorithms. However, it should be noted that there is a slight deviation between the measured and estimated fuel flow. This difference may explain the fuel errors observed in Figure 4.13. and is due to the dynamics of the engine which is difficult to model.

The two middle graphs in Figure 4.14 show the ground reactions acting on the nose gear and the main landing gear, respectively. As can be seen, the algorithms have also very well estimated these two parameters. The deviations that appear, especially for the main landing gear a few seconds before the rotation (i.e., between 20 and 28 s), are due to the increase in lift caused by the increase of the angle attack during the ground acceleration. Since the angle of attack was assumed to be constant during this segment, this lift increase cannot be predicted by the algorithms.

Regarding the angle of attack, the results indicated that this parameter was also very well estimated. It can be seen that the shape and magnitude of this parameter reflect the data measured with the RAFS on each segment of the takeoff phase (i.e., ground acceleration, rotation and transition).

Finally, the elevators deflection is the least well-predicted parameter. This aspect was expected because as explained in **Section 4.3.2.2**, the assumption of zero angular acceleration during the rotation phase and at the beginning of the transition phase is not fully justified. In addition, the fact that the elevators deflection is directly related to the pilot technique makes this parameter even more difficult to predict. This is the reason why the trim algorithm did not find a suitable solution during the time interval 28-32 s. However, it is interesting to note that after 32 s, the estimate becomes better and the error obtained is of the order of ±1.5°, which remains acceptable.

4.4.1.3 Validation Results for all Tests

The analyses presented in the previous sections were repeated for all 20 takeoff tests. For each test, the aircraft trajectory data and the fuel burned at the end of the takeoff phase were compared to their values predicted by the algorithms. The obtained results are presented in Figure 4.14 to Figure 4.16.

As shown in Figure 4.14 to Figure 4.16, the results are overall very good, since the takeoff distance, time-to-takeoff, and fuel burned are globally well estimated with less than 3% of relative error. It is also interesting to note that in addition to providing good estimates, the algorithms made it possible the analysis of the influence of several parameters on the aircraft takeoff performance.

The results of tests number 1 to 5 show for example that the weight has a very pronounced effect on the takeoff distance. According to the results, the aircraft required a takeoff distance of 2730 ft for a light configuration (26,000 lb), compared to 4494 ft for a heavy configuration (35,000 lb). This difference of 1764 ft (+64%) can be explained by the fact that a heavier weight leads to

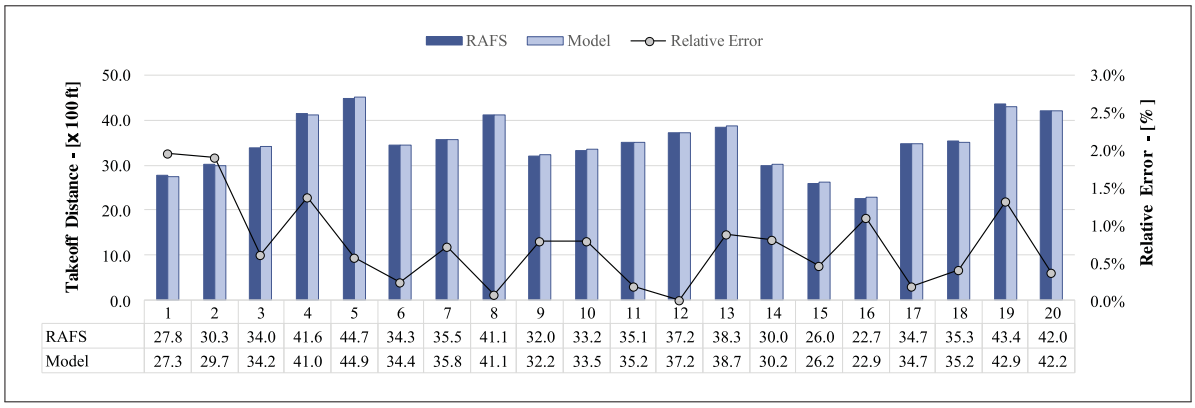

	1	2	3	4	5	6	7	8	9	10	11	12	13	14	15	16	17	18	19	20
RAFS	27.8	30.3	34.0	41.6	44.7	34.3	35.5	41.1	32.0	33.2	35.1	37.2	38.3	30.0	26.0	22.7	34.7	35.3	43.4	42.0
Model	27.3	29.7	34.2	41.0	44.9	34.4	35.8	41.1	32.2	33.5	35.2	37.2	38.7	30.2	26.2	22.9	34.7	35.2	42.9	42.2

Figure 4.15 Takeoff Distance Comparison

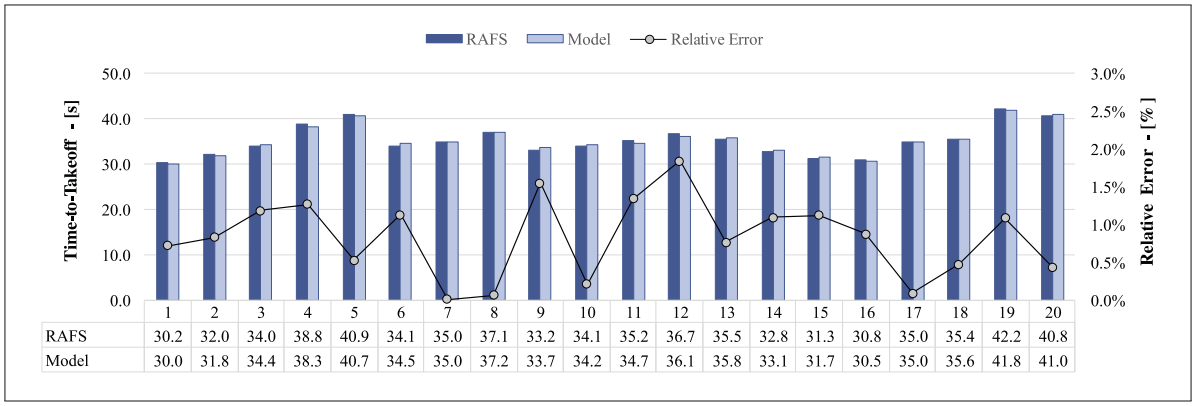

	1	2	3	4	5	6	7	8	9	10	11	12	13	14	15	16	17	18	19	20
RAFS	30.2	32.0	34.0	38.8	40.9	34.1	35.0	37.1	33.2	34.1	35.2	36.7	35.5	32.8	31.3	30.8	35.0	35.4	42.2	40.8
Model	30.0	31.8	34.4	38.3	40.7	34.5	35.0	37.2	33.7	34.2	34.7	36.1	35.8	33.1	31.7	30.5	35.0	35.6	41.8	41.0

Figure 4.16 Time-to-Takeoff Comparison

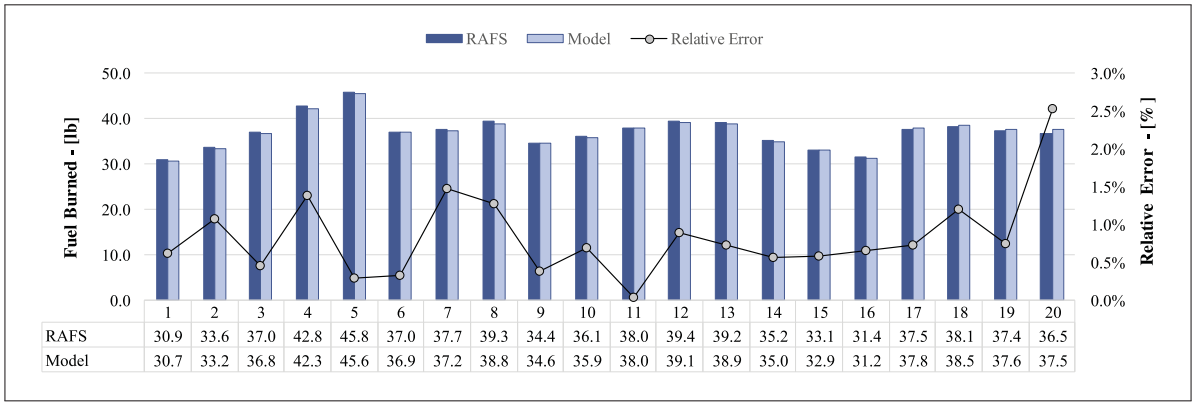

	1	2	3	4	5	6	7	8	9	10	11	12	13	14	15	16	17	18	19	20
RAFS	30.9	33.6	37.0	42.8	45.8	37.0	37.7	39.3	34.4	36.1	38.0	39.4	39.2	35.2	33.1	31.4	37.5	38.1	37.4	36.5
Model	30.7	33.2	36.8	42.3	45.6	36.9	37.2	38.8	34.6	35.9	38.0	39.1	38.9	35.0	32.9	31.2	37.8	38.5	37.6	37.5

Figure 4.17 Takeoff Fuel Burned Comparison

a slower acceleration. Similar observations can be made for the other two parameters which also increase with an increase in takeoff weight.

To further demonstrate the reliability of the proposed methodology, a second analysis was made by comparing the angle of attack and aircraft calibrated airspeed at the lift-off point. The results of this comparison are shown in Figure 4.18 and Figure 4.19. Note that the criteria recommended by the FAA to validate the model are that the predicted and measured angle of attack should agree within ±1.5°, and that the predicted and measured airspeed (CAS or TAS) should agree within ±3 kts.

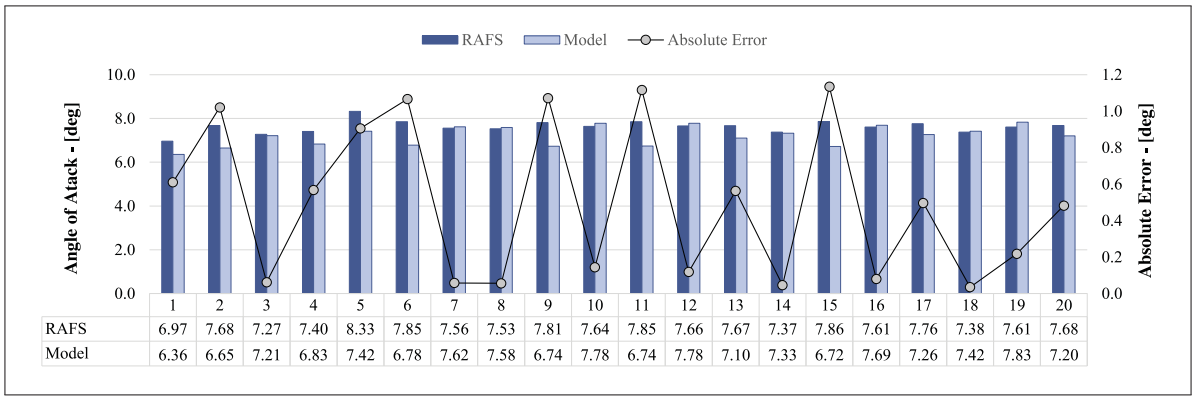

	1	2	3	4	5	6	7	8	9	10	11	12	13	14	15	16	17	18	19	20
RAFS	6.97	7.68	7.27	7.40	8.33	7.85	7.56	7.53	7.81	7.64	7.85	7.66	7.67	7.37	7.86	7.61	7.76	7.38	7.61	7.68
Model	6.36	6.65	7.21	6.83	7.42	6.78	7.62	7.58	6.74	7.78	6.74	7.78	7.10	7.33	6.72	7.69	7.26	7.42	7.83	7.20

Figure 4.18 Angle of Attack Comparison at Lift-Off Point

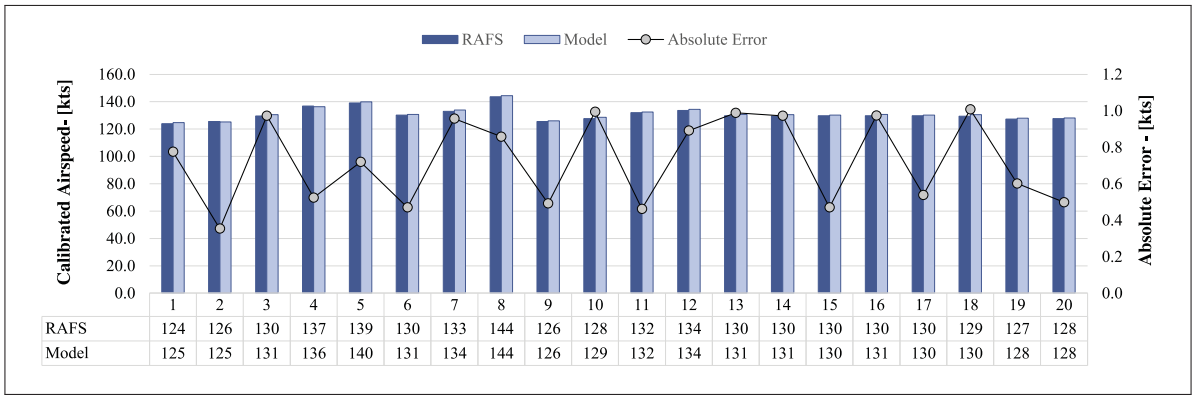

	1	2	3	4	5	6	7	8	9	10	11	12	13	14	15	16	17	18	19	20
RAFS	124	126	130	137	139	130	133	144	126	128	132	134	130	130	130	130	130	129	127	128
Model	125	125	131	136	140	131	134	144	126	129	132	134	131	131	130	131	130	130	128	128

Figure 4.19 Calibrated Airspeed Comparison at Lift-Off Point

As expected, the predicted parameters correspond very well to those measured with the RAFS. It can be seen that the angle of attack at the lift-off point was estimated with a maximum absolute

error of 1.13°, while the lift-off calibrated airspeed was predicted with less than 1.0 kt of absolute error. These results reinforce those obtained previously and demonstrate that the algorithms developed in this article can be used to carry out detailed analyzes of the performance of the aircraft during the takeoff phase.

4.4.2 Simulation Results for Complete Departure Trajectories

After the validation of the takeoff phase, the next step was to evaluate the effectiveness of the algorithms in predicting the complete trajectory of the aircraft for a given departure profile. For this purpose, 20 additional tests were conducted with the RAFS. Out of the 20 tests, 10 tests were performed by following a NADP 1, while the remaining 10 tests were performed by following a NADP 2. Table 4.3 shows the list of tests restrained with their corresponding flight conditions.

Table 4.3 Flight Tests for the Validation of the Complete Departure Trajectory

Test No. NADP 1/2	**Departure Airport**	**Elevation**	**Weight**	**TRH**	**AH**	**Wind Speed**	**Wind Gradient**	**ΔISA**
		[ft]	[lb]	[ft]	[ft]	[kts]	[kts/ft]	[°C]
1 / 11	CYUL	96	26,000	800	800	0	0	0
2 / 12	CYUL	96	30,000	800	800	0	0	0
3 / 13	CYUL	96	35,000	800	800	0	0	0
4 / 14	CYUL	96	30,000	1500	1500	0	0	-25
5 / 15	CYUL	96	30,000	1500	1500	0	0	+25
6 / 16	CYUL	96	30,000	1200	1200	-20	0	0
7 / 17	CYUL	96	30,000	1200	1200	-20	+15/1000	0
8 / 18	CYUL	96	30,000	1200	1200	-20	-15/1000	0
9 / 19	LOWI	1904	30,000	1000	1000	0	0	0
10 / 20	MMMX	7294	30,000	1000	1000	0	0	0

Note that 4 different profiles were used for the NAPDs by varying the thrust reduction height (TRH) and the acceleration height (AH) from 800 ft to 1500 ft (AGL). The CAS after acceleration for the NADP 2 was however always imposed at 220 kts for the sake of simplicity.

4.4.2.1 Example of Trajectory Comparison

Figure 4.20 shows two examples of results obtained for the tests number 7 (NADP 1) and number 17 (NADP 2). Note that for a better visualization of the results, the aircraft trajectory for the test number 17 has been shifted to the left.

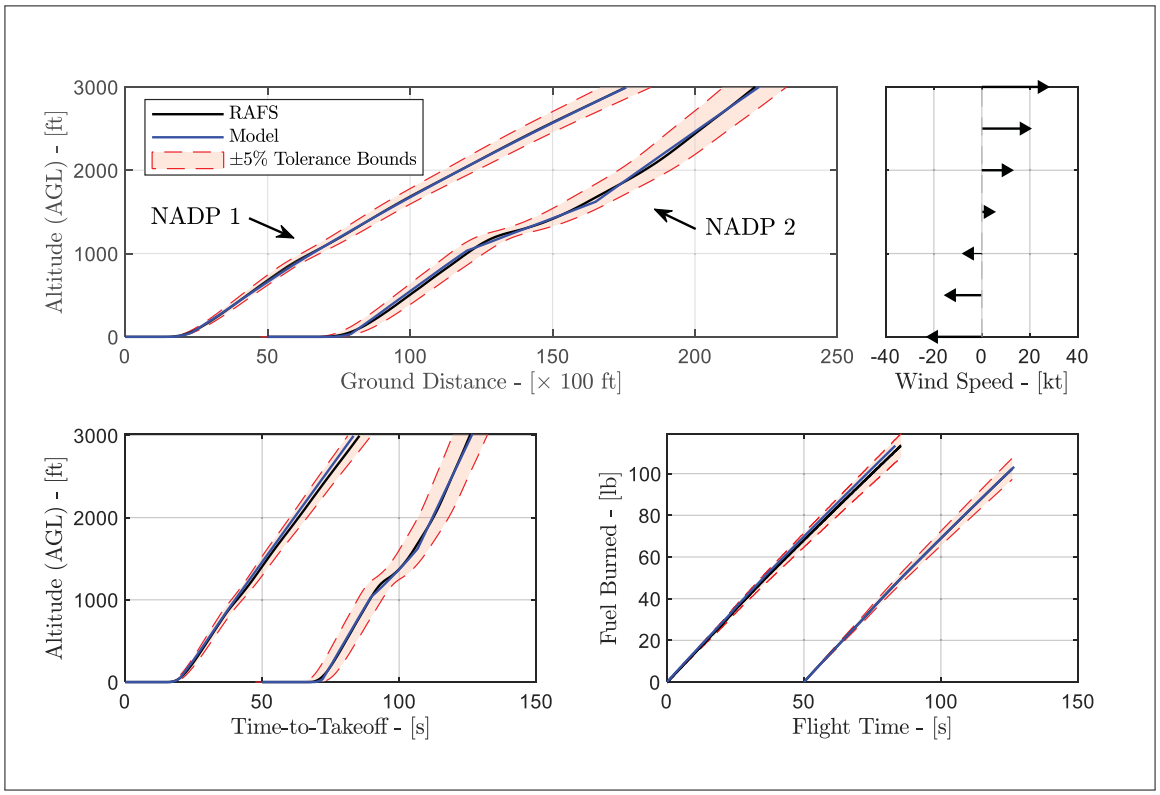

Figure 4.20 Aircraft Departure Trajectory and Fuel Burned Comparison for Tests number 7 and 17

As seen in Figure 4.20 a very good match of the predicted and measured data was obtained for the two departure procedures (NADP 1 and 2). The ground distance, flight time and fuel burned are all three well predicted, and gave less than 5% of relative error. It interesting to emphasize that both tests were conducted by imposing a constant wind gradient of 15/1000 kts/ft. This fact means that the aircraft initially benefited from a favorable headwind of 20 kts. However, as the aircraft climbed to 3000 ft, the wind changed progressively into an unfavorable tailwind

of 25 kts. This change in wind direction and wind magnitude has an impact on the aircraft performance and, as seen in Figure 4.20 , the algorithms were able to model this aspect.

Regarding the test number 17, it is also interesting to note that the algorithms predictions reflect very well the behavior of the aircraft, especially during the climb acceleration segment. In addition, attempts to model the aircraft acceleration with a constant climb gradient or with a constant rate of climb have led to less convincing results. This aspect reinforces the initial assumption of a climb acceleration at constant rate of TAS.

4.4.2.2 Results Validation for all Tests

The comparison made in the previous section was repeated for all the 20 tests. The results obtained are presented in Figure 4.21 to Figure 4.23 .

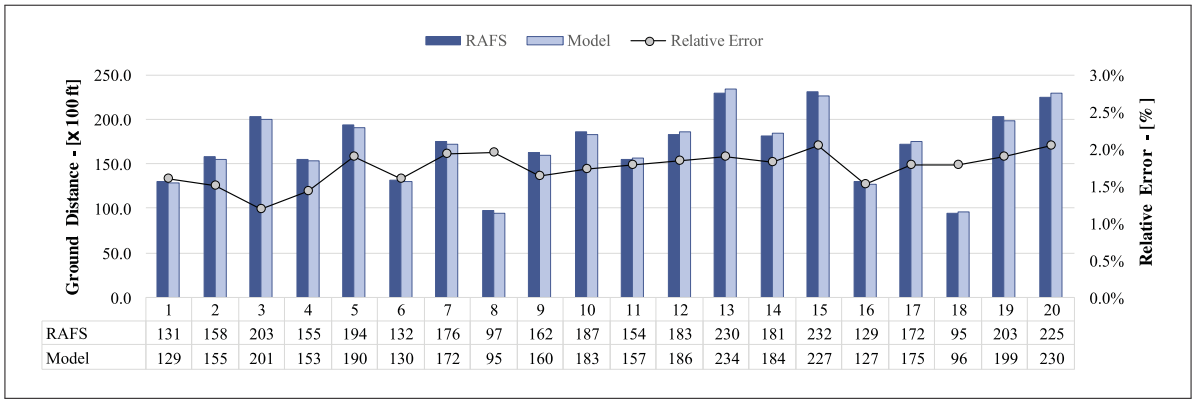

	1	2	3	4	5	6	7	8	9	10	11	12	13	14	15	16	17	18	19	20
RAFS	131	158	203	155	194	132	176	97	162	187	154	183	230	181	232	129	172	95	203	225
Model	129	155	201	153	190	130	172	95	160	183	157	186	234	184	227	127	175	96	199	230

Figure 4.21 Ground Distance Comparison for the Complete Departure Trajectory

The results presented in these figures are once again very good, and they reinforce those obtained for the takeoff phase. These results clearly demonstrate that the algorithms developed in this paper can be used to predict the takeoff and the departure trajectories of the Cessna Citation X in presence of a non-constant wind.

In the light of these results, it can be concluded that the methodology and algorithms presented in this paper could be used to develop dynamics tools for the study of aircraft takeoff and departure trajectories, and that the initial objective of this study was achieved.

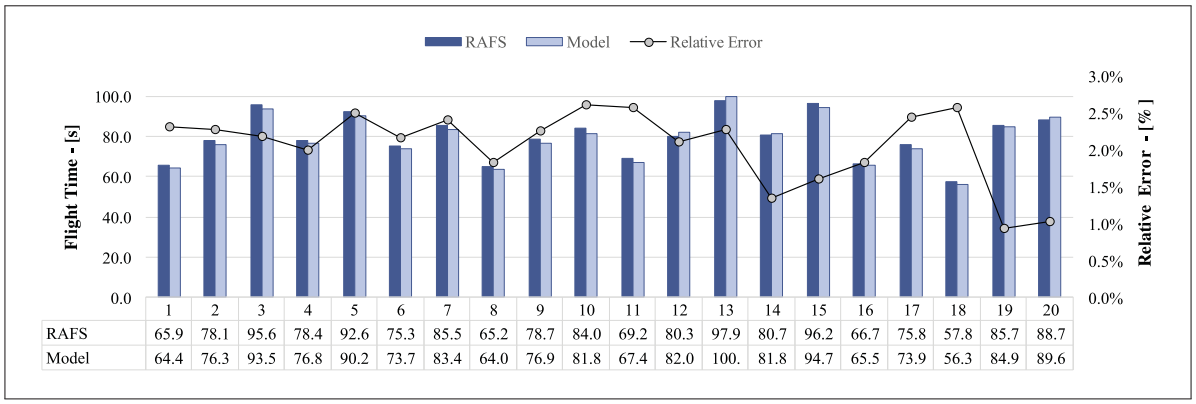

	1	2	3	4	5	6	7	8	9	10	11	12	13	14	15	16	17	18	19	20
RAFS	65.9	78.1	95.6	78.4	92.6	75.3	85.5	65.2	78.7	84.0	69.2	80.3	97.9	80.7	96.2	66.7	75.8	57.8	85.7	88.7
Model	64.4	76.3	93.5	76.8	90.2	73.7	83.4	64.0	76.9	81.8	67.4	82.0	100.	81.8	94.7	65.5	73.9	56.3	84.9	89.6

Figure 4.22 Flight Time Comparison for the Complete Departure Trajectory

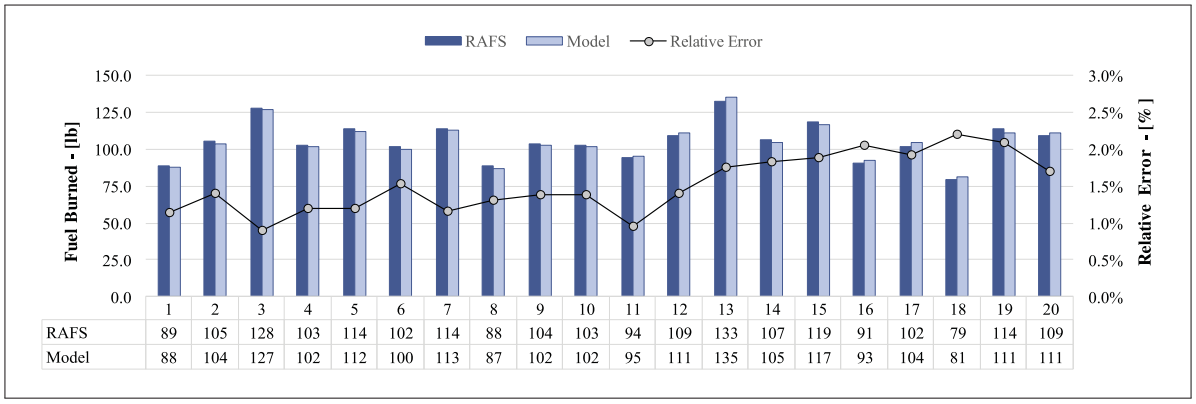

	1	2	3	4	5	6	7	8	9	10	11	12	13	14	15	16	17	18	19	20
RAFS	89	105	128	103	114	102	114	88	104	103	94	109	133	107	119	91	102	79	114	109
Model	88	104	127	102	112	100	113	87	102	102	95	111	135	105	117	93	104	81	111	111

Figure 4.23 Fuel Burned Comparison for the Complete Departure Trajectory

4.5 Conclusion

In this paper, a complete and detailed methodology to calculate the takeoff and departure trajectories of an aircraft was presented. To achieve this objective, the aircraft trajectory was divided into five types of segments: ground acceleration, rotation, transition, climb at constant speed, and climb-acceleration. For each segment, detailed algorithms were developed in order to solve and to integrate the equations of motion. Techniques to take into account piloting procedures were also presented. The methodology also allowed to consider the effects of headwinds and tailwinds, as well as non-zero wind gradients, on the vertical trajectory of the aircraft.

The methodology was tested and applied to the well-known Cessna Citation X business jet aircraft for which a qualified research aircraft flight simulator (RAFS) was available. A total of 40 tests for different flight and operation conditions were conducted; including 20 normal takeoff and 20 normal takeoff with initial-climb. The validation of the methodology was done by comparing the data measured with the RAFS to those calculated by the algorithms.

From a global point of view, it has been shown that the proposed algorithms were accurate enough to predict the aircraft trajectories with a relative error smaller than 5%. In addition, it has been also shown that the algorithms developed to trim the aircraft within each segment were able to predict various aircraft parameters, such as the ground reaction forces or the aircraft angle of attack with a very good degree of accuracy. Following the analyses of the results, it can therefore be concluded that the methodology presented in this paper is effective, and this methodology could be used to study the takeoff performance in the preliminary design of an aircraft, to generate takeoff performance databases required for the exploitation of the FMS, or to analyze and optimize aircraft takeoff and departure trajectories. Another advantage is that the algorithms are flexible, which makes the methodology applicable to other types of aircraft or adaptable according to the needs of the users.

The methodology developed in this paper can predict the departure trajectory of an aircraft, however it was limited to the vertical trajectory. As a future work, it would be interesting to improve the methodology by including the lateral motion of the aircraft. From this perspective, cross winds must also be considered in the methodology, as they can affect the aircraft takeoff performance, especially during the ground acceleration phase. Indeed, in the presence of crosswinds, pilots must use the rudder to compensate for wind direction and to maintain the aircraft at the center of the runway. This maneuver generates additional drag, which increases the takeoff distance. Future research will also focus on the adaptation of the methodology to the simulation of rejected takeoff scenario.

CHAPTER 5

METHOD FOR CALCULATING CESSNA CITATION X 4D FLIGHT TRAJECTORIES IN PRESENCE OF WINDS

Georges Ghazi [a], Ruxandra Mihaela Botez [b], Charles Bourrely [c] and Alina-Andreea Turculet [d]

[a, b, c, d] Department of Automated Production Engineering, École de Technologie Supérieure, 1100 Notre-Dame West, Montréal, Québec, Canada H3C 1K3

Paper submitted for publication in the *AIAA Journal of Aerospace Information Systems*, July 2020

Résumé

L'objectif de cet article est de présenter une méthode pratique développée au Laboratoire de Recherche en Commande Active en Contrôle, Avionique et AéroSevoÉlasticité (LARCASE) pour calculer les trajectoires de vol de l'avion Cessna Citation X en présence de vents. La méthode proposée consistait à intégrer numériquement les équations de mouvement de l'avion sur différents segments qui composent un profil de vol commercial typique. À cette fin, la trajectoire verticale de l'avion a été divisée en sept segments de vol typiques : montée sans restriction à vitesse constante, montée restreinte à vitesse constante, accélération en montée et en palier, vol en palier à vitesse constante, descente sans restriction à vitesse constante, descente restreinte à vitesse constante et décélération en descente et en palier. Pour chaque type de segment, des algorithmes détaillés ont été conçus pour résoudre et intégrer les équations de mouvement en utilisant un méthode d'Euler. La trajectoire latérale, d'autre part, a été construite en reliant une série de points de cheminement à des segments de droite et de virage. La méthode proposée a été testée et validée avec un simulateur de vol pour la recherche du Cessna Citation X. Un total de 130 tests ont été effectués avec le simulateur en considérant une large gamme de conditions de vol. Les résultats ont montré que les données de trajectoire prédites par les différents algorithmes correspondaient aux données de trajectoire obtenues à partir du RAFS avec moins de 5% d'erreur relative.

Abstract

This paper presents a practical method developed at the Laboratory of Applied Research in Actives Controls, Avionics, and AeroServoElasticity (LARCASE) for calculating aircraft flight trajectories of a Cessna Citation X in presence of winds. The proposed method consisted in numerically integrating the aircraft equations of motion over various segments that composed a typical commercial flight profile. For this purpose, the aircraft vertical trajectory was divided into seven typical flight segments: unrestricted climb at constant airspeed, restricted climb at constant airspeed, climb/level-off acceleration, level flight at constant airspeed, unrestricted descent at constant airspeed, restricted descent at constant airspeed, and descent/level-off deceleration. For each segment, detailed algorithms to solve and integrate the equations of motion using a simplified Euler scheme were designed. The lateral trajectory, on the other hand, was constructed by connecting a series of waypoints with straight and turn segments. The proposed method was tested and validated with a qualified Research Aircraft flight Simulator (RAFS) of the Cessna Citation X. A total of 130 tests were carried out with the RAFS over a wide range of operational conditions. Comparison results showed that the trajectory data predicted by the different algorithms matched the trajectory data obtained from the RAFS with less than 5% of relative error.

5.1 Introduction

During recent years, the release of pollutants into the atmosphere has become one of the main environmental problems for commercial airliners. Aircraft are energy-intensive and, like most transportation systems, depend on fossil fuels. By burning fuel, aircraft produce carbon dioxide (CO_2), which contributes to global warming, but also other substances such as nitrogen oxide (NO_x), which endangers human health and welfare. In 2018, the aviation industry was responsible for only about 2.5% of global emissions (Lee *et al.*, 2009). However, as the number of passengers is expected to double to 8.2 billion by 2037 (IATA, 2020), this share could increase considerably in the coming years.

Another problem facing commercial aviation is the airspace overload. In order to satisfy the high demand for air transport, airliner operators have to expand their fleets, which causes a saturation of the airspace. This saturation results in flight delays, inefficient routing, and complex air traffic control procedures.

Behind the environmental factor, there is also an economical factor. Indeed, "energy is not free", and fuel represents one of the major cost components for airlines. The International Air Transport Association (IATA) has estimated that in 2018, airlines spent an average of 23.5% of their operating expenses on fuel (IATA, 2018). Thus, any fuel saving strategy could turn into a significant competitive advantage. In addition, by reducing their fuel consumption, airlines are helping to reduce the aircraft carbon footprint, leading to a "win-win" scenario.

5.1.1 Research Problematic and Motivations

Today, the most promising solution to solve problems related to fuel consumption, emissions and airspace saturation in the short term relies on the optimization of flight trajectories. This solution becomes feasible mainly by the development of advanced flight planning tools and systems, such as the Flight Management System (FMS). The FMS is an avionics computer whose primary role is to assist the crew in a wide variety of in-flight tasks ranging from navigation and flight planning to performance prediction and flight trajectory optimization (Walter, 2001; Avery, 2011).

Although already very sophisticated, the next FMS generation will have to evolve to support future concepts, such as 4D Trajectory and Trajectory Based Operation (4D-TBO) (Ramasamy *et al.*, 2014; Gardi, Sabatini, Ramasamy & Kistan, 2014). Initiated by the Single European Sky Air Traffic Management Research (SESAR) and Next Generation Air Transportation System (NextGen) programs, these concepts aim to improve flight efficiency, flight times and schedule predictability through better prediction and harmonization of aircraft flight trajectories (Brooker, 2008). Under 4D-TBO, aircraft will be able to follow a predetermined optimal 4D trajectory

(i.e., three spatial dimensions plus a time constraint as the fourth dimension) as long as they comply with the restrictions issued by air traffic controllers.

In order to exploit the operational benefits of 4D-TBO concepts, it is necessary to develop algorithms to accurately calculate 4D flight trajectories. These algorithms are essential for the development of next FMS generation, but also for the design of decision support tools needed to reduce controllers' workload. For this reason, studies are conducted at the Laboratory of Applied Research in Active Controls and AeroServoElasticity (LARCASE) to develop techniques that could help manufacturers, sub-contractors, airliners and researchers in predicting aircraft performance and flight trajectories.

5.1.2 Methods for Calculating Aircraft Flight Trajectories

Today, one of the best alternatives for researchers to perform flight trajectory calculations is to use the Base of Aircraft Data (BADA, family 3). BADA is a collection of aircraft performance models developed and maintained by Eurocontrol (Nuic *et al.*, 2010). In addition to providing aircraft performance data, Eurocontrol has also included in the BADA user manual (Nuic, 2010) a very simple method and guidelines for calculating flight trajectories. The method consists in solving and integrating the total energy model equations, for which various simplifications have been applied.

Although widely accepted as a reference for trajectory prediction, optimization and simulation applications (Camilleri *et al.*, 2012; Abramson & Ali, 2012; Rodriguez-Sanz, Alvarez, Comendador, Valdes, Perez-Castan & Godoy, 2018), the method proposed in BADA has some limitations.

The first limitation is based on the fact that the lift force is calculated by assuming a zero flight path angle, for all flight phases. Such an assumption, although it simplifies the calculation process, can lead to prediction errors, especially during the climb and descent phases. Another limitation concerns trajectory prediction during the acceleration and deceleration phases, which are modelled by assuming a constant energy share factor, whereas in practice, commercial

aircraft accelerate or decelerate either at a constant vertical speed or at a constant rate of airspeed. Finally, the method does not allow to model the impact of the wind gradient on the aircraft flight trajectory.

There are other studies in the literature that used a method similar to the BADA approach but with some differences. Slattery & Zhao (1997), for instance, described a method implemented in the Center-TRACON Automation System (CTAS) tool developed by researchers from the NASA Ames Research Center to synthesize aircraft flight trajectories. Rodriguez, Deniz, Herrero, Portas & Corredera (2007) proposed an approach to model 4D descent flight trajectories using BADA performance parameters. Torres (2018) used an energy model to evaluate the influence of numerical integration methods on aircraft trajectory computation. Hartjes & Visser (2017) proposed a method to parameterized aircraft trajectories during departure procedures.

The inclusion of the wind acceleration and of the flight path angle introduces non-linearities in the aircraft equations of motion, and their resolution becomes very complex. This problem can nevertheless be overcome by using an optimization algorithm (Quanbeck, 1982), or an iterative process (Blake, 2009). In his report, Blake (2009) presented an iterative process used by Boeing to perform climb performance calculations. According to the author, this process makes it possible to obtain a very good estimate of aircraft flight path angle, thus improving the model predictions for the climb phase. Unfortunately, the method presented by Blake was only applied to the climb phase, and no solution was proposed for the other flight phases. In addition, the author did not consider the influence of the wind into the calculations.

Aircraft flight trajectories can be also calculated using lookup tables or performance databases. This approach was considered by various researchers of the LARCASE laboratory to optimize flight trajectories Patrón *et al.* (2014, 2015); Murrieta-Mendoza *et al.* (2017b). Murrieta-Mendoza & Botez (2015) described a complete method for calculating the vertical trajectory of a commercial aircraft using a set of performance databases. A close approach was also considered by Ghazi *et al.* (2015b; 2015a) for predicting the climb and cruise trajectories of a

Cessna Citation X using a lookup table-based aero-propulsive model. Tudor (2017) also used a lookup table approach to model the flight trajectories of two commercial aircraft.

One of the main advantages of using lookup table-based models is the simplicity of their structure. Indeed, because of their simplicity, these models are very easy to implement and above all computationally inexpensive. They can be used to generate flight trajectories over a few-seconds time period (Murrieta-Mendoza & Botez, 2015). However, their structure has a major default as they cannot be adapted to consider certain aspects, such as the influence of the wind or turns.

Most recently, several researchers have proposed to use machine learning techniques and artificial neural networks to model aircraft flight trajectories. Wu, Tian & Ma (2019), for instance, trained a backpropagation neural network based on ADS-B data to learn and predict future aircraft trajectories in China. Wang, Liang & Delahaye (2017) combined clustering and machine learning techniques to predict the arrival time of aircraft at the Beijing Capital International Airport. Similarly, Alligier, Gianazza & Durand (2016) used a neural network to improve aircraft trajectories predictions for the descent phase. In another study, Ayhan, Costas & Samet (2018) used a neural network for predicting the estimated time of arrival for commercial flights.

The results obtained so far in these studies have revealed that machine learning does not yet allow very precise predictions to be obtained. In addition, it should be noted that the learning process requires a very large quantity of historical data and, unfortunately, this information is generally not available to FMS manufacturers. For this reason, this approach cannot be considered in the context of this study.

5.1.3 Research Objectives and Paper Organization

The objective of this paper is to present a new methodology, which combines different algorithms, to calculate the 4D flight trajectories of a commercial aircraft. For this purpose, the vertical trajectory is divided into a series of flight segments. For each flight segment, algorithms for trimming the aircraft and solving the equations of motion are presented. The proposed

algorithms can be used to predict various flight parameters such as the flight path angle, or the angle of attack. In addition, techniques for implementing lateral turns and lateral transitions are also considered. The main idea behind this paper is to provide a detailed methodology that can be used for the analysis of aircraft flight performance, the optimization of flight trajectories or for air traffic management applications.

The methodology was applied to the business jet aircraft Cessna Citation X for which a Research Aircraft Flight Simulator (RAFS) was available (see Figure 5.1). The RAFS was designed and built by CAE Inc. based on flight-test data provided by Cessna Textron Aircraft. The flight dynamics and propulsion models encoded in the RAFS satisfy the criteria imposed by the Federal Aviation Administration (FAA) for the level-D (highest level of certification). The RAFS was therefore considered as a very good reference to evaluate the validity of the proposed method.

Figure 5.1 Cessna Citation X Research Aircraft Flight Simulator

The rest of the paper is structured as follows. **Section 5.2** introduces the main mathematical equations used in this study to model the aircraft behavior, and its aero-propulsive characteristics. **Section 5.3** deals with the complete methodology to predict the aircraft trajectory. **Section 5.4**

presents the comparison and validation results. Finally, the paper ends with conclusions and remarks concerning future possible research.

5.2 Background and Aircraft Mathematical Model

Before presenting the methodology proposed in this study, it may be useful to introduce several notations and mathematical equations related to the analysis of flight trajectories. From this perspective, the section begins with a brief presentation of the Cessna Citation X, as well as a description of the different flight segments that compose a typical commercial flight. The section then continues with the development of the aircraft mathematical model, which includes the equations of motion, the aero-propulsive model equations, and the environment model equations.

5.2.1 Cessna Citation X Description

The aircraft modeled in this study is the Cessna Citation X (model 750) produced and manufactured by the manufacturer Cessna Aircraft Company . The Cessna Citation X is a medium-sized long-range business jet designed to fly at a maximum operating altitude of 51,000 ft, and a maximum operating speed of Mach 0.92. The aircraft is equipped with two high bypass Rolls-Royce AE3007C-1 turbofan engines, installed at the rear of the fuselage. Each engine can produce a maximum takeoff thrust of 6442 lbf (28.65 kN) for an average fuel consumption of 2712 lb/h (1230 kg/h). With its well-designed aerodynamics and powerful engines, the Citation X can transport 10 passengers (including 2 crew members) and has a maximum range of 3390 n miles (6280 km).

Pertinent specifications and limitations relative to the Cessna Citation X are given in Table 5.1 for the convenience of the readers (Cessna Aircraft Company, 2002).

5.2.2 Flight Profile Generation and Flight Segment Definition

The flights studied in this paper are standard commercial flights between a departure airport and a destination airport. However, for the sake of simplicity, the take-off and landing phases are not

Table 5.1 Cessna Citation X Specifications and Limitations

Parameters	Values
Altitude Specifications	
Certified Altitude	51,000 ft 15,545 m
Typical Cruise Altitudes	37,000 to 45,000 ft
Airspeed Limitations	
Maximum Operating Mach number	Mach 0.92
Maximum Operating Speed (flaps 0 deg)	350 kts 649 km/h
Maximum Operating Speed (flaps 15 deg)	250 kts 463 km/h
Maximum Operating Speed (flaps > 15 deg)	180 kts 333 km/h
Certified Weights	
Maximum Takeoff Weight	36,100 lb 16,375 Kg
Maximum Landing Weight	31,800 lb 14,424 Kg
Maximum Zero Fuel Weight	4,400 lb 11,067 Kg

considered. It is therefore assumed that all flights begin and end at an altitude of 1500 ft above ground level (AGL). In addition, to simplify the discussion, the aircraft trajectory is divided into two parts: the lateral profile and the vertical profile.

5.2.2.1 Lateral Flight Profile Generation

The lateral flight profile specifies the horizontal route that the aircraft must follow to reach a given destination. It is generally represented by a sequence of waypoints (i.e., geographical points defined in terms of latitude/longitude coordinates) connected by straight and turn segments, as illustrated in Figure 5.2.

Waypoints are determined by selecting in a navigation database a departure airport, a takeoff runway, a Standard Instrument Departure (SID) procedure, a set of enroute waypoints or airways, a Standard Terminal Arrival Route (STAR) procedure, a destination airport, and a landing runway. On the basis of this information, the lateral profile is constructed by firstly connecting the waypoints one after the other with straight segments. This process leads to an approximate lateral profile which is used for synthetizing and optimizing the vertical flight profile.

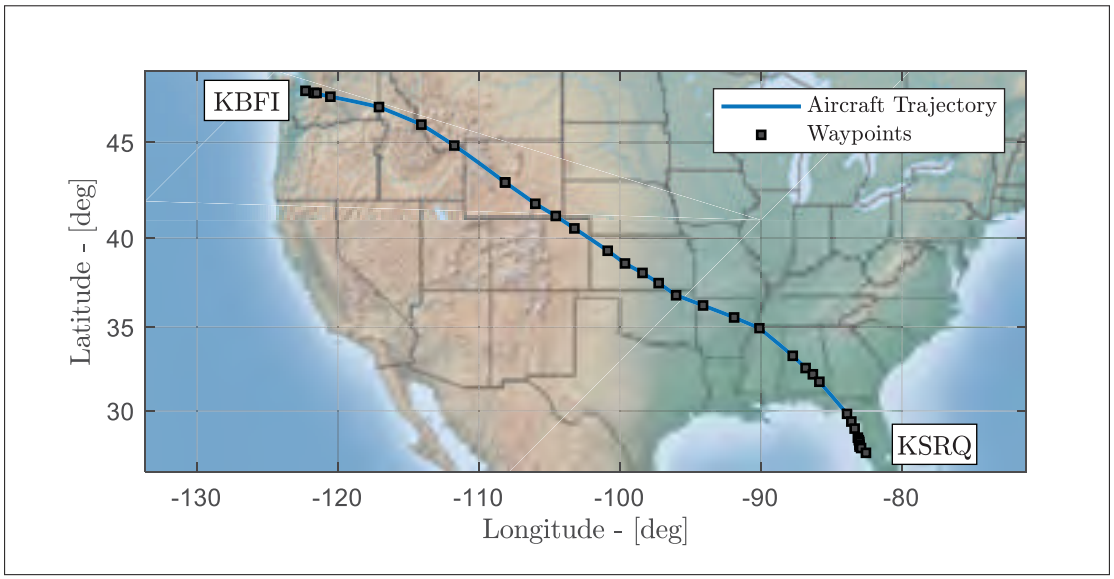

Figure 5.2 Example of Lateral Trajectory for a Flight from Seattle (KBFI) to Sarasota (KSRQ)

Turn segments are then added over the approximate lateral profile based on the required course change between two consecutive straight segments, the aircraft ground speed, and the type of lateral transition.

Turns Segments and Lateral Transitions Definition

There are two basic types of waypoints commonly used to define a lateral transition: “Fly-Over” (FO) waypoints and “Fly-By” (FB) waypoints (see Figure 5.3a and Figure 5.3b). Fly-over waypoints are used in terminal procedures (i.e., SID and STAR) when it is necessary to delay a turn for obstacle clearance or to protect areas from aircraft noise. In this case, the aircraft must first fly over the waypoint before heading to the next segment. Conversely, for fly-by waypoints, the turn can be initiated before reaching the waypoint to allow tangential interception of the next segment.

In addition to the waypoint type, a lateral transition also depends on the type of leg following a waypoint. A leg is defined by a two-letters alphabetic code, where the first letter refers to the mode of flight, and the second letter indicates how the leg should be completed. Nowadays,

most modern FMSs can handle up to 23 different leg types (Walter, 2001). However, only the three most commonly used leg types are considered in this study:

- Track to Fix (TF): a route segment between two geographic points (i.e., fixes or waypoints);
- Direct to Fix (DF): a route segment between the aircraft position and a given fix;
- Radius to Fix (RF): a constant radius circular route between two fixes.

By combining these three types of leg with the two types of waypoints, it become possible to obtain the four lateral transition types shown in Figure 5.3. Most of the transitions calculated by the FMS for flight conditions above 1500 ft can be reproduced by creating combinations of these four typical transitions.

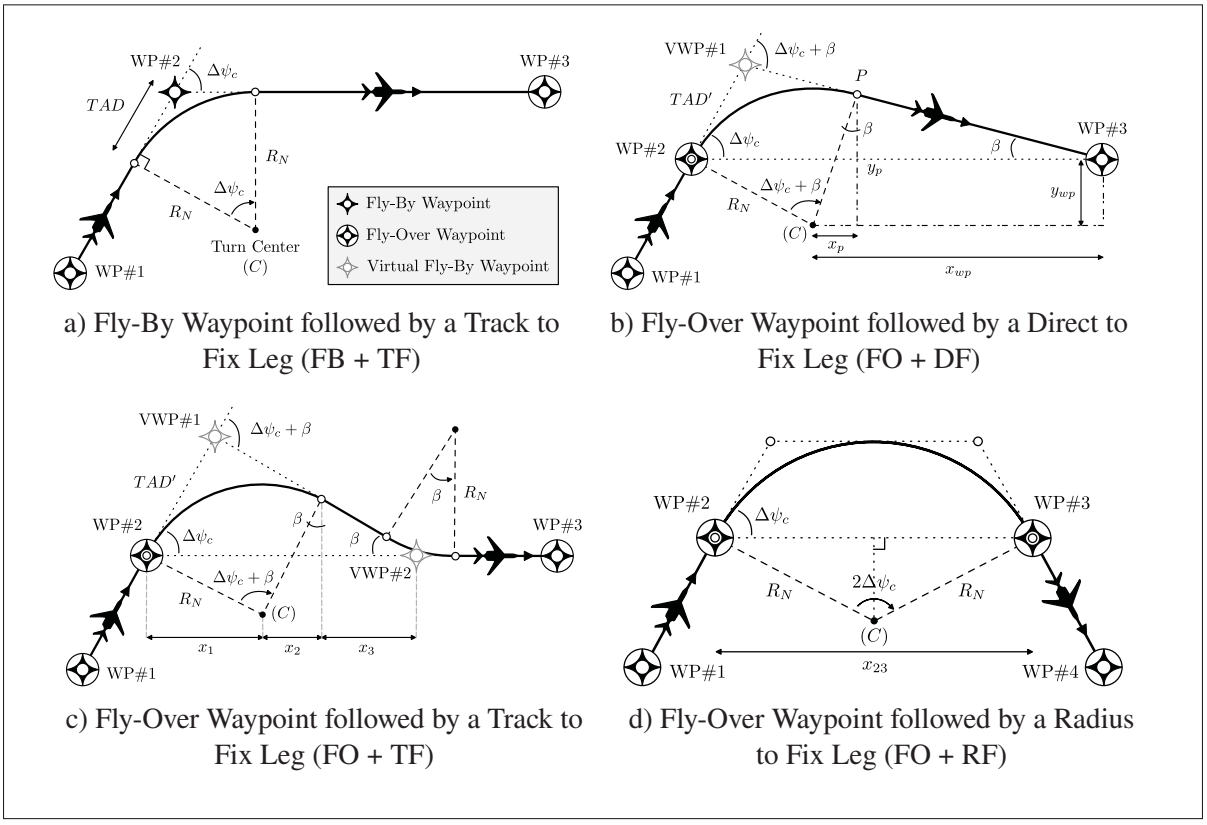

a) Fly-By Waypoint followed by a Track to Fix Leg (FB + TF)

b) Fly-Over Waypoint followed by a Direct to Fix Leg (FO + DF)

c) Fly-Over Waypoint followed by a Track to Fix Leg (FO + TF)

d) Fly-Over Waypoint followed by a Radius to Fix Leg (FO + RF)

Figure 5.3 Turn Segment and Lateral Transition Illustrations

Turns Segments and Lateral Transitions Construction

Turn segments and lateral transitions are constructed based on the required course change between two consecutive waypoints, the predicted aircraft ground speed, and several geometrical relationships.

By assuming that the aircraft is performing a coordinated turn, the nominal radius R_N of the turn can be calculated using the following equation (Walter, 2001):

$$R_N = \frac{\left[V_{GS}^{\max}\right]^2}{g_0 \tan(\phi_N)} \tag{5.1}$$

where ϕ_N is the nominal bank angle assumed to be the lesser of 5 deg or one-half the course change of the turn $\Delta\psi_c$, to a maximum of 25 deg. Similarly, the maximum ground speed $V_{GS}^{\max}$ is determined from the still-air ground speed at the start of the turn corrected for worst-case tailwinds.

Once the nominal turn radius determined, all lateral transitions can be constructed using geometrical relationships as explained in the following.

FB+TF Transition. A FB + TF transition is constructed by considering that the aircraft flies along a circular arc of radius R_N tangent to the two straight segments connecting waypoints #1 to #3, as illustrated in Figure 5.3a. For this purpose, the turn must be initiated when the aircraft is at a turn anticipation distance (TAD) from the active waypoint (i.e., WP#2). Using basic trigonometric relationships, the distance can be expressed as follows:

$$TAD = R_N \tan\left[\frac{|\Delta\psi_c|}{2}\right] \tag{5.2}$$

FO+DF Transition. A FO+DF transition is constructed by creating a virtual fly-by waypoint (VWP#1) between waypoints #2 and #3, as shown in Figure 5.3b. This technique allows to transform the original FO+DF transition into an equivalent FB+TF transition, which facilitate the calculation process as well as the activation logic of the waypoints. The VWP#1 is inserted

at an equivalent turn anticipation distance (TAD') from the active waypoint WP#2 defined as:

$$TAD' = R_N \tan\left[\frac{|\Delta\psi_c| + \beta}{2}\right] \tag{5.3}$$

where β is the interception angle. This angle should be defined so that the course of the aircraft at the end of the turn leads directly to the next waypoint (i.e., WP#3).

The interception angle β can be determined by introducing the point P (see Figure 5.3b), and by noting that this point belongs to a circle of radius R_N and to a tangent line formed by the VWP#1 and the WP#3. Mathematically, these two aspects imply:

$$\begin{cases} x_p^2 + y_p^2 = R_N^2 \\ \dfrac{y_p}{x_p} \times \dfrac{y_p - y_{wp}}{x_p - y_{wp}} = -1 \end{cases} \tag{5.4}$$

where $\{x_p, y_p\}$ are the distances of the point P relative to the turn center (C), and $\{x_{wp}, y_{wp}\}$ are the distances of the WP#3 relative to the turn center (C) defined such as:

$$\begin{aligned} x_{wp} &= x_{23} - |R_N \sin(\Delta\psi_c)| \\ y_{wp} &= R_N \cos(\Delta\psi_c) \end{aligned} \tag{5.5}$$

where x_{23} is the distance between the WP#2 and the WP#3.

By solving Eq. (5.5) with respect to x_p, two solutions can be obtained:

$$x_p^{(1,2)} = \frac{R_N \left[R_N x_{wp} \pm y_{wp}\sqrt{x_{wp}^2 + y_{wp}^2 - R_N^2}\right]}{x_{wp}^2 + y_{wp}^2} \tag{5.6}$$

Finally, based on these results, the interception angle can be then determined using the following equation:

$$\beta = \arcsin\left[\frac{\min\left\{x_p^1, x_p^2\right\}}{R_N}\right] \tag{5.7}$$

FO+TF Transition. A FO+TF transition is constructed by inserting two virtual fly-by waypoints as illustrated in Figure 5.3c. The first fly-by virtual waypoints (VWP#1) is inserted at equivalent turn anticipation distance (TAD') from the active waypoint WP#2, in the same way as for a FO+DF transition. The second virtual fly-by waypoint (VWP#2), is inserted at a distance $x = \Sigma x_i$, where x_i for $i = \{1, 2, 3\}$ are defined as follows:

$$x_1 = R_N \sin(|\psi_c|) \quad x_2 = R_N \sin(\beta) \quad x_3 = \left[1 - \frac{cos(\Delta\psi_c}{\cos(\beta)}\right] \frac{R_N^2 \cos^2(\beta)}{\sin(\beta)} \tag{5.8}$$

It should be noted that for a FO+TF transition, the interception angle β is always fixed at 30 deg as recommended by ICAO navigation procedures (ICAO, 2006). This value is typically used to ensure a "smoth" capture of the segment defined by the waypoints WP#2 and WP#3.

FO+RF Transition. A FO+RF transition (see Figure 5.3d) is constructed by considering that the aircraft moves along a circular arc of radius R_N defined such as:

$$R_N = \frac{x_{23}}{2 \sin(|\Delta\psi_c|)} \tag{5.9}$$

where x_{23} is the distance between the WP#2 and the WP#3.

5.2.2.2 Vertical Flight Profile Generation

In a complementary way, the vertical profile specifies the aircraft trajectory in the vertical plane in terms of altitude, speed and distance. It is generally divided into five flight phases: the on-course climb, the cruise climb, the cruise, the initial descent, and the approach descent. Each of these flight phases is in turn divided into several flight segments in order to emulate flight procedures. An example of a vertical profile for a commercial aircraft is shown in Figure 5.4.

It should be noted that for the purpose of this study, this profile is considered as the default vertical flight profile. However, it can be modified by adding or deleting one or more vertical flight segments.

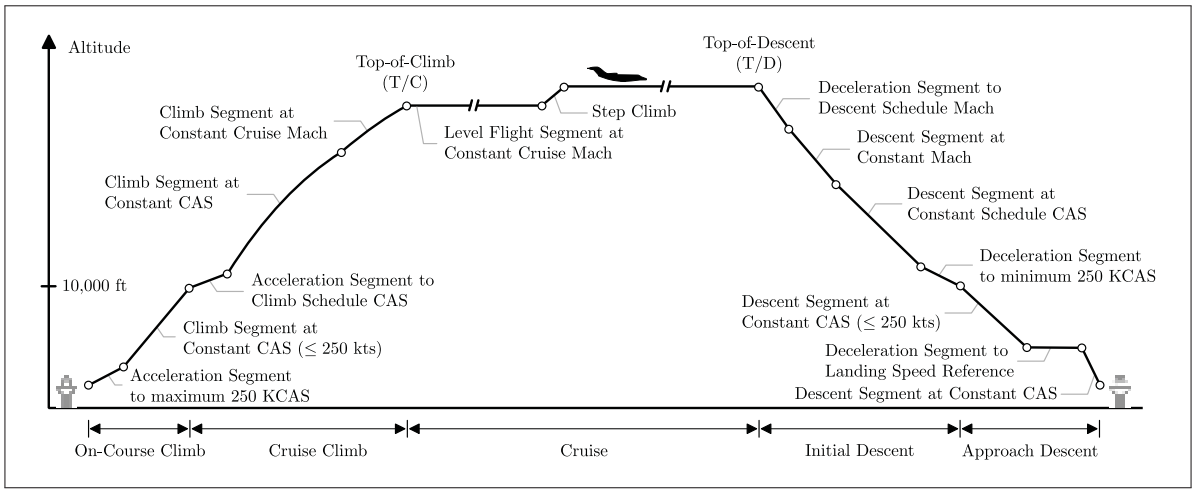

Figure 5.4 Typical Vertical Profile of a Commercial Flight

The On-Course Climb

The on-course climb phase begins at an altitude of 1500 ft AGL, or at an altitude where the engine power has been set to climb thrust. This flight phase is characterized by two vertical flight segments.

The first segment is an acceleration segment to the on-course climb speed. The objective of this segment is to accelerate the aircraft to an airspeed where the flaps can be fully retracted, and which offers good climb performance. However, due to airspace regulations which limit aircraft airspeed below 10,000 ft, the acceleration segment is limited to 250 KCAS (kts Calibrated Airspeed). A second climb segment at constant CAS up to 10,000 ft is then added to complete the on-course climb phase.

The Cruise Climb

Above 10,000 ft, the airspeed restriction no longer applies, and the pilot/FMS can initiate the cruise climb phase. This flight phase is characterized by three vertical flight segments.

The first segment is an acceleration segment to a pre-determined CAS higher than 250 kts. This segment is then followed by a climb segment at constant CAS up to an altitude where the aircraft

Mach number matches the desired cruise Mach number. At this altitude, the pilot/FMS has to change the climb reference speed to constant Mach, and the cruise climb phase is completed with a climb segment at constant Mach up to the Top-of-Climb (T/C).

The altitude at which the transition CAS to Mach takes place is called the “crossover altitude”. For most commercial flights, this altitude varies between 27,000 and 35,000 ft.

The Cruise

The cruise phase corresponds to the portion of the flight between the T/C and the Top-of-Descent (T/D). This flight phase is typically characterized by a level flight segment during which the pilot must adjust the engine power to maintain the desired cruise Mach number. If necessary, several step climbs/descents (i.e., local change of flight levels) can be applied to reduce fuel consumption. In this case, step climbs/descents are treated as restricted or unrestricted climb/descent segments at constant Mach. The word “restricted” in this context typically refers to a vertical restriction on either the vertical speed or the flight path angle.

In addition to these segments, level-off acceleration/deceleration segments can be also added during the cruise in order to meet RTA (Required Time of Arrival) constraints.

The Initial Descent

The initial descent phase is similar to the cruise climb phase, except that it is realized in the reverse order. This flight phase is characterized by four vertical flight segments.

Starting from the T/D, and after reducing the engine power to idle thrust, the first segment of the initial descent phase is a deceleration segment to a schedule descent Mach number. This segment is then followed by a descent segment at constant Mach until the crossover altitude, at which the reference speed is changed to constant CAS. The aircraft then continues to descent at constant CAS until a deceleration altitude where a second deceleration segment must be applied in order to comply with the airspeed restriction below 10,000 ft.

The Approach Descent

The last flight phase is the approach descent to the destination airport. This flight phase is characterized by three or four vertical flight segments.

The first segment is a descent segment at constant CAS (lower than or equal to 250 kts) to the approach altitude (e.g, 3000 to 4000 ft AGL). At this altitude, a deceleration segment is applied to decelerate the aircraft to the reference landing speed and to allow the time to the pilot to gradually deploy the flaps. If necessary, a level flight segment can be applied until the typical three-degree gradient descent of the glideslope is intercepted.

Finally, the approach descent phase ends with a restricted descent segment at constant CAS and fixed flight path angle to the altitude of 1500 ft AGL.

5.2.3 Aircraft Mathematical Equations and Flight Model

For the purposes of the study, the aircraft is modeled as a point mass and the Earth is assumed to be non-rotational. In addition, all engines are supposed to be operational, and there is no asymmetric thrust. The rates of change of flight-path angle and of bank angle are neglected, assuming quasi-steady flight. Finally, the aircraft is supposed to fly in an atmospheric wind field including its longitudinal and lateral components.

5.2.3.1 Aircraft Equations of Motion in presence of Winds

The forces acting on the aircraft in flight are shown in Figure 5.5. The lift L and the drag D are the aerodynamic forces, and they are defined to be normal and parallel to the aircraft airspeed. The total thrust of the engines, denoted by F_N, is oriented in the forward direction making an angle ϕ_T relative to the aircraft fuselage. Finally, the weight W is oriented towards the center of the Earth.

By summing the forces parallel and perpendicular to the airspeed, it can be shown that the equations describing the motion of the aircraft in the vertical plane (corrected for the bank angle)

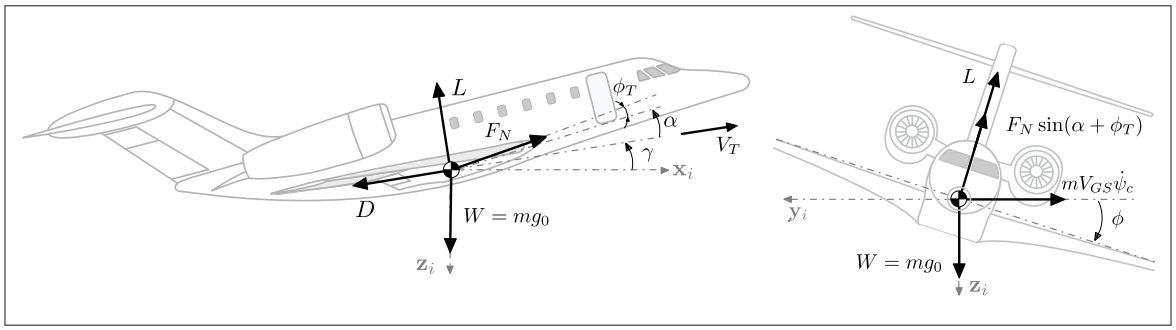

Figure 5.5 Forces Applied to the Cessna Citation X in Flight

are (Slattery & Zhao, 1997):

$$m\dot{V}_T + m\left[\dot{V}_{W,x}\cos(\gamma)\cos(\psi) + \dot{V}_{W,y}\cos(\gamma)\sin(\psi)\right] = F_N\cos(\alpha+\phi_T) - D - mg_0\sin(\gamma) \tag{5.10}$$

$$m\left[\dot{V}_{W,y}\sin(\gamma)\sin(\psi) - \dot{V}_{W,x}\sin(\gamma)\cos(\psi)\right] = [F_N\sin(\alpha+\phi_T) + L]\cos(\phi) - mg_0\cos(\gamma) \tag{5.11}$$

$$V_{GS} = \sqrt{[V_T\cos(\gamma)]^2 - [V_W\sin(\psi_c - \psi_w)]^2} + V_W\cos(\psi_c - \psi_w) \quad \text{and} \quad \dot{h} = V_T\sin(\gamma) \tag{5.12}$$

$$V_{W,x} = V_W\cos(\psi_w) \quad \text{and} \quad V_{W,y} = V_W\sin(\psi_w) \tag{5.13}$$

where m is the aircraft mass, g_0 is the acceleration of gravity, V_T is the true airspeed, $\{V_{W,x}, V_{W,y}\}$ are the horizontal components of the wind, V_W is the wind speed magnitude, α is the angle of attack, γ is the air relative flight path angle, ϕ is the aircraft bank angle, ψ is the aircraft heading, ψ_c is the aircraft course, ψ_w is the wind direction, and $\dot{h}$ is the aircraft rate of altitude.

Similarly, the aircraft motion in the horizontal plane can be described by the following equations:

$$\begin{aligned} mV_{GS}\dot{\psi}_c = {} & \{L + F_N\sin(\alpha+\phi_T)\}\{\sin(\phi)\cos(\psi_c - \psi) + \cos(\phi)\sin(\gamma)\sin(\psi_c - \psi)\} \\ & \cdots - \{F_N\cos(\alpha+\phi_T) - D\}\cos(\gamma)\sin(\psi_c - \psi) \end{aligned} \tag{5.14}$$

$$\dot{\lambda} = \frac{V_{GS}\sin(\psi_c)}{(R_E + h)\cos(\mu)} \quad \text{and} \quad \dot{\mu} = \frac{V_{GS}\cos(\psi_c)}{R_E + h} \tag{5.15}$$

where R_E is Earth's radius, and $\{\lambda, \mu\}$ are the aircraft longitude and latitude coordinates.

Finally, the aircraft mass variation due to engines fuel consumption is modeled as follows,

$$\dot{m} = -W_F \Rightarrow \Delta m = \Delta F_B = W_F \times \Delta t \tag{5.16}$$

where W_F is the engines fuel flow, and ΔF_B is the fuel burned during a given time interval Δt.

5.2.3.2 Aerodynamic Coefficients Model

The lift and drag in Eqs. (5.10) and (5.11) are the components of the aerodynamic force acting on the aircraft. These two quantities are represented using non-dimensional coefficients, such as:

$$L = 0.5\rho S V_T^2 CL_s \tag{5.17}$$

$$D = 0.5\rho S V_T^2 CD_s \tag{5.18}$$

where ρ is the air density, S is the aircraft wing reference area, and CL_s and CD_s are the lift and drag aerodynamic coefficients, respectively.

The model used to evaluate the aerodynamic coefficients was generated in-house by the LARCASE team based on the data encoded in the RAFS. The model consists of a set of lookup tables describing the variations of each aerodynamic coefficient as function of the angle of attack α, the Mach number M, the flaps setting δ_f, and the landing gear position δ_g.

Mathematically, these two coefficients are expressed as follows:

$$CL_s = CL_{WB}(\alpha, M) + \Delta CL_F(\alpha, M, \delta_f) + \Delta CL_{GR}(\alpha, M, \delta_g) \tag{5.19}$$

$$CD_s = CD_{WB}(\alpha, M) + \Delta CD_F(\alpha, M, \delta_f) + \Delta CD_{GR}(\alpha, M, \delta_g) \tag{5.20}$$

where each element in the above equations (i.e., CL_{WB}, ΔCL_F, ΔCL_{GR}, etc.) is a two- or three-dimensional lookup table representing the aerodynamic contributions of the wing-body (CX_{WB}), the flaps ΔCX_F, and the landing gear (ΔCX_{GR}).

5.2.3.3 Engine Thrust and Fuel Flow Models

In the same way as for the aerodynamic coefficients, the engine model is also composed of a set of four-dimensional lookup tables describing the variation of the thrust and fuel flow as function of the altitude h, the Mach number M, and temperature conditions. These lookup tables were developed and validated by the authors in a previous study using data provided by the RAFS (Ghazi *et al.*, 2015c; Ghazi & Botez, 2019). Mathematically, the thrust and fuel flow are expressed as follows:

$$F_N = F_N(N_1, h, M, \Delta\text{ISA}) \tag{5.21}$$

$$W_F = W_F(N_1, h, M, \Delta\text{ISA}) \tag{5.22}$$

where N_1 is the engine fan speed, and ΔISA is the temperature deviation from a standard day value.

The engine fan speed N_1 is also modeled by a four-dimensional lookup table, and is mathematically expressed as follows:

$$N_1 = N_1(h, M, \Delta\text{ISA}, TRP) - \Delta N_1 \tag{5.23}$$

where TRP is the Thrust Rating Parameter (i.e., idle, maximum cruise, maximum climb, etc.), and ΔN_1 is a parameter which quantifies the fan speed reduction in case of derated thrust operations.

5.2.4 Environment Model and Airspeed Conversions

The mathematical model used in this study to evaluate the atmosphere properties is based on the International Standard Atmosphere (ISA) (Young, 2017). The air temperature at a specific altitude is modeled by assuming a linear distribution with a temperature offset ΔISA, such as:

$$\begin{aligned} T &= T_0 - T'h + \Delta\text{ISA}, && \text{if } h \leq h_T \\ T &= T_T\Delta\text{ISA}, && \text{if } h \geq h_T \end{aligned} \tag{5.24}$$

where T_0 is the sea level air temperature, and T' is the temperature gradient, and T_T is the air temperature at the tropopause altitude h_T. Based on the temperature distribution law in Eq. (5.24), the air pressure is computed according to the two following relationships:

$$\begin{aligned} P &= P_0 \left[1 - T'h/T_0\right]^{g_0/(R_{\text{air}}T')}, && \text{if } h \leq h_T \\ P &= P_T \exp\left[-g_0(h - h_T)/(R_{\text{air}}T_T)\right], && \text{if } h \geq h_T \end{aligned} \tag{5.25}$$

while the air density is obtained as follows:

$$\rho = \rho_0 \left(\delta/\theta\right) \tag{5.26}$$

where P_0 and ρ_0 are the sea level pressure and density, respectively, R_{air} is the air gas constant, $\delta = P/P_0$ is pressure ratio, and $\theta = T/T_0$ is temperature ratio.

To obtain realistic trajectory simulations, the ISA model is combined with open source weather forecast data obtained from Environment Canada[1]. These data provide information relative to the air temperature, the mean sea level pressure, the horizontal wind speed, and the horizontal wind direction. The raw data are downloaded from Environment Canada website in a binary format called General Regularly-Distributed Information (GRIB2), and then restructured into lookup tables as function of longitude/latitude coordinates, isobaric levels and Coordinated Universal Time (UTC). A linear interpolation technique is used to obtain the weather data for a specific position/time condition.

Finally, the atmospheric parameters are also used in converting airspeed from calibrated airspeed (CAS, V_C), true airspeed (TAS, V_T), and Mach number (M). When V_C is known, the Mach number is first calculated as follows:

$$M = \sqrt{5\left\{\left[\frac{1}{\delta}\left\{\left[1 + 0.2\left(\frac{V_C}{a_0}\right)^2\right]^{3.5} - 1\right\} + 1\right]^{1/3.5} - 1\right\}} \tag{5.27}$$

[1] https://weather.gc.ca/grib/

and V_T is then obtained using the following equation:

$$V_T = a_0 M \sqrt{\theta} \tag{5.28}$$

Conversely, when V_T is known, the Mach number is first calculated from Eq. (5.28), and V_C is then obtained as follows:

$$V_C = a_0 \sqrt{5 \left\{ \left[\delta \left\{ \left(1 + 0.2M^2\right)^{3.5} - 1 \right\} + 1 \right]^{1/3.5} - 1 \right\}} \tag{5.29}$$

where a_0 is the sea level speed of sound.

5.3 Aircraft Trajectory Prediction Algorithm

The methodology developed in this study to calculate the aircraft 4D flight trajectory consists in numerically integrating the aircraft equations of motion presented in **Section 5.2.3** along a specified lateral flight profile from an initial state (i.e., weight, speed, altitude, etc.) and assuming environment conditions (i.e., temperature, pressure, density and winds). To simplify the calculations, the vertical trajectory is divided into seven basic vertical flight segments: unrestricted climb at constant CAS/Mach, restricted climb at constant CAS/Mach, climb acceleration, level flight at constant CAS/Mach, unrestricted descent at constant CAS/Mach, restricted descent at constant CAS/Mach, and descent deceleration. For each segment, algorithms to solve and integrate the equations of motion are presented.

The complete aircraft trajectory is constructed by combining these segments in a specified order depending on the vertical template profile, such as the one shown in Figure 5.4.

5.3.1 Unrestricted Climb at Constant CAS/Mach

The aircraft trajectory for an unrestricted climb at constant CAS/Mach segment is calculated by numerically integrating the aircraft equations of motion from an initial altitude $h_{[0]}$ to a

predetermined final altitude $h_{[N]}$. For this purpose, the aircraft trajectory is divided into N altitude intervals (or sub-segments) as illustrated in Figure 5.6.

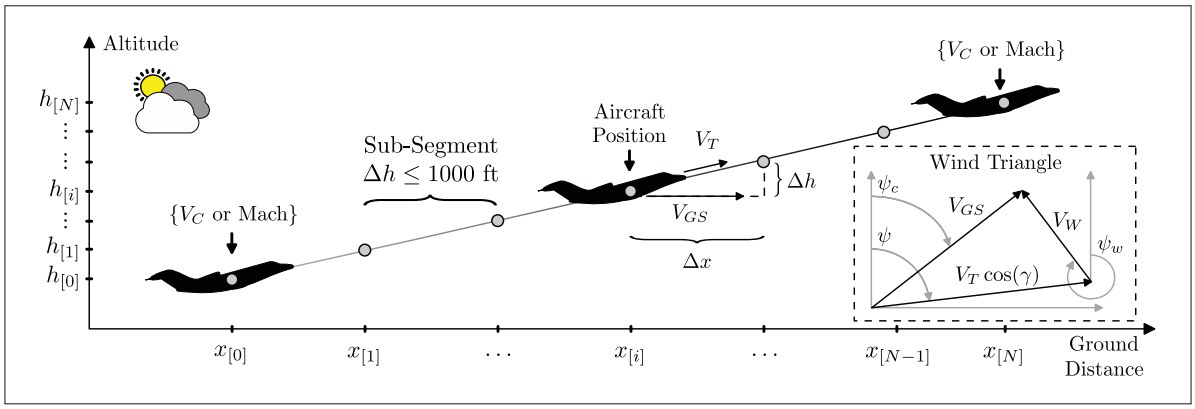

Figure 5.6 Calculation Procedure for an Unrestricted Climb at Constant CAS/Mach Segment

The step size for the altitude is arbitrary. In general, a small step size provides more accurate simulation results at the expense of the computational time, while a large step size reduces the computational time at the expense of accuracy. A suggested step size that offers a good trade-off between calculation time and accuracy is 1000 ft (Blake, 2009). Nevertheless, this step size can be reduced during the integration procedure depending on the aircraft position and performance.

5.3.1.1 Aircraft Equations of Motion Simplification and Model Parametrization

To simplify the calculations, several simplifications can be applied. Indeed, for a climb segment, it can be assumed that the change in wind conditions is mainly due to the change in aircraft altitude. Consequently, the time derivative of the wind components can be approximated by:

$$\dot{V}_{W,x} = \frac{\mathrm{d}V_{W,x}}{\mathrm{d}t} = \frac{\mathrm{d}V_{W,x}}{\mathrm{d}h} \times \frac{\mathrm{d}h}{\mathrm{d}t} = V'_{W,x} V_T \sin(\gamma) \tag{5.30}$$

$$\dot{V}_{W,y} = \frac{\mathrm{d}V_{W,y}}{\mathrm{d}t} = \frac{\mathrm{d}V_{W,y}}{\mathrm{d}h} \times \frac{\mathrm{d}h}{\mathrm{d}t} = V'_{W,y} V_T \sin(\gamma) \tag{5.31}$$

where $V'_{W,x}$ and $V'_{W,y}$ are the wind gradients along the x- and y-directions, respectively. These two parameters are determined based on a first-order finite difference at a given altitude.

In addition, given the fact that the aircraft is climbing at either constant CAS or constant Mach number, the time derivative of the true airspeed can also be approximated as follows:

$$\dot{V}_T = \frac{\mathrm{d}V_T}{\mathrm{d}t} = \frac{\mathrm{d}V_T}{\mathrm{d}h} \times \frac{\mathrm{d}h}{\mathrm{d}t} = \frac{\mathrm{d}V_T}{\mathrm{d}h} V_T \sin(\gamma) \tag{5.32}$$

By using these new expressions, Eq. (5.11) can be rewritten in the following more practical form:

$$\gamma = \arcsin\left[\frac{F_N \cos(\alpha + \phi_T) - D}{m g_0 \,(1 + \mathrm{AF})} - \frac{\left\{V'_{W,x} \cos(\psi) + V'_{W,y} \sin(\psi)\right\} V_T \sin(\gamma) \cos(\gamma)}{g_0 \,(1 + \mathrm{AF})}\right] \tag{5.33}$$

where $\mathrm{AF} = (V_T/g_0)(\mathrm{d}V_T/\mathrm{d}h)$ is called the "acceleration factor". This factor quantifies the variation of the aircraft true airspeed as function of altitude for a given CAS/Mach.

According to Blake Blake (2009) and Young (2017), the acceleration factor can be determined according to the following equations:

- For a climb segment at constant CAS:

$$\begin{aligned} \mathrm{AF} &= 0.7M^2 \left[\frac{(1 + 0.2M^2)^{3.5} - 1}{0.7M^2(1 + 0.2M^2)^{2.5}} - \frac{0.190263 \times T_{\mathrm{ISA}}}{T}\right], && \text{if } h \leq h_T \\ \mathrm{AF} &= \frac{(1 + 0.2M^2)^{3.5} - 1}{(1 + 0.2M^2)^{2.5}}, && \text{if } h \geq h_T \end{aligned} \tag{5.34}$$

- For a climb segment at constant Mach:

$$\begin{aligned} \mathrm{AF} &= \frac{-0.13318 \times M^2 T_{\mathrm{ISA}}}{T}, && \text{if } h \leq h_T \\ \mathrm{AF} &= 0, && \text{if } h \geq h_T \end{aligned} \tag{5.35}$$

where T_{ISA} is the standard temperature (i.e., for $\Delta\mathrm{ISA} = 0$).

Thus, by combining all these simplifications with Eqs. (5.10) to (5.16), the pertinent equations describing the motion of the aircraft for an unrestricted climb at constant CAS/Mach segment

can be summarized as follows:

$$L = F_N \sin(\alpha + \phi_T) - \frac{mg_0 \cos(\gamma)}{\cos(\phi)} + \frac{\left\{V'_{W,x} \cos(\psi) - V'_{W,y} \sin(\psi)\right\} V_T \sin(\gamma)^2}{\cos(\phi)} \tag{5.36}$$

$$\gamma = \arcsin\left[\frac{F_N \cos(\alpha + \phi_T) - D}{mg_0\,(1 + \mathrm{AF})} - \frac{\left\{V'_{W,x} \cos(\psi) + V'_{W,y} \sin(\psi)\right\} V_T \sin(\gamma) \cos(\gamma)}{g_0\,(1 + \mathrm{AF})}\right] \tag{5.37}$$

$$V_{GS} = \sqrt{[V_T \cos(\gamma)]^2 - [V_W \sin(\psi_c - \psi_w)]^2} + V_W \cos(\psi_c - \psi_w) \tag{5.38}$$

$$\dot{h} = V_T \sin(\gamma) \tag{5.39}$$

where AF is calculated from Eqs. (5.34) and (5.35).

It should be noted that unrestricted climb segments are normally performed at maximum climb thrust setting (MCLB). However, in practice, airlines prefer to use derated climb thrust to preserve engine wear (Young, 2017; Mori, 2020).

There are two derated thrust settings typically employed by airlines: Climb 1 (CLB-1) and Climb 2 (CLB-2). The former is achieved by reducing the engine fan speed by 3%, which is equivalent to a 10% thrust reduction; the latter is achieved by reducing the engine fan speed by 6%, which is equivalent to a thrust reduction of 20%.

In practice, the derating percentage is not applied through the climb phase. Rather, it is maintained up to 10,000 ft, after which it is linearly reduced to zero to allow the aircraft to recover the maximum climb thrust by 30,000 ft. Therefore, if a derated climb thrust is selected, the parameter ΔN_1 in Eq. (5.23) is modelled as follows:

$$\begin{aligned} \Delta N_1 &= \Delta N_{1,0}, && \text{if } h \leq 10,000 \text{ ft} \\ \Delta N_1 &= \min\left\{\frac{(30000 - h)\Delta N_{1,0}}{20000}, 0\right\}, && \text{if } h \geq 10,000 \text{ ft} \end{aligned} \tag{5.40}$$

where $\Delta N_{1,0} = -3\%$ for CLB-1 and $\Delta N_{1,0} = -6\%$ for CLB-2. Otherwise, this parameter is set to zero.

5.3.1.2 Aircraft Trim Procedure

To evaluate the lift and drag forces in Eqs. (5.36) and (5.37), it is necessary to know the values of the aircraft heading, angle of attack and flight path angle. These three parameters can be determined by considering that the aircraft is in quasi-static equilibrium, and by trimming the aircraft in each subsegment of the unrestricted climb segment.

The technique developed in this paper to trim the aircraft is summarized in Algorithm 5.1. This technique consists in iteratively searching for a combination of heading, angle of attack, and flight path angle that satisfies the equilibrium of the aircraft. For this purpose, the algorithm starts with an initial estimate of the angle of attack and flight path angle, denoted by $\{\alpha^{[k-1]}, \gamma^{[k-1]}\}$. Based on these two initial estimates, the algorithm computes the aircraft heading required to maintain a desired course from the wind triangle relationships, as shown in the next equation (Slattery & Zhao, 1997):

$$\psi = \psi_c - \arcsin\left[\frac{V_W \sin(\psi_c - \psi_w)}{V_T \cos(\gamma)}\right] \tag{5.41}$$

The algorithm then calculates the lift force and associated lift coefficient required to balance the aircraft along the vertical axis using Eq. (5.36). A“reverse lookup table” technique is next applied to find a new estimation of the angle of attack $\alpha^{[k]}$. This process is done by evaluating the lift coefficient for various angles of attack, and by using a linear interpolation technique to find the one that leads to the required lift coefficient, as illustrated in Figure 5.7.

Finally, the algorithm calculates a new estimate of the flight path angle $\gamma^{[k]}$ using Eq. (5.37) and the values $\{\alpha^{[k]}, \gamma^{[k-1]}\}$.

Because of the inaccuracy of the first iteration, it is necessary to redo the calculations by replacing the initial estimates $\{\alpha^{[k-1]}, \gamma^{[k-1]}\}$ with their new estimates $\{\alpha^{[k]}, \gamma^{[k]}\}$. This process should be repeated until the values of the angle of attack and the flight path angle between two consecutive iterations are acceptably close.

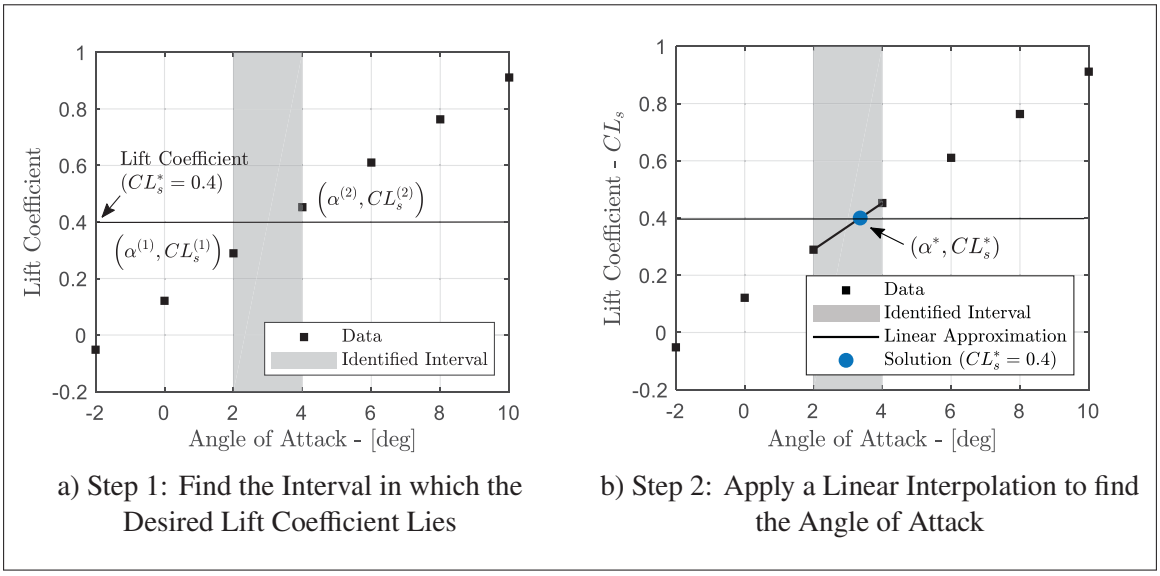

a) Step 1: Find the Interval in which the Desired Lift Coefficient Lies

b) Step 2: Apply a Linear Interpolation to find the Angle of Attack

Figure 5.7 Illustration of the "Reverse Lookup Table" Technique

5.3.1.3 Complete Integration Procedure

Equations (5.36) to (5.39) combined with Eqs. (5.14) and (5.15) form the system of equations describing the aircraft trajectory for an unrestricted climb at constant CAS/Mach segment. The complete procedure proposed to integrate these equations, and to compute the aircraft trajectory for this type of segment is given in Algorithm 5.2.

It should be noted that the altitude step size is by default 1000 ft. However, this step size can be reduced during the integration process depending on the following situations:

- If the aircraft is approaching the final altitude, the step size is reduced so that the final altitude will be reached in one iteration;
- If the aircraft is approaching a turn, the step size is reduced so that the beginning of the turn will be reached in one iteration;
- If the aircraft is in a turn, the step size is chosen so that either the aircraft will turn 5° in one iteration or the turn will be completed in one iteration;
- If the aircraft vertical speed is lower than 500 ft/min, then the step size is reduced based on a maximum time step of 60 seconds.

In the case where more than one situation applies, the altitude step size is then chosen to be the smallest among all the possible sizes.

Algorithm 5.1 Trim Procedure for an Unrestricted Climb at Constant CAS/Mach Segment

0. Initialization: For the trim algorithm, it is assumed that all aircraft parameters are known except the aircraft heading ψ, the angle of attack α, and the flight path angle γ.

1. Define Initial Estimates: Set $\alpha^{[0]} = 0$, and $\gamma^{[0]} = 0$. Note that in order to accelerate the convergence of the algorithm, these two parameters can be initialized based on the results obtained for the previous sub-segment. Set $k = 0$.

2. Main Loop: repeat

a) Update the number of iterations: $k = k + 1$.

b) From the current estimate of the flight path angle $\gamma^{[k-1]}$, compute the aircraft heading required to maintain the desired course:

$$\psi = \psi_c - \arcsin\left[\frac{V_W \sin(\psi_c - \psi_w)}{V_T \cos(\gamma^{[k-1]})}\right]$$

c) From the current estimate of the angle of attack $\alpha^{[k-1]}$ and flight path angle $\gamma^{[k-1]}$, compute the lift force required to balance the aircraft along the vertical axis:

$$L^* = F_N \sin(\alpha^{[k-1]} + \phi_T) - \frac{mg_0 \cos(\gamma^{[k-1]})}{\cos(\phi)} + \frac{\left\{V_{W,x} \cos(\psi) - V_{W,y} \sin(\psi)\right\} V_T \sin(\gamma^{[k-1]})^2}{\cos(\phi)}$$

d) Compute the corresponding lift coefficient: $CL_s^* = L^*/0.5\rho S V_T^2$.

e) Perform a reverse lookup table to find the new estimate for the angle of attack $\alpha^{[k]}$ which leads to the lift coefficient CL_s^*.

f) Based on $\alpha^{[k]}$, interpolate the drag coefficient CD_s, and compute the drag force: $D = 0.5\rho S V_T^2 CD_s$.

g) Knowing $\alpha^{[k]}$ and $\gamma^{[k-1]}$, compute a new estimate for the flight path angle $\gamma^{[k]}$:

$$\gamma^{[k]} = \arcsin\left[\frac{F_N \cos(\alpha^{[k]} + \phi_T) - D}{mg_0\,(1 + \mathrm{AF})} - \frac{\left\{V'_{W,x} \cos(\psi) + V'_{W,y} \sin(\psi)\right\} V_T \sin(\gamma^{[k-1]}) \cos(\gamma^{[k-1]})}{g_0\,(1 + \mathrm{AF})}\right]$$

while $|\alpha^{[k]} - \alpha^{[k-1]}| \geq 0.1$ ***OR*** $|\gamma^{[k]} - \gamma^{[k-1]}| \geq 0.1$ ***AND*** $k \leq 25$;

3. Return the last trim parameters: $\alpha^{[k]}$**,** $\gamma^{[k]}$ **and** ψ**.**

Algorithm 5.2 Integration Procedure for an Unrestricted Climb at Constant CAS/Mach Segment

0. Initialization: Set the aircraft initial states/position; latitude $\lambda_{[0]}$, longitude $\mu_{[0]}$, course $\psi_{c[0]}$, mass $m_{[0]}$, altitudes $h_{[0]}$, elapsed time $t_{[0]}$, ground distance $x_{[0]}$, and fuel burned $F_{B[0]}$.

1. Integration and Model Parameters Definition: Define the final altitude $h_{[N]}$, and set the altitude step Δh. Initialise the number of iterations $i = 0$, the bank angle ϕ, and rate of change of course $\dot{\psi}_c$.

2. Main Loop: repeat

a) From the atmosphere and wind models find the following parameters: air density ρ, temperature ratio θ, pressure ratio δ, Mach number M from $V_{T[i]}$, and wind parameters: V_W, ψ_w, $V_{W,x}$, $V_{W,y}$, $V'_{W,x}$, and $V'_{W,y}$.

b) Based on the speed strategy, determine the TAS V_T, the CAS V_C, and the Mach number M.

c) From the knowledge of the Mach number M and temperature, compute the acceleration factor AF.

d) Based on the engine model and flight conditions, compute the thrust F_N and fuel flow W_F by assuming MCLB, CLB-1 or CLB-2 setting.

e) Use Algorithm 5.1 to trim the aircraft for the current flight condition, and to determine the aircraft heading ψ, the angle of attack α, and the flight path angle γ.

f) Compute the altitude, distance, and mass variations for the current sub-segment:

$$\Delta h = V_{T[i]} \sin(\gamma)\Delta t \quad \Delta x = V_{GS}\Delta t \quad \Delta m = W_F \Delta t$$

g) Update aircraft states :

$$h_{[i+1]} = h_{[i]} + \Delta h \quad \lambda_{[i+1]} = \lambda_{[i]} + \dot{\lambda}\Delta t \quad t_{[i+1]} = t_{[i]} + \Delta t \quad \psi_{c[i+1]} = \psi_{c[i]} + \dot{\psi}_c \Delta t$$
$$x_{[i+1]} = x_{[i]} + \Delta x \quad \mu_{[i+1]} = \mu_{[i]} + \dot{\mu}\Delta t \quad m_{[i+1]} = m_{[i]} - \Delta m \quad F_{B[i+1]} = F_{B[i]} + \Delta m$$

h) If the next segment is a turn segment, then adjust the bank angle based on the actual ground speed and nominal turn radius, and then compute the rate of change of course using Eq. (5.14). Otherwise, set $\phi = \dot{\psi}_c = 0$, and determine the aircraft course according to the next waypoint in the list.

i) Update the number of iterations: $i = i + 1$.

while $h_{[i]} < h_{[N]}$;

3. Return all flight parameters, including altitude, distance, time and fuel burned.

5.3.2 Restricted Climb at Constant CAS/Mach

The aircraft trajectory for a restricted climb at constant CAS/Mach is calculated by following a procedure quasi similar to that developed for an unrestricted climb at constant CAS/Mach. The difference comes mainly from the fact that for this type of segment the aircraft flight path is no longer an unknown parameter, while the thrust is.

5.3.2.1 Aircraft Equations of Motion Simplification and Model Parametrization

Restricted climb segments are used when the vertical profile contains one or more vertical constraints. Theses constraints can either be directly specified in terms of a fixed rate of climb or fixed flight path angle, or indirectly created by an altitude restriction at a given waypoint. In the case where the rate of climb (or flight path angle) is specified, then the flight path angle (or rate of climb) can be calculated based on the following equations:

$$\gamma^* = \arcsin\left[\frac{V/S}{V_T}\right] \quad \text{or} \quad \dot{h} = V/S = V_T \sin(\gamma^*) \tag{5.42}$$

where V/S is the specified rate of climb, and γ^* is the specified flight path angle.

In the case where the vertical constraint is created by an altitude restriction at a waypoint, then the flight path angle is determined based on a point-to-point vertical flight path as follows:

$$\gamma^* = \arctan\left[\frac{\Delta h_{wp}}{\Delta x_{wp}}\right] \tag{5.43}$$

where Δh_{wp} and Δx_{wp} are the altitude and distance of the waypoint relative to the aircraft position. It should be noted that the computed flight path angle should be verified for "flyability" (i.e., not steeper than unrestricted descent).

Once the vertical speed and flight path angle determined, the thrust required to maintain the aircraft airspeed along the climb segment can then be found from Eq. (5.37).

Thus, the pertinent equations describing the motion of the aircraft for a restricted climb at constant CAS/Mach segment can be summarized as follows:

$$L = F_N \sin(\alpha + \phi_T) - \frac{mg_0 \cos(\gamma^*)}{\cos(\phi)} + \frac{\left\{V'_{W,x} \cos(\psi) - V'_{W,y} \sin(\psi)\right\} V_T \sin(\gamma^*)^2}{\cos(\phi)} \tag{5.44}$$

$$F_N = \frac{mg_0 \mathrm{AF} \sin(\gamma^*) + D}{\cos(\alpha + \phi_T)} + \frac{m\left\{V'_{W,x} \cos(\psi) + V'_{W,y} \sin(\psi)\right\} V_T \sin(\gamma^*) \cos(\gamma^*)}{\cos(\alpha + \phi_T)} \tag{5.45}$$

$$V_{GS} = \sqrt{[V_T \cos(\gamma)]^2 - [V_W \sin(\psi_c - \psi_w)]^2} + V_W \cos(\psi_c - \psi_w) \tag{5.46}$$

$$\dot{h} = V_T \sin(\gamma) \tag{5.47}$$

where the expression of the acceleration factor is the same as that in Eqs. (5.34) and (5.35).

5.3.2.2 Aircraft Trim Procedure

To complete the calculation procedure, it necessary to determine the values of the angle of attack and thrust required to solve Eqs. (5.44) and (5.45). The technique used to estimate these two parameters is similar to the one developed for an unrestricted climb at constant CAS/Mach, with the main difference that the flight path angle is assumed to be known and that the thrust is determined iteratively based on the result obtained from Eq. (5.45). In addition, given the required thrust, the engine fan speed is computed, and the latter becomes the basis for computing the engine fuel flow. Algorithm 5.3 illustrates the trim procedure for the convenience of the reader.

5.3.2.3 Complete Integration Procedure

Equations (5.44) to (5.47) combined with Eqs. (5.14) and (5.15) fform the system of equations describing the aircraft trajectory for a restricted climb at constant CAS/Mach segment. The complete procedure proposed to integrate these equations, and to compute the aircraft trajectory for this type of segment is given in Algorithm 5.4.

It worth noting that the altitude step size is by default 1000 ft, but this step size can be reduced during the integration process by following a logic similar to that described for an unrestricted climb at constant CAS/Mach in **Section 5.3.1.3**.

Algorithm 5.3 Trim Procedure for a Restricted Climb at Constant CAS/Mach Segment

0. Initialization: For the trim algorithm, it is assumed that all aircraft parameters are known except the aircraft heading ψ, the angle of attack α, and the engine thrust F_N.

1. Define Initial Estimates: Set $\alpha^{[0]} = 0$, and $F_N^{[0]} = 0.6F_N^{MCLB}$. Note that in order to accelerate the convergence of the algorithm, these two parameters can be initialized based on the results obtained for the previous sub-segment. Set $k = 0$.

2. Main Loop: repeat

a) Update the number of iterations: $k = k + 1$.

b) From the value of the flight path angle γ^*, compute the aircraft heading required to maintain the desired course:

$$\psi = \psi_c - \arcsin\left[\frac{V_W \sin(\psi_c - \psi_w)}{V_T \cos(\gamma^*)}\right]$$

c) From the current estimate of the angle of attack $\alpha^{[k-1]}$ and engine thrust $F_N^{[k-1]}$, compute the lift force required to balance the aircraft along the vertical axis:

$$L^* = F_N^{[k-1]} \sin(\alpha^{[k-1]} + \phi_T) - \frac{mg_0 \cos(\gamma^*)}{\cos(\phi)} + \frac{\left\{V_{W,x} \cos(\psi) - V_{W,y} \sin(\psi)\right\} V_T \sin(\gamma^*)^2}{\cos(\phi)}$$

d) Compute the corresponding lift coefficient: $CL_s^* = L^*/0.5\rho S V_T^2$.

e) Perform a reverse lookup table to find the new estimate for the angle of attack $\alpha^{[k]}$ which leads to the lift coefficient CL_s^*.

f) Based on $\alpha^{[k]}$, interpolate the drag coefficient CD_s, and compute the drag force.

g) Knowing $\alpha^{[k]}$, compute a new estimate for the engine thrust $F_N^{[k]}$:

$$F_N^{[k]} = \frac{mg_0 \mathrm{AF} \sin(\gamma^*) + D}{\cos(\alpha^{[k]} + \phi_T)} + \frac{m\left\{V'_{W,x} \cos(\psi) + V'_{W,y} \sin(\psi)\right\} V_T \sin(\gamma^*) \cos(\gamma^*)}{\cos(\alpha^{[k]} + \phi_T)}$$

while $|\alpha^{[k]} - \alpha^{[k-1]}| \geq 0.1$ ***OR*** $|F_N^{[k]} - F_N^{[k-1]}|/F_N^{[k-1]} \geq 0.01$ ***AND*** $k \leq 25$;

3. Engine fuel flow calculation: Based on the engine model, perform a reverse lookup table in order to find the engine fan speed N_1. Then, use this value to find the engine fuel flow W_F by interpolation.

4. Return the last trim parameters: $\alpha^{[k]}$**,** $F_N^{[k]}$**,** W_F**, and** ψ**.**

Algorithm 5.4 Integration Procedure for a Restricted Climb at Constant CAS/Mach Segment

0. Initialization: Set the aircraft initial states/position; latitude $\lambda_{[0]}$, longitude $\mu_{[0]}$, course $\psi_{c[0]}$, mass $m_{[0]}$, altitudes $h_{[0]}$, elapsed time $t_{[0]}$, ground distance $x_{[0]}$, and fuel burned $F_{B[0]}$.

1. Integration and Model Parameters Definition: Define the final altitude $h_{[N]}$, and set the altitude step Δh. Initialise the number of iterations $i = 0$, the bank angle ϕ, and rate of change of course $\dot{\psi}_c$.

2. Main Loop: repeat

a) From the atmosphere and wind models find the following parameters: air density ρ, temperature ratio θ, pressure ratio δ, Mach number M from $V_{T[i]}$, and wind parameters: V_W, ψ_w, $V_{W,x}$, $V_{W,y}$, $V'_{W,x}$, and $V'_{W,y}$.

b) Based on the speed strategy, determine the TAS V_T, the CAS V_C, and the Mach number M.

c) From the knowledge of the Mach number M and temperature, compute the acceleration factor AF.

d) Based on the vertical restriction, find the required flight path angle γ^*.

e) Use Algorithm 5.3 to trim the aircraft for the current flight condition, and to determine the aircraft heading ψ, the angle of attack α, and the engine thrust F_N.

f) Compute the altitude, distance, and mass variations for the current sub-segment:

$$\Delta h = V_{T[i]} \sin(\gamma)\Delta t \quad \Delta x = V_{GS}\Delta t \quad \Delta m = W_F \Delta t$$

g) Update aircraft states :

$$h_{[i+1]} = h_{[i]} + \Delta h \quad \lambda_{[i+1]} = \lambda_{[i]} + \dot{\lambda}\Delta t \quad t_{[i+1]} = t_{[i]} + \Delta t \quad \psi_{c[i+1]} = \psi_{c[i]} + \dot{\psi}_c \Delta t$$
$$x_{[i+1]} = x_{[i]} + \Delta x \quad \mu_{[i+1]} = \mu_{[i]} + \dot{\mu}\Delta t \quad m_{[i+1]} = m_{[i]} - \Delta m \quad F_{B[i+1]} = F_{B[i]} + \Delta m$$

h) If the next segment is a turn segment, then adjust the bank angle based on the actual ground speed and nominal turn radius, and then compute the rate of change of course using Eq. (5.14). Otherwise, set $\phi = \dot{\psi}_c = 0$, and determine the aircraft course according to the next waypoint in the list.

i) Update the number of iterations: $i = i + 1$.

while $h_{[i]} < h_{[N]}$;

3. Return all flight parameters, including altitude, distance, time and fuel burned.

5.3.3 Climb and Level-Off Acceleration Segment

The aircraft trajectory for a climb or level-off acceleration segment is calculated by numerically integrating the aircraft equations of motion from an initial airspeed V_C (or Mach number M) to a specified final airspeed $V_C + \Delta V_C$ (or Mach number $M + \Delta M$).

Although the acceleration segment is delimited in terms of airspeed, it is more convenient to integrate the aircraft equations as function of time rather than as function of airspeed. For this reason, the acceleration segment is divided into N time intervals as illustrated in Figure 5.8. A suggested size for the time step is 2.0 s, however, however, this step size can be adjusted depending on the airspeed increment.

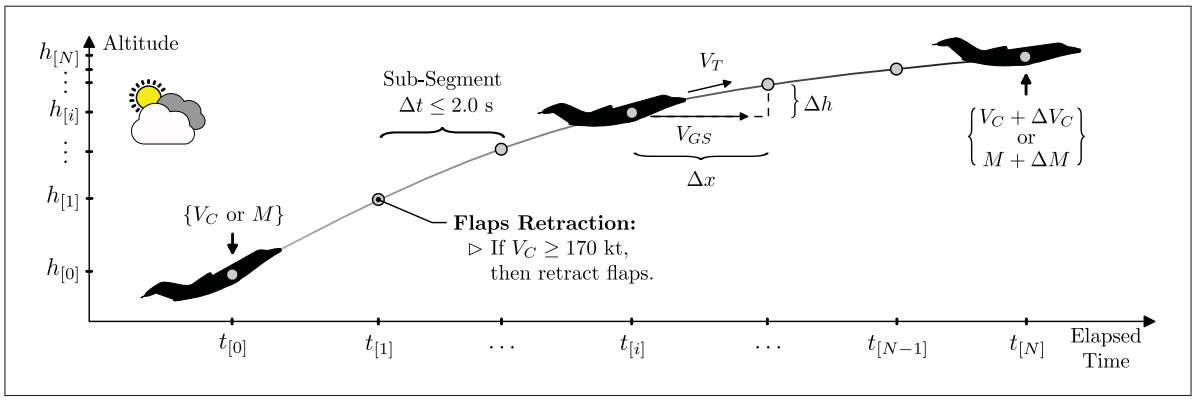

Figure 5.8 Calculation Procedure for a Climb Acceleration Segment

5.3.3.1 Aircraft Equations of Motion Simplification and Model Parametrization

The way in which an aircraft accelerates in climb is dependent upon the autopilot flight control laws. In general, most of commercial aircraft accelerate by either maintaining a constant climb gradient, or a constant rate of climb. However, by performing several simulations with the RAFS, it was found that the logic that reflected best the behavior of the Cessna Citation X was an acceleration at a constant rate of TAS.

In this case, the pertinent equations describing the motion of the aircraft for a climb acceleration segment can be expressed as follows:

$$L = F_N \sin(\alpha + \phi_T) - \frac{mg_0 \cos(\gamma)}{\cos(\phi)} + \frac{\left\{V'_{W,x} \cos(\psi) - V'_{W,y} \sin(\psi)\right\} V_T \sin(\gamma)^2}{\cos(\phi)} \tag{5.48}$$

$$\gamma = \text{asin}\left[\frac{F_N \cos(\alpha + \phi_T) - D}{mg_0\,(1 + \text{AF})} - \frac{\dot{V}_T^{ACC} + \left\{V'_{W,x} \cos(\psi) + V'_{W,y} \sin(\psi)\right\} V_T \sin(\gamma) \cos(\gamma)}{g_0\,(1 + \text{AF})}\right] \tag{5.49}$$

$$V_{GS} = \sqrt{[V_T \cos(\gamma)]^2 - [V_W \sin(\psi_c - \psi_w)]^2} + V_W \cos(\psi_c - \psi_w) \tag{5.50}$$

$$\dot{h} = V_T \sin(\gamma) \tag{5.51}$$

where $\text{asin}(x) = \arcsin(x)$, and $\dot{V}_T^{ACC}$ is the desired rate of TAS. This parameter was estimated in average at 3.11 ft/s^2 for the Cessna Citation X.

It should be noted that if the acceleration is performed during the on-course climb phase, the flaps should be retracted progressively as the aircraft airspeed increases. This aspect was modeled by assuming a linear variation of the flaps from their initial positions (e.g., 15° or 5°) to 0° (i.e., fully retracted) at a rate of -1.29°/s. This value was obtained based on several tests conducted with the RAFS.

Moreover, in case when the acceleration is carried out during the on-course or cruise climb phases, the thrust should be interpolated from the engine model by using either the maximum climb thrust setting (MCLB) or one of the two derated climb thrust settings (i.e., CLB-1 or CLB-2). However, if the acceleration is carried out during the cruise phase, the thrust should be interpolated based on the maximum cruise thrust setting (MCR).

5.3.3.2 Aircraft Trim Procedure

As for the other vertical flight segments, to complete the calculation procedure, it is necessary to determine the angle of attack and flight path angle required to compute the lift and drag forces

in Eqs. (5.48) and (5.49). Once again, the technique used to estimate two parameters is similar to the one developed for an unrestricted climb at constant CAS/Mach, except that the flight path angle in step g) is updated using the result in Eq. (5.48). All the other steps remain exactly the same. Algorithm 5.5 illustrates the trim procedure for the convenience of the reader.

Algorithm 5.5 Trim Procedure for a Climb Acceleration Segment

0. Initialization: For the trim algorithm, it is assumed that all aircraft parameters are known except the aircraft heading ψ, the angle of attack α, and the flight path angle γ.

1. Define Initial Estimates: Set $\alpha^{[0]} = 0$, and $\gamma^{[0]} = 0$. Note that in order to accelerate the convergence of the algorithm, these two parameters can be initialized based on the results obtained for the previous sub-segment. Set $k = 0$.

2. Main Loop: repeat

a) Update the number of iterations: $k = k + 1$.

b) From the current estimate of the flight path angle $\gamma^{[k-1]}$, compute the aircraft heading required to maintain the desired course:

$$\psi = \psi_c - \arcsin\left[\frac{V_W \sin(\psi_c - \psi_w)}{V_T \cos(\gamma^{[k-1]})}\right]$$

c) From the current estimate of the angle of attack $\alpha^{[k-1]}$ and flight path angle $\gamma^{[k-1]}$, compute the lift force required to balance the aircraft along the vertical axis:

$$L^* = F_N \sin(\alpha^{[k-1]}+\phi_T) - \frac{mg_0 \cos(\gamma^{[k-1]})}{\cos(\phi)} + \frac{\left\{V_{W,x}\cos(\psi) - V_{W,y}\sin(\psi)\right\} V_T \sin(\gamma^{[k-1]})^2}{\cos(\phi)}$$

d) Compute the corresponding lift coefficient: $CL_s^* = L^*/0.5\rho S V_T^2$.

e) Perform a reverse lookup table to find the new estimate for the angle of attack $\alpha^{[k]}$ which leads to the lift coefficient CL_s^*.

f) Based on $\alpha^{[k]}$, interpolate the drag coefficient CD_s, and compute the drag force: $D = 0.5\rho S V_T^2 CD_s$.

g) Knowing $\alpha^{[k]}$ and $\gamma^{[k-1]}$, compute a new estimate for the flight path angle $\gamma^{[k]}$:

$$\gamma^{[k]} = \arcsin\left[\frac{F_N \cos(\alpha^{[k]} + \phi_T) - D}{mg_0\,(1 + \mathrm{AF})} - \frac{\dot{V}_T^{ACC} + \{\cdots{}^{2}\} V_T \sin(\gamma^{[k-1]})\cos(\gamma^{[k-1]})}{g_0\,(1 + \mathrm{AF})}\right]$$

while $|\alpha^{[k]} - \alpha^{[k-1]}| \geq 0.1$ ***OR*** $|\gamma^{[k]} - \gamma^{[k-1]}| \geq 0.1$ ***AND*** $k \leq 25$;

3. Return the last trim parameters: $\alpha^{[k]}$**,** $\gamma^{[k]}$ **and** ψ**.**

[2] Note that $\{\cdots\} = \left\{V'_{W,x}\cos(\psi) + V'_{W,y}\sin(\psi)\right\}$

In case when the aircraft accelerates at constant climb gradient or at constant rate of climb, Algorithm 5.5 can be used by replacing the equation in step g) with the following one:

$$\dot{V}_T^{ACC} = \frac{F_N \cos(\alpha + \phi_T) - D - g_0 \sin(\gamma)}{m} - \left\{ V'_{W,x} \cos(\psi) + V'_{W,y} \sin(\psi) \right\} V_T \sin(\gamma) \cos(\gamma) \tag{5.52}$$

and by imposing the flight path angle value using one of the following two equations:

$$\gamma = \arcsin\left[\frac{V/S}{V_T}\right] \quad \text{or} \quad \gamma = \arctan\left[\frac{CG\%}{100}\right] \tag{5.53}$$

where V/S is the rate of climb (e.g., 500 or 1000 ft/min), and $CG\%$ is the climb gradient expressed in percentage. Similarly, the particular case of a level-off acceleration can be obtained by simply imposing zero flight path angle (i.e., $\gamma = 0$).

5.3.3.3 Complete Calculation Process

Equations (5.48) to (5.51) combined with Eqs. (5.14) and (5.15) form the system of equations describing the aircraft performance for a climb acceleration segment. The complete procedure proposed to integrate these equations and compute the aircraft trajectory for this type of segment is described in Algorithm 5.6.

It should be noted that the time step size is by default 2.0 s. However, this step size can be reduced during the integration process depending on the following situations:

- If the aircraft is approaching the final airspeed, the step size is reduced so that the final airspeed will be reached in one iteration;
- If the aircraft is approaching a turn, the step size is reduced so that the beginning of the turn will be reached in one iteration;
- If the aircraft is in a turn, the step size is reduced sot that the turn will be completed in one iteration.

In the case where more than one situation applies, the time step size is then chosen to be the smallest among all the possible sizes.

Algorithm 5.6 Integration Procedure for a Climb/Level-Off Acceleration Segment

0. Initialization: Set the aircraft initial states/position; latitude $\lambda_{[0]}$, longitude $\mu_{[0]}$, course $\psi_{c[0]}$, mass $m_{[0]}$, altitudes $h_{[0]}$, elapsed time $t_{[0]}$, ground distance $x_{[0]}$, and fuel burned $F_{B[0]}$.

1. Integration and Model Parameters Definition: Set the time step Δt and compute the TAS $V_{T[0]}$ from the initial CAS $V_{C[0]}$ (or initial Mach number $M_{[0]}$). Select the desired airspeed increment ΔV_C (or ΔM). Initialise the number of iterations $i = 0$, the bank angle ϕ, and rate of change of course $\dot{\psi}_c$.

2. Main Loop: repeat

a) From the atmosphere and wind models find the following parameters: air density ρ, temperature ratio θ, pressure ratio δ, Mach number M from $V_{T[i]}$, and wind parameters: V_W, ψ_w, $V_{W,x}$, $V_{W,y}$, $V'_{W,x}$, and $V'_{W,y}$.

b) Based on the engine model, flight conditions and flaps/slats configuration, interpolate the thrust F_N and fuel flow W_F by assuming MCLB, CLB-1/2 or MCR.

c) Use Algorithm 5.5 to trim the aircraft for the current flight condition, and to determine the aircraft heading ψ, the angle of attack α, and the flight path angle γ.

d) For a climb acceleration at constant rate of TAS, set $\dot{V}_T = \dot{V}_T^{ACC}$. For a climb acceleration at constant climb gradient, constant rate of climb or level-off, compute the aircraft acceleration using the following equation:

$$\dot{V}_T^{ACC} = m^{-1}\left[F_N \cos(\alpha + \phi_T) - D - g_0 \sin(\gamma)\right] - \{\cdots^2\} V_T \sin(\gamma)\cos(\gamma)$$

e) Compute the altitude, distance, and mass variations for the current sub-segment:

$$\Delta h = V_{T[i]} \sin(\gamma)\Delta t \quad \Delta x = V_{GS}\Delta t \quad \Delta m = W_F \Delta t$$

f) Update aircraft states :

$$h_{[i+1]} = h_{[i]} + \Delta h \quad \lambda_{[i+1]} = \lambda_{[i]} + \dot{\lambda}\Delta t \quad t_{[i+1]} = t_{[i]} + \Delta t \quad \psi_{c[i+1]} = \psi_{c[i]} + \dot{\psi}_c \Delta t$$
$$x_{[i+1]} = x_{[i]} + \Delta x \quad \mu_{[i+1]} = \mu_{[i]} + \dot{\mu}\Delta t \quad m_{[i+1]} = m_{[i]} - \Delta m \quad V_{T[i+1]} = V_{T[i]} + \dot{V}_T^{ACC}\Delta t$$

g) Compute the new CAS $V_{C[i+1]}$ and new Mach number $M_{[i+1]}$ from the TAS $V_{T[i+1]}$, and update the number of iterations: $i = i + 1$.

h) If the next segment is a turn segment, then adjust the bank angle based on the actual ground speed and nominal turn radius, and then compute the rate of change of course using Eq. (5.11). Otherwise, set $\phi = \dot{\psi}_c = 0$, and determine the aircraft course according to the next waypoint in the list.

while $\left(V_{C[i]} < V_{C[0]} + \Delta V_C\right)$ ***OR*** $\left(M_{[i]} < M_{[0]} + \Delta M\right)$;

3. Return all flight parameters, including altitude, distance, time and fuel burned.

5.3.4 Level Flight at Constant CAS/Mach

The aircraft trajectory for a level flight at constant CAS/Mach segment is calculated by numerically integrating the aircraft equations of motion with respect to the distance. For this purpose, the aircraft trajectory is divided into multiple distance intervals (or sub-segments) as illustrated in Figure 5.9.

In the same way as for the other vertical flight segments, the distance step size is arbitrary. A suggested value for the step size is 25 n miles. This value has proven to provide a good compromise between time calculation and results accuracy.

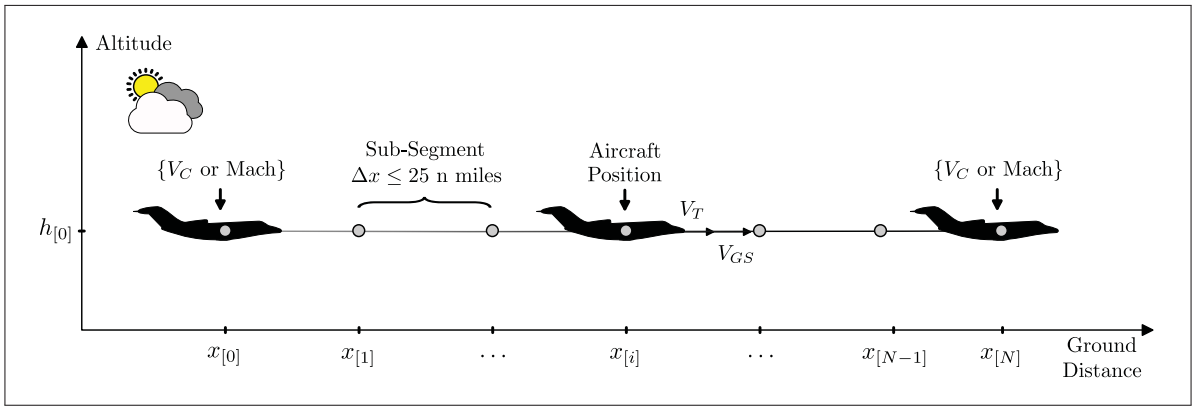

Figure 5.9 Illustration of the Calculation Procedure for a Level Flight Segment

5.3.4.1 Aircraft Equations of Motion Simplification and Model Parametrization

Level flight at constant CAS/Mach segments are special cases where the equations of motion for which the aircraft flight path angle and acceleration (i.e., rate of TAS) are by definition zero.

In addition, the fact that the aircraft altitude is also constant by definition implies that the time derivatives of the wind speed components as defined in Eqs. (5.30) and (5.31) are zero. In reality, a better approximation of these two components could be obtained by replacing the wind gradients with respect to altitude in Eqs. (5.30) and (5.31) by the wind gradients in the x- and y-directions. However, at high altitudes, the wind conditions change relatively slowly in these

two directions, and to a good approximation can be assumed locally constant. For that reason, the time derivatives of the wind speed components are considered to be zero for a level flight segment.

Thus, by considering all these simplifications in Eqs. (5.10) to (5.16), the equations describing the motion of the aircraft for level flight at constant CAS/Mach segment can be summarized as follows:

$$L = F_N \sin(\alpha + \phi_T) - mg_0 \cos(\phi)^{-1} \tag{5.54}$$

$$F_N = D \cos(\alpha + \phi_T)^{-1} \tag{5.55}$$

$$V_{GS} = \sqrt{[V_T]^2 - [V_W \sin(\psi_c - \psi_w)]^2} + V_W \cos(\psi_c - \psi_w) \tag{5.56}$$

$$\dot{h} = \gamma = 0 \tag{5.57}$$

5.3.4.2 Aircraft Trim Procedure

To complete the calculation procedure, it necessary to determine the values of the angle of attack and thrust required to solve Eqs. (5.54) and (5.55). FFor this purpose, the trim procedure developed for an unrestricted climb segment at constant CAS/Mach can be reused by imposing a zero flight path angle. Algorithm 5.7 illustrates the trim procedure for the convenience of the reader.

5.3.4.3 Complete Integration Procedure

Equations (5.54) to (5.57) combined with Eqs. (5.14) and (5.15) form the system of equations describing the aircraft trajectory for a level flight at constant CAS/Mach segment. The complete procedure proposed to integrate these equations, and to compute the aircraft trajectory for this type of segment is given in Algorithm 5.8.

Algorithm 5.7 Procedure for a Level Flight at Constant CAS/Mach Segment

0. Initialization: For the trim algorithm, it is assumed that all aircraft parameters are known except the aircraft heading ψ, the angle of attack α, and the engine thrust F_N.

1. Define Initial Estimates: Set $\alpha^{[0]} = 0$, and $F_N^{[0]} = 0.6F_N^{MCR}$. Note that in order to accelerate the convergence of the algorithm, these two parameters can be initialized based on the results obtained for the previous sub-segment. Set $k = 0$.

2. Main Loop: repeat

a) Update the number of iterations: $k = k + 1$.

b) Considering a zero flight path angle $\gamma = 0$, compute the aircraft heading required to maintain the desired course:

$$\psi = \psi_c - \arcsin\left[\frac{V_W \sin(\psi_c - \psi_w)}{V_T}\right]$$

c) From the current estimate of the angle of attack $\alpha^{[k-1]}$ and engine thrust $F_N^{[k-1]}$, compute the lift force required to balance the aircraft along the vertical axis:

$$L^* = F_N^{[k-1]} \sin(\alpha^{[k-1]} + \phi_T) - \frac{mg_0}{\cos(\phi)}$$

d) Compute the corresponding lift coefficient: $CL_s^* = L^*/0.5\rho SV_T^2$.

e) Perform a reverse lookup table to find the new estimate for the angle of attack $\alpha^{[k]}$ which leads to the lift coefficient CL_s^*.

f) Based on $\alpha^{[k]}$, interpolate the drag coefficient CD_s, and compute the drag force: $D = 0.5\rho SV_T^2 CD_s$.

g) Knowing $\alpha^{[k]}$, compute a new estimate for the engine thrust $F_N^{[k]}$:

$$F_N^{[k]} = \frac{D}{\cos(\alpha^{[k]} + \phi_T)}$$

while $|\alpha^{[k]} - \alpha^{[k-1]}| \geq 0.1$ ***OR*** $|F_N^{[k]} - F_N^{[k-1]}|/F_N^{[k-1]} \geq 0.01$ ***AND*** $k \leq 25$;

3. Engine fuel flow calculation: Based on the engine model, perform a reverse lookup table in order to find the engine fan speed N_1. Then, use this value to find the engine fuel flow W_F by interpolation.

4. Return the last trim parameters: $\alpha^{[k]}$, $F_N^{[k]}$, W_F, **and** ψ.

Algorithm 5.8 Integration Procedure for a Level Flight at Constant CAS/Mach Segment

0. Initialization: Set the aircraft initial states/position; latitude $\lambda_{[0]}$, longitude $\mu_{[0]}$, course $\psi_{c[0]}$, mass $m_{[0]}$, altitudes $h_{[0]}$, elapsed time $t_{[0]}$, ground distance $x_{[0]}$, and fuel burned $F_{B[0]}$.

1. Integration and Model Parameters Definition: Define the total distance $x_{[N]}$, and set the distance step Δx. Initialise the number of iterations $i = 0$, the bank angle ϕ, and rate of change of course $\dot{\psi}_c$.

2. Main Loop: repeat

a) From the atmosphere and wind models find the following parameters: air density ρ, temperature ratio θ, pressure ratio δ, and wind parameters: V_W, ψ_w, $V_{W,x}$, and $V_{W,y}$.

b) Based on the speed strategy, determine the TAS V_T, the CAS V_C, and the Mach number M.

c) Use Algorithm 5.7 to trim the aircraft for the current flight condition, and to determine the aircraft heading ψ, the angle of attack α, the engine thrust F_N, and the engine fuel flow W_F.

f) Compute the altitude, distance, and mass variations for the current sub-segment:

$$\Delta h = 0 \quad \Delta x = V_{GS}\Delta t \quad \Delta m = W_F \Delta t$$

g) Update aircraft states :

$$h_{[i+1]} = h_{[i]} + \Delta h \quad \lambda_{[i+1]} = \lambda_{[i]} + \dot{\lambda}\Delta t \quad t_{[i+1]} = t_{[i]} + \Delta t \quad \psi_{c[i+1]} = \psi_{c[i]} + \dot{\psi}_c \Delta t$$
$$x_{[i+1]} = x_{[i]} + \Delta x \quad \mu_{[i+1]} = \mu_{[i]} + \dot{\mu}\Delta t \quad m_{[i+1]} = m_{[i]} - \Delta m \quad F_{B[i+1]} = F_{B[i]} + \Delta m$$

h) If the next segment is a turn segment, then adjust the bank angle based on the actual ground speed and nominal turn radius, and then compute the rate of change of course using Eq. (5.11). Otherwise, set $\phi = \dot{\psi}_c = 0$, and determine the aircraft course according to the next waypoint in the list.

i) Update the number of iterations: $i = i + 1$.

while $x_{[i]} < x_{[N]}$;

3. Return all flight parameters, including altitude, distance, time and fuel burned.

The distance step size is by default 25 n miles. However, this step size can be reduced during the integration process depending on the following situations: It should be noted that the time step size is by default 2.0 s. However, this step size can be reduced during the integration process depending on the following situations:

- if the aircraft is approaching the final distance, the step size is reduced so that the final distance will be reached in one iteration;
- If the aircraft is approaching a turn, the step size is reduced so that the beginning of the turn will be reached in one iteration;
- If the aircraft is in a turn, the step size is chosen so that either the aircraft will turn 5° in one iteration or the turn will be completed in one iteration.

In the case where more than one situation applies, the distance step size is then chosen to be the smallest among all the possible step sizes.

5.3.5 Unrestricted/Restricted Descent at Constant CAS/Mach and Descent/Level-Off Deceleration

The aircraft trajectory for unrestricted/restricted descent segments is obtained by following exactly the same procedures as those used for the climb segments. The only differences are that the aircraft altitude varies in the opposite direction (i.e., $\Delta h < 0$, $\Delta\gamma < 0$, and $V/S < 0$), and that the engines are set to idle thrust instead of maximum climb thrust. All the other steps of Algorithms 5.1 to 5.4 remain the same.

Regarding the deceleration segments, here also, the procedure is identical to the one presented for the climb acceleration segment in Algorithms 5.5 to 5.6. However, it should be noted that decelerations are generally executed either at constant rate of descent (e.g., -500 or -1000 ft/min) or at constant descent gradient (for a level-off deceleration, the rate of descent is set to zero). As a result, the case of a descent acceleration at constant rate of TAS should not be considered. Finally, for all deceleration types, the engines are set to idle thrust.

5.3.6 Estimation of the Top-of-Descent Location

The last study to be presented in this section concerns the estimation of the top-of-descent (T/D) location. The technique developed in this study to estimate the T/D location consists in using an approximate descent profile which assumes a 1000 ft descent for every 3 n miles

(Slattery & Zhao, 1997). Under this condition, the horizontal distance of the T/D point relative to the destination airport can be obtained as follows:

$$x_{T/D} = \frac{(h_{CRZ} - h_{APT})/100}{3} \tag{5.58}$$

where h_{CRZ} is the aircraft cruise altitude, and h_{APT} is the airport pressure altitude (i.e., elevation). It should be noted that the distance $x_{T/D}$ in Eq. (5.58) is obtained in [n miles] if the altitudes are given in [ft]. In addition, if a deceleration is performed during descent, the distance $x_{T/D}$ is corrected with the basic rule of 1 n mile for 10 kts.

Once the T/D position has been determined, the complete aircraft trajectory is calculated up to 1500 ft above the destination airport level. If the distance between the aircraft position at 1500 ft and the airport position is more than 5 n miles, the T/D is corrected as follows

$$x^{+}_{T/D} = x^{-}_{T/D} + \Delta x_{APT} \tag{5.59}$$

where $x^{+}_{T/D}$ is the new estimation of the T/D location, $x^{-}_{T/D}$ is the hold estimation of the T/D location, and Δx_{APT} is the distance of the aircraft relative to the airport.

The descent phase is then recalculated based on the new T/D location. This process is repeated as long as the error distance is greater than 5 n miles. In general, only few (i.e., two or three) number of iterations are required to obtain a satisfactory result.

5.4 Simulation and Validation Results

This section presents the simulation results for the validation of the algorithms proposed in this paper to predict the aircraft trajectory. For this purpose, several flight tests were conducted with the Cessna Citation X RAFS. In order to evaluate the validity of the algorithms over a wide range of operating conditions, three categories of tests were considered: (1) continuous climb to cruise altitude, (2) idle descent from cruise altitude, and (3) complete flight from a departure

airport to a destination airport. In parallel, the algorithms developed in **Section 5.3** were used to calculate the aircraft trajectory for the same simulation conditions.

The validation of the algorithms was accomplished by comparing the aircraft trajectory data measured from the RAFS with those calculated by the algorithms.

5.4.1 Simulation Results for the Climb Phase

To test and validate the algorithms for the climb phase (including the, on-course climb phase, and the cruise climb phase), a first series of 60 flight tests was conducted with the Cessna Citation X RAFS.

The strategy adopted to choose the tests, and to evaluate the accuracy of the algorithms over a wide range of flight conditions was to establish 20 climb scenarios based on the vertical profile shown in Figure 5.4, and to reproduce these scenarios for three different aircraft weight configurations: light (26,000 lb), medium (30,000 lb) and heavy (36,000 lb). For the sake of simplicity, the crossover altitude for all scenarios was always assumed to be 30,000 ft, while the cruise altitude was fixed at 40,000 ft. In addition, random environmental conditions (i.e., winds and temperature) were imposed for each of the 20 climb scenarios.

5.4.1.1 Example of Results for three Climb Tests

To illustrate the way in which each flight test was compared, and then validated, an example of results obtained for a climb scenario is shown in Figure 5.10. In this figure, the trajectory data measured with the RAFS are represented by the black squares, while those predicted by the algorithms (i.e., model) are represented by solid lines of different colors, where each color corresponds to one of the three weight configurations.

From a general point of view, it can be seen that the algorithm predictions reflect very well the trajectory data obtained from the RAFS, especially during the climb acceleration segment at 10,000 ft. It should be noted that attempts to model aircraft acceleration with a constant

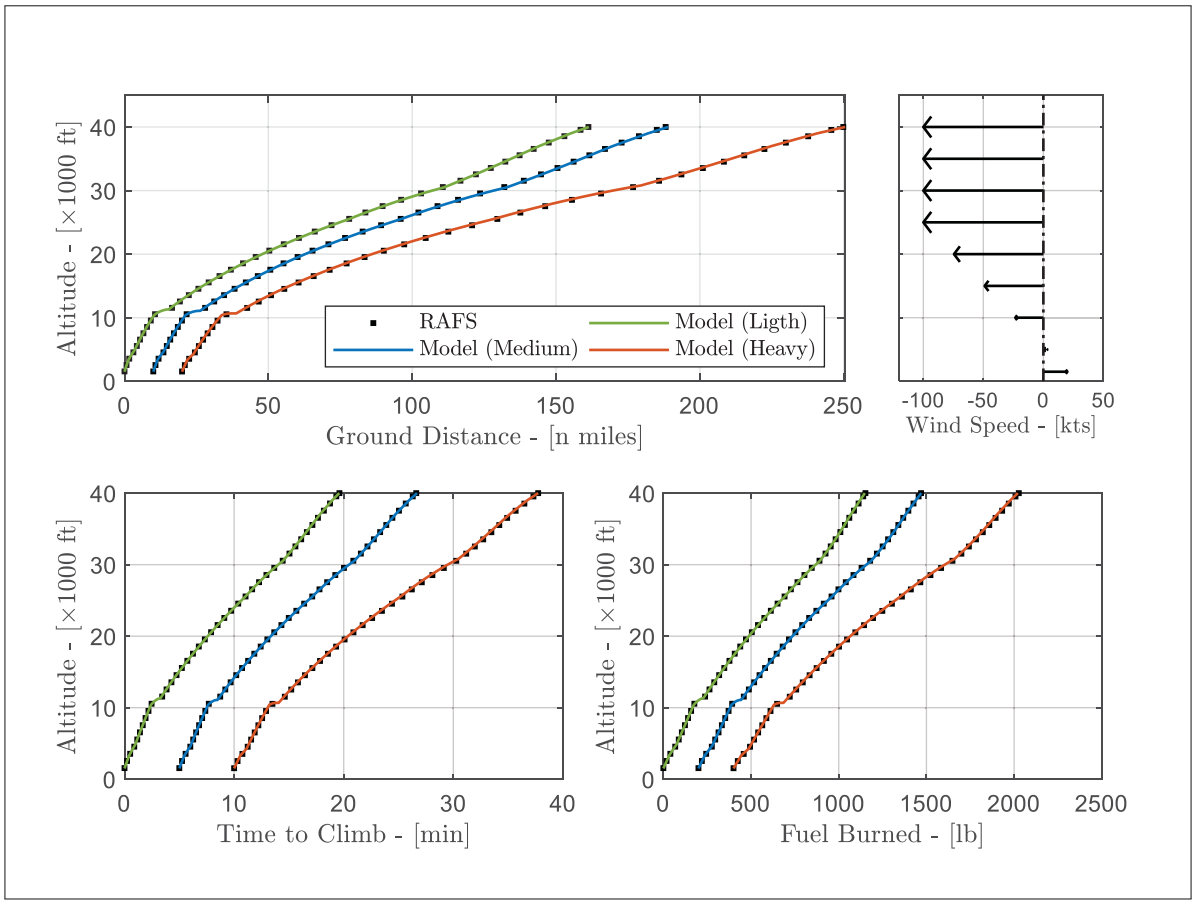

Figure 5.10 Aircraft Climb Trajectory Results for the Three Weight Configurations

climb gradient or with a constant rate of climb have yielded less convincing results. This aspect therefore reinforces the assumption of a climb acceleration at constant rate of TAS.

By analyzing the results for the three weight configurations, it was noted that the highest errors were obtained the heaviest weight (represented by the red color). The distance error at the end of the climb for this weight was found to be about 0.87 n miles (0.49%), while the errors for the time to climb and fuel burned were found to be approximately 4.12 s (0.31%) and 5.26 lb (0.32%), respectively. These differences are clearly negligible, leading to the conclusion that the algorithms predicted very well the aircraft trajectory and fuel consumption for these three climb tests.

5.4.1.2 Example of Trim Parameters Comparison for three Climb Tests

To further evaluate the efficiency of the algorithms, another comparison was made for the aircraft trim parameters. For this purpose, Figure 5.11 shows the angle of attack and flight path angle variations as function of altitude for the three climb tests.

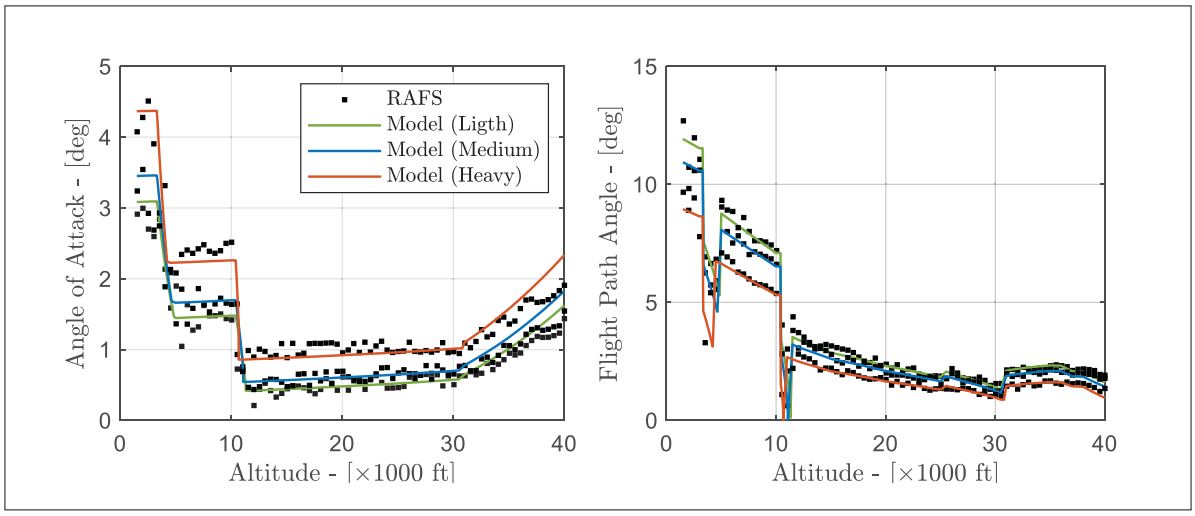

Figure 5.11 Aircraft Trim Results for the Three Weight Configurations

As seen in Figure 5.11, the two parameters are well estimated, despite a slight deviation that can be observed on the curves of the angle of attack especially above 30,000 ft. This deviation can be justified by the aerodynamic model structure. Indeed, the aerodynamic model used in this study was generated by assuming an average position of the horizontal stabilizer, and a center of gravity location at 25% of the wing mean aerodynamic chord. In reality, these two parameters are not constant during the flight, and their values affect the aircraft lift force. Since the aircraft angle of attack is determined as a function of the lift force, it is therefore normal to obtain errors if the horizontal stabilizer position, and the aircraft center of gravity location are not explicitly considered in the calculations.

Nevertheless, the errors between the measured and predicted angle of attack were found to be smaller than 0.5 deg, which remains acceptable.

5.4.1.3 Results Validation for all Climb Scenarios

The analyses presented in the previous sections were repeated for all 60 climb flight tests. For each test, the aircraft trajectory data measured with the RAFS were compared with their values predicted by the algorithms at each 500 ft. The resulting relative errors for the time to climb, ground distance, and fuel burned are presented in Figure 5.12.

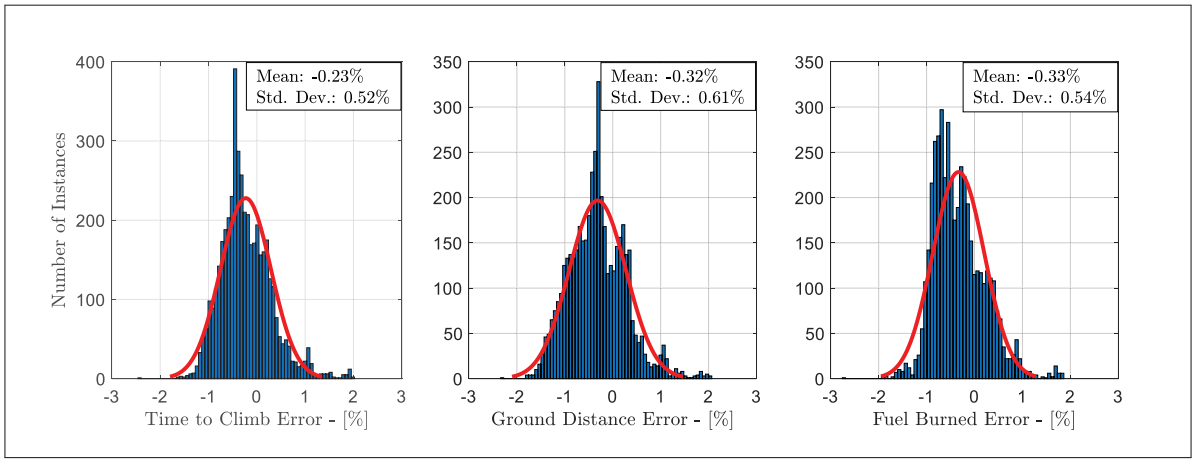

Figure 5.12 Flight Time, Ground Distance and Fuel Burned Comparison Results for the Climb Phase

From an overall point of view, it can be seen that the results shown in Figure 5.12 are very good. Indeed, the time to climb, the ground distance, and the fuel burned are all very well estimated with relative errors less than 2.5%. In addition, it can be noted that the relative error for the three parameters follows a normal distribution almost centered around zero, and it has a standard deviation of the order of 0.60%.

Based on these results presented in this section, it can be concluded that the algorithms developed in this paper can predict very well the trajectory and fuel consumption of the Cessna Citation X for the climb phase.

5.4.2 Simulation Results for the Descent Phase

The descent phase (including the initial descent phase, and the descent approach phase) was validated by using exactly the same methodology as that used for the climb phase. For this purpose, 60 additional flight tests were conducted with the RAFS. In the same way as for the climb phase, these flight tests were determined by defining 20 descent scenarios based on the vertical profile shown in Figure 5.4, and by reproducing these scenarios for three different aircraft weight configurations: light (26,000 lb), medium (30,000 lb) and heavy (34,000 lb). The initial altitude for all scenarios was fixed at 40,000 ft, while the crossover altitude was imposed at 30,000 ft. Finally, random environmental conditions (i.e., winds and temperature) were assumed for each descent scenario.

Figure 5.13 shows the relative errors obtained for the descent phase in terms of time to descent, ground distance, and fuel burned. As expected, the results are globally very good. Indeed, it can be seen that the time to descent is once again very well estimated with an average relative error of 0.07%, and a standard deviation of 0.79%. Similarly, the ground distance is also very well estimated with an average error of 0.16%, and a standard deviation of 0.14%.

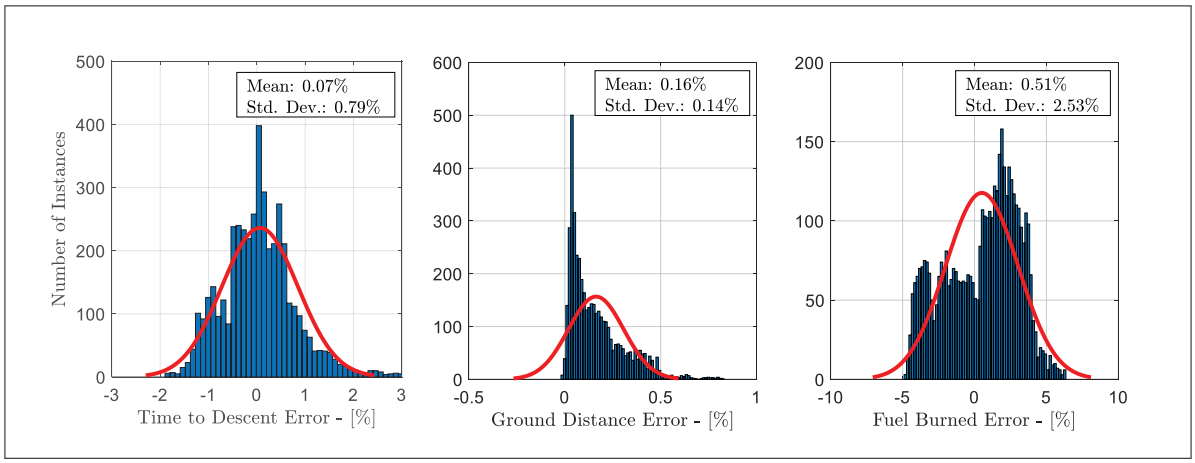

Figure 5.13 Flight Time, Ground Distance and Fuel Burned Comparison Results for the Descent Phase

Regarding the fuel burned, the results in Figure 5.13 indicate that this parameter is less well estimated than the other two parameters with a narrower relative error distribution varying in the range of -5 to 6%. In fact, these errors are negligible because they correspond to a maximum error of ±10 lb. By comparison to the total fuel that the aircraft should burn during a flight, a 10 lb error is relatively small, if not negligible. For this reason, the results obtained for the burnt fuel can still be considered very good.

5.4.3 Complete Flight Trajectory Simulation Results

After the validation of the climb and descent phases results, the next step in the validation process was to evaluate the effectiveness of the algorithms in predicting the complete trajectory of the aircraft for a given flight profile.

For this purpose, 10 additional tests were conducted with the RAFS. For each of the 10 flight tests, a complete lateral profile was established by selecting in a navigation database a departure airport, a takeoff runway, a Standard Departure Procedure (SID), a set of enroute waypoints, a Standard Arrival Route (STAR) procedure, and a runway at a given destination airport. The vertical profile, on the other hand, was established according to the template shown in Figure 5.4. The 4D aircraft trajectory was next computed using the various algorithms presented in **Section 5.3**. The T/D (top-of-descent) location as well was estimated using the method described in **Section 5.3.6**. It should be noted that for simplicity, the departure airport has always been assumed to be Montreal's Pierre Elliot-Trudeau Airport (CYUL), while the destination airports have been chosen to vary the duration of the flight.

In parallel, the lateral profile was also entered into the Flight Management System of the RAFS. The flight was performed with the assistance of the autopilot, and by engaging the lateral navigation mode (i.e., LNAV). The vertical profile, however, was managed by activating manually the various vertical modes of the autopilot.

5.4.3.1 Example of Results for a given Flight Profile

Figure 5.14 shows an example of results comparison for a complete flight from the Montreal Pierre-Elliot Trudeau Airport (CYUL) to Washington Dulles International Airport (KIAD).

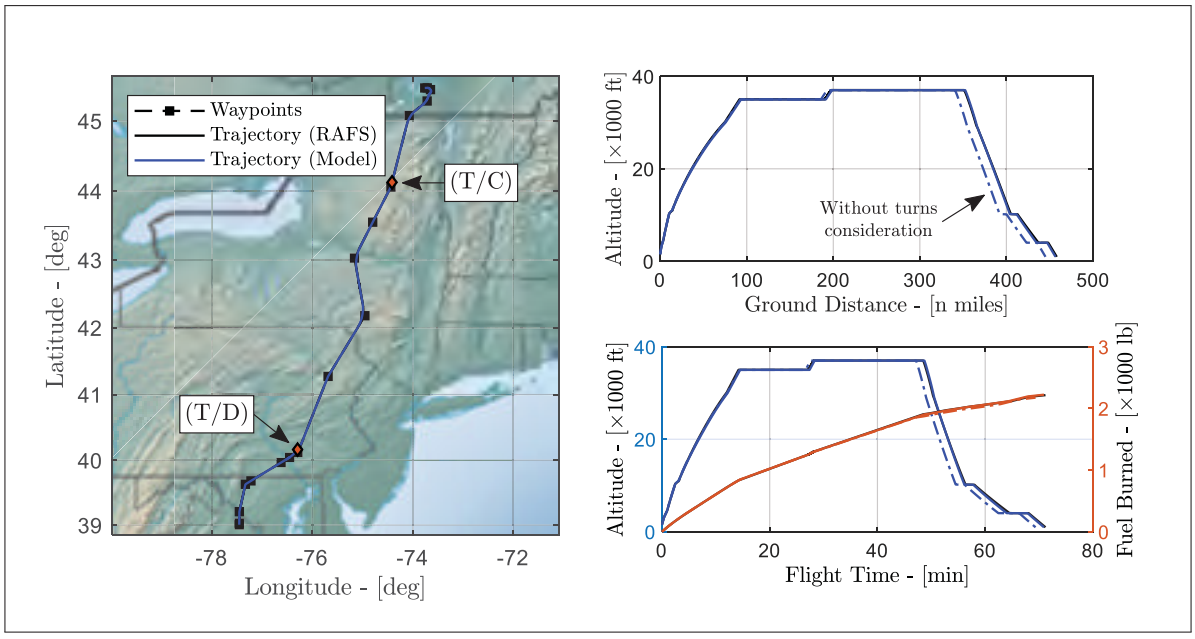

Figure 5.14 Example of Trajectory Comparison Results for a Flight from CYUL to KIAD

As seen in Figure 5.14, there is a very good match between the predicted and simulated trajectory results. The flight time and fuel burned are both very well estimated. The errors at the end of the flight for these two parameters were found to be approximately 0.6 min (0.88%) and 5.07 lb (0.23%), respectively. Regarding the ground distance, the error was found to be 2.59 n miles (0.56%). In fact, this last result was expected, because of the fact that the T/D point is calculated so that the aircraft at the end of the descent phase is located at a distance of ±5% n miles from the arrival airport (or the selected runway).

It is interesting to emphasize that the T/C and T/D locations in terms of distance and time to reach these points are estimated with less than 2% of errors.

Another aspect that might be interesting to mentioned is the consideration of turns segments in the calculation of the aircraft trajectory. Indeed, the trajectory data plotted with a dash-dotted line in Figure 5.14, corresponds to the aircraft trajectory calculated by neglecting all lateral transitions and turns segments. The difference between the trajectory with turns and the one without turns was found to be relatively small (less than 5% of difference). Therefore, if the algorithms presented in this paper are used for the purpose of optimizing flight trajectories, it is strongly recommended to neglect turns. This fact allows trajectories to be generated in less than a second while maintaining an acceptable level of precision. Once the optimal solution has been found, it can be refined by adding the turn segments.

5.4.3.2 Results for All Flight Tests

The comparison made in the previous section was repeated for all the 10 flights. The results obtained for the total ground distance, the total flight time and the total fuel burned are presented in Figure 5.15 to Figure 5.17.

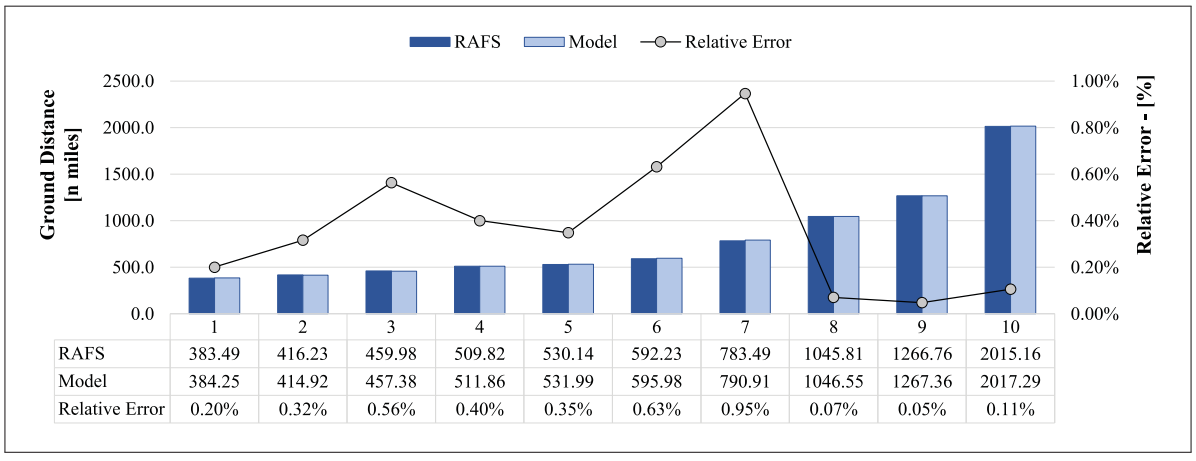

	1	2	3	4	5	6	7	8	9	10
RAFS	383.49	416.23	459.98	509.82	530.14	592.23	783.49	1045.81	1266.76	2015.16
Model	384.25	414.92	457.38	511.86	531.99	595.98	790.91	1046.55	1267.36	2017.29
Relative Error	0.20%	0.32%	0.56%	0.40%	0.35%	0.63%	0.95%	0.07%	0.05%	0.11%

Figure 5.15 Ground Distance Comparison for All Flights

From a general point of view, the results show a very good agreement between the data obtained from the RAFS and those estimated by the algorithms. As shown in Figure 5.15, the ground distance is estimated with less than 1.0% error. The average error for this parameter was found to be 0.36% with a standard deviation of 0.29%. Regarding the flight time, it can be seen in

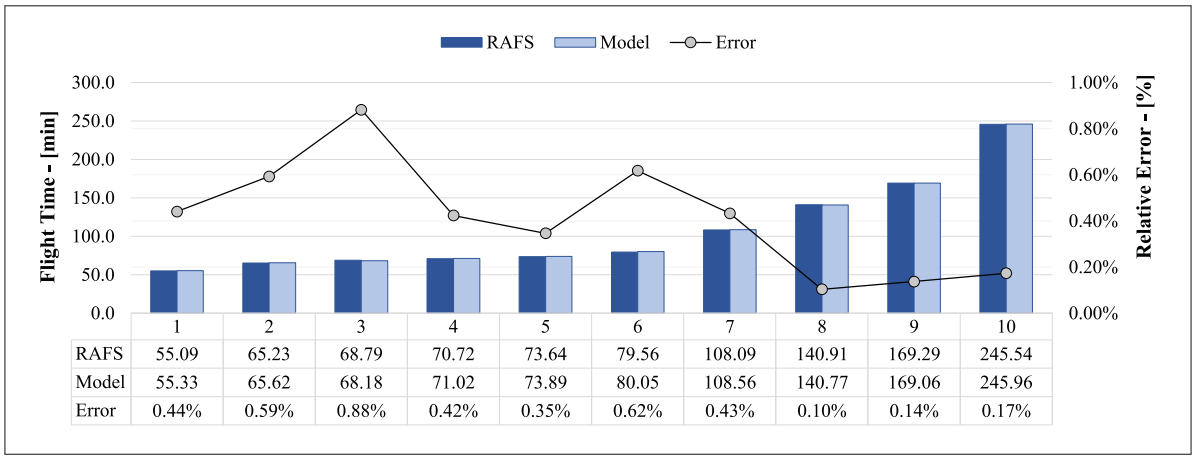

	1	2	3	4	5	6	7	8	9	10
RAFS	55.09	65.23	68.79	70.72	73.64	79.56	108.09	140.91	169.29	245.54
Model	55.33	65.62	68.18	71.02	73.89	80.05	108.56	140.77	169.06	245.96
Error	0.44%	0.59%	0.88%	0.42%	0.35%	0.62%	0.43%	0.10%	0.14%	0.17%

Figure 5.16 Flight Time Comparison for All Flights

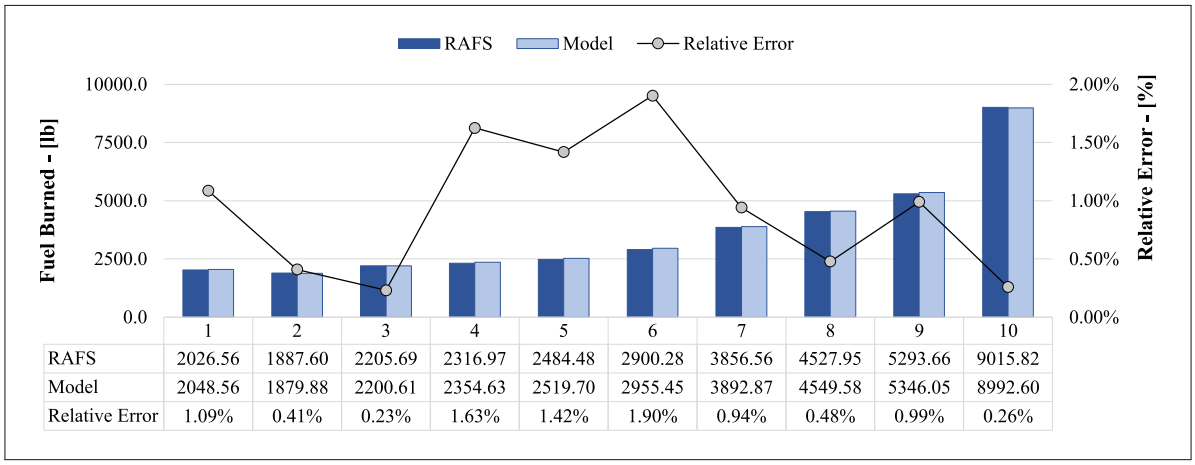

	1	2	3	4	5	6	7	8	9	10
RAFS	2026.56	1887.60	2205.69	2316.97	2484.48	2900.28	3856.56	4527.95	5293.66	9015.82
Model	2048.56	1879.88	2200.61	2354.63	2519.70	2955.45	3892.87	4549.58	5346.05	8992.60
Relative Error	1.09%	0.41%	0.23%	1.63%	1.42%	1.90%	0.94%	0.48%	0.99%	0.26%

Figure 5.17 Fuel Burned Comparison for All Flights

Figure 5.16 that this parameter is also very well estimated with less than 1.0% of relative error. The average error for the flight time was found to be 0.42% with a standard deviation of 0.24%. Finally, Figure 5.17 shows that the fuel burned was also estimated with less than 2.0% error. The average error for this parameter was found to be 1.93% with a standard deviation of about 0.59%.

The results presented in this section reinforce those obtained for the climb and descent phases. They demonstrate that the various algorithms developed in this paper can be used to predict the

flight trajectories of the Cessna Citation X in the presence of winds. Based on these results, it can therefore be concluded that the methodology and algorithms presented in this paper could be used to develop dynamics tools for the study of aircraft flight trajectories, and that the initial objective of this study was achieved.

5.5 Conclusion

In this paper, a complete and useful methodology to calculate the 4D flight trajectories of an aircraft was presented. The method consisted in solving and integrating the general equations of motion used to describe the motion of the aircraft in the vertical and lateral profiles. To achieve this objective, the aircraft vertical trajectory was divided into seven basic flight segments: unrestricted climb at constant CAS/Mach, restricted climb at constant CAS/Mach, climb/level-off acceleration, level flight at constant CAS/Mach, unrestricted descent at constant CAS/Mach, restricted descent at constant CAS/Mach, and descent/level-off deceleration. For each segment, detailed algorithms for solving and integrating the equations of motion was developed. Techniques have also been developed to include lateral transitionsm and turns segments in the calculation process.

The methodology described in this paper was tested, and then applied to the well-known Cessna Citation X business jet aircraft for which a qualified research aircraft flight simulator (RAFS) was available. A total of 130 tests for different flight and operation conditions were conducted. These flight tests were grouped into three categories: (1) continuous climb to cruise altitude, (2) idle descent from cruise altitude, and (3) complete flight from a departure airport to a destination airport. The validation of the methodology was accomplished by comparing the performance data measured with the RAFS with those calculated by the algorithms. From a global point of view, it has been shown that the proposed algorithms were precise enough to predict the aircraft trajectory and fuel consumption with a relative error smaller than 5%.

Following the analyses of the results, it can therefore be concluded that the methodology and algorithms presented in this paper are adequate, and that they could be further used to predict the flight trajectories of other types of aircraft.

The methodology developed in this paper can predict the 4D trajectory of an aircraft, however it was limited to flight phase above 1500 ft. As future work, it would be interesting to improve the methodology by including the takeoff and landing phases trajectories studies. In this way, it will be possible to obtain a complete model over the entire flight envelope of the aircraft.

CHAPTER 6

NEW ADAPTIVE ALGORITHM DEVELOPMENT FOR MONITORING AIRCRAFT PERFORMANCE AND IMPROVING FMS PREDICTIONS

Georges Ghazi [a], Benoit Gerardin [b], Magali Gelhaye [c] and Ruxandra Mihaela Botez [d]

[a, b, c, d] Department of Automated Production Engineering, École de Technologie Supérieure, 1100 Notre-Dame West, Montréal, Québec, Canada H3C 1K3

Paper published in the *AIAA Journal of Aerospace Information Systems*, Vol. 17, No. 2, December 2019, pp. 97-112.
DOI: https://doi.org/10.2514/1.I010748

Résumé

Pour calculer la route la plus efficace que l'avion doit emprunter, le système de gestion de vol (FMS) a besoin d'une représentation mathématique des performances de l'avion. Cependant, après plusieurs années d'exploitation, divers facteurs peuvent dégrader les performances globales de l'avion. Une telle dégradation peut affecter la fiabilité du modèle de l'avion, et l'équipage perdrait confiance dans la planification du carburant estimée par le FMS. Cet article présente les résultats d'une étude dans laquelle un nouvel algorithme adaptatif est proposé pour la mise à jour continue du modèle de performance du FMS en utilisant les données de vol en croisière. L'algorithme proposé combine des techniques de surveillance des performances de l'avion avec des tables adaptatives pour modéliser les caractéristiques aérodynamiques de l'avion. La méthodologie a été appliquée à l'avion d'affaires Cessna Citation X, pour lequel un simulateur de vol pour la recherche était disponible. Le développement de cette méthodologie a été accompli en créant un modèle de performance initial, en l'adaptant à l'aide de données de vol en croisière, et enfin en comparant sa prédiction avec une série de données de vol recueillies avec le simulateur de vol. Les résultats ont montré que la méthodologie proposée a permis de réduire les erreurs moyennes de prévision du débit de carburant d'environ 5%, tandis que l'écart-type a été réduit d'un facteur de 3.4.

Abstract

To compute the most efficient route that the aircraft has to fly, the Flight Management System

(FMS) needs a mathematical representation of the aircraft performance. However, after several years of operation, various factors can degrade the overall performance of the aircraft. Such degradation can affect the reliability of the aircraft model, and the crew would lose confidence in the fuel planning estimated by the FMS. This paper presents the results of a study in which a new adaptive algorithm is proposed for continuously updating the FMS performance model using cruise flight data. The proposed algorithm combines aircraft performance monitoring techniques with adaptive lookup tables to model the aerodynamic characteristics of the aircraft. The methodology was applied to the well-known Cessna Citation X business aircraft, for which a Research Aircraft Flight Simulator (RAFS) was available. The development of this methodology was accomplished by creating an initial performance model, adapting it using flight data in cruise, and finally comparing its prediction with a series of flight data collected with the flight simulator. Results have shown that the proposed methodology was able to reduce fuel flow prediction mean errors by about 5%, while the standard deviation was reduced by a factor of 3.4.

6.1 Introduction

In recent years, environmental problems related to the emissions of polluting particles into the atmosphere, global warming, and climate change have been of particular concern. One of the main reasons why aircraft produce and emit CO_2 is due to their engines, which require burning a large amount of fuel to generate a propulsive force. According to the International Air Transportation Association (IATA), during the year 2017, the civil aviation, including commercial and private operations, produced around 859 million tons of CO_2 (IATA, 2018). In comparison with other modes of transport, aircraft are responsible for roughly 1.5 to 2% of global CO_2 emissions (IATA, 2018). Although this percentage may seem insignificant, it has unfortunately a disproportionate effect on the atmosphere. Indeed, studies suggest that the impact per kilogram of CO_2 emissions taking place above 10,000 ft on the climate system is around twice than that of the emissions at ground-level (Lee *et al.*, 2009).

In parallel to the environmental factor, there is also a cost factor. Indeed, “energy is not free”, and most of airlines spend around 17% of their total budget on fuel (IATA, 2018). According to

a report published by the Lufthansa Group (2013), during the year 2013, the fuel consumption associated with their flight operations was estimated at more than 9 million tons. Considering the average price of fuel per kilogram during this period, their fuel costs amounted for approximately EUR 7.3 billion (USD 8.6 billion). This example clearly illustrates the potential savings that could be obtained by achieving a substantial reduction in fuel consumption associated to a fleet of aircraft. Moreover, since the amount of CO_2 emitted by an aircraft is directly related to the quantity of fuel burned, reducing the fuel consumption is also a way to address the challenge of climate change and to mitigate CO_2 emissions.

Faced with this dual ecological and economic challenge, various approaches have been proposed by industry and academics to reduce aircraft fuel consumption. These approaches include the use of alternative fuel (Sandquist & Guell, 2012; Hendricks *et al.*, 2011; Yilmaz & Atmanli, 2017), the development of next-generation engines (Haselbach *et al.*, 2015; Brouckaert *et al.*, 2018), the use of lightweight materials to reduce aircraft/engine weights (Marsh, 2012; Calado *et al.*, 2018), the improvement of aircraft aerodynamic characteristics using morphing wing concepts (Segui & Botez, 2018; Segui *et al.*, 2018; Koreanschi *et al.*, 2017a,b), the development of modern avionics systems (Sabatini *et al.*, 2015; Ramasamy, Sabatini & Gardi, 2015; Li & Hansman, 2018), and the optimization of flight trajectories (Patrón *et al.*, 2014, 2015; Murrieta-Mendoza *et al.*, 2017a,b).

6.1.1 Research Problematic and Motivations

A fundamental requirement for optimizing aircraft flight trajectories and flight procedures is the availability of a quality flight planning system, such as the Flight Management System (FMS). Introduced during the 80s by Boeing (Avery, 2011), the FMS is an on-board computer capable of providing the crew members with the optimal route by evaluating multiple possible scenarios, and by choosing the route that would best satisfy the airline's economic objectives (Liden, 1994; Walter, 2001; Avery, 2011). To accomplish all these functions, the FMS includes several sophisticated algorithms with advanced optimization capabilities and an explicit mathematical definition of the aircraft performance (Murrieta-Mendoza & Botez, 2015; Walter, 2001). The

word “performance” in this context refers mainly to the motion of the aircraft in the vertical plane, but also to the estimate of fuel required to complete the flight (Blake, 2009).

Although the functionalities of the FMS have evolved considerably since its first commercialization (Avery, 2011; Ramasamy *et al.*, 2014), there are two main factors that can still affect the reliability of its computerized flight plan.

The first factor is directly related to the accuracy of the data used to create the aircraft performance model (Sibin *et al.*, 2010). Generally, the aircraft performance model encoded in the FMS memory is composed of a set of non-linear mathematical equations and a set of databases (Walter, 2001). These databases, also called performance databases (Murrieta-Mendoza & Botez, 2015; Murrieta-Mendoza *et al.*, 2015), contain all the aero-propulsive model data required to characterize the lift and drag aerodynamic forces, thrust and fuel flow with respect to aircraft operating conditions (Walter, 2001; Sibin *et al.*, 2010). Therefore, the performance databases are the central element of the FMS mathematical model and are unique to each aircraft. Unfortunately, because of the highly competitive nature of the market, manufacturers are increasingly reluctant to provide aero-propulsive data of their aircraft/engine. This difficulty in obtaining data from manufacturers is forcing FMS designers to develop performance models with modeling uncertainties.

The second factor that can affect the reliability of FMS is the wear of some components due to the aging of the aircraft over time (Airbus, 2002a; ATR Customer Services, 2011). Indeed, since aircraft operate under a wide variety of operating conditions, they are constantly exposed to dynamic loads that can degrade their flight characteristics (Airbus, 2001; Krajcek, Nikolic & Domitrovic, 2015). These degradations can be classified into two categories: (1) airframe deterioration and (2) engine performance degradation **?** Airframe deterioration includes, for instance, missing or damaged door seals, deformations of the wing/fuselage surface, or increase in roughness due to the accumulation of contaminants on the aircraft surfaces (Airbus, 2001). According to Airbus, the accumulation of imperfections on the surface of the wings or the fuselage can cause the drag of an aircraft to increase by up to 2% every five years (Airbus,

2001). This increase in drag is manifested directly by an increase in fuel consumption during the cruise (the longest portion of the flight) as more thrust will be required to maintain the airspeed. Regarding the engine degradations, the consequences are the same. Indeed, engines operate most of the time under extreme temperature and pressure conditions, and are by consequence constantly exposed to high levels of wear and degradation (ATR Customer Services, 2011). In this case also, such a degradation has a direct impact on the aircraft performance in terms of fuel consumption because more fuel will be required to produce a required level of thrust in cruise.

By ignoring these two factors when operating the FMS, it is clear that after several years of service, the performance databases encoded in its memory will no longer be representative of the actual performance of the aircraft. Consequently, the crew will gradually lose confidence in the fuel planning estimated by the FMS and will have to add their own reserves. It is, therefore, important for airlines to monitor the performance of their aircraft and to apply appropriate corrective measures to maintain the level of reliability of their FMS.

6.1.2 Aircraft/Engine Performance Monitoring Techniques

In recent years, the importance of aircraft performance monitoring has been well recognized by airlines in order to preserve as much as possible aircraft's operational efficiency (Li, Das, John Hansman, Palacios & Srivastava, 2015; Li, Hansman, Palacios & Welsch, 2016). Among all parts of an aircraft, engines are probably the most critical component because of their high exposure to highly variable conditions (Nayyeri, 2013). Consequently, any major fault in an aircraft engine can result in a considerable increase in fuel consumption, and in a decrease in the performance of the aircraft. A traditional approach for maintaining the efficiency of aircraft engines is to perform regular checks. To estimate the optimal time when engines must be checked, researchers have developed Engine Health Monitoring (EHM) systems which allow airlines to detect early engine degradation, and to predict critical conditions (Ray, Hicks & Wichman, 1991; Tumer & Bajwa, 1999). EHM systems analyze engine health by monitoring key engine parameters such as rotational speeds (N_1 or N_2), fuel flow, or Exhausted Gas Temperature (EGT), and by comparing them with nominal values predetermined by the manufacturer (Yildirim & Kurt,

2016; Woike, 2018). Any change in the monitored parameters is used to detect early failures and assess engine performance. However, as pointed out by Airbus, even after engine replacement, the "specific range" (distance covered per unit quantity of fuel consumed) for an aircraft can be reduced by 0.3% every year (Airbus, 2002a; Krajcek *et al.*, 2015). Moreover, carrying out engine maintenance frequently will inevitably increase maintenance costs (ATR Customer Services, 2011).

To help airlines in monitoring the overall performance of their aircraft at low costs, Airbus and Boeing have developed Aircraft Performance Monitoring (APM) programs (Airbus, 2002a; Anderson & Hanreiter, 2008). These programs aim to compare the actual aircraft performance recorded in-flight with the theoretical performance computed by the FMS, or by an equivalent flight planning system. For new-generation aircraft equipped with multi-purpose computers, the data recording can be done automatically during the cruise phase, and then can be stored into an external memory device. After each flight, a "cruise report" file is generated (ATR Customer Services, 2011). This file is next fed into the APM in order to compute the average fuel consumption and the average specific range corresponding to the cruise phase (Airbus, 2002a; ATR Customer Services, 2011). These values are then compared to the values predicted by the FMS for the same flight conditions and aircraft configuration. Based on this analysis, airlines can determine a correction factor called Fuel Factor (FF) (Airbus, 2002a). This factor is a percentage that reflects the level of performance of the model with respect to the actual performance of the aircraft. Basically, a positive (or negative) fuel factor means that the FMS tends to underestimate (or overestimate) the actual fuel consumption of the aircraft. Such a technique has the advantage of being simple and effective, but also has the disadvantage of generalizing the correction to all flight conditions. Consequently, the fuel flow factor could be optimal for certain regions of the flight envelope, but not suitable for the other regions.

Another alternative that could also be considered for monitoring aircraft performance, and improving FMS performance predictions is the use of "adaptive algorithms". In recent years, several researchers have studied different methods to improve trajectory predictions in climb using observed track data. The main idea behind the proposed techniques was to reduce trajectory

prediction errors by dynamically adjusting one modelling parameter of the aircraft performance model, such as the aircraft weight (Schultz, Thipphavong & Erzberger, 2012; Thipphavong, Schultz, Lee & Chan, 2013) or the engine net thrust (Slater, 2002). Typically, each time when the algorithm received a track data update, the energy rate of the aircraft (defined as the sum of the kinetic and potential energy per unit weight) was computed. In parallel, the same energy rate was estimated using the aircraft performance model. Then by comparing the observed to the estimated energy rate, the modelling parameter (i.e., aircraft weight or engine net thrust) is adjusted to bring the value of the estimated energy rate closer to the observed energy rate value. However, although very promising results have been obtained, it is important to mention that these methods do not make it possible to update or correct the modeling uncertainties of the aircraft performance databases.

In a similar direction of research, adaptive algorithms combined with adaptive lookup tables have been also explored by several researchers in the automotive field (Vogt, Muller & Isermann, 2004; Hausberg, Hecker, Pfeffer, Plochl & Rupp, 2014; Guardiola, Pla, Blanco-Rodriguez & Cabrera, 2013). In addition to their advantages to be easily interpreted and visualized, adaptive lookup tables can also provide a very interesting way to capture the time-varying behavior of a complex physical system. Indeed, unlike a normal static lookup table, an adaptive lookup table receives a set of measurements from the system to be modelled, and continuously improves its structure. This continuous improvement can be referred to as an "adaptation process" or a "learning process" (Guardiola *et al.*, 2013). Faced with this learning potential, it would be interesting to be able to combine adaptive lookup tables with performance monitoring problems. The result would be a system that would be capable of learning the aircraft performance while taking into account performance deviation due to the aging of the aircraft.

6.1.3 Research Objectives and Paper Organization

The main objective of this research is to propose a new adaptive algorithm to monitor the fuel consumption of an aircraft, and to update the performance databases of the FMS. After each flight, the algorithm takes as inputs a set of parameters that have been recorded automatically

during the cruise phase. These parameters are then analyzed and filtered in order to detect all cruise segments, and to evaluate the equilibrium of the aircraft. By comparing the performance observed during the cruise with the theoretical performance predicted by the FMS, the proposed algorithm identifies the region of the flight envelope in which the performance databases must be corrected, and applies a correction in order to minimize the fuel consumption error. Thus, as the aircraft flies, the performance databases will be continuously adapted, making the FMS predictions increasingly reliable.

To develop, test and validate such an algorithm, a Research Aircraft Flight Simulator (RAFS) of the Cessna Citation X available at the LARCASE was used as a reference aircraft (see Figure 6.1). This simulator was designed and built by CAE Inc. based on flight tests data provided by the Cessna Textron aircraft manufacturer. The flight dynamics and engine models encoded in the RAFS have been validated with real flight tests data, and satisfy all criteria imposed in the Airplane Simulator Qualification (FAA, AC 120-40B) corresponding to highest level of certification, Level-D. The RAFS is therefore a reliable and adequate source of data for the verification and validation of the proposed algorithm.

Figure 6.1 Cessna Citation X Research Aircraft Flight Simulator

The structure of this paper is the following: **Section 6.2** gives a brief description the Cessna Citation X, as well as the main mathematical relationships required to model the aircraft performance in cruise. **Section 6.3** deals with the complete methodology used to design and correct the aircraft performance model. In **Section 6.4**, comparisons between flight parameters estimated with the aircraft performance model and flight parameters measured with the flight simulator are presented and discussed. Finally, the paper ends with conclusions and remarks concerning further possible research and developments ideas.

6.2 Mathematical Background and Aircraft Performance Model

The main purpose of this section is to establish a series of suitable mathematical expressions while determining which data are required for evaluating the performance of an aircraft in cruise. To this end, the section begins with a brief presentation of the Cessna Citation X business aircraft. Then a description of the equations of motion is given, along with the drag and engine model equations considered in this study to determine the aero-propulsive characteristics of the Cessna Citation X. The combination of all these mathematical relationships defines the performance model that will be used for most of the development in the subsequent sections. Finally, the concept of lookup table, and the aerodynamic database considered in this study to quantify the aerodynamic characteristics of the Cessna Citation X are presented.

6.2.1 Cessna Citation X Aircraft Description

The aircraft considered in this study is the well-known Cessna Citation X (Model 750). The Citation X is a long-range mid-sized business jet aircraft produced and manufactured by Cessna Aircraft Company (that became a brand of Textron Aviation in 2014). This aircraft is powered by two powerful Rolls-Royce AE3007C1 high-bypass turbofans installed at the rear of its fuselage. Each engine can produce a maximum thrust of 6,764 lbs at the sea level for an average fuel consumption of 325 gallons per hour. The Cessna Citation X is capable of flying at a maximum operating altitude of 51,000 ft and at a maximum operating Mach number of 0.92. Typical

configuration features 8 passengers and 2 crew seats. Since its first flight in December 1993, the Cessna Citation X is ranked still among the fastest civilian aircraft in the world.

Pertinent physical and performance characteristics of the Citation X are given in Table 6.1 (Cessna Aircraft Company, 2002). These characteristics include the aircraft dimensions and several limitations that must be considered for its safe operation.

Table 6.1 Cessna Citation X Specifications and Limitations

Parameters	**Values**	
Exterior Dimensions		
Length	72 ft 4 in	22.04 m
Height	19 ft 3 in	5.86 m
Wing Span	63 ft 11 in	19.48 m
Altitude		
Certified Altitude	51,000 ft	15,545 m
Typical Cruise Altitudes	37,000 to 45,000 ft	
Airspeed Limitations		
Maximum Operating Mach number	Mach 0.92	
Maximum Operating Speed	350 kts	649 km/h
Certified Weights		
Maximum Takeoff Weight	36,100 lb	16,375 Kg
Maximum Zero Fuel Weight	4,400 lb	11,067 Kg
Maximum Fuel Capacity	12,931 lb	5,865 Kg

6.2.2 Aircraft Mathematical Model in Cruise

For the study of flight performance, it is convenient to model the aircraft as a point-mass and to constrain its motion in a vertical plane on a non-rotating flat earth (Young, 2017). The point-mass model considers that all the external forces acting on the aircraft are directly applied to its center of gravity. As shown in Figure 6.2, the external forces acting on an aircraft typically result from the combination between their aerodynamic, propulsive and gravitational components. The lift and drag, denoted by L and D respectively, are the aerodynamic force components. The thrust

is the net propulsive force produced by the two turbofan engines, and is denoted by F_N. Finally, the weight of the aircraft W corresponds to the gravitational component.

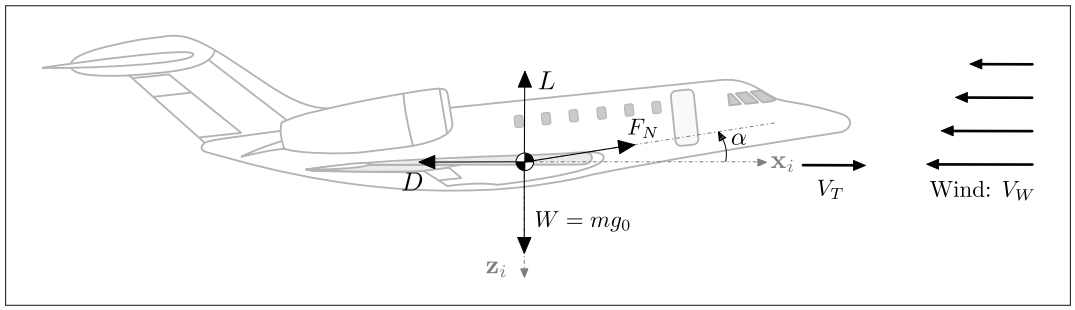

Figure 6.2 Forces acting on the Cessna Citation X

6.2.2.1 Aircraft Equations of Motion in Cruise

Since the cruise is a particular phase where the aircraft is supposed to fly at constant altitude and constant flight speed, additional approximations of parameters are commonly made for the sake of simplicity (Young, 2017). These approximations are listed here for the convenience of the reader.

The flight path angle is by definition equal to zero. The angle of attack (denoted by α in Figure 6.2) is assumed small, so that the thrust direction is considered the same as the flight path. The drift angle is assumed to be small and the aircraft is supposed to fly in an atmospheric wind field comprising only horizontal wind components that is dependent on altitude, time and geographic coordinates. The acceleration of the aircraft is approximated by the rate of ground speed in order to take into consideration the horizontal acceleration due to wind horizontal component. Finally, weight reduction of the aircraft is solely due to its engines fuel consumption. Thus, applying all these simplifications to the point-mass model in Figure 6.2, and projecting the forces along the horizontal and vertical directions, the pertinent equations of motion for the

cruise phase can be written in their simplified form as follows:

$$m\dot{V}_{GS} = F_N - D \tag{6.1}$$

$$0 = L - mg_0 \tag{6.2}$$

$$V_{GS} = V_T + V_W \tag{6.3}$$

where m is the aircraft mass, g_0 is the acceleration due to gravity (assumed to be constant and equal to 9.81 m/s^2 or 32.174 ft/s^2), V_{GS} is the aircraft ground speed, V_T is the true airspeed, V_W is the horizontal wind component. Finally, Eqs. (1) to (3) are the aircraft equations of motion simplified and adapted to the cruise phase.

6.2.2.2 Engine Fundamental Relationships

During the cruise, part of the fuel is consumed by the two engines to generate a propulsive force that propels the Cessna Citation X forward. As a result, the mass of the aircraft decreases at a rate which is proportional to the amount of thrust produced by the engines (Young, 2017; Mattingly *et al.*, 2018). According to several references in the literature (Bartel & Young, 2008), the fuel flow W_F, which translates to the amount of fuel burned per unit of time, can be determined by:

$$W_F = F_N \times \text{TSFC} \tag{6.4}$$

where TSFC is the thrust-specific fuel consumption. This parameter represents in a certain way the fuel efficiency of an engine and can vary significantly depending on the engine type. For turbojet and turbofan engine technologies, the TSFC in cruise can be modeled as a function of the Mach number M and the temperature ratio $\theta = T/T_0$ (ratio between the static air temperature at a specific altitude T and the static air temperature at seat level T_0) using the following equation (Daidzic, 2016):

$$\text{TSFC}(\theta, M) = \text{TSFC}_0\sqrt{\theta}\,(1 + M)^n \tag{6.5}$$

where $TSFC_0$ corresponds to the static sea level installed thrust-specific fuel consumption of the engine at maximum cruise setting, and the exponent n is a constant that depends on the engine characteristics.

The AE3007C1, that equips the Cessna Citation X, is a high-bypass ratio (approximately 5:1) turbofan engine, which was produced in the 90's. Based on these specifications, and according to data available in reference (Daidzic, 2016), the $TSFC_0$ was determined to be 0.04 kg/h/N and the coefficient n to be 0.8. Although these values are semi-empirical, they were assumed accurate enough to represent the actual fuel efficiency of the Cessna Citation X engines.

6.2.2.3 Aerodynamic Fundamental Relationships

To complete the aircraft mathematical model, additional definitions of lift and drag are usually required. As explained in several references (Raymer, 2012; Young, 2017), these two aerodynamic components can be expressed with, on the one hand, the lift coefficient CL_s, and on the other hand, the drag coefficient CD_s, according to the following equations:

$$L = 0.5\rho S V_T^2 CL_s \tag{6.6}$$

$$L = 0.5\rho S V_T^2 CL_s \tag{6.7}$$

where ρ is the static air density function of the altitude and the static air temperature, and S is the wing reference surface of the aircraft. Furthermore, for altitudes and speed regimes, in which cruise range and endurance are typically optimized, the total drag coefficient in Eq. (6.7) can be determined using the next drag polar equation:

$$\begin{aligned} CD_s &= f(CL_s, M) \\ &= CD_0(M) + K(M)CL_s^2 \end{aligned} \tag{6.8}$$

where CD_0 is the zero-lift drag coefficient, and K is the lift-dependent drag coefficient factor. Both parameters are complex unknown functions of flaps/slats configuration, Mach number,

and many other conditions, such as air compressibility effects, which cannot be neglected for nominal cruising speeds.

Although there exist in the literature various semi-empirical equations to describe the evolution of these two parameters with respect to flight conditions and aircraft configurations, for most of the existing aircraft, the drag coefficient cannot be adequately described by such simplified expressions. Indeed, exact calculations of the drag coefficient of an aircraft are rather carried out using tabular data or lookup tables. This is the reason why, in this study, an approach based on a grid-based lookup table instead of mathematical equations was preferred to model the drag coefficient of the Cessna Citation X.

6.2.3 Aerodynamic Data Modeling using Grid-Based Lookup Table

As mentioned in the previous section, the total drag coefficient of the Cessna Citation X was modeled using a grid-based lookup table. A considerable advantage of using lookup tables instead of continuous functions is that they provide a suitable means of capturing the input-output mapping of a complex physical system. The typical representation of a two-dimensional lookup table describing the variation of a variable z as a function of two variables x and y is illustrated in Figure 6.3. As shown in this figure, a two-dimensional lookup table can be compared to a two-dimensional matrix, where each element of the matrix corresponds to a sampled value of the variable z for a specific combination of breakpoints $(x_{[i]}, y_{[j]})$, also called "nodes". The set of all breakpoints defines the domain of the lookup table and is called the "grid". In the example given in Figure 6.3, the two variables x and y are defined with five breakpoints varying from -1 to 1 with a step increment of 0.5. The output data of the lookup table is therefore represented by a two-dimensional matrix of 25 nodes.

Because of the discrete nature of the lookup table, an interpolation algorithm is always required in order to compute the output corresponding to a specific input, that is not a direct combination of the breakpoints. A bilinear interpolation along the y- and x-directions is used for this reason. To better explain this, an arbitrary point θ defined by the coordinates $(z|x, y)$ is considered. As shown

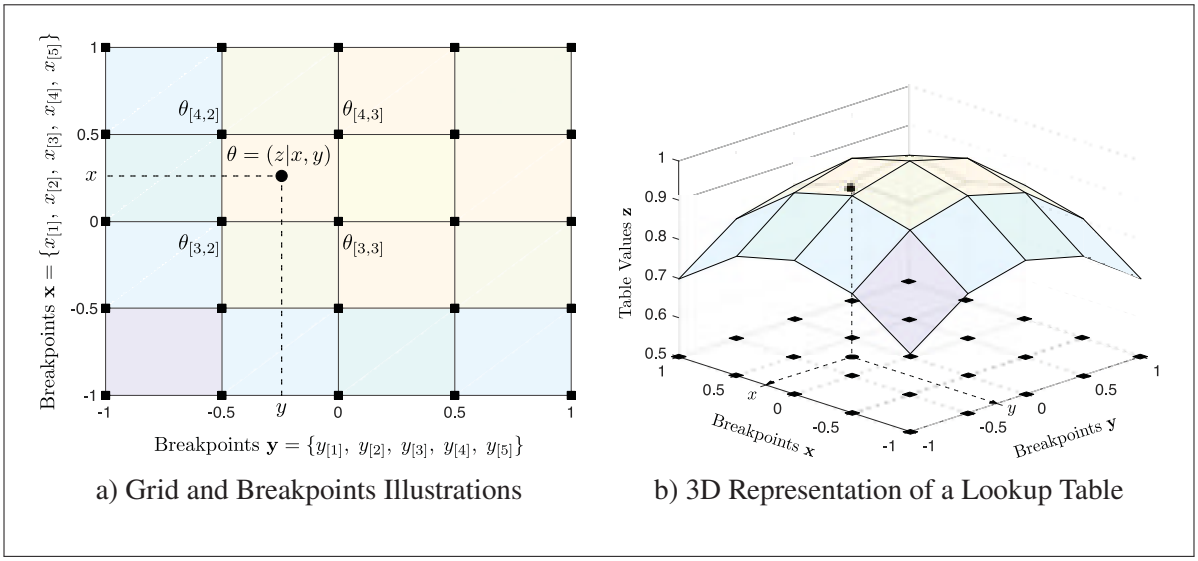

a) Grid and Breakpoints Illustrations

b) 3D Representation of a Lookup Table

Figure 6.3 Two-Dimensional Grid-Based Lookup Table Representation

in Figure 6.3a, this point is surrounded by the four nodes denoted by $\theta_{[3,2]} = (z_{[3,2]}|x_{[3]}, y_{[2]})$, $\theta_{[3,3]} = (z_{[3,3]}|x_{[3]}, y_{[3]})$, $\theta_{[4,3]} = (z_{[4,3]}|x_{[4]}, y_{[3]})$ and $\theta_{[4,2]} = (z_{[4,2]}|x_{[4]}, y_{[2]})$. By applying a first linear interpolation in the y-direction, the two following relationships are obtained:

$$z(x_{[3]}, y) = \frac{y_{[3]} - y}{y_{[3]} - y_{[2]}} z(x_{[3]}, y_{[2]}) + \frac{y - y_{[2]}}{y_{[3]} - y_{[2]}} z(x_{[3]}, y_{[3]}) \tag{6.9}$$

$$z(x_{[4]}, y) = \frac{y_{[3]} - y}{y_{[3]} - y_{[2]}} z(x_{[4]}, y_{[2]}) + \frac{y - y_{[2]}}{y_{[3]} - y_{[2]}} z(x_{[4]}, y_{[3]}) \tag{6.10}$$

Then, by applying a second linear interpolation in the x-direction this time, the desired output can be calculated using the following equation:

$$z(x, y) = \frac{x_{[4]} - x}{x_{[4]} - x_{[3]}} z(x_{[3]}, y) + \frac{x - x_{[3]}}{x_{[4]} - x_{[3]}} z(x_{[4]}, y) \tag{6.11}$$

It is worth noticing that the process gives exactly the same results if the interpolation was first done along the x-direction and then along the y-direction.

For the problem considered in this study, two lookup tables were used to model the aerodynamic characteristics of the Cessna Citation X in cruise. These two lookup tables are presented in Table 6.2, together with their inputs and outputs.

Table 6.2 Cessna Citation X Aerodynamic Lookup Tables

Input(s)	**Output**
Lift Aerodynamic Coefficient, CL_s Mach Number, M	Drag Aerodynamic Coefficient, CD_s
Lift Aerodynamic Coefficient, CL_s Mach Number, M	Confidence Coefficient, λ

The first lookup table represents the "parabolic drag polar" of the aircraft. The required inputs for this lookup table are the lift coefficient, CL_s, and the Mach number, M. The corresponding output is the total drag coefficient of the aircraft, CD_s. The second lookup table represents the confidence level of the drag model and has the same inputs as the previous one. The corresponding output parameter is called the confidence coefficient, λ. This parameter is a positive constant that must be greater than or equal to 1, and that quantifies the reliability of the data stored in the drag coefficient lookup table. To be more specific, the higher the confidence coefficient, the more reliable the drag coefficient model can be.

6.2.4 Proposed Approach

Based on the information provided in this section, it is now possible to conclude that the reliability of the global performance model depends mainly on the reliability of the associated thrust-specific fuel consumption and the drag aerodynamic coefficient models. Therefore, if a prediction error on the fuel flow is observed during the flight, it is necessary to interrogate one of the two models in order to find the source of the error. Unfortunately, since commercial aircraft are not adequately instrumented to measure all the parameters required to estimate the thrust and drag forces, it is usually difficult, if not impossible, to determine which one of the two models is responsible for the prediction error. A way to simplify this problem is to consider the thrust-specific fuel consumption model as a reference and to correct the drag model accordingly.

Thus, any error in the fuel flow prediction will be automatically transferred into an error in drag coefficient.

From this point of view, the adaptation of the aircraft performance model in cruise can be simply reduced to the adaptation of the drag coefficient lookup table using available flight data in cruise. Such a methodology is presented in **Section 6.3**.

6.3 Methodology: Adaptive Algorithm and Performance Prediction Algorithm

Now that the fundamentals and mathematical relationships describing the aircraft performance model have been introduced, the complete methodology developed at the LARCASE laboratory to adapt the drag coefficient lookup table in cruise can be presented. To this end, this section begins with the creation of two "initial" lookup tables; one for the drag coefficient and one for the confidence coefficient. Afterward, the second part of this section describes the procedure used in this study to simulate the performance of the Cessna Citation X for the cruise regime. Finally, the section presents with the main purpose of this study that is, the development of the adaptive algorithm. The result of this section is, therefore, the development a complete method through which a mathematical model of an aircraft can be determined using a minimum amount of reference data, and could be further adapted using cruise flight data to improve the prediction of the fuel consumption. A block diagram, which summarizes this concept, is presented in Figure 6.4.

6.3.1 Creation of Drag and Confidence Coefficient Initial Lookup Tables

Before going into the details of the adaptive algorithm, it was necessary to create an initial model for the drag coefficient. To do this model, a set of performance data available in the Cessna Citation X Flight Planning Guide (FPG) manual was used as reference. This manual is a document produced by the aircraft manufacturer, and it is generally consulted by the crew for evaluating the performance of the aircraft for various flight phases such as takeoff, climb, cruise, descent and landing.

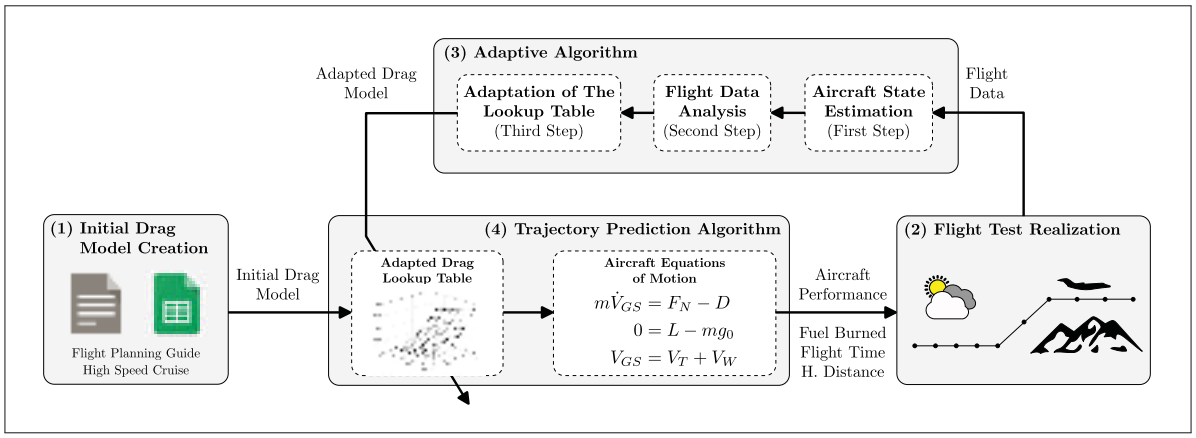

Figure 6.4 Block Diagram describing the Main Steps of the Proposed Methodology

The performance data published in the FPG are usually derived from data contained in the Aircraft Flight Manual (AFM) and Flight Crew Operating Manual (FCOM). However, it may be interesting to mention that, unlike the AFM and FCOM, the FPG is not approved by the FAA, and the data published in this document are subject to change without notice. Consequently, the data provided in the FPG do not constitute a reliable source. This is the main reason why this document was selected among the other two, the objective being to create an initial model that is not representative of the actual aircraft performance, and verify if the proposed adaptive algorithm can correct the uncertainties of this model.

An example of typical data published in the FPG for the cruise phase is given in Figure 6.5. As can be seen in this figure, the aircraft performance is presented in the form of a table describing the fuel flow in lb/hr required to operate the aircraft at various aircraft weights (from 26,000 to 36,000 lb at 2,000 lb intervals), pressure altitudes (from 5,000 to 49,000 ft) and cruising true airspeeds (from 291 to 470 KTAS). Moreover, a notice at the bottom of the table specifies that the data is provided only for standard atmosphere conditions (ISA) and with anti-ice systems off. Note that the values presented in Figure 6.5 are not the real values due to confidentiality reasons.

The combination of all this information makes it possible to obtain a model for the drag coefficient of the Cessna Citation X in cruise. Indeed, starting from a given weight and specific flight conditions in terms of altitude and true airspeed, the aerodynamic lift coefficient of the aircraft

HIGH SPEED CRUISE
ISA, Anti-Ice Off

Cruise Speed & Fuel Flow

Pressure Altitude (ft)		Cruise Weight (lb) 36,000	34,000	32,000	30,000	28,000	26,000
5,000	KTAS	291	291	291	291	291	291
	Lb/Hr	2,449	2,420	2,394	2,369	2,346	2,324
10,000	KTAS	402	402	402	402	402	402
	Lb/Hr	3,503	3,485	3,451	3,436	3,436	3,422
15,000	KTAS	431	431	431	431	431	431
	Lb/Hr	3,372	3,353	3,335	3,319	3,303	3,289
21,000	KTAS	460	462	464	465	467	468
	Lb/Hr	3,121	3,124	3,127	3,130	3,132	3,135

Figure 6.5 Example of High Speed Cruise Performance Data Published in the FPG

can be estimated using the relationships in Eq. (6.2) and Eq. (6.6) as follows:

$$CL_s = \frac{L}{0.5\rho S V_T^2} = \frac{mg_0}{0.5\rho S V_T^2} \tag{6.12}$$

Then, by considering that the data published in the FPG is given only for level-flight conditions at constant speed (i.e., no acceleration) and for zero-wind condition, the thrust force required to balance the aircraft is assumed to be equal to the drag force. Based on this assumption, the total drag coefficient can be obtained by substituting the drag force with the thrust in Eq. (6.7), which gives:

$$CD_s = \frac{D}{0.5\rho S V_T^2} = \frac{F_N}{0.5\rho S V_T^2} \tag{6.13}$$

Finally, by recalling the definition of the thrust specific fuel consumption in Eq. (6.5), the expression of the aircraft drag coefficient in Eq. (6.13) can be rewritten in the following form:

$$CD_s = \frac{W_F/\mathrm{TSFC}}{0.5\rho S V_T^2} = \frac{W_F/[\mathrm{TSFC}_0\sqrt{\theta}(1+M)^n]}{0.5\rho S V_T^2} \tag{6.14}$$

This last result states that the drag coefficient in cruise can be determined according to the knowledge of the fuel flow, and the corresponding flight condition defined by the physical parameters ρ, θ, V_T, and M. Thus, by applying the aerodynamic CL_s and CD_s coefficients

results obtained from Eq. (6.12) to Eq. (6.14) to all flight conditions available in the FPG, a set of data describing the evolution of the drag coefficient as a function of the lift coefficient and the Mach number was obtained. This data set was subsequently approximated using the following polynomial model:

$$\begin{aligned} CD_s &= CD_0(M) + K(M)CL_s^2 \\ \text{with: } CD_0(M) &= p_0 + p_1 M + p_2 M^2 \\ K(M) &= p_3 + p_4 M + p_5 M^2 \end{aligned} \tag{6.15}$$

where $\{p_0, \ldots, p_5\}$ are coefficients that were determined using the Least Squares Method (LSM).

Finally, the lookup table for the drag coefficient was created by sampling the model in Eq. (6.15) for different Mach numbers ranging from 0.40 to 0.90 with an increment of 0.05, and different lift coefficients ranging from 0.10 to 1.00 with an increment of 0.025. Regarding the lookup table for the confidence coefficient, all the elements were initialized with the value 1. Figure 6.6 shows a graphical representation of the two resulting lookup tables.

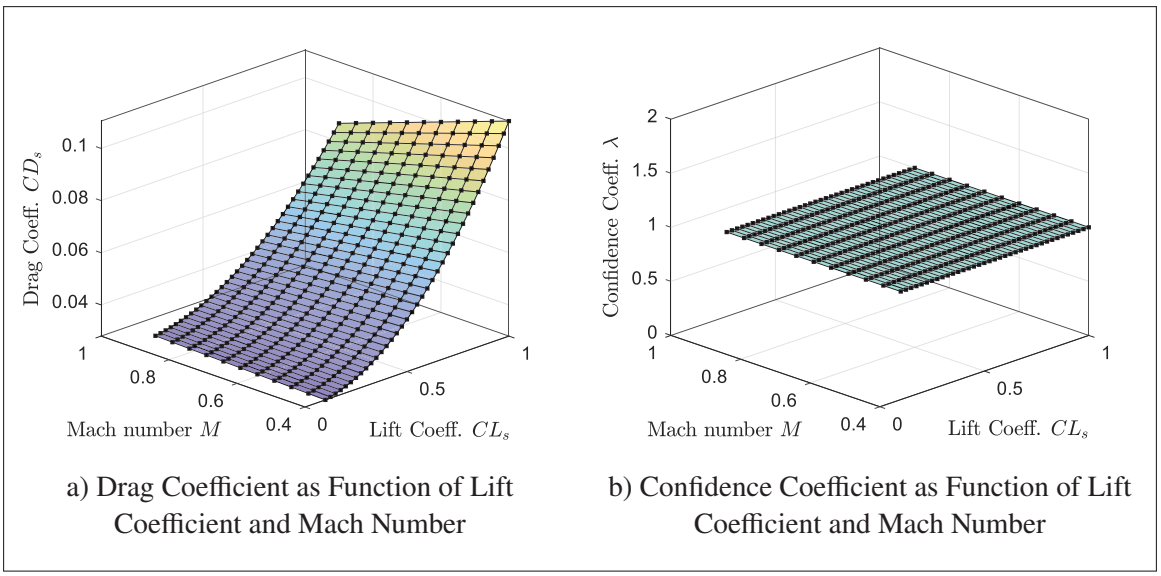

a) Drag Coefficient as Function of Lift Coefficient and Mach Number

b) Confidence Coefficient as Function of Lift Coefficient and Mach Number

Figure 6.6 Initial Drag Coefficient and Confidence Coefficient Lookup Tables

It should be emphasized that the values of lookup table shown in Figure 6.6a do not represent the actual drag of the Cessna Citation X. Indeed, the lookup table obtained here is rather a model of the drag which, combined with the thrust-specific fuel consumption model in Eq. (6.5), allows a prediction of the fuel flow that matches the data provided in the FPG.

6.3.2 Flight Test Realization and In-Flight Data Recording

Once the initial drag and confidence coefficient models were created, the next step in the methodology consisted in realizing flight tests using the flight simulator available at the LARCASE laboratory. Each flight test aimed to reproduce, as much as possible, an actual flight scenario between two airports. For the sake of simplicity, the airport of Montreal (Pierre Elliott Trudeau International Airport, CYUL) was always selected as the departure airport. The destination airport, however, was different from one test to the next in order to vary the duration of the flights. In this way, it has been possible to reproduce different flight scenarios that are all representative of the actual air traffic in North America and Europe.

6.3.2.1 Flight Planning and Flight Test Realization

In order to reproduce operating conditions that are similar to those of actual commercial and business flights, all the flight tests considered in this study were conducted with the assistance of the FMS located on the flight deck of the Cessna Citation X RAFS. To do this type of operation, prior to each test, a flight plan was established based on real aircraft trajectory data obtained from the website Flight-Aware[1]. This website allows tracking the real-time flight status of any aircraft around the world. The raw data provided by Flight-Aware typically include the aircraft altitude, ground speed, heading, flight time (expressed in Coordinated Universal Time, UTC), and geographic coordinates (longitude and latitude). After selecting a flight on the website, its corresponding information was imported into Matlab. The aircraft trajectory was then analyzed and decomposed into a series of waypoints that best described the observed route that the real aircraft used. These waypoints were next introduced manually into the FMS of the Cessna

[1] https://flightaware.com

Citation X to create the complete lateral flight profile. Similarly, the vertical flight profile (climb speed, cruise altitude, etc.) was also configured using the assistance of the FMS.

Since atmospheric conditions can significantly affect the flight characteristics of the aircraft during the cruise, non-standard atmosphere data comprising both temperature deviations and wind field components was considered for each flight test. The temperature and wind data was obtained from Environment Canada. The data is given under Global Deterministic Prediction System (GDPS) format and includes horizontal wind direction, horizontal wind speed, and static air temperature for various combinations of geographical coordinates (latitudes/longitudes), altitudes and hours (given in UTC). To complete the wind model, a turbulence model was also considered in order to simulate temporary disturbances that could occur during the cruise phase. The turbulence at a given point in space was stochastically modeled by means of its power spectrum using the Dryden power spectral model.

Finally, to help the pilots in performing all the required maneuvers during the flight (climb, turn, maintain altitude and speed, etc.), the vertical and lateral navigation modes (VNAV/LNAV) were engaged from the autopilot panel, so that the aircraft can follow the desired trajectory computed by the FMS even in presence of wind.

6.3.2.2 In-Flight Data Recording and Output Data File Creation

For the purposes of this study, it was assumed that all flight parameters shown in Table 6.3 were available and recordable during the flight. These flight parameters were sampled every minute (i.e., 60 seconds) from the various electronic systems on-board the aircraft. These systems include the Air Data Computer (ADC), the Attitude Heading Reference System (AHRS), the Global Positioning System (GPS), and the Electronic Flight Instrument System (EFIS). The accuracy tolerance for each of these flight instruments was supposed to be within the industrial tolerances (Airbus, 2002a). Based on this assumption, rounding errors and measurement noise were considered to be negligible in comparison to other potential sources of larger errors, such as

uncertainties of the initial/current aircraft performance model, airframe degradations or engine components deterioration.

Table 6.3 Flight Parameters Recorded during the Cruise

Flight Parameter	Physical Unit	On-Board Computer/System
Flight Conditions		
Pressure Altitude	[ft] or [m]	From the ADC
Static Air Temperature	[°C]	From the ADC
Flight Velocities		
True Airspeed	[ft/s] or [m/s]	From the ADC
Mach number		From the ADC
Ground Speed	[ft/s] or [m/s]	From the GPS
Aircraft References Angles		
Drift Angle	[deg]	From the AHRS
Roll Angle	[deg]	From the AHRS
Engine Performance		
Engine Speed	[%RPM]	From the FADEC or the EFIS
Actual Fuel Flow	[lb/h] or [kg/h]	From the FADEC or the EFIS
Total Fuel Used	[lb] or [kg]	From the FADEC or the EFIS

In order to avoid analysis error due to engine transient behavior and also to limit the number of data collected during the flight, the recording of the data was started 15 minutes after the aircraft has reached the Top-of-Climb (T/C, altitude at which the climb phase ends), and was stopped 15 minutes before the aircraft has arrived to the Top-of-Descent (T/D, point where the aircraft begins the descent to the destination airport).

Finally, once the flight test was completed, all flight parameters collected during the cruise, as well as the aircraft initial weight data, were stored into a “text file”, so that it can be used and analyzed by the adaptive algorithm. An example of cruise report file that was generated for a cruise of 600 seconds (i.e., 10 minutes) is given in Figure 6.7.

In Figure 6.7, `ALT` is the pressure altitude, `SAT` is the static air temperature, `MACH` is the Mach number, `VTAS` is the true airspeed, `GSPD` is the aircraft ground speed, `ROLL` is the aircraft roll

```
* LARCASE LABORATORY - CRUISE PERFORMANCE                          A/C: CESSNA CITATION X *
* ================================================================================== *
    WEIGHT DATA (AT ENG. START)                                      ADD. INFORMATION
-------------------------------------                          ---------------------------
- FUEL ON BOARD : 11200 [LB]                                   - SAMPLING RATE  : 060 [SEC]
- ZERO FUEL WEIGHT : 23800 [LB]                                - NUMBER OF DATA : 010 [N/A]
- AIRCRAFT GROSS WEIGHT : 35000 [LB]

                      FLIGHT DATA                                          ENGINE DATA
-------------------------------------------------------------------------------------------
No. ALT    SAT     MACH   VTAS  GSPD    ROLL   DRIFT || N2(1)  N2(2)  WF(1)  WF(2) FU
    FEET   C               KTS   KTS     DEG    DEG   || %RPM   %RPM   LB/H   LB/H  LB
-------------------------------------------------------------------------------------------

 1  37011  -32.50  0.801  250.0  250.0 -10.9  -0.92  ||  85.04  85.04  2410   2410  2679
 2  37011  -32.50  0.801  250.0  250.0 -10.9  -0.92  ||  85.04  85.04  2410   2410  2679
 3  37011  -32.50  0.801  250.0  250.0 -10.9  -0.92  ||  85.04  85.04  2410   2410  2679
 :    :       :      :      :      :     :     :    ||    :      :      :      :     :
 9  37011  -32.50  0.801  250.0  250.0 -10.9  -0.92  ||  85.04  85.04  2410   2410  2679
10  37011  -32.50  0.801  250.0  250.0 -10.9  -0.92  ||  85.04  85.04  2410   2410  2679

* END OF FILE                                                     A/C: CESSNA CITATION X *
* ================================================================================== *
```

Figure 6.7 Example of a Cruise Report File created at the End of a Flight Test

angle, `DRIFT` is the aircraft drift angle, `N2(1)` and `N2(2)` are respectively the left and right engine turbine speeds, `WF(1)` and `WF(2)` are respectively the left and right engine fuel flows, and `FU` is the total fuel used since the two engines start.

6.3.3 Adaptive Algorithm and Adaptive Lookup Table

So far, the methodology has allowed to create an initial drag coefficient model in the form of a grid-based lookup table, and to establish a list of variables that can be recorded in-flight, and which reflect the actual aircraft performance. The next step of the methodology consists, therefore, in proposing an adaptive algorithm that verifies the degree of accuracy of the drag coefficient model after each flight, and performs a correction of the model, if necessary. As shown previously in Figure 6.4, the adaptive algorithm developed in this study can be divided into three main steps. Each of these steps is presented more in details in the following sections, together with relevant comments as to their purpose.

6.3.3.1 Estimation of the Aircraft Weight, Acceleration and Vertical Speed

The first step of the adaptive algorithm is to estimate the aircraft gross weight, longitudinal acceleration, and vertical speed. The two first parameters are the most important since they are necessary to calculate the lift and drag aerodynamic coefficients of the aircraft. The vertical speed is also required to analyze the equilibrium of the aircraft along its flight trajectory. Based on the recorded flight data available in the cruise report file, the aircraft gross weight at a specific time was determined by subtracting the total fuel used from the aircraft ramp weight at engine start as follows:

$$\begin{aligned} m[i] &= m_{\mathrm{RAMP}} - m_{\mathrm{FU}}[i] \\ &= (m_{\mathrm{ZFW}} + m_{\mathrm{FOB}}) - m_{\mathrm{FU}}[i] \end{aligned} \tag{6.16}$$

where m_{RAMP} is the aircraft ramp weight (defined as the sum of the aircraft zero fuel weight m_{ZFW} and the fuel on board at main engine start m_{FOB}), m_{FU} is the total fuel-used since the starting of the two engines (denoted by `FU` in Figure 6.7), $i = \{1, \ldots, N\}$ is the discrete-time index, and N the number of sampled data.

The value of the aircraft acceleration along the flight path was determined using a first-order approximation of the derivative of the ground speed with respect to time as follows:

$$\left.\frac{\mathrm{d}V_{GS}}{\mathrm{d}t}\right|_{[i]} = \frac{V_{GS}[i+1] - V_{GS}[i]}{\Delta t} \tag{6.17}$$

where V_{GS} is the aircraft ground speed (denoted by `GSPD` in Figure 6.7), and Δt is the sampling rate (constant and equal to 60 seconds).

It is worth noticing that because of discrete nature of Eq. (6.17), the acceleration at the last point $i = N$ cannot be computed. For this reason, the value of the acceleration for this point was obtained by applying a linear regression technique to the three previous points, and by extrapolating the value for the last point N.

Using the same technique, the vertical speed of the aircraft was also calculated based on a first-order approximation of the derivative of the pressure altitude with respect to time, such as:

$$V/S[i] = \left.\frac{\mathrm{d}h}{\mathrm{d}t}\right|_{[i]} = \frac{h[i+1] - h[i]}{\Delta t} \tag{6.18}$$

where V/S is the aircraft vertical speed, and h is the pressure altitude denoted by `ALT` in Figure 6.7.

6.3.3.2 Flight Data Analysis and Decomposition into Stabilized Flight Segments

Once the aircraft gross weight, longitudinal acceleration and vertical speed are estimated, the next step of the adaptive algorithm is to analyze the recorded flight data and search for all cruising segments where the aircraft is stabilized. To do this analysis, the algorithm scans all the flight parameters available in the output data file and detects all flight segments where favorable trim conditions are maintained for at least three minutes. In this study, eight criteria were used to evaluate the equilibrium of the aircraft along a given flight segment. These criteria were obtained from a technical report published by Airbus (2002a) and are given in Table 6.4.

Table 6.4 Trim Criteria for a Level Flight Segment in Cruise

Flight Parameter	**Criteria/Limit**
Pressure Altitude	Δ`ALT` $\leq$ 20 ft
Vertical Speed	Δ`VS` $\leq$ 100 ft/min
Mach number	Δ`MACH` $\leq$ 0.003
Ground Speed	Δ`GSPD` $\leq$ 1 kt
Static Air temperature	Δ`SAT` $\leq$ 1°C
Engine Turbine Speed	Δ`N2` $\leq$ 1.6 %RPM
Drift Angle	`DRIFT` $\leq$ 5.0 deg
Roll Angle	`ROLL` $\leq$ 0.8 deg

To illustrate how the aircraft cruise trajectory is processed and decomposed into a series of stabilized flight segments, an example of analysis performed for a 30-minute cruise at 37,000 ft

is shown in Figure 6.8. However, for reasons of simplicity and clarity, only the analysis for the altitude pressure variable is discussed here. The results for the other seven flight parameters could be obtained by following a similar procedure.

As illustrated in Figure 6.8, the data analysis procedure relies on three successive filtering processes. Each of these processes aims to progressively remove all flight data that do not meet the altitude criteria imposed in Table 6.4. For this, the algorithm starts by scanning the vector of altitudes (represented by the black squares in Figure 6.8a) and then removes all altitude points $h[i]$, $i = \{1, \ldots, N\}$, that do not satisfy the following constraints:

$$\begin{aligned}
&|h[i] - h[i-1]| \leq 20 \text{ ft} \quad \text{and} \quad |h[i] - h[i+1]| \leq 20 \text{ ft}, \quad \text{if } i \in [\![2, \ldots, N-1]\!] \\
&|h[i] - h[i+1]| \leq 20 \text{ ft} \quad \text{and} \quad |h[i] - h[i+2]| \leq 20 \text{ ft}, \quad \text{if } i = 1 \\
&|h[i] - h[i-2]| \leq 20 \text{ ft} \quad \text{and} \quad |h[i] - h[i-1]| \leq 20 \text{ ft}, \quad \text{if } i = N
\end{aligned} \tag{6.19}$$

As shown in Figure 6.8b, this first filtering process makes it possible to detect two flight segments of duration of 8 minutes and 16 minutes, respectively.

Each flight segment identified by the algorithm is then divided into sub-segments with a maximum duration of 10 minutes. The maximum time constraint of 10 minutes was imposed in this study in order to avoid an excessive variation of the aircraft gross weight. In this way, it is possible to assume that the mass of the aircraft is constant along a given sub-segment. This second filtering process leads to the results shown in Figure 6.8c. As can be seen in this figure, the second segment was divided into two new sub-segments of 10 minutes and 6 minutes, respectively.

Finally, the algorithm applied a third and final filtering process that discards all altitude points in a sub-segment that are outside the 95% confidence interval defined by $[\mu - 2\sigma; \mu + 2\sigma]$, where μ is the mean value of the altitude over the sub-segment and σ the corresponding standard deviation. The result of this third filtering process is presented in Figure 6.8d. Thus, by using this step-by-step analysis, it has been possible to identify three flight segments that are "altitude-stable".

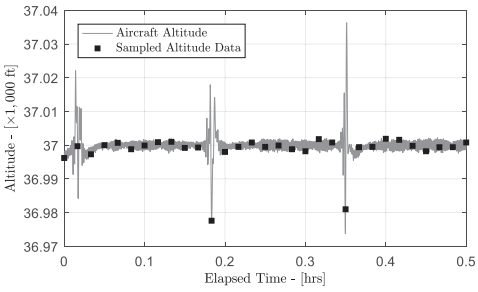

a) Simulated Aircraft Altitude versus Elapsed Time (Trajectory Simulated with the RAFS)

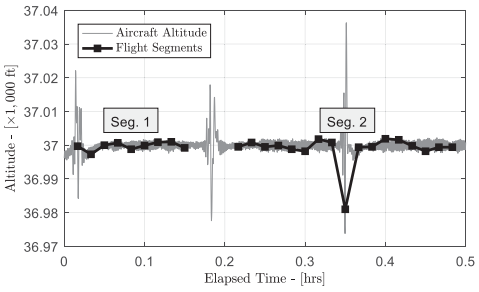

b) First Filtering Process: Detection of All Flight Segments that are "Altitude-Stable"

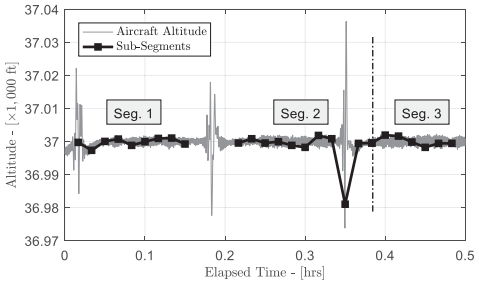

c) Second Filtering Process: Division into Flight Segments of Maximum 10 Minutes

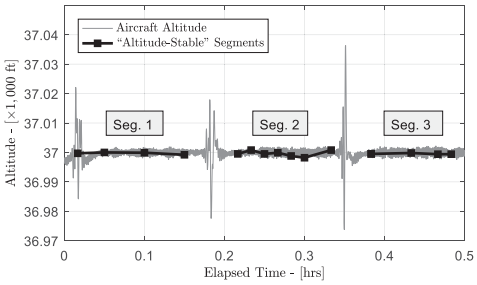

d) Third Filtering Process: Elimination of Data that are outside the Confidence Interval

Figure 6.8 Example of Flight Data Analysis using the Aircraft Pressure Altitude

The procedure presented for the altitude variable is repeated for all flight parameters given in the cruise report file, and for all trim conditions specified in Table 6.4. For each flight parameter, the algorithm removes all points in the initial data set that do not satisfy one of the conditions. At the end, one or more flight segments of minimum 3 minutes and maximum 10 minutes such as those presented in Figure 6.8d are retained depending on the quality of the initial raw data recorded during the flight.

6.3.3.3 Drag Coefficient Lookup Table Adaptation

The last step of the adaptive algorithm is to verify the accuracy of the current drag coefficient lookup table and to apply a correction if necessary. Typically, for each flight segment detected

in the previous step, the algorithm computes the average value for each flight parameter (i.e., average altitude, average Mach number, average aircraft mass, average acceleration, etc.). These average values are supposed to represent the actual aircraft state, and are next used to calculate the lift coefficient of the aircraft as follows:

$$CL_s = \frac{mg_0}{0.5\rho S V_T^2} \tag{6.20}$$

Similarly, based on the average fuel flow for the two engines, the algorithm computes the fuel flow and drag coefficient of the aircraft according to the following two equations:

$$W_F = W_{F(1)} + W_{F(2)} \tag{6.21}$$

$$CD_s = \frac{1}{0.5\rho S V_T^2}\left[\frac{W_F}{\text{TSFC}_0\sqrt{\theta}(1+M)^2} - m\dot{V}_{GS}\right] \tag{6.22}$$

where $W_{F(1)}$ and $W_{F(2)}$ is the average fuel flow of the left and right engine, respectively.

In parallel, the algorithm also makes an estimation of the drag coefficient of the aircraft, $\hat{CD}_s$, by interpolating the actual drag coefficient lookup table for the same flight conditions (for more details about the interpolation technique, see **Section 6.2.3**). This last result is next combined with the set of equations (6.1) to (6.5) in order to determine an estimate of the total fuel flow of the aircraft such as:

$$\begin{aligned}\hat{W}_F &= \left[\hat{D} + m\dot{V}_{GS}\right] \times [\text{TSFC}] \\ &= \left[0.5\rho S V_T^2 \hat{CD}_s + m\dot{V}_{GS}\right] \times \left[\text{TSFC}_0\sqrt{\theta}(1+M)^n\right]\end{aligned} \tag{6.23}$$

The estimated value of the fuel flow obtained in Eq. (6.23) is subsequently compared to the value of the fuel flow obtained in Eq. (6.21) in order to the determine a prediction error in percentage of fuel flow ε_{wf} as follows:

$$\varepsilon_{wf} = \frac{W_F - \hat{W}_F}{W_F} \times 100 \tag{6.24}$$

The fuel flow prediction error in Eq. (6.24) reflects the current deviation of the performance model from the actual performance of the aircraft. As it was explained in **Section 6.1.1**, such a deviation can have three main origins: (1) a poor estimation of the fuel flow due to modeling uncertainties of the initial aircraft performance model, (2) an increase in aerodynamic drag of the aircraft due to airframe degradations, or (3) an increase in fuel flow due to a possible degradation of the engine components. However, because of the structure of the aircraft performance model considered in this study, it is not possible to determine which one of the three causes is actually responsible for the observable fuel flow deviation. This is the reason why, it was always assumed in this study that any deviation in fuel flow should be transferred into a deviation in drag coefficient. Thus, if the prediction error between the theoretical fuel flow and the observed fuel flow is higher than predetermined threshold (e.g. 5%), the algorithm considers that the current performance model is no longer accurate to represent the actual aircraft performance, and a correction of the drag coefficient lookup table must be performed. Such modification is applied in two steps.

Local Adaptation and Local Modification of the Drag Coefficient Lookup Table

By further analyzing the structure of the lookup table, it is possible to conclude that if a prediction error in fuel flow coefficient is observed, this error mainly comes from the four nodes used during the interpolation of the drag coefficient. Based on this observation, it was decided that the correction should apply only to the four nodes used to interpolate the drag coefficient instead to all the nodes of the lookup table. The complete process for the modification of the four nodes is illustrated in Figure 6.9.

As can be seen in Figure 6.9a, the algorithm begins by determining the position in the grid of the flight point defined by the coordinates $\theta = (CD_s|CL_s, M)$. Then, the algorithm extracts the four nodes in the grid that surrounds the flight point. These nodes are shown in Figure 6.9b and Figure 6.9c , and are denoted in the following text by $\theta_{[i,j]} = (CD_{s[i,j]}|CL_{s[i]}, M_{[j]})$ for $i = \{3, 4\}$ and $j = \{2, 3\}$.

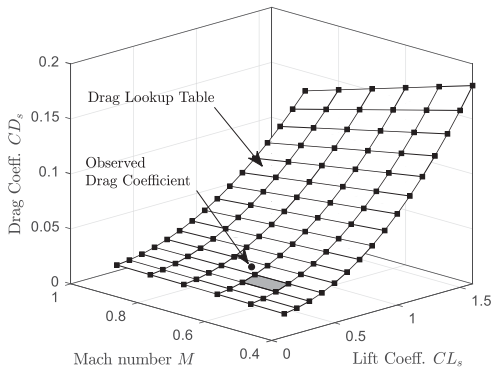

a) Step 1: Locate the Flight Point within the Grid of the Drag Coefficient Lookup Table

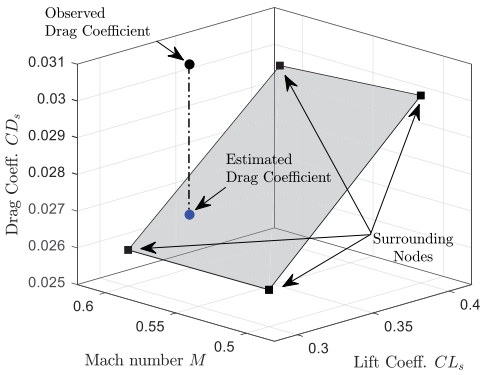

b) Step 2: Extract the Four Nodes that Surround the Flight Point

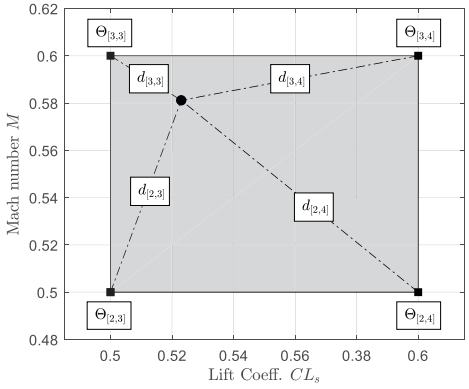

c) Step 3: Compute the Euclidian Distances between the Flight Point and the Nodes

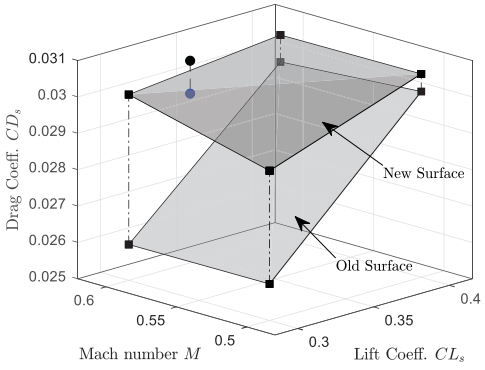

d) Step 4: Adapt the Four Surrounding Nodes to obtain a New Surface

Figure 6.9 Proposed Adaptation Algorithm Illustration

Once the four surrounding nodes are located, the algorithm calculates the Euclidian distance between each node and the flight point (see Figure 6.9c) according to the following equation:

$$d_{[i,j]} = \sqrt{\left(CL_s - CL_{s[i]}\right)^2 + \left(M - M_{[j]}\right)^2} \tag{6.25}$$

The distance obtained in Eq. (6.25) is next normalized by dividing its value to the length of the diagonal of the rectangle formed by the four surrounding nodes, such as:

$$\delta_{[i,j]} = \frac{d_{[i,j]}}{\sqrt{\left(CL_{s[4]} - CL_{s[3]}\right)^2 + \left(M_{[3]} - M_{[2]}\right)^2}} \tag{6.26}$$

Subsequently, the value of the drag coefficient for each of the four nodes is modified according to the following adaptation law:

$$CD^{+}_{s[i,j]} = \underbrace{\left[\frac{\delta_{[i,j]} - \delta^{\lambda_{[i,j]}}_{[i,j]}}{1 - \delta^{\lambda_{[i,j]}}_{[i,j]}}\right]}_{k_c} CD^{-}_{s[i,j]} + \underbrace{\left[\frac{1 - \delta_{[i,j]}}{1 - \delta^{\lambda_{[i,j]}}_{[i,j]}}\right]}_{k_a} CD_s, \text{ for } \delta_{[i,j]} \in]0,1[\tag{6.27}$$

As can be seen in Eq. (6.27), the adaptation law proposed for the drag coefficient lookup table is governed by two parameters. The first parameter, referred to as k_c, is called the conservative gain, while the second one, referred to as k_a, is called the adaptive gain.

These gains are both functions of the normalized distance and the confidence coefficient, and control the tradeoff between keeping the old values stored in the lookup table, and updating their values. To illustrate how these two gains affect the adaptation law proposed in Eq. (6.27), Figure 6.10 shows their variations with respect to the confidence coefficient and for three normalized distance values.

The first observation that can be made when analyzing the three graphs in Figure 6.10 is the variation of the two gains with respect to the confidence coefficient. Indeed, in the three graphs, it is possible to see that whatever the value of the normalized distance is, when the confidence coefficient is equal to 1, the conservative gain is always equal to 0, while the adaptive gain is always equal to 1. This fact means that when a node in the grid is adapted for the first time, the algorithm will directly replace the value of the drag coefficient associated to the node by the value of the drag coefficient observed during the cruise. This aspect of the adaptation law makes it possible to correct very quickly the modeling uncertainties of the initial model. Nevertheless,

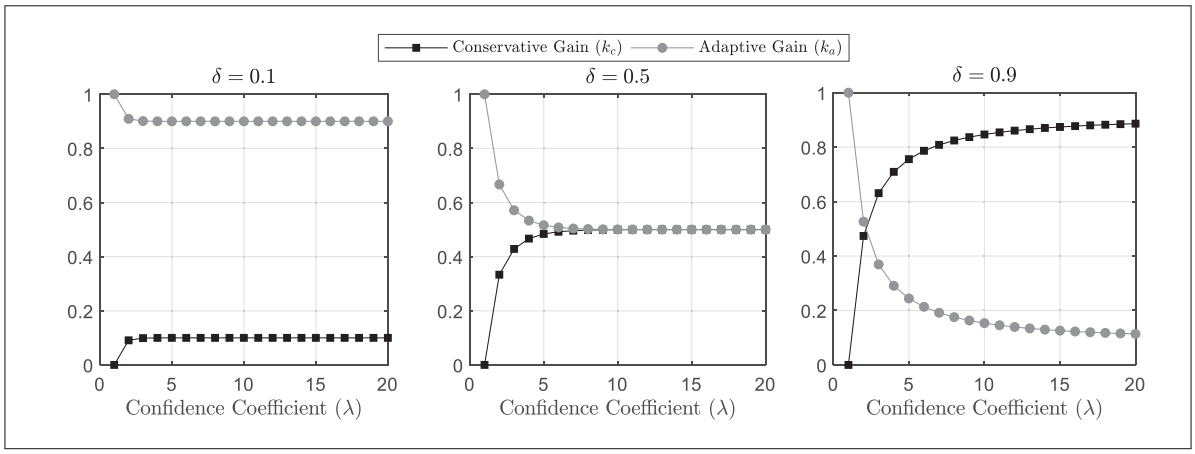

Figure 6.10 Variation of the Adaptive and Conservative Gains as Function of Confidence Coefficient and for Three Normalized Distance Values

as the aircraft flies, the confidence coefficient will increase, and the drag model will become more reliable. Consequently, future adaptations will be made on the basis of a compromise between the old values stored in the lookup table and the values observed during the cruise.

Regarding the effect of the normalized distance on the adaptation law, the three graphs in Figure 6.10 clearly show that, the closer a point is to a node, the greater is the impact on the node. Indeed, it can be observed in the first graph that for a normalized distance of 0.1 (i.e., the point is very close to a node) the value for the adaptive gain converges very quickly to 0.9, while the conservative gain converges to a lower value of 0.1. This observation means that the algorithm will give more importance to the drag coefficient observed in flight than to its value stored in the lookup table. In the opposite case, where the normalized distance is equal to 0.9 (i.e., the point is very far from a node), the value of the adaptive gain converges slowly to 0.1, while the conservative gain converges to a higher value of 0.9. In this case, the algorithm tends to keep the old value of the drag coefficient rather than updating its value.

Finally, similarly to the drag coefficient lookup table, the confidence coefficient lookup table is also adapted according to the following simplified law:

$$\lambda^{+}_{[i,j]} = \lambda^{-}_{[i,j]} + (1 - \delta_{[i,j]}) \tag{6.28}$$

where $\lambda^{+}_{[i,j]}$ is the new value of the confidence lookup table at the node $\theta_{[i,j]}$, and $\lambda^{-}_{[i,j]}$ is the old value of the confidence table at the same node. However, unlike for the drag coefficient, the confidence coefficient is modified only depending on the normalized distance δ. According to proposed relationship in Eq. (6.28), the closer a flight point is to a node, the greater the impact on the node.

Global Adaptation and Generalization to the Others Nodes of the Lookup Table

A considerable disadvantage of the adaptive algorithm, as presented in the previous section, is that it only affects the drag lookup table locally. Indeed, when a correction is applied, only four nodes on all the nodes forming the grid are affected. Therefore, as long as a region of the lookup table has not been explored by the aircraft, it cannot be modified, adapted and corrected. In addition, by locally modifying the drag lookup table, several irregularities can be introduced into the structure of the model. The combination of these two problems results in a non-smooth drag coefficient surface that is reliable only for certain regions of the aircraft flight envelope.

To solve this problem, it was decided to extend the adaptation of the drag and confidence coefficients when sufficient information has been collected over time. To detect the right moment to realize this process, the algorithm counts the number of nodes that have a confidence coefficient value strictly greater than 1. This number is then divided by the total number of nodes to calculate the percentage of nodes that has been adapted since the last reset of the lookup tables. If the percentage of adapted nodes is greater than 30%, the algorithm considers that enough data was collected, and that a global adaptation of the model can be done.

The global adaptation of the drag lookup table is realized by following the same procedure as the one of creating the initial model in **Section 6.3.1**. However, by taking advantage of the confidence coefficient this time, the least squares problem is modified into a weighted least square problem, and the new coefficients of the polynomial in Eq. (6.15) are obtained by solving the following equation:

$$\mathbf{p} = \left(\mathbf{X}^T\mathbf{W}\mathbf{X}\right)\mathbf{X}^T\mathbf{W}\mathbf{Z} \tag{6.29}$$

where $\mathbf{p} = \{p_0, p_1, \ldots, p_5\}$ is the vector containing the polynomial coefficients, $\mathbf{X}$ is the information matrix constructed based on the structure of the polynomial and the values of the breakpoints of the drag lookup table, $\mathbf{W}$ is the diagonal weighting matrix defined such that each element of the diagonal corresponds to a confidence coefficient, and $\mathbf{Z}$ is the vector containing the values of the drag coefficient stored in the lookup table.

Finally, the value of the drag coefficient for all nodes that have a confidence coefficient equal to 1 was replaced by the value of the drag coefficient calculated using the new polynomial shown in Eq. (6.29). Regarding the confidence coefficient, all the values of the lookup table were reset to 1.

Summary of the Complete Calculation Process for the Adaptation of the Drag Coefficient Model

Algorithm 1 summarizes all the steps for the adaptation of the drag lookup table. That is, the selection of the cruise report file, the estimation of the aircraft gross weight, acceleration and vertical speed, the data analysis to detect all stabilized cruise segments, the adaptation of the nodes, and finally, the generalization of the adaptation to the others nodes.

6.4 Results and Validation of the Methodology

The last section of this paper presents the results for the validation of the proposed methodology for adaptation of the drag coefficient model. To this end, a series of flight tests was conducted with the Cessna Citation X Research Aircraft Flight Simulator (RAFS) available at the LARCASE laboratory. Two categories of flight tests were considered: adaptation flight tests and static performance flight tests. These two categories aimed to verify and validate a specific aspect of the proposed methodology, as well as the final adapted drag coefficient model.

Algorithm 6.1 Adaptive Algorithm (Local Adaptation and Global Adaptation)

0. Initialization: Select a flight test and extract the corresponding output data file (see Figure 6.8).

1. Predict the aircraft additional flight parameters: Using the information available in the output data file, and based on the results in Eqs. (6.16) to (6.18), compute the aircraft gross weight, acceleration and vertical speed.

2. Find all flight segments where favorable trim conditions are maintained for at least 3 minutes, and for a maximum of 10 minutes.

3. Main Adaptation Loop. for *For each stabilized flight segment detected* **do**
- a) For the current flight condition, compute the parameters θ and ρ.
- b) Determine the observed lift and drag coefficients, and fuel flow.
- c) Using the actual drag lookup table, make an estimation of the drag coefficient.
- d) Compute the theoretical fuel flow.
- e) Compute the fuel flow error between the observed fuel flow and theoretical one, then: **if** $\varepsilon > 5\%$ **then**
  1. Find the four surrounding nodes.
  2. Compute the normalized distance for each node.
  3. Adapt the nodes using the two adaptation laws in Eq. (6.27) and in Eq. (6.28).

end if

end for

4. Perform a global adaptation: Compute the percentage of nodes that has been adapted, and then: **if** *the percentage of adapted node* $\geq 30\%$ **then**
- a) Construct the matrices: **X**, **W**, and **Y**.
- b) Solve the weighted least squares problem.
- c) Replace all drag coefficient values that has a confidence coefficient equal to 1.
- d) Reset the confidence coefficient lookup table (i.e., set all values to 1).

end if

5. Return the Drag and Confidence Lookup Tables.

6.4.1 Validation of the Adaptation Algorithm

To validate the adaptation algorithm developed in this study, 10 flight tests were conducted by following the procedure described in **Section 6.3.2**. For each flight test, the aircraft takeoff weight and flight conditions for the cruise phase (i.e., altitude and speed) were selected differently in order to cover as much as possible the aircraft flight envelope. Similarly, the destination

airport entered in the FMS to construct the flight plan relative to each test was chosen so that the duration of the cruise could vary between 1 and 4 hours. The list of flight tests used for the validation of the adaptation algorithm is given in Table 6.5. Note that the information contained herein only corresponds to the cruise phase. For example, the weight is the weight of the aircraft at the top-of-climb; the time is the flight time from the top-of-climb to the top-of-descent, and the same for the distance.

Table 6.5 Flight Conditions for the Validation of the Adaptation Algorithm

No.	**Altitude** [ft]	**Mach**	**Weight** [lb]	**Time** [hrs : min]	**Distance** [n miles]
1	25,000	0.58	31,100	1h 23min	476.0
2	38,500	0.79	28,700	1h 35min	721.0
3	32,500	0.79	32,300	1h 45min	750.0
4	27,000	0.55	33,800	1h 56min	551.0
5	28,000	0.61	29,800	2h 30min	882.0
6	28,000	0.71	30,200	2h 32min	1,026
7	31,000	0.84	33,600	2h 38min	1,289
8	41,000	0.78	33,400	2h 40min	1,106
9	39,000	0.84	34,100	2h 46min	1,338
10	40,000	0.73	34,200	3h 40min	1,431

Finally, after each flight, an output data file such as the one shown in Figure 6.7 was generated. The resulting files were next introduced one by one into the adaptation algorithm in order to verify the drag lookup table, and to perform a correction if necessary.

Figure 6.11 shows the validation results for the initial drag coefficient lookup table that was generated using the performance data published in the FPG (see **Section 6.3.1**). The first remark that can be made when analyzing these results is the distribution of the fuel flow error for the initial drag model. Indeed, by analyzing the results in Figure 6.11b, it is possible to see that the distribution of the error is centered around -5.02%, with a standard deviation of 4.97%. Moreover, the maximum error in absolute value for this model was found to be about 19%.

These results clearly demonstrate that the initial drag lookup table derived from the FPG is not accurate enough to predict the performance of the aircraft in cruise. Furthermore, it can be also noted that the relative error for this model is mostly negative. This means that the fuel flow predicted by the model overestimates the actual fuel flow of the aircraft. Going deeper in this analysis, it can be said that an overestimation of fuel consumption results from an overestimation of the drag of the aircraft. Thus, to reduce the fuel flow prediction error, it is necessary to reduce the value of the drag coefficient.

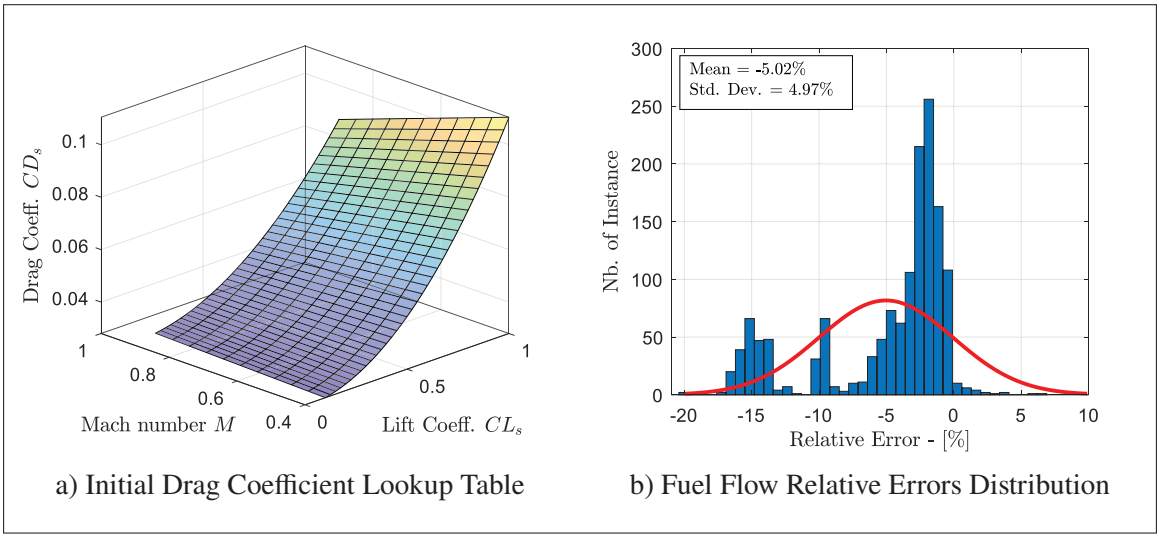

a) Initial Drag Coefficient Lookup Table

b) Fuel Flow Relative Errors Distribution

Figure 6.11 Results for the Initial Drag Coefficient Lookup Table (FPG)

Figure 6.12 shows the resulting drag coefficient lookup table obtained after applying a local adaptation. The most important feature to note in this figure is the local deformation of the surface around the center of the grid. This region of the grid corresponds to the region that has been modified by the adaptation algorithm, and it is also the region that has been explored by the aircraft. As can be seen in this figure, the algorithm has somehow “dug” the surface by lowering the values of the drag coefficient. This fact means that the algorithm has detected that the fuel flow was overestimated, and took the decision to adjust the drag coefficient so that the resulting fuel flow prediction more closely matched the observed fuel flow of the aircraft. Such a deformation of the surface led to the results presented in Figure 6.12a . As shown in this figure, the maximum relative error has been drastically reduced from 19% for the initial drag

coefficient model to 5% for the locally adapted model. Moreover, it can be also observed that the distribution of the fuel flow error in Figure 6.12b is bell-shaped around zero, and that the standard deviation was reduced from 4.97% for the initial model to 1.45% for the adapted model.

These results demonstrate the capability of the adaptation algorithm to correct the drag coefficient lookup table for a given set of flight data in cruise. However, these data also highlight a disadvantage of the local adaptation process, which involves disrupting the structure of the lookup table by creating a non-homogeneous surface.

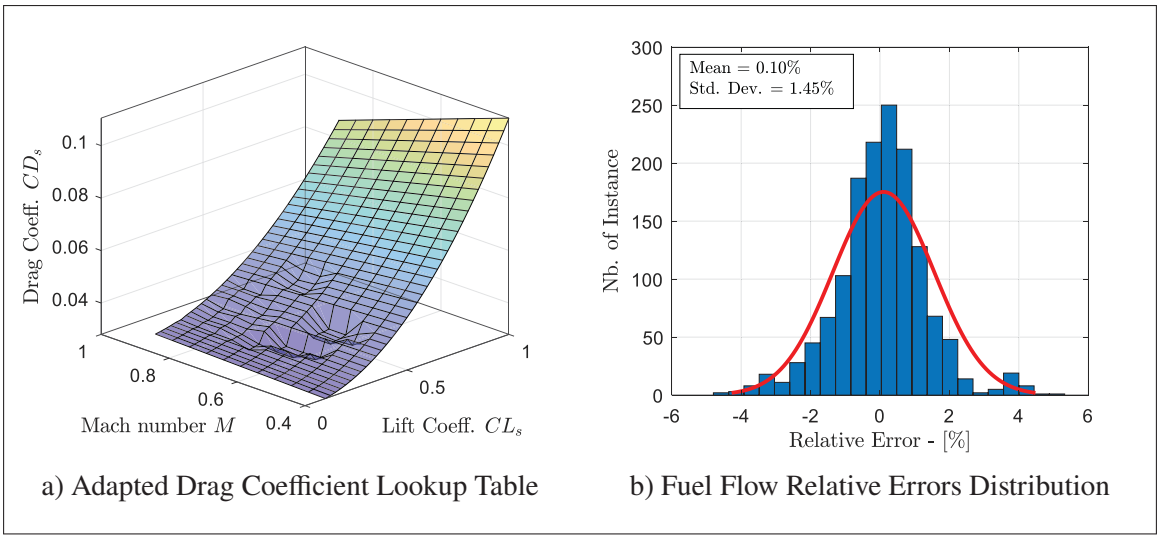

a) Adapted Drag Coefficient Lookup Table

b) Fuel Flow Relative Errors Distribution

Figure 6.12 Results for the Adapted Drag Coefficient Lookup Table (Local Adaptation)

Finally, Figure 6.13 shows the drag coefficient lookup table obtained after applying a local and global adaptation. As a reminder, the global adaptation makes it possible to generalize the local deformation of the surface to all the other nodes of the grid. A considerable advantage of this process is that it allows the adaptation of the overall trend of the drag coefficient lookup table while slightly smoothing the surface. By analyzing the surface obtained in Figure 6.13a, it can be seen that the maximum value of the drag coefficient has been reduced from 0.11 (see in Figure 6.12a) to 0.080. This means that the general trend of the drag coefficient has been shifted down. Finally, it can be also noted from Figure 6.13b that the global adaption process

did not affect the reliability of the drag model obtained from the local adaptation process since the distribution of the fuel flow error remained the same for the two models.

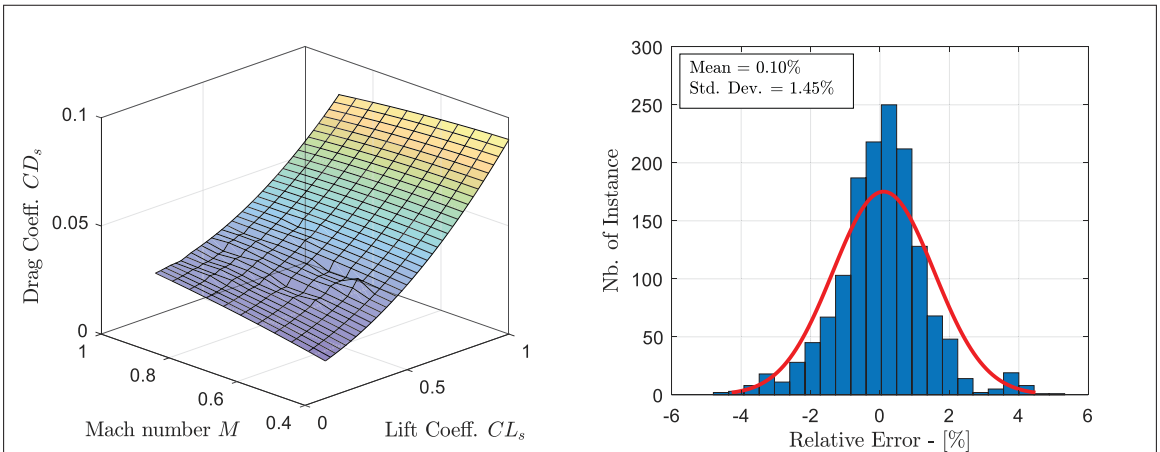

a) Adapted Drag Coefficient Lookup Table

b) Fuel Flow Relative Errors Distribution

Figure 6.13 Results for the Adapted Drag Coefficient Lookup Table (Local Adaptation)

Based on the results presented in this section, it can be concluded that the adaptation algorithm developed in this study corrected the initial drag model by significantly reducing the fuel flow prediction error by 14%. The final adapted drag model is therefore more accurate than the initial model generated with the FPG, and can be used to predict the fuel flow of the aircraft within a tolerance of ±5%.

6.4.2 Validation of the Adapted Drag Coefficient Lookup Table

To further validate the adaptation algorithm proposed in this study, as well as the adapted drag model obtained in Figure 6.13a, a second validation process was carried out using static performance flight tests this time.

The procedure used to perform the static performance flight tests consisted in selecting a particular weight, positioning the aircraft in a given flight condition in terms of altitude and Mach number, and then manually trimming the aircraft to cancel its accelerations. Once the aircraft was completely trimmed, the fuel flow was sampled every 10 seconds over a period

of 60 seconds. The average of the 6 measurements was assumed to be the fuel flow for the corresponding flight condition. In parallel, using the aircraft performance model and the adapted drag coefficient lookup table, the fuel flow was estimated for the same flight condition in order to be compared with the fuel flow value measured with the flight simulator.

As a basis for comparison and evaluation of the aircraft modeling predictions, 15 flight conditions were selected within the aircraft flight envelope by varying the aircraft altitude from 30,000 to 45,000 ft and the Mach number from 0.60 to 0.90. Furthermore, the flight tests were realized for three aircraft weight configurations: 25,000 lb (light), 30,000 lb (medium), and 35,000 lb (heavy). At the end, the combination of all these parameters led to a total of 45 static performance flight tests (15 flight conditions for 3 weight configurations).

Figure 6.14 to Figure 6.16 show the results of comparisons between the fuel flow measured with the flight simulator (RAFS), and the fuel flow estimated with the aircraft performance model (A/C Model) for each of the three weight configurations considered.

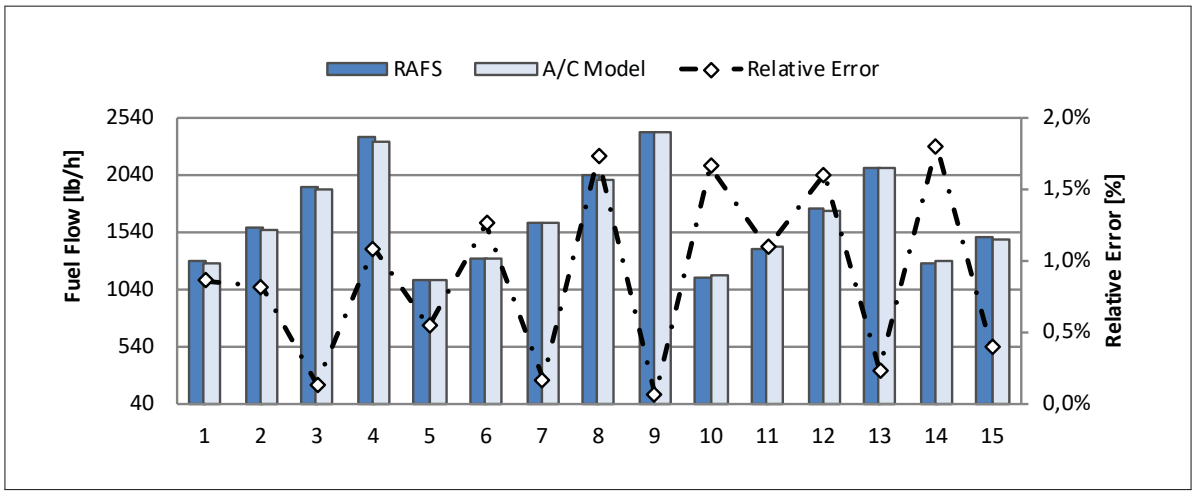

Figure 6.14 Aircraft Fuel Flow Comparison for a Weight of 25,000 lb

From an overall point of view, the results demonstrate that for a given cruise condition, the performance model can predict very well the aircraft fuel flow. Indeed, as can be seen in all three graphics, the maximum relative error is always smaller than 4.5%. This result reinforces the results of analyses made in the previous section because it demonstrates once again that the

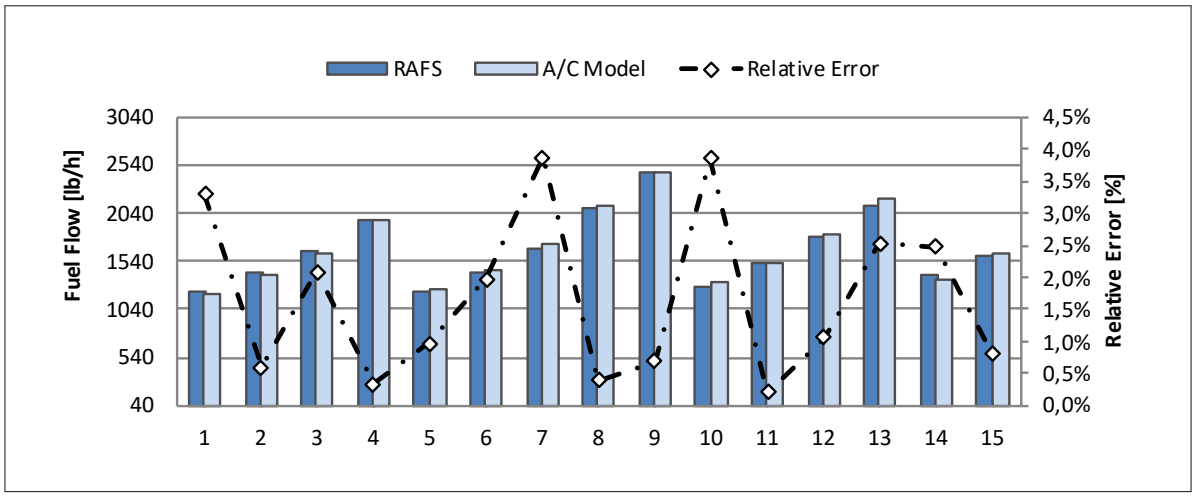

Figure 6.15 Aircraft Fuel Flow Comparison for a Weight of 30,000 lb

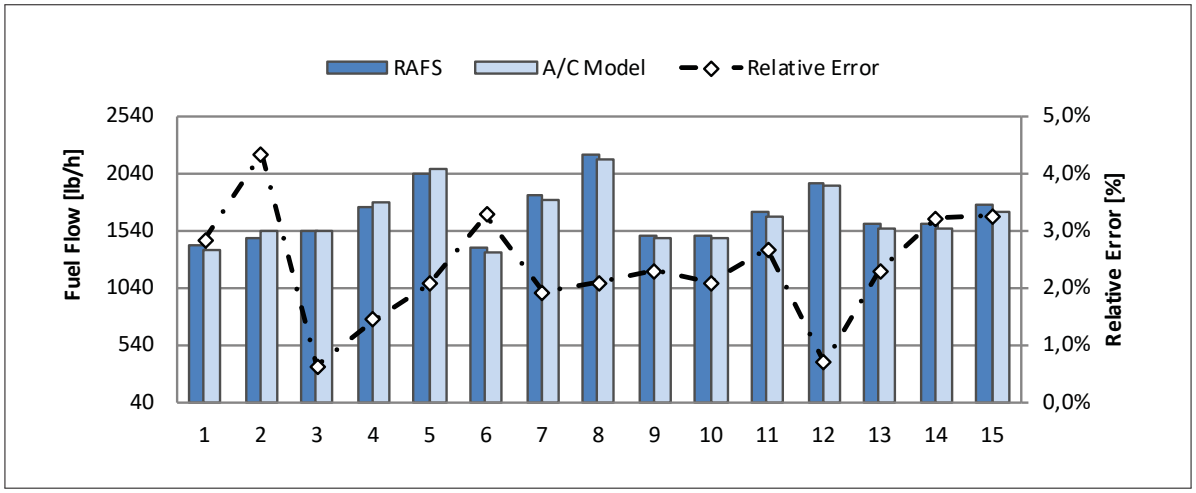

Figure 6.16 Aircraft Fuel Flow Comparison for a Weight of 35,000 lb

drag model generated by the adaptive algorithm remains reliable even in regions of the flight envelope that have not been used in the adaptation process.

6.5 Conclusion

In this paper, a complete methodology and a new adaptive algorithm to continuously monitor the fuel flow of the Cessna Citation X and to update its aerodynamic performance database was

presented. The general methodology consisted in three main steps. Firstly, an initial performance model was created using available data in the Cessna Citation X flight planning guide. This model was intended to represent the fuel consumption of the aircraft in the cruise phase. Once the initial model was created, the second part of the methodology focused on the development of the adaptive algorithm. As it was shown in this paper, the proposed algorithm can be divided into three main parts. The first part of the algorithm consisted in collecting the information recorded during the cruise to estimate several additional flight parameters, such as the aircraft weight and acceleration. The second part of the algorithm consisted in evaluating the equilibrium of the aircraft by identifying all the stabilized flight segments during the cruise. The last part of the algorithm consisted in verifying the accuracy of the current drag coefficient model, and in the application of a correction when necessary. The result of the adaptive algorithm is a drag coefficient model that brings the value of the estimated fuel flow closer to the observed fuel flow in cruise.

The validation of the complete methodology was accomplished using data from a research aircraft flight simulator of the Cessna Citation X, designed and manufactured by CAE Inc. A total of 55 flight tests were conducted and divided into two categories: adaptation flight tests and static performance flight tests. Each of the two categories aimed to verify and validate a specific aspect of the proposed methodology. From a general point of view, it has been demonstrated that the adaptive algorithm proposed in this paper can be used to correct the modelling uncertainties of the initial drag coefficient lookup table obtained with the flight planning guide. As shown in the results section, the fuel flow prediction mean errors were reduced by about 5%, while the standard deviation was divided by a factor of 3.4. Another advantage of the proposed algorithm relies on its capability to correct in advance the regions of the flight envelope that have not yet been explored by the aircraft.

The adaptive algorithm developed in this paper can be used to update a performance model by continuously correcting the drag coefficient of the aircraft. The results obtained are very encouraging and demonstrate the potential of the proposed adaptation algorithm. However, the proposed approach has some limitations, as it is not able to detect if the performance deviation

is due to an aerodynamic degradation or to an engine degradation. Moreover, the study was limited to the cruise phase for which the aircraft mathematical model can be greatly simplified.

As future work, it is desired to take the study a step further by extending the methodology to take into account the engines. In this way, it would be possible to identify the cause of the performance deviation, and to update accordingly either the engine model or the aerodynamic model. This new feature would result in a performance model that would more accurately reflect the actual aero-propulsive characteristics of the aircraft. Future research will also focus on the generalization of the method to other flight phases, such as climb and descent.

GENERAL DISCUSSION AND CONCLUSION

The main problem presented in this thesis was to design, and further develop new methods and algorithms for the study of aircraft performance and flight trajectories. This problem was addressed through three different themes (or parts), including 1) the modeling of aircraft performance, 2) the prediction of aircraft flight trajectories, and 3) the automatic correction (or update) of a performance model.

Aircraft Performance Modeling

The first theme was addressed in **Chapters 2** and **3**, through which two directions were used to propose a solution.

In **Chapter 2**, a first methodology was presented to identify an engine performance model using a CLM approach and lookup tables. Based on the analysis provided in this chapter, it was concluded that a model of engine thrust ratings for certain flight regimes and fuel flow could be identified based on the typical data published in aircraft flight manuals (i.e., AFM and FCOM). It was also pointed out that performance data published in these documents was unfortunately not sufficient to allow the modelling of thrust. To overcome this problem, it was necessary to supplement the data from the flight manuals with other more detailed data obtained from a performance program. Once all the data gathered, a practical technique to identify each parameter of the engine using splines was presented. The results obtained in this first study have shown that the identified model was capable of predicting the engine performance with less than 5% of relative error for various operating conditions and different flight phases (i.e., takeoff, climb, cruise and descent).

The methodology presented in this chapter focused mainly on modelling engine performance. However, by combining the identified model with the trajectory data, it is possible to obtain an aerodynamic model of the aircraft. Nevertheless, in the case when the available data for

the identification process is not detailed enough to obtain firstly an engine model, and then to deduce the aerodynamic model accordingly, it is necessary to consider another approach.

Therefore, in **Chapter 3**, a second new methodology was presented to obtain an aircraft performance model by assuming that only flight trajectory data was available for the identification process. Unlike in **Chapter 2**, it was assumed that no information regarding the engine thrust and thrust ratings was available, and because of this fact, it was explained that it was not possible to identify the engine and aerodynamic models one after the other. The technique proposed in this chapter to overcome this problem consisted in using an iterative process to find a combination of thrust and drag models that reflected the aircraft excess-thrust in descent. Then, based on the results obtained for the descent phase, the engine performance for the other flight phases (i.e., climb and cruise) were modeled. The validation results obtained in this study demonstrated that the aircraft performance model identified with the proposed methodology was capable of predicting the aircraft fuel consumption and flight trajectories with a very good level of accuracy.

In conclusion, the two methods proposed in **Chapters 2** and **3** have given very good results. However, depending on the type, quality and granularity of the data available for the identification process, one or the other method should be considered.

Aircraft Trajectories Prediction

The second theme of this research thesis, which dealt with the prediction of aircraft flight paths, was discussed in **Chapters 4** and **5**. Once again, this subject was treated in two parts.

Chapter 4 dealt with the prediction of aircraft flight trajectories for the takeoff phase and the initial-climb phase up to 3000 ft. The approach proposed in this study consisted in dividing the entire aircraft trajectory into five typical segments (i.e., ground acceleration, rotation, transition, climb at constant airspeed and climb-acceleration). For each of these five segments, algorithms to solve, and to integrate the equations of motion were presented. The aircraft mathematical

model considered for this study was a point-mass model, for which the rotational motion around the pitching axis was included in order to well reflect the aircraft performance during rotation and transition phases. Various techniques were implemented to consider the winds influence, piloting procedures, and runway conditions. Results demonstrated that the methods and algorithms developed in this study were capable of predicting the aircraft performance and departure trajectories with relative errors of less than 5%.

Chapter 5 completed the study shown in **Chapter 4** by presenting additional methods and algorithms for aircraft trajectories prediction above 3000 ft. The methods and algorithms developed in this second study were mainly based on those proposed for the takeoff and initial-climb phases. Indeed, in this study, the entire aircraft trajectory was divided into various flight segments, and for each flight segment, methods and algorithms were developed with the aim to solve and integrate the equations of motion. Results obtained following this second study, once again, was very good as they demonstrated that the prediction algorithms were capable of calculating the aircraft flight trajectories and fuel consumption with relative errors of less than 5%.

The main difference between the **Chapter 4** and the **Chapter 5** was the structure of the aircraft mathematical model, and more specifically the structure of the aerodynamic model. In **Chapter 4**, the model was a so-called "Tail-Off" model, which means that the aircraft tail aerodynamic contributions were explicitly represented into the aerodynamic model, while in **Chapter 5**, the model was a so-called "Tail-On", in which the aircraft tail aerodynamic contributions were implicitly considered. The use of two different structures for the aerodynamic model was a requirement of the project carried out in collaboration with CMC Electronics-Esterline.

In general, "Tail-Off" models are more adapted for the study of terminal procedures, such as takeoff and landing as they make it possible to model the pitch behavior of the aircraft. This aspect is important notably for the study of the aircraft motion in the takeoff phase in order to

well predict its behavior during the rotation and transition segments. However, for the study of aircraft behavior in other flight phases (i.e., climb, cruise and descent), its pitch motion can be ignored. This aspect can be justified by the fact that the rate of attitude change in commercial aircraft is relatively small during these flight phases. Thus, in this case, a "Tail-On" model is preferred.

The main advantage of using a "Tail-Off" model is that it reduces the complexity of the equations of motion, thus facilitating their resolution and integration. Another advantage, which follows from the previous one, is that this type of model facilitates the calculation of the forces, and makes it possible to simulate flight trajectories faster. However, by neglecting the equation of moments, the results may be slightly less accurate since it is not possible to consider the influence of the aircraft's center of gravity position.

In conclusion, the two methods proposed in **Chapters 4** and **5** have given very good results. However, depending on the structure of the aerodynamic model, one or the other method should be considered. Another factor that can be considered is the calculation time, as methods using a "Tail-Off" model require more computational efforts than methods based on a "Tail-On" model. Finally, it is advisable to use a "Tail-Off" model for the takeoff study because it will provide better results for the rotation and transition segments, than the "Tail-On".

Performance Monitoring and Automatic Correction of a Performance Model

Finally, the last theme of this thesis research was discussed in **Chapter 6**. In this chapter new and innovative methods were presented for monitoring aircraft performance in cruise, and then for automatically correcting the aircraft performance model to take into account the airframe/engine degradation due to aging.

The approach consisted in designing an initial performance model that was voluntary not accurate enough to simulate initial modeling uncertainties (or errors). The engine model was designed

based on an empirical specific-fuel consumption model found in the literature. The lift-to-drag model, on the other hand, was identified based on cruise performance data available in the aircraft flight planning guide. An adaptative algorithm was next developed in order to perform various tasks. The first task was to gather all the cruise data, then to analyze them in order to find all the flight segments where the aircraft was in trim (i.e. stabilized) conditions. Based on this first analysis, the actual aircraft fuel flow was estimated, then compared to that predicted by the model.

When the difference between the estimated and predicted fuel flow was too large (greater than 5%), the algorithms developed in this research considered that the model was no longer representative of the aircraft actual performance, and that it was necessary to update the model. This aspect was achieved by using an adaptive law to correct locally the aircraft drag model, in the way that the model with the corrected drag was able to predict the fuel flow with less than 5% of relative error. Finally, when sufficient part of the aircraft flight envelope was explored by the algorithm, a global adaptation was performed to generalize the local corrections and to improve future predictions.

The results presented in this study demonstrated that the algorithms were capable of correcting the initial drag model, and of reducing fuel flow prediction mean errors by around 5%, while the standard deviation was reduced by a factor of 3.4.

RECOMMENDATIONS

The research presented in this thesis focussed on the development of methods and algorithms for calculating aircraft performance and flight trajectories. Clearly, following the results presented in the different studies, it can be concluded that the three objectives considered were successfully achieved. Nevertheless, even if the results obtained in this thesis were globally very good, there is still a lot of work to be done in the study of aircraft performance and flight paths. Several perspectives can be suggested for future work.

Regarding the modelling of aircraft performance, some improvements could be considered. Firstly, it would be interesting to study the possibility of combining the analyses provided in **Chapters 2** and **3** with current knowledge from the literature with the aim to propose new and more reliable engine empirical models, particularly for the study of engine performance during the descent phase. Therefore, it would be possible to propose new empirical models more suited to the next-generation engines. In the same direction, the use of techniques based on artificial intelligence could also be considered to improve the model identification process.

Another improvement that could be considered concerns the definition of the "thrust-drag" ratio introduced in **Chapter 3**. It was assumed that this ratio for the descent phase was constant and varied between 0 and 0.5. Although this ratio was only used to initiate the identification procedure, it might be interesting to find a better way to approximate this parameter. Indeed, based on several analyses, it was found that this ratio depended mainly on the Mach number, and that it behaved in the same way as the lift-to-drag ratio. Also, the method presented in **Chapter 3** did not considered the effects of the flaps/slats and landing gear on the aircraft drag. Thus, future work could focus on techniques able to integrate these elements into the aerodynamic model.

Regarding the prediction of aircraft flight trajectories, future works and investigations should focus on the takeoff phase. First, it would be important to include the lateral motion of the

aircraft by including turn segments. In addition, to obtain a complete tool for the study of departure trajectories, it would also be interesting to combine the prediction algorithms presented in **Chapter 4** with noise and emission models. This aspect would make it possible to assess the impact of aircraft noise and emissions during takeoff and departure procedures. Finally, the only flight phase that was not considered in this thesis, was the landing phase. Thus, future work could be carried out in this direction by adapting the methods and algorithms proposed to this phase of flight.

Regarding the adaptive algorithm proposed in **Chapter 6**, given that the study carried out in this thesis was preliminary, it is clear that more research can be continued in this direction. First of all, the proposed adaptation algorithm was capable of locally modifying four nodes only. However, it should be interesting to find out if more nodes could be adapted and to analyse how the number of "adapted nodes" affects the reliability of the model. Thereafter, it would be very good to improve, thus to complete the methodology for the adaptation of the engine model, and not only of the aerodynamic model. This research would make it possible to determine whether the identified degradation is due to the engines or to the aerodynamics of the aircraft. Finally, investigations to adapt the method for other flight phases should be also considered.

LIST OF REFERENCES

Abramson, M. & Ali, K. (2012). *Integrating the Base of Aircraft Data (BADA) in CTAS Trajectory Synthesizer* (NASA/TM–2012–216051). Hanover, MD, USA. NASA Center for AeroSpace Information.

Airbus. (2001). *Getting Hands on Experience with Aerodynamic Deterioration*. Toulouse, France. Flight Operations Support & Line Assistance.

Airbus. (2002a). *Getting to Grips with Aircraft Performance Monitoring*. Toulouse, France. Flight Operations Support & Line Assistance.

Airbus. (2002b). *Getting to Grips with Aircraft Performance*. Toulouse, France. Flight Operations Support & Line Assistance.

Alligier, R., Gianazza, D. & Durand, N. (2016). Predicting Aircraft Descent Length with MachineLearning. *In 7th International Conference on Research in Air Transportation*. Philadelphia, PA, USA. ICRAT 2016.

Altus, S. (2009). Effective Flight Plans Can Help Airlines Economize. *AERO Magazine, Boeing Commercial Airplanes*, QTR03(09), 26–30. Retrieved from https://www.boeing.com/commercial/aeromagazine/articles/qtr_03_09/article_08_1.html.

Anderson, D. & Hanreiter, C. (2008). Cruise Performance Monitoring - Boeing. *AERO Magazine, Boeing Commercial Airplanes*, QTR04(06), 5–11. Retrieved from https://www.boeing.com/commercial/aeromagazine/articles/qtr_4_06/article_02_1.html.

Angeiras, T. (2015). *A Semi-Empirical Methodology for Balanced Field Length Estimation of Jet-Engined Aircraft in Early Design Phases*. Presented at 5th CEAS Air & Space conference: Challenges in European Aerospace, Delft, Netherland.

Antuñano, M. J. & Spanyers, J. P. (1998). *Hearing and Noise in Aviation* (AM-400-98/3). Oklahoma City, OK, USA. FAA Civil Aerospace Medical Institute Aeromedical Education Division.

Apuleo, G. (2018). Aircraft Morphing - An Industry Vision. In *Morphing Wing Technologies* (ch. 8, pp. 85–101). Elsevier. DOI:https://doi.org/ 10.1016/B978-0-08-100964-2.00002-2.

Asselin, M. (1997). *An Introduction to Aircraft Performance*. Reston, VA, USA: American Institute of Aeronautics and Astronautics. DOI:https://doi.org/ 10.2514/4.861529.

ATR Customer Services. (2011). Fuel Saving Contributing to a Sustainable Air Transport Development. Retrieved from http://www.atraircraft.com/userfiles/files/Fuel_Saving_2011.pdf.

Avery, D. (2011). The Evolution of Flight Management Systems. *IEEE Software*, 28(1), 11–13. DOI:https://doi.org/ 10.1109/MS.2011.17.

Ayhan, S., Costas, P. & Samet, H. (2018). Predicting Estimated Time of Arrival for Commercial Flights. *In Proceedings of the 24th ACM SIGKDD International Conference on Knowledge Discovery & Data Mining*, pp. 33–42. London, United Kingdom. ACM. DOI:https://doi.org/ 10.1145/3219819.3219874.

Baklacioglu, T. & Cavcar, M. (2014). Aero-Propulsive Modelling for Climb and Descent Trajectory Prediction of Transport Aircraft using Genetic Algorithms. *The Aeronautical Journal*, 118(1199), 65–79. DOI:https://doi.org/ 10.1017/S0001924000008939.

Baklacioglu, T. (2016). Modeling the Fuel Flow-Rate of Transport Aircraft during Flight Phases using Genetic Algorithm-Optimized Neural Networks. *Aerospace Science and Technology*, 49, 52–62. DOI:https://doi.org/ 10.1016/j.ast.2015.11.031.

Balakrishnan, H. (2016). Control and Optimization Algorithms for Air Transportation Systems. *Annual Reviews in Control*, 41, 39–46. DOI:https://doi.org/ 10.1016/j.arcontrol.2016.04.019.

Bardela, P. A. & Botez, R. M. (2017). Identification and Validation of the Cessna Citation X Engine Component Level Modeling with Flight Tests. *In AIAA Modeling and Simulation Technologies Conference*. Grapevine, TX, USA. American Institute of Aeronautics and Astronautics. DOI:https://doi.org/ 10.2514/6.2017-1942.

Bartel, M. & Young, T. M. (2008). Simplified Thrust and Fuel Consumption Models for Modern Two-Shaft Turbofan Engines. *Journal of Aircraft*, 45(4), 1450–1456. DOI:https://doi.org/ 10.2514/1.35589.

Basner, M., Clark, C., Hansell, A., Hileman, J. I., Janssen, S., Shepherd, K. & Sparrow, V. (2017). Aviation Noise Impacts: State of the Science. *Noise Health*, 19(87), 41–50. DOI:https://doi.org/ 10.4103/nah.NAH_104_16.

Bazazzade, M., Shahriari, A. & Badihi, H. (2009). Improved Turbine Engine Hierarchical Modeling and Simulation Based on Engine Fuel Control System. *In 45th AIAA/ASME/SAE/ASEE Joint Propulsion Conference & Exhibit*. Denver, Colorado, USA. American Institute of Aeronautics and Astronautics. DOI:https://doi.org/ 10.2514/6.2009-5525.

Blackburn, J., Frendt, G., Gagné, M., Genest, J.-D., Kohler, T. & Nolan, B. (2007). Performance Enhancements to the Industrial Avon Gas Turbine. *In Turbo Expo: Power for Lan, Sea, and Air*, pp. 1521–1530. Montreal, Canada. The American Society of Mechanical Engineers (ASME). DOI:https://doi.org/ 10.1115/GT2007-28315.

Blake, W. (2009). *Jet Transport Performance Methods* (D6-1420). Seattle, WA, USA. Boeing Commercial Airplanes.

Boely, N. & Botez, R. M. (2010). New Approach for the Identification and Validation of a Nonlinear F/A-18 Model by Use of Neural Networks. *IEEE Transactions on Neural Networks*, 21(11), 1759–1765. DOI:https://doi.org/ 10.1109/tnn.2010.2071398.

Boely, N., Botez, R. M. & Kouba, G. (2011). Identification of a Non-Linear F/A-18 Model by the use of Fuzzy Logic and Neural Network Methods. *Proceedings of the Institution of Mechanical Engineers, Part G: Journal of Aerospace Engineering*, 225(5), 559–574. DOI:https://doi.org/ 10.1177/2041302510392871.

Botez, R. M., Bardela, P.-A. & Bournisien, T. (2019). Cessna Citation X Simulation Turbofan Modelling: Identification and Identified Model Validation using Simulated Flight Tests. *The Aeronautical Journal*, 123(1262), 433–463. DOI:https://doi.org/ 10.1017/aer.2018.166.

Brooker, P. (2008). SESAR and NextGen: Investing In New Paradigms. *Journal of Navigation*, 61(2), 195–208. DOI:https://doi.org/ 10.1017/S0373463307004596.

Brouckaert, J.-F., Mirville, F., Phuah, K. & Taferner, P. (2018). Clean Sky Research and Demonstration Programmes for Next-Generation Aircraft Engines. *The Aeronautical Journal*, 122(1254), 1163–1175. DOI:https://doi.org/ 10.1017/aer.2018.37.

Buckingham, E. (1914). On Physically Similar Systems; Illustrations of the Use of Dimensional Equations. *Physical Review*, 4(4), 345–376. DOI:https://doi.org/ 10.1103/PhysRev.4.345.

Calado, E. A., Leite, M. & Silva, A. (2018). Selecting Composite Materials Considering Cost and Environmental Impact in the Early Phases of Aircraft Structure Design. *Journal of Cleaner Production*, 186, 113–122. DOI:https://doi.org/ 10.1016/j.jclepro.2018.02.048.

Camilleri, W., Chircop, K., Zammit-Mangion, D., Sabatini, R. & Sethi, V. (2012). Design and Validation of a Detailed Aircraft Performance Model for Trajectory Optimisation. *In AIAA Modeling and Simulation Technologies Conference*. Minneapolis, MN, USA. American Institute of Aeronautics and Astronautics. DOI:https://doi.org/ 10.2514/6.2012-4566.

Cavcar, M. & Cavcar, A. (2004). Aero-Propulsive Modeling of Transport Aircraft for Air Traffic Management Applications. *In AIAA Guidance, Navigation, and Control Conference and Exhibit*. Providence, RI, USA. American Institute of Aeronautics and Astronautics. DOI:https://doi.org/ 10.2514/6.2004-4792.

Celis, C., Sethi, V., Singh, R. & Pilidis, P. (2015). On Optimisation of Environmentally Friendly Aircraft Engine Cycles. *Journal of Aerospace Technology and Management*, 7(2), 143–156. DOI:https://doi.org/ 10.5028/jatm.v7i2.406.

Cessna Aircraft Company. (2002). *Cessna Citation X Operating Manual (Model 750)* (Airplanes 750-0001 THRU-0172). Witchita, KS, USA. Cessna Aircraft Company.

Chen, Z. X., Langella, I. & Swaminathan, N. (2019). The Role of CFD in Modern Jet Engine Combustor Design. In *Advances in Jet Engines*. IntechOpen. DOI:https://doi.org/ 10.5772/intechopen.88267.

Correia, A. W., Peters, J. L., Levy, J. I., Melly, S. & Dominici, F. (2013). Residential Exposure to Aircraft Noise and Hospital Admissions for Cardiovascular Diseases: Multi-Airport Retrospective Study. *British Medical Journal*, 347, 1–11. DOI:https://doi.org/ 10.1136/bmj.f5561.

Daidzic, N. E. (2016). Estimation of Performance Airspeeds for High-Bypass Turbofans Equipped Transport-Category Airplanes. *Journal of Aviation Technology and Engineering*, 5(2). DOI:https://doi.org/ 10.7771/2159-6670.1122.

Dancila, B., Botez, R. & Labour, D. (2013). Fuel Burn Prediction Algorithm for Cruise, Constant Speed and Level Flight Segments. *The Aeronautical Journal*, 117(1191), 491–504. DOI:https://doi.org/ 10.1017/S0001924000008149.

Dancila, B. D. & Botez, R. M. (2016). Geographical Area Selection and Construction of a Corresponding Routing Grid used for In-Flight Management System Flight Trajectory Optimization. *Proceedings of the Institution of Mechanical Engineers, Part G: Journal of Aerospace Engineering*, 231(5), 809–822. DOI:https://doi.org/ 10.1177/0954410016643104.

Dancila, B. D. & Botez, R. M. (2018). Vertical Flight Path Segments Sets for Aircraft Flight Plan Prediction and Optimisation. *The Aeronautical Journal*, 122(1255), 1371–1424. DOI:https://doi.org/ 10.1017/aer.2018.67.

DARcoporation. (2019). Aircraft Performance Program (Version 7.0) [Computer program]. Retrieved from https://www.darcorp.com/aircraft-performance-program-software/.

De Jesus Mota, S. & Botez, R. M. (2011). New Helicopter Model Identification Method based on a Neural Network Optimization Algorithm and on Flight Test Data. *The Aeronautical Journal*, 115(1167), 295–314. DOI:https://doi.org/ 10.1017/s0001924000005789.

De Jesus Mota, S., Nadeau Beaulieu, M. & Botez, R. M. (2009). Identification of a MIMO State Space Model of an F/A-18 Aircraft using a Subspace Method. *The Aeronautical Journal*, 113(1141), 183–190. DOI:https://doi.org/ 10.1017/s0001924000700418.

Erzberger, H. & Lee, H. Q. (1969). *Technique for calculating optimum takeoff and climbout trajectories for noise abatement* (NASA TN D-5182). Moffett Field, CA, USA. NASA Ames Research Center.

Federal Aviation Administration (FAA). (1991). *Airplane Simulator Qualification* (AC 120–40B). Washington, DC, USA. US. Department of Transportation.

Filippone, A. (2006). *Flight Performance of Fixed and Rotary Wing Aircraft*. American Institute of Aeronautics and Astronautics. DOI:https://doi.org/ 10.2514/4.478390.

Filippone, A. (2008). Comprehensive Analysis of Transport Aircraft Flight Performance. *Progress in Aerospace Sciences*, 44(3), 192–236. DOI:https://doi.org/ 10.1016/j.paerosci.2007.10.005.

Gardi, A., Sabatini, R., Ramasamy, S. & Kistan, T. (2014). Real-Time Trajectory Optimisation Models for Next Generation Air Traffic Management Systems. *Applied Mechanics and Materials*, 629, 327–332. DOI:https://doi.org/ 10.4028/www.scientific.net/AMM.629.327.

Ghazi, G. (2014). *Développement d'une Plateforme de Simulation et d'un Pilote Automatique - Application aux Cessna Citation X et Hawker 800XP*. (Master's thesis, École Polytechnique de Montréal, Montreal, QC, CA).

Ghazi, G. & Botez, R. M. (2015). Development of a High-Fidelity Simulation Model for a Research Environment. *In SAE 2015 AeroTech Congress & Exhibition*, pp. 01–2569. Seattle, WA, USA. SAE International. DOI:https://doi.org/ 10.4271/2015-01-2569.

Ghazi, G. & Botez, R. M. (2019). Identification and Validation of an Engine Performance Database Model for the Flight Management System. *Journal of Aerospace Information Systems*, 16(8), 307–326. DOI:https://doi.org/ 10.2514/1.I010663.

Ghazi, G., Botez, R. M. & Tudor, M. (2015a, November). Identification of a Cessna Citation X Aero-Propulsive Model in Climb Regime from Flight Tests. *In International Conference on Air Transport 2015*. Amsterdam, Netherlands. Aviation Academy of the Amsterdam University of Applied Sciences.

Ghazi, G., Botez, R. M. & Tudor, M. (2015b). Performance Database Creation for Cessna Citation X Aircraft in Climb Regime using an Aero-Propulsive Model developed from Flight Tests. *In AHS Sustainability 2015*. Montreal, QC, CA. American Helicopter Society International.

Ghazi, G., Botez, R. M. & Messi Achigui, J. (2015c). Cessna Citation X Engine Model Identification from Flight Tests. *SAE International Journal of Aerospace*, 8(2), 203–213. DOI:https://doi.org/ 10.4271/2015-01-2390.

Ghazi, G., Botez, R. M. & Domanti, S. (2020). New Methodology for Aircraft Performance Model Identification for Flight Management System Applications. *Journal of Aerospace Information Systems*, 17(6), 294–310. DOI:https://doi.org/ 10.2514/1.I010791.

Gong, C. & Chan, W. (2002). Using Flight Manual Data to Derive Aero-Propulsive Models for Predicting Aircraft Trajectories. *In AIAA's Aircraft Technology, Integration, and Operations (ATIO) 2002 Technical Forum*. Los Angeles, CA, USA. American Institute of Aeronautics and Astronautics. DOI:https://doi.org/ 10.2514/6.2002-5844.

Guardiola, C., Pla, B., Blanco-Rodriguez, D. & Cabrera, P. (2013). A Learning Algorithm Concept for Updating Look-Up Tables for Automotive Applications. *Mathematical and Computer Modelling*, 57(7-8), 1979–1989. DOI:https://doi.org/ 10.1016/j.mcm.2012.02.001.

Hartjes, S. & Visser, H. (2017). Efficient Trajectory Parameterization for Environmental Optimization of Departure Flight Paths using a Genetic Algorithm. *Proceedings of the Institution of Mechanical Engineers, Part G: Journal of Aerospace Engineering*, 231(6), 1115–1123. DOI:https://doi.org/ 10.1177/0954410016648980.

Haselbach, F., Newby, A. & Parker, R. (2015). Next Generation of Large Civil Aircraft Engines-Concepts & Technologies. *In 11th European Conference on Turbomachinery Fluid dynamics & Thermodynamics*. Madrid, Spain. European Turbomachinery Society.

Hausberg, O., Hecker, S., Pfeffer, P., Plochl, M. & Rupp, M. (2014, September). *Incorporation of Adaptive Grid-Based Look-Up Tables in Adaptive Feedforward Algorithms for Active Engine Mounts*. Presented at 12th International Symposium on Advanced Vehicle Control, Tokyo, Japan.

Hebly, S. J. & Visser, H. G. (2008). Advanced Noise Abatement Departure Procedures: Custom Optimized Departure Profiles. *In AIAA Guidance, Navigation and Control Conference and Exhibit*. Honolulu, Hawaii. American Institute of Aeronautics and Astronautics. DOI:https://doi.org/ 10.2514/6.2008-7405.

Hendricks, R. C., Bushnell, D. M. & Shouse, D. T. (2011). Aviation Fueling: A Cleaner, Greener Approach. *International Journal of Rotating Machinery*, 2011, 1–13. DOI:https://doi.org/ 10.1155/2011/782969.

Hiliuta, A. & Botez, R. M. (2007). Flight Dynamics Helicopter Model Validation based on Flight Test Data. *Proceedings of the Institution of Mechanical Engineers, Part G: Journal of Aerospace Engineering*, 221(5), 757–765. DOI:https://doi.org/ 10.1243/09544100jaero205.

Hiliuta, A., Botez, R. M. & Brenner, M. (2005). Approximation of Unsteady Aerodynamic Forces Q(k, M) by use of Fuzzy Techniques. *In 46th AIAA/ASME/ASCE/AHS/ASC Structures, Structural Dynamics and Materials Conference*. American Institute of Aeronautics and Astronautics. DOI:https://doi.org/ 10.2514/6.2005-2079.

Howe, D. (2000). *Aircraft conceptual design synthesis*. Chippenham, England: Professional Engineering.

ICAO. (2010). *Noise Abatement Procedures: Review of Research, Development and Implementation Projects Discussion of Survey Results* (doc. 9888). Montreal, QC, CA. International Civil Aviation Organisation, Montreal.

International Air Transport Association (IATA). (2018). Fact Sheet: Climate Change & CORSIA. Retrieved from https://www.iata.org/en/iata-repository/pressroom/fact-sheets/fact-sheet---climate-change/.

International Air Transport Association (IATA). (2019). More Connectivity and Improved Efficiency - 2018 Airline Industry Statistics Released. Retrieved from https://www.iata.org/en/pressroom/pr/2019-07-31-01/.

International Air Transport Association (IATA). (2020). IATA Forecast Predicts 8.2 billion Air Travelers in 2037. Retrieved from https://www.iata.org/en/pressroom/pr/2018-10-24-02/.

International Civil Aviation Organization (ICAO). (2006). *Procedures for Air Navigation Services, Aircraft Operations (PANS–OPS), Volume II, Construction of Visual and Instrument Flight Procedures* (doc. 8168). Montreal, QC, CA. International Civil Aviation Organisation.

International Civil Aviation Organization (ICAO). (2016). ICAO Environmental Report 2016: Aviation and Climb Change. Retrieved from https://www.icao.int/environmental-protection/Documents/ICAO%20Environmental%20Report%202016.pdf.

Jensen, L., Hansman, R. J., Venuti, J. C. & Reynolds, T. (2013). Commercial Airline Speed Optimization Strategies for Reduced Cruise Fuel Consumption. *In 2013 Aviation Technology, Integration, and Operations Conference*. Los Angeles, CA, USA. American Institute of Aeronautics and Astronautics. DOI:https://doi.org/ 10.2514/6.2013-4289.

Jensen, L., Hansman, R. J., Venuti, J. & Reynolds, T. (2014). Commercial Airline Altitude Optimization Strategies for Reduced Cruise Fuel Consumption. *In 14th AIAA Aviation Technology, Integration, and Operations Conference*. Atlanta, GA, USA. American Institute of Aeronautics and Astronautics. DOI:https://doi.org/ 10.2514/6.2014-3006.

Junjie Lu, Feng Lu & Jinquan Huang. (2018). Performance Estimation and Fault Diagnosis Based on Levenberg–Marquardt Algorithm for a Turbofan Engine. *Energies*, 11(1), 181. DOI:https://doi.org/ 10.3390/en11010181.

Khardi, S. (2009). Reduction of Commercial Aircraft Noise Emission Around Airports. A New Environmental Challenge. *European Transport Research Review*, 1(4), 175–184. DOI:https://doi.org/ 10.1007/s12544-009-0020-7.

Kobayashi, T. & Simon, D. L. (2005). Hybrid Neural-Network Genetic-Algorithm Technique for Aircraft Engine Performance Diagnostics. *Journal of Propulsion and Power*, 21(4), 751–758. DOI:https://doi.org/ 10.2514/1.9881.

Koreanschi, A., Gabor, O. S., Acotto, J., Brianchon, G., Portier, G., Botez, R. M., Mamou, M. & Mebarki, Y. (2017a). Optimization and Design of an Aircraft's Morphing Wing-Tip Demonstrator for Drag Reduction at Low Speeds, Part I - Experimental Validation Using Infra-Red Transition Measurement from Wind Tunnel Tests. *Chinese Journal of Aeronautics*, 30(1), 149–163. DOI:https://doi.org/ 10.1016/j.cja.2016.12.013.

Koreanschi, A., Gabor, O. S., Acotto, J., Brianchon, G., Portier, G., Botez, R. M., Mamou, M. & Mebarki, Y. (2017b). Optimization and Design of an Aircraft's Morphing Wing-Tip Demonstrator for Drag Reduction at Low Speeds, Part II - Experimental Validation Using Infra-Red Transition Measurement from Wind Tunnel Tests. *Chinese Journal of Aeronautics*, 30(1), 164–174. DOI:https://doi.org/ 10.1016/j.cja.2016.12.018.

Kouba, G., Botez, R. M. & Boely, N. (2010). Fuzzy Logic Method Use in F/A-18 Aircraft Model Identification. *Journal of Aircraft*, 47(1), 10–17. DOI:https://doi.org/ 10.2514/1.40714.

Krajcek, K., Nikolic, D. & Domitrovic, A. (2015). Aircraft Performance Monitoring from Flight Data. *Tehnicki vjesnik - Technical Gazette*, 22(5). DOI:https://doi.org/ 10.17559/TV-20131220145918.

Lambrecht, M. & Slater, G. (1999). Departure Trajectory Modeling for Air Traffic Control Automation Tools. *In Guidance, Navigation, and Control Conference and Exhibit*. Portland, OR, USA. American Institute of Aeronautics and Astronautics. DOI:https://doi.org/ 10.2514/6.1999-4234.

Lee, D. S., Fahey, D. W., Forster, P. M., Newton, P. J., Wit, R. C., Lim, L. L., Owen, B. & Sausen, R. (2009). Aviation and Global Climate Change in the 21st Century. *Atmospheric Environment*, 43(22-23), 3520–3537. DOI:https://doi.org/ 10.1016/j.atmosenv.2009.04.024.

Li, C. & Hansman, R. J. (2018). Preliminary Development of a Cruise Altitude and Speed Optimization Decision Support Tool. *In 2018 Aviation Technology, Integration, and Operations Conference*. Atlanta, GA, USA. American Institute of Aeronautics and Astronautics. DOI:https://doi.org/ 10.2514/6.2018-3513.

Li, L., Das, S., John Hansman, R., Palacios, R. & Srivastava, A. N. (2015). Analysis of Flight Data Using Clustering Techniques for Detecting Abnormal Operations. *Journal of Aerospace Information Systems*, 12(9), 587–598. DOI:https://doi.org/ 10.2514/1.I010329.

Li, L., Hansman, R. J., Palacios, R. & Welsch, R. (2016). Anomaly Detection via a Gaussian Mixture Model for Flight Operation and Safety Monitoring. *Transportation Research Part C: Emerging Technologies*, 64, 45–57. DOI:https://doi.org/ 10.1016/j.trc.2016.01.007.

Liden, S. (1994). The evolution of Flight Management Systems. *In AIAA/IEEE Digital Avionics Systems Conference. 13th DASC*, pp. 157–169. Phoenix, AZ, USA. DOI:https://doi.org/ 10.1109/DASC.1994.369487.

Longmuir, M. & Ahmed, N. A. (2009). Commercial Aircraft Exterior Cleaning Optimization. *Journal of Aircraft*, 46(1), 284–290. DOI:https://doi.org/ 10.2514/1.38472.

Lufthansa Group. (2013). Every Liter Counts: Reducing Fuel Consumption and Protecting the Environment Through Product Bundling.

Marsh, G. (2012). Aero Engines Lose Weight thanks to Composites. *Reinforced Plastics*, 56(6), 32–35. DOI:https://doi.org/ 10.1016/S0034-3617(12)70146-7.

Marshall, R. T. & Schweikhard, W. G. (1973). *Modeling of Airplane Performance From Flight-Test Results Validation with an F-104G Airplane* (NASA TN D-7137). Washington, DC, USA. NASA Fligh Research Center.

Martin, S., Wallace, I. & Bates, D. G. (2008). Development and Validation of a Civil Aircraft Engine Simulation Model for Advanced Controller Design. *Journal of Engineering for Gas Turbines and Power*, 130(5), 051601. DOI:https://doi.org/ 10.1115/1.2939015.

Mattingly, J. D., Heiser, W. H., Pratt, D. T., Boyer, K. M. & Haven, B. A. (2018). *Aircraft Engine Design* (ed. 3). Washington, DC, USA: American Institute of Aeronautics and Astronautics. DOI:https://doi.org/ 10.2514/4.105173.

McCormick, B. W. (1995). *Aerodynamics, aeronautics, and flight mechanics* (ed. 2). New York, NY, USA: Wiley.

McEnteggart, Q. & Whidborne, J. F. (2018). Multiobjective Environmental Departure Procedure Optimization. *Journal of Aircraft*, 55(3), 905–917. DOI:https://doi.org/ 10.2514/1.C033132.

Metz, I., Hoekstra, J., Ellerbroek, J. & Kügler, D. (2016). Aircraft Performance for Open Air Traffic Simulations. *In AIAA Modeling and Simulation Technologies Conference*. Washington, DC, USA. American Institute of Aeronautics and Astronautics. DOI:https://doi.org/ 10.2514/6.2016-3522.

Michaud, F., Dalir, H. & Joncas, S. (2018). Structural Design and Optimization of an Aircraft Morphing Wing: Composite Skin. *Journal of Aircraft*, 55(1), 195–211. DOI:https://doi.org/ 10.2514/1.C034340.

Miller, S. (2009). Contribution of Flight Systems to Performance-Based Navigation. *AERO Magazine, Boeing Commercial Airplanes*, QTR2(9), 20–29. Retrieved from https://www.boeing.com/commercial/aeromagazine/articles/qtr_02_09/pdfs/AERO_Q209_article05.pdf.

Mori, R. (2020). Fuel-Saving Climb Procedure by Reduced Thrust near Top of Climb. *Journal of Aircraft*, 1–7. DOI:https://doi.org/ 10.2514/1.C035200.

Murrieta-Mendoza, A. & Botez, R. M. (2015). Methodology for Vertical-Navigation Flight-Trajectory Cost Calculation Using a Performance Database. *Journal of Aerospace Information Systems*, 12(8), 519–532. DOI:https://doi.org/ 10.2514/1.I010347.

Murrieta-Mendoza, A., Demange, S., George, F. & Botez, R. M. (2015). Performance Database Creation using a Level D Simulator for Cessna Citation X Aircraft in Cruise Regime. *In Modelling, Identification and Control / 827: Computational Intelligence*, pp. 826–028. Innsbruck, Austria. ACTAPRESS. DOI:https://doi.org/ 10.2316/P.2015.826-028.

Murrieta-Mendoza, A., Beuze, B., Ternisien, L. & Botez, R. M. (2017a). New Reference Trajectory Optimization Algorithm for a Flight Management System Inspired in Beam Search. *Chinese Journal of Aeronautics*, 30(4), 1459–1472. DOI:https://doi.org/ 10.1016/j.cja.2017.06.006.

Murrieta-Mendoza, A., Hamy, A. & Botez, R. M. (2017b). Four- and Three-Dimensional Aircraft Reference Trajectory Optimization Inspired by Ant Colony Optimization. *Journal of Aerospace Information Systems*, 14(11), 597–616. DOI:https://doi.org/ 10.2514/1.I010540.

Murrieta-Mendoza, A., Botez, R. M. & Bunel, A. (2018a). Four-Dimensional Aircraft En Route Optimization Algorithm using the Artificial Bee Colony. *Journal of Aerospace Information Systems*, 15(6), 307–334. DOI:https://doi.org/ 10.2514/1.I010523.

Murrieta-Mendoza, A., Ternisien, L., Beuze, B. & Botez, R. M. (2018b). Aircraft Vertical Route Optimization by Beam Search and Initial Search Space Reduction. *Journal of Aerospace Information Systems*, 15(3), 157–171. DOI:https://doi.org/ 10.2514/1.I010561.

Nadeau Beaulieu, M. & Botez, R. M. (2008). Simulation and Prediction of Main Rotor, Tail Rotor, and Engine Parameters from Flight Tests. *Proceedings of the Institution of Mechanical Engineers, Part G: Journal of Aerospace Engineering*, 222(6), 817–834. DOI:https://doi.org/ 10.1243/09544100jaero313.

Nadeau Beaulieu, M., Botez, R. M. & Hiliuta, A. (2007). Ground Dynamics Model Validation by Use of Landing Flight Test. *Journal of Aircraft*, 44(6), 2063–2068. DOI:https://doi.org/ 10.2514/1.26625.

Nayyeri, S. (2013). *Aircraft Jet Engine Condition Monitoring Through System Identification by Using Genetic Programming*. (Master's thesis, Concordia University, Montreal, QC, CA).

Nuic, A. (2010). *User Manual for the Base of Aircraft Data (BADA - Revision 3.8)* (2010-003). Brétigny-sur-Orge, France. European Organisation for the Safety of Air Navigation (EUROCONTROL).

Nuic, A., Poinsot, C., Iagaru, M., Gallo, E., Navarro, F. & Querejeta, C. (2005). Advanced Aircraft Performance Modeling for ATM: Enhancements to the BADA Model. *In 24th Digital Avionics Systems Conference*, 1, 2.B.4–1–2.B.4–1. Washington, DC, USA. IEEE. DOI:https://doi.org/ 10.1109/DASC.2005.1563320.

Nuic, A., Poles, D. & Mouillet, V. (2010). BADA: An Advanced Aircraft Performance Model for Present and Future ATM Systems. *International Journal of Adaptive Control and Signal Processing*, 24(10), 850–866. DOI:https://doi.org/ 10.1002/acs.1176.

Nygren, E., Aleklett, K. & Höök, M. (2009). Aviation Fuel and Future Oil Production Scenarios. *Energy Policy*, 37(10), 4003–4010. DOI:https://doi.org/ 10.1016/j.enpol.2009.04.048.

Obert, E., Slingerland, R., Leusink, D. J. W., Berg, T. v. d., Koning, J. H. & Tooren, M. J. L. v. (2009). *Aerodynamic design of transport aircraft*. Amsterdam, The Netherlands: Ios Press; Delft University of Technology, Faculty of Aerospace Engineering, Section Design of Aircraft and Rotorcraft.

Ogaji, S., Sampath, S., Singh, R. & Probert, S. (2002). Parameter Selection for Diagnosing a Gas-Turbine's Performance-Deterioration. *Applied Energy*, 73(1), 25–46. DOI:https://doi.org/ 10.1016/S0306-2619(02)00042-9.

Ojha, S. K. (1995). *Flight Performance of Aircraft*. Washington, DC, USA: American Institute of Aeronautics and Astronautics. DOI:https://doi.org/ 10.2514/4.861826.

Okamoto, N. D., Rhee, J. & Mourtos, N. J. (2005, February). *Educating Students to Understand the Impact of Engineering Solutions in a Global/Societal Context*. Presented at 8th UICEE Annual Conference on Engeneering Education, Kingston, Jamaica.

Patrón, R. S. F. & Botez, R. M. (2015). Flight Trajectory Optimization Through Genetic Algorithms for Lateral and Vertical Integrated Navigation. *Journal of Aerospace Information Systems*, 12(8), 533–544. DOI:https://doi.org/ 10.2514/1.I010348.

Patrón, R. S. F., Botez, R. M. & Labour, D. (2013). New Altitude Optimisation Algorithm for the Flight Management System CMA-9000 Improvement on the A310 and L-1011 Aircraft. *The Aeronautical Journal*, 117(1194), 787–805. DOI:https://doi.org/ 10.1017/s0001924000008459.

Patrón, R. S. F., Kessaci, A. & Botez, R. M. (2014). Horizontal Flight Trajectories Optimisation for Commercial Aircraft through a Flight Management System. *The Aeronautical Journal*, 118(1210), 1499–1518. DOI:https://doi.org/ 10.1017/S0001924000010162.

Patrón, R. S. F., Berrou, Y. & Botez, R. M. (2015). New Methods of Optimization of the Flight Profiles for Performance Database-Modeled Aircraft. *Proceedings of the Institution of Mechanical Engineers, Part G: Journal of Aerospace Engineering*, 229(10), 1853–1867. DOI:https://doi.org/ 10.1177/0954410014561772.

Poles, D. (2009). *Base of Aircraft Data (BADA) Aircraft Performance Modelling Repport* (EEC Technical/Scientific Report 2009-009). Brétigny-sur-Orge, France. European Organisation for the Safety of Air Navigation (EUROCONTROL).

Prats, X., Puig, V. & Quevedo, J. (2011). Equitable Aircraft Noise-Abatement Departure Procedures. *Journal of Guidance, Control, and Dynamics*, 34(1), 192–203. DOI:https://doi.org/ 10.2514/1.49530.

Pratt & Whitney. (2018). Pratt & Whitney GTF Engine. Retrieved from https://prattwhitney.com/en/products-and-services/products/commercial-engines/pratt-and-whitney-gtf.

Quanbeck, D. B. (1982). *Methods for Generating Aircraft Trajectories* (AD-A122386). Alexandria, VA, USA. Center for Naval Analyses.

Ramasamy, S., Sabatini, R., Gardi, A. & Kistan, T. (2014). Next Generation Flight Management System for Real-Time Trajectory Based Operations. *Applied Mechanics and Materials*, 629, 344–349. DOI:https://doi.org/ 10.4028/www.scientific.net/AMM.629.344.

Ramasamy, S., Sabatini, R. & Gardi, A. (2015). Novel Flight Management System for Improved Safety and Sustainability in the CNS+A Context. *In 2015 Integrated Communication, Navigation and Surveillance Conference (ICNS)*, pp. G3–1–G3–11. Herdon, VA, USA. IEEE. DOI:https://doi.org/ 10.1109/ICNSURV.2015.7121225.

Ray, R. J., Hicks, J. W. & Wichman, K. D. (1991). *Real-Time In-Flight Engine Performance and Health Monitoring Techniques for Flight Research Application* (NASA-TM-104239). Edwards, CA USA. NASA Dryden Flight Research Facility.

Raymer, D. (2012). *Aircraft Design: A Conceptual Approach* (ed. 5). Washington, DC, USA: American Institute of Aeronautics and Astronautics. DOI:https://doi.org/ 10.2514/4.869112.

Roberson, W. & Johns, J. A. (2007). Fuel Conservation Strategies: Cost Index Explained. *AERO Magazine, Boeing Commercial Airplanes*, QTR4(7), 26–28. Retrieved from https://www.boeing.com/commercial/aeromagazine/articles/qtr_02_10/pdfs/AERO_FuelConsSeries.pdf.

Roberts, R. A. & Eastbourn, S. M. (2014). Modeling Techniques for a Computational Efficient Dynamic Turbofan Engine Model. *International Journal of Aerospace Engineering*, 2014, 1–11. DOI:https://doi.org/ 10.1155/2014/283479.

Robinson, J. E. & Kamgarpour, M. (2010). Benefits of Continuous Descent Operations in High-Density Terminal Airspace Considering Scheduling Constraints. *In 10th AIAA Aviation Technology, Integration, and Operations (ATIO) Conference*. Fort Worth, TX, USA. American Institute of Aeronautics and Astronautics. DOI:https://doi.org/ 10.2514/6.2010-9115.

Rodriguez, J. M. C., Deniz, L. G., Herrero, J. G., Portas, J. B. & Corredera, J. R. C. (2007). A model to 4D Descent Trajectory Guidance. *In 2007 IEEE/AIAA 26th Digital Avionics Systems Conference*, pp. 1.C.2–1–1.C.2–12. Dallas, TX, USA. IEEE. DOI:https://doi.org/ 10.1109/DASC.2007.4391828.

Rodriguez, L. F. & Botez, R. M. (2013). Generic New Modeling Technique for Turbofan Engine Thrust. *Journal of Propulsion and Power*, 29(6), 1492–1495. DOI:https://doi.org/ 10.2514/1.B34795.

Rodriguez-Sanz, A., Alvarez, D. A., Comendador, F. G., Valdes, R. A., Perez-Castan, J. & Godoy, M. N. (2018). Air Traffic Management based on 4D Trajectories: A Reliability Analysis using Multi-State Systems Theory. *Transportation Research Procedia*, 33, 355–362. DOI:https://doi.org/ 10.1016/j.trpro.2018.11.001.

Roskam, J. (1985). *Airplane Design, volume I to VIII*. Lawrence, KA, USA: Roskam Aviation and Engineering Corp.

Sabatini, R., Gardi, A., Ramasamy, S., Kistan, T. & Marino, M. (2015). Modern Avionics and ATM Systems for Green Operations. In *Encyclopedia of Aerospace Engineering* (pp. 1–17). John Wiley & Sons, Ltd.

SAE International, Committee A-21, Aircraft Noise. (1998). *Procedure for the Calculation of Airplane Noise in the Vicinity of Airports* (1845). Warrendale, PA, USA. SAE International.

Safran Aircraft Engines. (2017). A technological LEAP forward. Retrieved from https://www.safran-aircraft-engines.com/commercial-engines/single-aisle-commercial-jets/leap/leap-1b.

Sandquist, J. & Guell, B. M. (2012). Overview of biofuels for aviation. *Chemical Engineering Transactions*, 29, 1147–1152. DOI:https://doi.org/ 10.3303/CET1229192.

Schultz, C., Thipphavong, D. & Erzberger, H. (2012). Adaptive Trajectory Prediction Algorithm for Climbing Flights. *In AIAA Guidance, Navigation, and Control Conference*. Minneapolis, MN, USA. American Institute of Aeronautics and Astronautics. DOI:https://doi.org/ 10.2514/6.2012-4931.

Segui, M. & Botez, R. M. (2018, October). *Cessna Citation X Climb and Cruise Performance Improvement using Adaptive Winglet*. Presented at Advanced Aircraft Efficiency in a Global Air Transport System (AEGATS), Toulouse, France.

Segui, M., Mantilla, M., Ghazi, G. & Botez, R. M. (2018). New Economical Cruise Methodology for the Cessna Citation X Business Jet by an Original Morphing Horizontal Tail Application. *In Modeling and Simulation Technologies Conference*. Atlanta, GA, USA. American Institute of Aeronautics and Astronautics. DOI:https://doi.org/ 10.2514/6.2018-3895.

Segui, M., Rogoli, V. & Botez, R. M. (2019, July). *Cessna Citation X Static Cruise Improvement using Morphing Wing Application on its Horizontal Tail*. Presented at 8th European Conference for Aeronautics and Space Sciences (EUCASS), Madrid, Spain, DOI:https://doi.org/ 10.13009/EUCASS2019-494.

Senzig, D. A., Fleming, G. G. & Iovinelli, R. J. (2009). Modeling of Terminal-Area Airplane Fuel Consumption. *Journal of Aircraft*, 46(4), 1089–1093. DOI:https://doi.org/ 10.2514/1.42025.

Sibin, Z., Guixian, L. & Junwei, H. (2010). Research and Modelling on Performance Database of Flight Management System. *In 2010 2nd International Asia Conference on Informatics in Control, Automation and Robotics (CAR 2010)*, pp. 295–298. Wuhan, China. IEEE. DOI:https://doi.org/ 10.1109/CAR.2010.5456841.

Silk, R. (2017). More and More Airports Running Out of Space. Retrieved from https://www.travelweekly.com/Travel-News/Airline-News/More-and-more-airports-running-out-of-space.

Simos, D. (2006). *PIANO: a Tool for Preliminary Design, Competitor Evaluation, Performance Analysis*. Presented at ICAO Committee on Aviation Environmental Protection (CAEP), Rome, Italy.

Slater, G. (2002). Adaptive improvement of aircraft climb performance for air traffic control applications. *In Proceedings of the IEEE Internatinal Symposium on Intelligent Control*, pp. 602–607. Vancouver, BC, CA. IEEE. DOI:https://doi.org/ 10.1109/ISIC.2002.1157831.

Slattery, R. & Zhao, Y. (1997). Trajectory Synthesis for Air Traffic Automation. *Journal of Guidance, Control, and Dynamics*, 20(2), 232–238. DOI:https://doi.org/ 10.2514/2.4056.

Suchkov, A., Swierstra, S. & Nuic, A. (2003). Aircraft Performance Modeling for Air Traffic Management Applications. *In 5th USA/Europe Air Traffic Management Research and Development Seminar*, pp. 23–27. Budapest, Hungary.

Sun, J., Ellerbroek, J. & Hoekstra, J. (2017). Modeling Aircraft Performance Parameters with Open ADS-B Data. *In 12th USA/Europe Air Traffic Management Research and Development Seminar*. Seattle, WA, USA.

Sun, J., Ellerbroek, J. & Hoekstra, J. M. (2018a). Aircraft Initial Mass Estimation using Bayesian Inference Method. *Transportation Research Part C: Emerging Technologies*, 90, 59–73. DOI:https://doi.org/ 10.1016/j.trc.2018.02.022.

Sun, J., Hoekstra, J. M. & Ellerbroek, J. (2018b, June). *Aircraft Drag Polar Estimation Based on a Stochastic Hierarchical Model."*. Presented at SESAR Innovation Days, Salzburg, Austria.

Sun, J., Ellerbroek, J. & Hoekstra, J. M. (2019). WRAP: An Open-Source Kinematic Aircraft Performance Model. *Transportation Research Part C: Emerging Technologies*, 98, 118–138. DOI:https://doi.org/ 10.1016/j.trc.2018.11.009.

Sun, J., Hoekstra, J. M. & Ellerbroek, J. (2020). Estimating Aircraft Drag Polar using Open Flight Surveillance Data and a Stochastic Total Energy Model. *Transportation Research Part C: Emerging Technologies*, 114, 391–404. DOI:https://doi.org/ 10.1016/j.trc.2020.01.026.

Thipphavong, D. P., Schultz, C. A., Lee, A. G. & Chan, S. H. (2013). Adaptive Algorithm to Improve Trajectory Prediction Accuracy of Climbing Aircraft. *Journal of Guidance, Control, and Dynamics*, 36(1), 15–24. DOI:https://doi.org/ 10.2514/1.58508.

Torenbeek, E. (2013). *Synthesis of Subsonic Airplane Design*. Delft, Netherland: Delft University Press.

Torres, S. (2018). Evaluation of Numerical Methods for Aircraft Trajectory Computation. *In 2018 IEEE/AIAA 37th Digital Avionics Systems Conference (DASC)*, pp. 1–10. London, UK. IEEE. DOI:https://doi.org/ 10.1109/DASC.2018.8569850.

Trani, A., Wing-Ho, F., Schilling, G., Baik, H. & Seshadri, A. (2004). A Neural Network Model to Estimate Aircraft Fuel Consumption. *In AIAA 4th Aviation Technology, Integration and Operations (ATIO) Forum*. Chicago, IL, USA. American Institute of Aeronautics and Astronautics. DOI:https://doi.org/ 10.2514/6.2004-6401.

Tudor, M. (2017). *Aero-Propulsive Model Design from a Commercial Aircraft in Climb and Cruise Regime using Performance Data*. (Master's thesis, École de technologie supérieure (ÉTS), Montreal, QC, CA).

Tumer, I. & Bajwa, A. (1999). A Survey of Aircraft Engine Health Monitoring Systems. *In 35th Joint Propulsion Conference and Exhibit*. Los Angeles, CA, USA. American Institute of Aeronautics and Astronautics. DOI:https://doi.org/ 10.2514/6.1999-2528.

Turgut, E. T. & Rosen, M. A. (2012). Relationship Between Fuel Consumption and Altitude for Commercial Aircraft during Descent: Preliminary Assessment with a Genetic Algorithm. *Aerospace Science and Technology*, 17(1), 65–73. DOI:https://doi.org/ 10.1016/j.ast.2011.03.007.

Van Bavel, L. (2014). A Takeoff Rotation Model Including Pilot Technique Parameters for Flight Test Data Reduction and Expansion. *In AIAA Atmospheric Flight Mechanics Conference*. Atlanta, GA, USA. American Institute of Aeronautics and Astronautics. DOI:https://doi.org/ 10.2514/6.2014-2059.

Van Es, G. W. H. (2002). Rapid Estimation of the Zero-Lift Drag Coefficient of Transport Aircraft. *Journal of Aircraft*, 39(4), 597–599. DOI:https://doi.org/ 10.2514/2.2997.

Visser, H. G. & Wijnen, R. A. A. (2001). Optimization of Noise Abatement Departure Trajectories. *Journal of Aircraft*, 38(4), 620–627. DOI:https://doi.org/ 10.2514/2.2838.

Vogt, M., Muller, N. & Isermann, R. (2004). On-Line Adaptation of Grid-Based Look-up Tables Using a Fast Linear Regression Technique. *Journal of Dynamic Systems, Measurement, and Control*, 126(4), 732–739. DOI:https://doi.org/ 10.1115/1.1849241.

Volponi, A. J. (1999). Gas Turbine Parameter Corrections. *Journal of Engineering for Gas Turbines and Power*, 121(4), 613–621. DOI:https://doi.org/ 10.1115/1.2818516.

Walter, R. (2001). Flight Management Systems. In *The Avionics Handbook* (ed. 2, ch. 15). Boca Raton, FL, USA: CRC Press LLC.

Wang, Z., Liang, M. & Delahaye, D. (2017). Short-term 4D Trajectory Prediction Using MachineLearning Methods. *In 7th SESAR Innovation Days*. Belgrade, Serbia.

Woike, M. R. (2018). *New Sensors and Techniques for Aircraft Engine Health Monitoring* (GRC-E-DAA-TN54758). Cleveland, OH, USA. NASA Glenn Research Center.

Wu, Z.-J., Tian, S. & Ma, L. (2019). A 4D Trajectory Prediction Model Based on the BP Neural Network. *Journal of Intelligent Systems*, 29(1), 1545–1557. DOI:https://doi.org/ 10.1515/jisys-2019-0077.

Yildirim, M. T. & Kurt, B. (2016). Engine Health Monitoring in an Aircraft by using Levenberg-Marquardt Feedforward Neural Network and Radial Basis Function Network. *In 2016 International Symposium on INnovations in Intelligent SysTems and Applications (INISTA)*, pp. 1–5. Sinaia, Romania. IEEE. DOI:https://doi.org/ 10.1109/INISTA.2016.7571847.

Yilmaz, N. & Atmanli, A. (2017). Sustainable alternative fuels in aviation. *Energy*, 140, 1378–1386. DOI:https://doi.org/ 10.1016/j.energy.2017.07.077.

Young, T. M. (2017). *Performance of the Jet Transport Airplane: Analysis Methods, Flight Operations, and Regulations*. John Wiley & Sons.

Zaag, M., Botez, R. M. & Wong, T. (2019). Cessna Citation X Engine Model Identification using Neural Networks and Extended Great Deluge Algorithms. *INCAS BULLETIN*, 11(2), 195–207. DOI:https://doi.org/ 10.13111/2066-8201.2019.11.2.16.

Zammit-Mangion, D. & Eshelby, M. (2008). Simplified Algorithm to Model Aircraft Acceleration During Takeoff. *Journal of Aircraft*, 45(4), 1090–1097. DOI:https://doi.org/ 10.2514/1.22966.

Zhao, Y. & Vaddi, V. V. (2013). Algorithms of FMS Reference Trajectory Synthesis to Support NextGen Capability Studies. *In 2013 Aviation Technology, Integration, and Operations Conference*. Los Angeles, CA, USA. American Institute of Aeronautics and Astronautics. DOI:https://doi.org/ 10.2514/6.2013-4264.

Zhu, Y., Wang, J., Chen, Y. & Wu, Y. (2016). Calculation of Takeoff and Landing Performance under Different Environments. *International Journal of Modern Physics: Conference Series*, 42, 1660174. DOI:https://doi.org/ 10.1142/S2010194516601745.